EXPLORATION OF THE ANTIMICROBIAL AND MAGNETIC PROPERTIES OF η^6-ARENE-η^5-CYCLOPENTADIENYLIRON(II)-DERIVED DENDRIMERS

by

CHRISTIAN AGATEMOR

A THESIS SUBMITTED IN PARTIAL FULFILLMENT OF
THE REQUIREMENTS FOR THE DEGREE OF

DOCTOR OF PHILOSOPHY

IN

MOLECULAR AND MACROMOLECULAR SCIENCES

DEPARTMENT OF CHEMISTRY
FACULTY OF SCIENCE
UNIVERSITY OF PRINCE EDWARD ISLAND

ABSTRACT

This thesis reports a new family of cationic organometallic dendrimers as an antimicrobial platform and a magnetoceramic precursor. The synthesis of these dendrimers involved well-established chemistries, especially the facile nucleophilic aromatic substitution (S_NAr) reaction of η^6-chloroarene-η^5-cyclopentadienyliron(II) ([η^6-chloroarene-η^5-CpFe]$^+$) complex with a phenolic nucleophile. The use of [η^6-chloroarene-η^5-CpFe]$^+$ resulted in iron-containing dendrimers that undergo S_NAr reaction with nucleophilic functional molecules to give bifunctional dendrimers, and also have implications for antimicrobial activity and ferromagnetism. Indeed, the dendrimers yielded bifunctional, photoactive and redox-active, as well as dual-emissive dendrimers. Importantly, the dendrimers were active against drug-resistant bacteria, including methicillin-resistant *Staphylococcus aureus* (MRSA) and vancomycin-resistant *Enterococcus faecium*. The activity depends on the nature of the counteranion because changing from BF_4^- to PF_6^- counteranion enhanced activity. Also, the dendrimers induced oxidative stress on MRSA and disrupted the microbial cell membrane. Functionalization of the dendrimers with known antimicrobial agents, quaternary ammonium groups or 2-mercaptobenzothiazole, yielded hybrid antimicrobial dendrimers with enhanced activity, especially at higher generation. On pyrolysis at 900 °C in an inert atmosphere, these dendrimers yielded ceramics with room temperature, soft ferromagnetism. The magnetism was tuned *via* dendritic effects or functionalization with cobalt. Indeed, saturation magnetization (M_s) and coercivity (H_c) decreased with increase in dendrimer generation. Incorporating Co increased M_s and H_c at the second-generation but decreased these properties at the zeroth- and first-generations. Overall, [η^6-chloroarene-η^5-CpFe]$^+$-derived dendrimers are a versatile platform for accessing functional, in particular antimicrobial and magnetic, materials.

TABLE OF CONTENTS

LIST OF TABLES

LIST OF FIGURES

LIST OF SCHEMES

LIST OF ABBREVIATIONS AND SYMBOLS

Abbreviation and symbol	Description
$[\eta^6$-arene-η^5-CpFe$]^+$	η^6-arene-η^5-cyclopentadienyliron(II) complex
%	Percentage
3D	Three-dimensional
a.u	Arbitrary units
AAS	Atomic absorption spectroscopy
ATCC	American Type Culture Collection
ATR-FTIR	Attenuated Total Reflectance Fourier transform infrared spectroscopy
br	Broad
CAMHB	Cation-adjusted Mueller Hinton Broth
CFU	Colony-forming units
CLFM	Confocal confocal laser fluorescence microscope
CLSI	Clinical & Laboratory Standard Institute
cm^{-1}	*Per* centimeter
CpFe	Cyclopentadienyliron(II)
CV	Cyclic voltammetry
d	Doublet
DAPI	4′,6-Diamidino-2-phenylindole
DCC	*N*,*N*′-Dicyclohexylcarboiimide
DCM	Dichloromethane
DCU	Dicyclohexylurea
DMAP	4-(Dimethylamino)pyridine
DMF	*N*,*N*′-Dimethylformamide
DMSO	Dimethyl sulfoxide
D_o	Diffusion coefficient
DOSY	Diffusion-ordered spectroscopy
DPP	9,10-Diphenylphenanthrene
DSC	Differential scanning calorimetry
$E_{1/2}$	Half-wave potential
EDX	Energy dispersive X-ray analysis
emu/g	Electromagnetic units *per* grams
E_{pa}	Anodic peak
E_{pc}	Cathodic peak
ESR	Electron spin resonance spectroscopy
FE-SEM	Field-emission scanning electron microscope
G_0	Zeroth generation
G_1	First generation
G_2	Second generation
GPC	Gel permeation chromatography
h	Hours
H_2DCF	Dichlorodihydrofluorescein
H_c	Coercivity
HEKa	Human Epidermal Keratinocytes, adult

IC_{50}	Concentration that inhibits 50% of microorganism activity
IC_{90}	Concentration that inhibits 90% of microorganism activity
K	Kelvin
k_B	Boltzmann constant
mg	Milligram
MHz	Megahertz
mL	Milliliter
mm	Millimeter
mM	Millimolar
MOPS	3-(*N*-Morpholino)propanesulfonic acid
M_r	Remanent magnetization
MRSA	Methicillin-resistant *Staphylococcus aureus*
M_s	Saturation magnetization
ms	Milliseconds
nm	Nanometer
NMR	Nuclear magnetic resonance
Oe	Oersted
p-XRD	Powder X-ray diffraction
Pa s	Pascal second
ppm	Part *per* million
RBC	Red blood cells
R_h	Hydrodynamic volume
rt	Room temperature
s	Singlet
SEM	Scanning electron microscope
S_NAr	Nucleophilic aromatic substitution
T	Absolute temperature
TEM	Transmission electron microscope
T_g	Glass transition temperature
TGA	Thermogravimetric analysis
THF	Tetrahydrofuran
T_m	Melting transition temperature
T_{onset}	Onset of rapid thermal degradation
TPE	Tetraphenylethylene
UV-vis	Ultraviolet-visible
VRE	Vancomycin-resistant *Enterococcus faecium*
W/g	Watt *per* gram
α-Fe	Alpha-iron or ferrite
β	Beta
δ	Chemical shift
η	Eta
η_s	Viscosity
λ_{max}	Wavelength at band maximum
μg	Microgram
μL	Microliter
μM	Micromolar

μs	Microseconds
θ	Angle of diffraction
τ	Tau
°	Degree
°C	Degree Celsius

ACKNOWLEDGMENT

I thank Professors Alaa Abd-El-Aziz and Nola Etkin for being my supervisors for the past four years. Their kind mentorship, as well as the resources and space provided resulted in the experience and success reported in this thesis. The lessons learned in working with them is immense, and I am forever grateful to them. Thanks to Professor Michael Shaver, with whom I started this journey and who introduced me to materials chemistry.

I am also grateful to members of my supervisory committee, Professors Barry Linkletter, Stephanie MacQuarrie, and Tarek Saleh, for the time, direction and suggestions provided throughout these years. I also thank Professor Rabin Bissessur, who has been very helpful, encouraging me, as well as allowing unrestricted access to his research facilities and reading through the various manuscripts.

Thanks to faculty and staff at the Department of Chemistry, University of Prince Edward Island. Professor Brian Wagner assisted in fluorescence spectroscopy measurements; indeed, none of the fluorescence lifetimes measurement would have been possible without his assistance. Mr. Stephen Scully was very valuable especially in helping and training me on how operate the numerous instruments used during the research. The collaboration with the Professor R. G. Kerr group is also appreciated. Without this collaboration and the help of Dr. D. P. Overy, M. Lanteigne, and K. McQuillan, efforts in assessing the biological activity of the dendrimers would have been futile. I am grateful to Dr. Christopher Kirby and Ms. Maike Fischer, who assisted with diffusion-order spectroscopy experiments. Also, I must thank Janette Paquet, Patricia Boland, Shiv Veer Singh, Dr. Prashanth Poddutoori, Mike Johnson, Dorota Wadowska, and Patricia Scallion for their support. Members of the Abd-El-Aziz and Etkin labs as well as students of the Department of Chemistry, University of Prince Edward Island are also appreciated.

The Natural Science and Engineering Research Council of Canada postgraduate scholarship is deeply appreciated. Also, I would like to thank the Department of Chemistry for a laboratory instructorship position as well as the Faculty of Science Graduate Committee and the University of Prince Edward Island Scholarship Committee for the various scholarship awards. The financial assistance of Dr. J. Regis Duffy, through the Dr. J. Regis Duffy Scholarship in Science, is also appreciated.

My family has been the fountain of love, strength and inspiration. I thank them for their love, sacrifices, and prayers. My parents' exemplary fortitude in times of difficulty inspires me in troubled times. My siblings: Oghale, Ajiri, Eloho, Maro, Ovoke, Karo and Mamoke, have always encouraged and supported me in my pursuit. I am forever indebted to my wife, Patience, for her love, understanding, sacrifice, and for encouraging me to complete the thesis when I almost quit.

DEDICATION

To all members of the Clifford Agatemor family, born and unborn.

Chapter One: Introduction[†]

1.1. Towards iron-containing functional materials

Arguably, innovations in science and technology rely on the discovery and development of new materials. A classic example is the independent findings by Kealy *et al*.[1] and Miller *et al*.[2] in 1951, of a new and highly stable organometallic compound (**1.1**) that consist of iron sandwiched between two cyclopentadienyl ligands. Before this discovery, organometallic compounds with a transition metal-carbon bond were rare, making this compound a subject of wonder in the chemistry community, especially after the right structure – $[Fe(\eta^5\text{-}C_5H_5)_2]$ – was independently elucidated by Wilkinson *et al*.[3] and Fischer *et al*.[4] in 1952. More importantly, these developments expanded the frontiers of chemistry, interfacing organic chemistry with inorganic chemistry, and ultimately leading to the development of modern organometallic chemistry. The compound, later named ferrocene by Woodward *et al*.[5] remains an icon of organometallic chemistry, fostering breakthroughs in fundamental and applied research, and expanding the frontiers of organometallic chemistry into areas such as medicine and materials science. The persistent interest in ferrocene as an organometallic motif is due to its low cost, stability, and reactivity.[6-8] Ferrocene chemistry is versatile, involving reactions at the iron center as well as the cyclopentadienyl ligands.[9] For instance, strong acids protonate the iron center (Scheme 1.1),[6,9] various reagents react at the cyclopentadienyl ligands (η^5-Cp) (Scheme 1.2),[6,9] and arene ligands replace a cyclopentadienyl

[†] A part of this chapter is published as Abd-El-Aziz, A. S.; Agatemor, C.; Etkin, N.; *Biomaterials*, **2017**, *118*, 27 and is reproduced by permission of Elsevier Ltd. Another part is published as Abd-El-Aziz, A. S.; Agatemor, C.; Etkin, N.; *Macromol. Rapid Commun.* **2014**, *35*, 513 and is reproduced by permission of WILEY-VCH Verlag GmbH & KgaA, Weinheim.

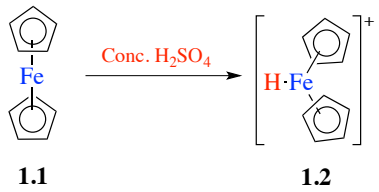

Scheme 1.1. Strong acid protonates the iron in ferrocene.

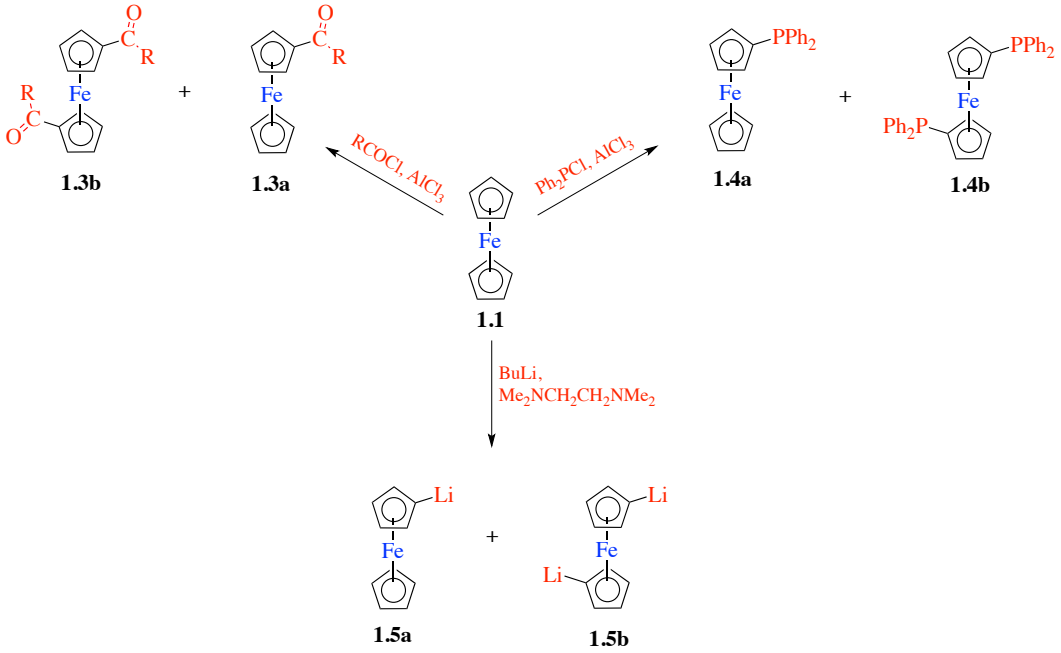

Scheme 1.2. Various reagents react at the cyclopentadienyl ligand in ferrocene.

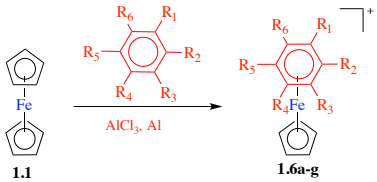

	R_1	R_2	R_3	R_4	R_5	R_6
1.6a	H	H	H	H	H	H
1.6b	CH_3	CH_3	CH_3	CH_3	CH_3	CH_3
1.6c	Cl	H	H	H	H	H
1.6d	Cl	H	H	Cl	H	H
1.6e	Br	H	H	H	H	H
1.6f	Ph	H	H	H	H	H
1.6g	OCH_3	H	H	H	H	H

Scheme 1.3. Various arene ligands replace η^5-cyclopentadienyl ligand in ferrocene.

ligand (Scheme 1.3).[9] These reactions afford many derivatives that are now important precursors in the development of new functional materials.

1.2. Functional materials from η^6-arene-η^5-cyclopentadienyliron(II) complex

The ligand exchange reaction (Scheme 1.3), first reported in 1963 by Nesmeyanov,[10] is a general synthesis route to a series of ferrocene derivatives, the mixed ligand, 18-electron, cationic η^6-arene-η^5-cyclopentadienyliron(II) ([η^6-arene-η^5-CpFe]$^+$) complexes. From the functional materials perspective, these complexes are important for a few reasons. First, the presence of an iron in these complexes imparts redox activity which has implications for biological and catalytic applications.[11-21] Further, the iron activates the arene ligand towards deprotonation[16,18,19] as well as nucleophilic addition and substitution reactions, mediating the facile syntheses of small molecules as well as polymers.[11-15,22-28] Indeed, many polymer chemists exploit the chemistry of [η^6-arene-η^5-CpFe]$^+$ complexes to mediate the facile syntheses of polymers of different structures, including linear, branched, hyperbranched and star polymers.[28-37]

1.2.1. [η^6-Arene-η^5-CpFe]$^+$ mediated synthesis of functional molecules

The η^5-CpFe moiety activates the arene ligand towards facile nucleophilic aromatic substitution or addition reactions, which are synthesis routes to some functional organic molecules.[26,28] As an example, Sutherland *et al*. synthesized benzonitrile and phthalonitrile using these reactions.[26] In their approach, a cyanide ion adds to the arene ligand or replaces a chloro group when [η^6-chlorobenzene-η^5-CpFe]$^+$ complex (**1.6c**) was reacted with excess sodium cyanide in dimethylformamide (DMF) at room temperature (Scheme 1.4). They found that the substitution and addition reactions simultaneously occur with the overall product being dependent on the

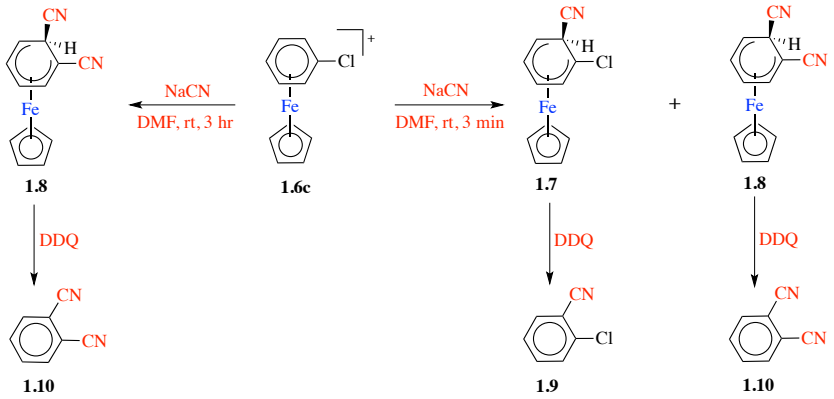

Scheme 1.4. $[\eta^6\text{-Arene-}\eta^5\text{-CpFe}]^+$ mediated synthesis of aromatic nitriles.

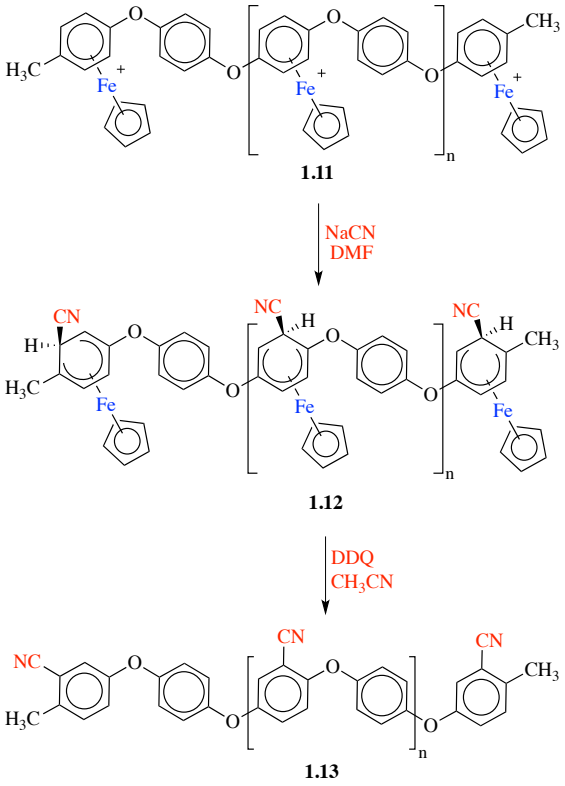

Scheme 1.5. $[\eta^6\text{-Arene-}\eta^5\text{-CpFe}]^+$ mediated functionalization poly(aromatic ethers).

reaction time. Conducting the reaction for three minutes gives an approximate 90:10 mixture of the addition product (**1.7**) and the addition/substitution product (**1.8**), whereas three hours gives only **1.8** (Scheme 1.4). Subsequent demetallation/oxidation of **1.7** or **1.8** with 2,3-dichloro-5,6-dicyano-1,4-benzoquinone afforded benzonitrile (**1.9**) or phthalonitrile (**1.10**), respectively. Inspired by the work of Sutherland, Abd-El-Aziz *et al*. successfully functionalized poly(aromatic ether)s with nitrile (CN) groups (Scheme 1.5).[38] The facile introduction of CN functional group to aromatic rings is attractive because this group is essential to the activity of many pharmaceuticals, agrochemicals, and dyes.[39-43] Conventional and emerging synthesis methods to aromatic nitriles employ stringent conditions such as high or low temperatures,[39-42] making the $[\eta^6$-arene-η^5-CpFe$]^+$ mediated room temperature synthesis a desirable alternative.

1.2.2. $[\eta^6$-Arene-η^5-CpFe$]^+$ mediated synthesis of high-temperature polymers

New materials with high-temperature properties are in constant demand in engineering fields, for instance in spacecraft and defense applications. These materials exhibit good mechanical properties and stability in harsh environments, such as chemical and UV environments, at higher temperatures. Poly(aromatic ether)s are one of the first commercial successes in the search for high-temperature polymers and remain a prime member of this family of materials. Traditional synthesis route to these polymers is *via* high-temperature nucleophilic aromatic substitution polymerization of activated dihaloarenes with bisphenolates,[44-46] therefore, stressing a need for less stringent synthesis strategies to access these polymers. Towards this, Abd-El-Aziz *et al*. and Pearson *et al*. pioneered $[\eta^6$-dichloroarene-η^5-CpFe$]^+$ mediated nucleophilic aromatic substitution polymerization at 65 °C, aiming for less stringent conditions (**1.15a** and **1.16a**).[28,30,35] A typical polymerization involves reacting $[\eta^6$-dichlorobenzene-η^5-CpFe$]^+$ (**1.6c**) with a dihydroxyarene

nucleophile in the presence of a weak base, such as potassium carbonate (Scheme 1.6).[30,35] The $[\eta^6$-arene-η^5-CpFe$]^+$ mediated nucleophilic substitution polymerization also facilitates the syntheses of poly(amine)s (**1.15b** and **1.16b**) and poly(sulfide)s (**1.15c** and **1.16c**) under mild conditions by using the appropriate nucleophile (Scheme 1.6).[29,35] In addition to the less stringent conditions, the route also allows access to organometallic as well as organic polymers. Indeed, simple UV photolysis yields the organic from the organometallic polymer with a good recovery of ferrocene (Scheme 1.6).[28-30,35] These polymers are potentially high-temperature materials because their thermogravimetric analysis show that the organometallic poly(aromatic ether)s are thermally stable up to 200 °C, and the organic analog, up to 500 °C.[35]

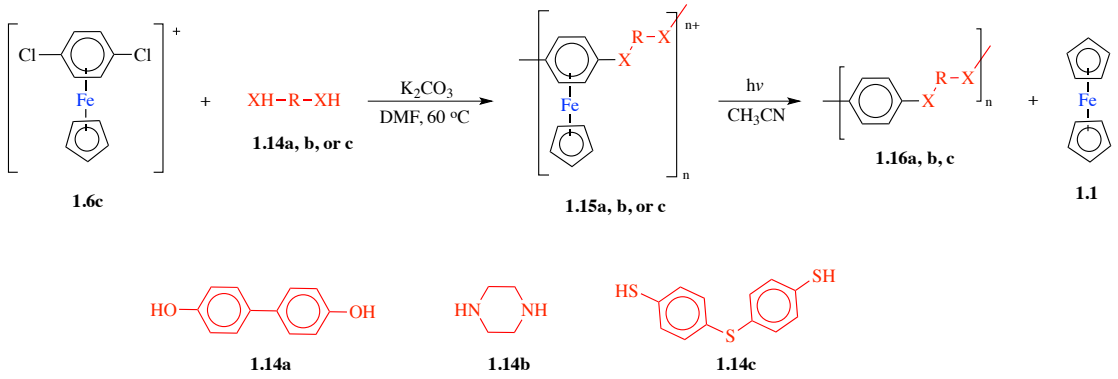

Scheme 1.6. $[\eta^6$-Arene-η^5-CpFe$]^+$ mediated polymerization.

1.2.3. $[\eta^6$-Arene-η^5-CpFe$]^+$ mediated synthesis of dendrimer cores

Dendrimers are an attractive class of polymers given their potential applications in many fields ranging from catalysis to drug delivery.[47-51] Structurally, dendrimers are tree-like polymers characterized by a core from which several branched monomers stem, yielding multiple termini. A goal in dendrimer research targets nanospaces for drug delivery applications.[50] Towards this, efforts have been made to design dendrimers with many branched monomers, because this leads

to the space saturation at the periphery, eventually creating the inner nanospaces for drug encapsulation.[50] Synthesizing such dendrimers requires a multifunctional core that reacts with many branched monomers. Astruc *et al*. have successfully established a synthesis route to multifunctional cores.[52-57] Their route exploits the ability of the η^5-CpFe moiety to activate the arene ligand in $[\eta^6$-arene-η^5-CpFe$]^+$ towards benzylic CH deprotonation when an alkyl substituent is attached to the ligand.[18] After deprotonation, nucleophilic substitution of a halide in an organohalide yields a multi-functionalized arene ligand in one pot under ambient conditions (Scheme 1.7).[18] This reaction can be rationally designed, as demonstrated by Astruc *et al*., to give up to nine functional handles that react with several branched monomers. In an approach, they reacted $[\eta^6$-mesitylene-η^5-CpFe$]^+$ (**1.17**) with allyl bromide in the presence of potassium hydroxide under ambient conditions, followed by photolysis to synthesize a dendrimer core (**1.18**) with nine double bonds (Scheme 1.7).[52]

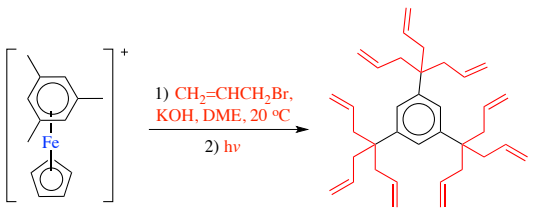

1.17 **1.18**

Scheme 1.7. $[\eta^6$-Arene-η^5-CpFe$]^+$ mediated synthesis of a multifunctional dendrimer core.

1.2.4. $[\eta^6$-Arene-η^5-CpFe$]^+$-based redox-active polymers

The design of functional polymers is at the forefront of polymer research. Characteristically, these polymers have latent reactive centers that can engage in chemical reactions without degrading the polymer. The iron in the 18-electron monocation $[\eta^6$-arene-η^5-CpFe$]^+$ is redox active, and can participate in electron transfer reactions to give either the reduced 19-electron neutral $[\eta^6$-arene-η^5-CpFe], or the oxidized 17-electron, dicationic $[\eta^6$-arene-η^5-CpFe$]^{2+}$ complex (Scheme 1.8).[20]

Conjugating these [η^6-arene-η^5-CpFe] complexes to polymers is, therefore, a synthesis route towards redox active materials[16-21,31,58-60] that have significant implications for catalysis and biology. For instance, the 19-electron complex is an electron rich, strong reducing agent[61,62] whereas the 17-electron complex is a strong oxidizing agent,[63] both of which have catalytic applications.[61-63] Using these complexes, Astruc *et al*.[52,57,58,61] as well as Abd-El-Aziz *et al*.[31,36,37,64] have built a library of redox active polymers, some of which are excellent reducing systems (Figure 1.1).

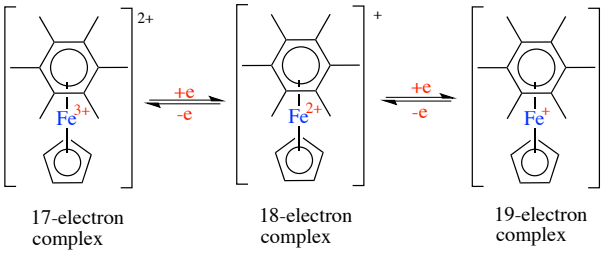

Scheme 1.8. Electron transfer reactions of [η^6-arene-η^5-CpFe] complexes.

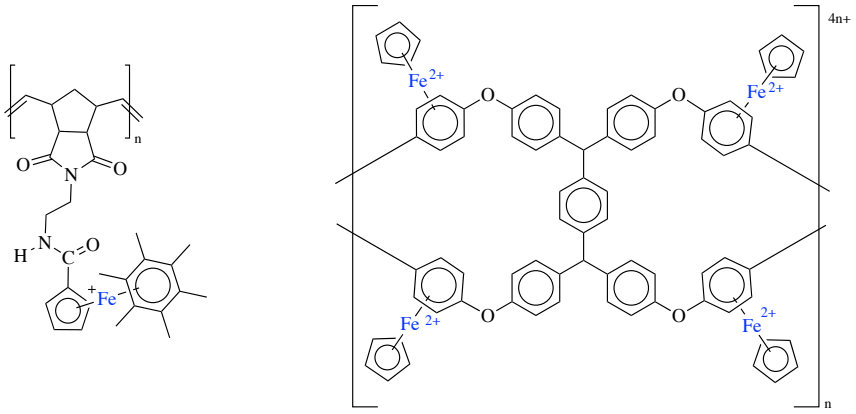

1.19 **1.20**

Figure 1.1. Some examples of redox active [η^6-arene-η^5-CpFe]$^+$ polymers.

1.3. State-of-the-art and gaps in $[\eta^6$-arene-η^5-CpFe$]^+$ research

Since the pioneering work of Nesmeyanov on the synthesis of $[\eta^6$-arene-η^5-CpFe$]^+$ complexes from ferrocene, extensive investigations have been carried out on these complexes with the focus directed at two areas:

1. facile syntheses of small molecules and polymers.
2. design of redox-active polymers.

While these investigations have resulted in numerous achievements, major gaps exist. For instance, it remains to be established:

1. if these redox-active complexes are antimicrobial given that redox activity is linked with many biological functions.
2. if materials derived from these complexes are magnetic given that they contain a ferromagnetic metal, iron.

1.4. Research goal and objectives

This research focuses on bridging the identified gaps. The overall goal, therefore, is to "*Explore the Antimicrobial Activity and Magnetic Property of* $[\eta^6$*-Arene-*η^5*-CpFe*$]^+$*-derived Materials*" with the expectation of developing new functional materials. This goal will be achieved *via* three objectives.

1.4.1. First objective: Synthesis of functional dendrimers

The first objective, addressed in *Chapters Two and Three*, is the synthesis of functional polymers that incorporate $[\eta^6$-arene-η^5-CpFe$]^+$ within their framework and are amenable to further functionalization. The polymers will be applied to test the hypothesis that $[\eta^6$-arene-η^5-CpFe$]^+$-

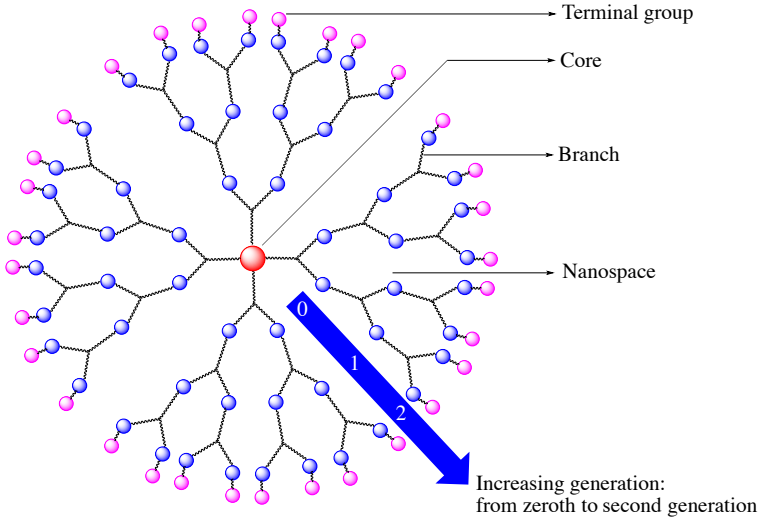

Figure 1.2. A general representation of dendrimer.

derived materials are antimicrobial, and are magnetic. Towards this, dendrimer (Figure 1.2), a special type of highly branched polymer composed of a central core from which several branched monomers stem to yield multiple surface terminal groups, was selected. From a functional polymer standpoint, the core, branches and multiple terminal groups are structural sites where functional groups can be precisely placed to impart and tune functional properties. Further, the iterative synthesis route of dendrimers affords structures with close to uniform dispersity,[65] providing the homogeneity required in most biological applications.[66] Also, the synthesis route can be rationally designed to afford dendrimers of various generations (sizes), which is an approach to tuning properties. Again, whereas reports on dendrimers containing 19-electron neutral [η^6-arene-η^5-CpFe] complex as terminal groups are common in the literature,[52,57,58,61] reports on dendrimers with the 18-electron cationic [η^6-arene-η^5-CpFe]$^+$ complex located on the branch and is amenable to functionalization are far less common,[64] creating a need to explore the potentials of this type of dendrimer. Such dendrimer design allows access to multifunctional materials and offers opportunity to impart new properties or tune intrinsic ones *via* functionalization. More importantly,

in the emerging field of antimicrobial organometallic polymers, the dendrimer structure is yet to be explored. It will, therefore, be worthwhile to expand the frontiers of antimicrobial organometallic polymers into dendrimer science. The last argument also inform the choice of dendrimer as the polymer structure to investigate the magnetic property of $[\eta^6$-arene-η^5-CpFe$]^+$-derived materials. Indeed, reports of organometallic linear, crosslinked and hyperbranched polymer-derived magnetic ceramics exist,[67-80] but reports on organometallic dendrimer-derived magnetic ceramics are unavailable.

To synthesize the dendrimers, the traditional convergent and divergent strategies will be explored. The divergent strategy construct the dendrimer outwards, starting with a multifunctional core molecule that reacts with several monomers in a series of reactions to access the target generations. Conversely, in the convergent strategy, the terminal groups are first synthesized, and in a series of reactions, the dendrimer is constructed inwards with the last step being reaction with the multifunctional core. Two key reactions, S_NAr and Steglich esterification reactions, will be used to construct the dendrimers because these reactions take place under mild conditions. For instance, the Steglich esterification reaction proceeds at room temperature and takes up water, a byproduct of esterification reaction, by forming dicyclohexylurea, therefore eliminating the need for special water removal techniques. Importantly, the Steglich esterification reaction takes place in the presence of the $[\eta^6$-arene-η^5-CpFe$]^+$ complex and affords the target products without destroying the functionality of the iron centers.

1.4.2. Second objective: Characterization for antimicrobial activity

The second objective of this work, addressed in *Chapter Three*, is to evaluate the antimicrobial activity of the $[\eta^6$-arene-η^5-CpFe$]^+$-derived dendrimers against drug-resistant microorganisms.

The expectation is new antimicrobial materials and new insights on how to control the antimicrobial activity *via* a structure-property relationship. This objective is attractive given the threat of drug resistant infections to public health. An acknowledged strategy to combating resistance is a continued supply of new antimicrobial agents that act *via* mechanisms of action that bypass the resistance pathway.[81] The discovery of new antimicrobial agents is, therefore, critical to the fight against drug-resistant infections. Antimicrobial polymers are attractive since they are less volatile, more chemically robust, and therefore possess longer lifetimes, and better environmental compatibility compared with small molecules.[82] Again, from the application perspective, polymers can be extruded into fibers for sterile bandages and surgical gowns, or fabricated into medical devices and implants, or used as surface coatings in medical devices, hospital furniture and shower walls to minimize microbial colonization.[82]

In the quest for potent antimicrobial polymers, greater focus is on organic polymers with organometallic polymers being less investigated, creating a need to explore the potential of the latter class of polymers.[83] The antimalarial property of ferroquine,[84] a ferrocene-containing molecule in clinical trials, contributes to the current interest in organometallic molecules as antimicrobial platforms. It is postulated that iron in ferrocene mediates redox processes that induce oxidative stress on microorganisms, contributing to the biological activity.[84,85] It is, therefore, reasonable to presume that $[\eta^6\text{-arene-}\eta^5\text{-CpFe}]^+$ complexes, ferrocene derivatives, may mediate redox processes that may lead to antimicrobial activity. The antimicrobial activity of organometallic compounds extends beyond oxidative stress. Indeed, many discoveries in this area suggest that this class of antimicrobials damage and selectively kill microbial cells by inducing oxidative stress, causing protein dysfunction, or damaging the cell membrane.[86-88] Arguably, organometallic polymers can combine multiple mechanisms of action, which in synergy pose a

potent challenge to drug-resistant microorganisms. For instance, Metzler-Nolte *et al*. found that the antimicrobial organometallic compounds (**1.21**) or ruthenocene (**1.22**) (Figure 1.3) act *via* multiple mechanisms.[85] These compounds are active against methicillin-resistant *Staphylococcus aureus* (MRSA), and act by simultaneously interfering with cell wall biosynthesis, targeting cytoplasmic membrane, depolarizing membrane potential, and inducing oxidative stress.[85] It is logical to assume that the combined effects of these mechanisms of action contributed to the effectiveness of these compounds.

The presence of a cationic charge on organometallic polymers also offers a mechanism of action for by-passing the resistance pathway. For instance, Tang *et al*. exploited the presence of cationic charges to bypass resistance in MRSA,[83] a drug-resistant microorganism that deactivates β-lactam antibiotics by producing and secreting β-lactamase to hydrolyze the β-lactam ring in the antibiotic. Tang and his team developed a strategy that involves the formation of ion-pair bioconjugates between anionic charge in β-lactam antibiotics and cationic charge in a cobaltocenium-containing metallopolymers (**1.23**) (Scheme 1.9).[83] The formation of the bioconjugates protects the antibiotic from β-lactamase hydrolysis. The cationic charge on the polymer also interacts with the negatively charged cell membrane, disrupting the cell membrane of MRSA, eventually killing the cell.[83]

Given the presence of a cationic charge, and redox-active iron in the $[\eta^6\text{-arene-}\eta^5\text{-CpFe}]^+$ complex, it is expected to function as an antimicrobial agent *via* multiple mechanisms of action and be more active than the neutral ferrocene. It is really unfortunate that while ferrocene is well-exploited in organometallic medicinal chemistry research to advance the development of biologically active materials,[7,8,89] $[\eta^6\text{-arene-}\eta^5\text{-CpFe}]^+$ complexes receive little consideration for their biological activity. We, therefore, consider it a good research challenge to examine the

biological, specifically the antimicrobial activity, of these $[\eta^6$-arene-η^5-CpFe$]^+$ -derived dendrimers.

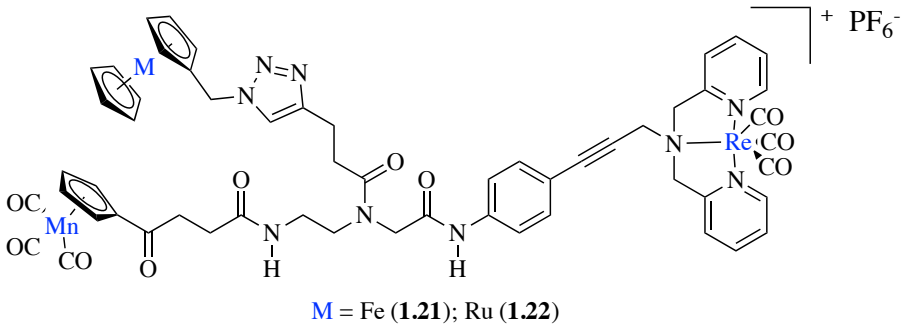

M = Fe (**1.21**); Ru (**1.22**)

Figure 1.3. Example of antimicrobial organometallic compound.

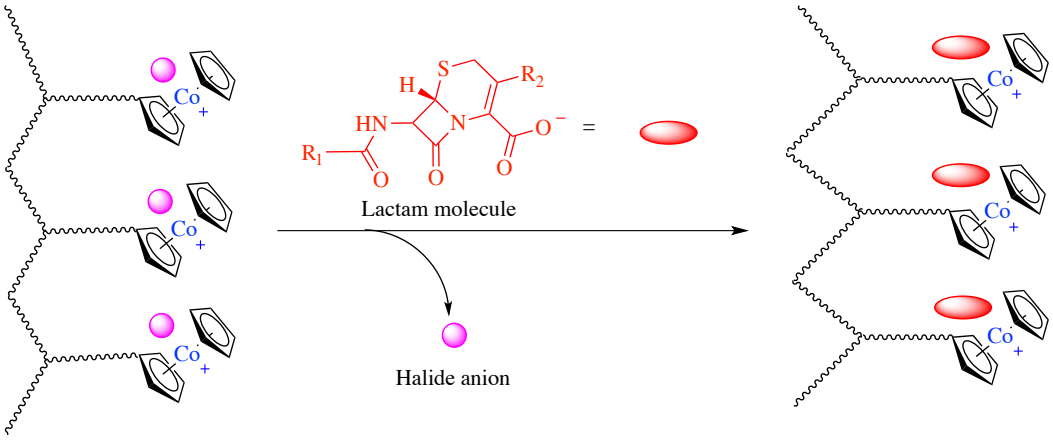

Scheme 1.9. Illustrated mechanism of action of a cationic polymer. The polymer (left: **1.23**) exchanges its counteranion for lactam antibiotic, thereby protecting the antibiotic from hydrolysis.

1.4.3. Third objective: Characterization for magnetic properties

The final objective of the work, addressed in *Chapter Four*, is to evaluate the magnetic property of ceramics derived from the dendrimers. Undoubtedly, magnetic materials drive many of today's technological innovations in the electronic industry.[90-94] Magnetic ceramics, for instance, represent a significant niche in the magnetic materials market where they are in demand as permanent

magnets in loudspeakers, in magnetic recording heads, in antennas, and as magnetic printers.[95] Interest in magnetic ceramics is driven by their low electrical conductivity and low production cost compared with other magnetic materials.[95] Consequently, the synthesis of magnetic ceramics continue to attract attention. The conversion of organometallic polymers to magnetic ceramics is an emerging chemical process with several advantages. The conventional route to ceramics is the powder technology, which requires sintering additives that limit technical applications. The polymer route enables the integration of the good thermal and chemical stability, and mechanical strength of ceramics with the functional properties of metals into a single system. Further, the preceramic polymer (precursor) can be rationally designed to control critical parameters, such as the number of magnetic species per unit volume and the macrostructure, to tune the magnetic property as well as the ceramic yield. Again, it is possible to shape the ceramics at the precursor stage by using traditional polymer-forming techniques to shape the precursor, and subsequently convert the shaped component to ceramics. Indeed, ceramic fibers,[96] films,[67,71,74] and nanoparticles,[68-70,73] have been developed using the polymer route.

To synthesize magnetic ceramics, the precursor is heated in a non-oxidative atmosphere at relatively high temperature but usually below 1500 ºC.[97] Typical precursors include polysiloxanes, polysilylcarbodiimides, polysilazanes, polycarbosilazanes, polyborosilazanes and polysilanes containing a ferromagnetic metal such as iron, cobalt, nickel, or a combination of these metals. As an example, Manners *et al*. derived magnetic ceramics from the pyrolysis of polyferrocenylsilanes (Figure 1.4).[67,69-71,73,74] Pyrolysis of these precursors yields ceramics with unique chemical composition and metallic nanoparticle phases.[96,98] By changing the pyrolytic temperature, it is possible to control the composition and phases, and eventually tune the magnetic property. Indeed,

Manners *et al*. tuned the magnetic property of ceramics, switching between superparamagnetism and ferromagnetism, by changing the pyrolytic temperature.[74]

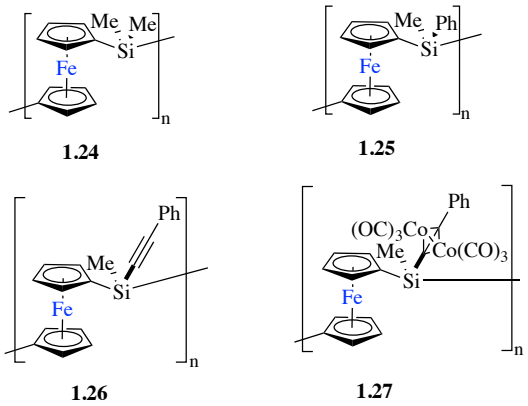

Figure 1.4. Examples of preceramic polymers.

In choosing a precursor, certain properties are desirable. For example, to reduce volatilization and obtain high ceramic yield, it is preferable to use high molecular weight polymers.[97] Also, the polymer should have appropriate rheological and solubility properties for the shaping process, as well as latent reactivity for the curing and crosslinking steps.[97] To better retain pyrolyzed species for high ceramic yields as well as promote a steadier growth of magnetic nanoparticles for high saturation magnetization (M_s), it is desirable to use polymers with “cage” structures.[97] Indeed, Tang *et al*. attributed the higher ceramic yield and M_s of hyperbranched polymers to their "cages" structures.[76]

From the requirements outlined above, it seems that dendrimers offer a promising structure for the design of preceramic precursors. First, high molecular weight dendrimers are attainable through the traditional iterative synthesis methods of dendrimers. Second, dendrimers are amorphous, leading to better solubility compared with the linear polymers or crosslinked

polymers.[65] Third, functional groups can be precisely introduced into the core, the branches, or the termini, yielding latent reactive sites for curing and crosslinking, if desirable. Last and most importantly, it is the "shell effect" of dendrimers, especially at high-generations, where overcrowding at the periphery provides a "dense shell" with "inner nanospaces" that mimic "cages."[50] The attractive features of dendrimers notwithstanding, they have not been investigated as precursors for ceramics. This gap and the growing interest in magnetic materials provides the motivation to investigate $[\eta^6$-arene-η^5-CpFe$]^+$-derived dendrimers as precursors for magnetic ceramics.

1.5. Conclusion

In brief, functional materials are needed to tackle many of today's problems and to foster technological innovations. As an example, new antimicrobial materials are urgently needed to combat the persistent threat of drug resistant infections. Also, many technologies, especially in the electronic industry, rely on magnetic materials with magnetic ceramics being preferred in some cases due their low electrical conductivity and low production cost.[95] The $[\eta^6$-arene-η^5-CpFe$]^+$ complexes feature a redox-active iron center that has implications for antimicrobial activity and ferromagnetism. This research seeks to exploit these features to develop an antimicrobial platform and magnetic precursors.

References

1. Kealy, T.; Pauson, P. *Nature* **1951***, 168*, 1039.
2. Miller, S. A.; Tebboth, J. A.; Tremaine, J. F. *J. Chem. Soc*. **1952**, 632.
3. Wilkinson, G.; Rosenblum, M.; Whiting, M.; Woodward, R. *J. Am. Chem. Soc.* **1952***, 74*, 2125.
4. Fischer, E. O.; Pfab, W. *Z. Naturforsch. B.* **1952***, 7*, 377.
5. Woodward, R.; Rosenblum, M.; Whiting, M. *J. Am. Chem. Soc.* **1952***, 74*, 3458.
6. Astruc, D. *E. J. Inorg. Chem.* **2017***, 2017*, 6.

7. Van Staveren, D. R.; Metzler-Nolte, N. *Chem. Rev.* **2004***, 104*, 5931.
8. Fouda, M. F.; Abd-El-Zaher, M. M.; Abdelsamaia, R. A.; Labib, A. A. *Appl. Organomet. Chem.* **2007***, 21*, 613.
9. Housecroft, C.; Sharpe, A. G. *Inorganic Chemistry;* Pearson Education Limited: Essex, England, 2012.
10. Nesmeyanov, A.; Vol'kenau, N.; Bolesova, I. *Tetrahedron Lett.* **1963***, 4*, 1725.
11. Abd-El-Aziz, A. S.; Strohm, E. A. *Polymer* **2012***, 53*, 4879.
12. Abd-El-Aziz, A. S.; Manners, I. *J. Inorg. Organomet. Polym. Mater.* **2005***, 15*, 157.
13. Abd-El-Aziz, A. S. Overview of Organoiron Polymers. In *Macromolecules Containing Metal and Metal-like Elements*; Abd-El-Aziz, A. S., Carraher Jr., C. E., Pittman Jr., C. U., Sheats, J. E., Zeldin, M., Eds.; John Wiley & Sons: New York, **2004**; Vol. 2, pp 1-27.
14. Abd-El-Aziz, A. S.; Todd, E. K. *Coord. Chem. Rev.* **2003***, 246*, 3.
15. Abd-El-Aziz, A. S.; Bernardin, S. *Coord. Chem. Rev.* **2000***, 203*, 219.
16. Gu, H.; Ciganda, R.; Gatard, S.; Lu, F.; Zhao, P.; Ruiz, J.; Astruc, D. *J. Organomet. Chem.* **2016***, 813*, 95.
17. Astruc, D.; Ruiz, J. *J. Inorg. Organomet. Polym. Mater.* **2015***, 25*, 330.
18. Astruc, D.; Wang, Y.; Rapakousiou, A.; Diallo, A.; Djeda, R.; Ruiz, J.; Ornelas, C. *Polyhedron* **2015***, 86*, 24.
19. Astruc, D.; Ornelas, C.; Ruiz, J. *Acc. Chem. Res.* **2008***, 41*, 841.
20. Astruc, D. *Acc. Chem. Res.* **2000***, 33*, 287.
21. Astruc, D. *Acc. Chem. Res.* **1986***, 19*, 377.
22. Abd-El-Aziz, A. S. *Coord. Chem. Rev.* **2002***, 233*, 177.
23. Abd-El-Aziz, A. S. *Macromol. Rapid Commun.* **2002***, 23*, 995.
24. Pearson, A. J.; Park, J. G.; Zhu, P. Y. *J. Org. Chem.* **1992***, 57*, 3583.
25. Sutherland, R. G.; Chowdhury, R. L.; Piórko, A.; Lee, C. C. *Can J. Chem.* **1986***, 64*, 2031.
26. Sutherland, R. G.; Zhang, C.; Piórko, A.; Lee, C. C. *Can. J. Chem.* **1989***, 67*, 137.
27. Sutherland, R. G.; Chowdhury, R. L.; Piórko, A.; Lee, C. C. *J. Chem. Soc., Chem. Commun.* **1985**, 1296.
28. Pearson, A. J.; Gelormini, A. M. *J. Org. Chem.* **1994***, 59*, 4561.
29. Abd-El-Aziz, A. S.; Epp, K. M.; de Denus, C. R.; Fisher-Smith, G. *Organometallics* **1994***, 13*, 2299.
30. Abd-El-Aziz, A. S.; Schriemer, D. C.; de Denus, C. R. *Organometallics* **1994***, 13*, 374.
31. Abd-El-Aziz, A. S.; Todd, E. K.; Okasha, R. M.; Shipman, P. O.; Wood, T. E. *Macromolecules* **2005***, 38*, 9411.
32. Abd-El-Aziz, A. S.; Pereira, N. M.; Winram, D. J.; Sidhu, P.; Kroeker, S. *J. Inorg. Organomet. Polym. Mater.* **2007***, 17*, 275.
33. Abd-El-Aziz, A. S.; Afifi, T. H.; Budakowski, W. R.; Friesen, K. J.; Todd, E. K. *Macromolecules* **2002***, 35*, 8929.
34. Abd-El-Aziz, A. S.; de Denus, C. R.; Zaworotko, M. J.; MacGillivray, L. R. *J. Chem. Soc., Dalton Trans.* **1995**, 3375.
35. Abd-El-Aziz, A. S.; Todd, E.; Ma, G. *J. Polym. Sci. Part A: Polym. Chem.* **2001***, 39*, 1216.
36. Abd-El-Aziz, A. S.; Todd, E. K.; Okasha, R. M.; Wood, T. E. *Macromol. Rapid Commun.* **2002***, 23*, 743.
37. Abd-El-Aziz, A. S.; Todd, E. K.; Afifi, T. H. *Macromol. Rapid Commun.* **2002***, 23*, 113.

38. Abd-El-Aziz, A. S.; Armstrong, D. A.; Bernardin, S.; Hutton, H. M. *Can. J. Chem.* **1996***, 74*, 2073.
39. Anbarasan, P.; Neumann, H.; Beller, M. *Chem. Eur, J.* **2010***, 16*, 4725.
40. Anbarasan, P.; Neumann, H.; Beller, M. *Chem. Eur. J.* **2011***, 17*, 4217.
41. Ushkov, A. V.; Grushin, V. V. *J. Am. Chem. Soc.* **2011***, 133*, 10999.
42. Reeves, J. T.; Malapit, C. A.; Buono, F. G.; Sidhu, K. P.; Marsini, M. A.; Sader, C. A.; Fandrick, K. R.; Busacca, C. A.; Senanayake, C. H. *J. Am. Chem. Soc.* **2015***, 137*, 9481.
43. Magano, J.; Dunetz, J. R. *Chem. Rev.* **2011***, 111*, 2177.
44. Labadie, J. W.; Hedrick, J. L.; Ueda, M. Poly (aryl ether) synthesis. In *Step-growth Polymers for High-performance Materials*. Eds Hedrick, J. L.; Labadie, J. W. ACS Symposium Series, **1996**, Vol. 624, pp 210-225.
45. Ueda, M.; Ichikawa, F. *Macromolecules* **1990***, 23*, 926.
46. Fukawa, I.; Tanabe, T.; Dozono, T. *Macromolecules* **1991***, 24*, 3838.
47. Astruc, D.; Boisselier, E.; Ornelas, C. *Chem. Rev.* **2010***, 110*, 1857.
48. Frechet, J. M. *Science* **1994***, 263*, 1710.
49. Svenson, S.; Tomalia, D. A. *Adv. Drug Deliv. Rev.* **2012***, 64*, 102.
50. Yamamoto, K.; Imaoka, T. *Acc. Chem. Res.* **2014***, 47*, 1127.
51. Caminade, A.; Yan, D.; Smith, D. K. *Chem. Soc. Rev.* **2015***, 44*, 3870.
52. Ruiz, J.; Lafuente, G.; Marcen, S.; Ornelas, C.; Lazare, S.; Cloutet, E.; Blais, J.; Astruc, D. *J. Am. Chem. Soc.* **2003***, 125*, 7250.
53. Moulines, F.; Astruc, D. *Angew. Chem. Int. Ed.* **1988***, 27*, 1347.
54. Sartor, V.; Djakovitch, L.; Fillaut, J.; Moulines, F.; Neveu, F.; Marvaud, V.; Guittard, J.; Blais, J.; Astruc, D. *J. Am. Chem. Soc.* **1999***, 121*, 2929.
55. Moulines, F.; Djakovitch, L.; Gloaguen, B.; Thiel, W.; Fillaut, J.; Delville, M.; Astruc, D.; Boese, R. *Angew. Chem. Int. Ed.* **1993***, 32*, 1075.
56. Moulines, F.; Gloaguen, B.; Astruc, D. *Angew. Chem. Int. Ed.* **1992***, 31*, 458.
57. Rapakousiou, A.; Wang, Y.; Ciganda, R.; Lasnier, J.; Astruc, D. *Organometallics* **2014***, 33*, 3583.
58. Valério, C.; Alonso, E.; Ruiz, J.; Blais, J.; Astruc, D. *Angew. Chem. Int. Ed.* **1999***, 38*, 1747.
59. Astruc, D. *Acc. Chem. Res.* **1991***, 24*, 36.
60. Astruc, D.; Hamon, J. R.; Roman, E.; Michaud, P. *J. Am. Chem. Soc.* **1981***, 103*, 7502.
61. Djeda, R.; Ornelas, C.; Ruiz, J.; Astruc, D. *Inorg. Chem.* **2010***, 49*, 6085.
62. Bossard, C.; Rigaut, S.; Astruc, D.; Delville, M.; Félix, G.; Février-Bouvier, A.; Amiell, J.; Flandrois, S.; Delhaès, P. *J. Chem. Soc., Chem. Commun.* **1993**, 333.
63. Ruiz, J.; Ogliaro, F.; Saillard, J.; Halet, J.; Varret, F.; Astruc, D. *J. Am. Chem. Soc.* **1998***, 120*, 11693.
64. Abd-El-Aziz, A. S.; Shipman, P. O.; Shipley, P. R. *Macromol. Rapid Commun.* **2010***, 31*, 459.
65. Bosman, A.; Janssen, H.; Meijer, E. *Chem. Rev.* **1999***, 99*, 1665.
66. Knop, K.; Hoogenboom, R.; Fischer, D.; Schubert, U. S. *Angew. Chem. Int. Ed.* **2010***, 49*, 6288.
67. Liu, K.; Clendenning, S. B.; Friebe, L.; Chan, W. Y.; Zhu, X.; Freeman, M. R.; Yang, G. C.; Yip, C. M.; Grozea, D.; Lu, Z. *Chem. Mater.* **2006***, 18*, 2591.

68. Ginzburg-Margau, M.; Fournier-Bidoz, S.; Coombs, N.; Ozin, G. A.; Manners, I. *Chem. Commun.* **2002**, 3022.
69. Kulbaba, K.; Cheng, A.; Bartole, A.; Greenberg, S.; Resendes, R.; Coombs, N.; Safa-Sefat, A.; Greedan, J. E.; Stöver, H. D.; Ozin, G. A. *J. Am. Chem. Soc.* **2002***, 124*, 12522.
70. Friebe, L.; Liu, K.; Obermeier, B.; Petrov, S.; Dube, P.; Manners, I. *Chem. Mater.* **2007***, 19*, 2630.
71. Rider, D. A.; Liu, K.; Eloi, J.; Vanderark, L.; Yang, L.; Wang, J.; Grozea, D.; Lu, Z.; Russell, T. P.; Manners, I. *ACS Nano* **2008***, 2*, 263.
72. Cheng, A. Y.; Clendenning, S. B.; Yang, G.; Lu, Z.; Yip, C. M.; Manners, I. *Chem. Commun.* **2004**, 780.
73. Liu, K.; Fournier-Bidoz, S.; Ozin, G. A.; Manners, I. *Chem. Mater.* **2009***, 21*, 1781.
74. MacLachlan, M. J.; Ginzburg, M.; Coombs, N.; Coyle, T. W.; Raju, N. P.; Greedan, J. E.; Ozin, G. A.; Manners, I. *Science* **2000***, 287*, 1460.
75. Sun, Q.; Lam, J. W.; Xu, K.; Xu, H.; Cha, J. A.; Wong, P. C.; Wen, G.; Zhang, X.; Jing, X.; Wang, F. *Chem. Mater.* **2000***, 12*, 2617.
76. Shi, J.; Tong, B.; Li, Z.; Shen, J.; Zhao, W.; Fu, H.; Zhi, J.; Dong, Y.; Häussler, M.; Lam, J. W. *Macromolecules* **2007***, 40*, 8195.
77. Häussler, M.; Zheng, R.; Lam, J. W.; Tong, H.; Dong, H.; Tang, B. Z. *J. Phys. Chem. B* **2004***, 108*, 10645.
78. Jim, C. K.; Lam, J. W.; Qin, A.; Leung, C. W.; Jianzhao, L.; Sung, H. H.; Williams, I. D.; Tang, B. Z. *J. Inorg. Organomet. Polym. Mater.* **2013***, 23*, 147.
79. Kong, J.; Kong, M.; Zhang, X.; Chen, L.; An, L. *ACS Appl. Mater. Interfaces* **2013***, 5*, 10367.
80. Kong, J.; Schmalz, T.; Motz, G.; Müller, A. H. *J. Mater. Chem. C* **2013***, 1*, 1507.
81. Shallcross, L. J.; Howard, S. J.; Fowler, T.; Davies, S. C. *Philos. Trans. R. Soc., B.* **2015***, 370*, 20140082.
82. Kenawy, E.; Worley, S.; Broughton, R. *Biomacromolecules* **2007***, 8*, 1359.
83. Zhang, J.; Chen, Y. P.; Miller, K. P.; Ganewatta, M. S.; Bam, M.; Yan, Y.; Nagarkatti, M.; Decho, A. W.; Tang, C. *J. Am. Chem. Soc.* **2014***, 136*, 4873.
84. Dubar, F.; Slomianny, C.; Khalife, J.; Dive, D.; Kalamou, H.; Guérardel, Y.; Grellier, P.; Biot, C. *Angew. Chem. Int. Ed.* **2013***, 52*, 7690.
85. Wenzel, M.; Patra, M.; Senges, C. H. R.; Ott, I.; Stepanek, J. J.; Pinto, A.; Prochnow, P.; Vuong, C.; Langklotz, S.; Metzler-Nolte, N. *ACS Chem. Biol.* **2013***, 8*, 1442.
86. Lemire, J. A.; Harrison, J. J.; Turner, R. J. *Nat. Rev. Microbiol.* **2013***, 11*, 371.
87. Harrison, J. J.; Ceri, H.; Turner, R. J. *Nat. Rev. Microbiol.* **2007***, 5*, 928.
88. Workentine, M. L.; Harrison, J. J.; Stenroos, P. U.; Ceri, H.; Turner, R. J. *Environ. Microbiol.* **2008***, 10*, 238.
89. Schatzschneider, U.; Metzler-Nolte, N. *Angew. Chem. Int. Ed.* **2006***, 45*, 1504.
90. Liu, J.; Qiao, S. Z.; Hu, Q. H. *Small* **2011***, 7*, 425.
91. Lu, A.; Salabas, E. e.; Schüth, F. *Angew. Chem. Int. Ed.* **2007***, 46*, 1222.
92. Reddy, L. H.; Arias, J. L.; Nicolas, J.; Couvreur, P. *Chem. Rev.* **2012***, 112*, 5818.
93. Frey, N. A.; Peng, S.; Cheng, K.; Sun, S. *Chem. Soc. Rev.* **2009***, 38*, 2532.
94. Gutfleisch, O.; Willard, M. A.; Brück, E.; Chen, C. H.; Sankar, S.; Liu, J. P. *Adv. Mater.* **2011***, 23*, 821.

95. Valenzuela, R. *Magnetic Ceramics*, Cambridge University Press: New York, United States, 1994.
96. Zaheer, M.; Schmalz, T.; Motz, G.; Kempe, R. *Chem. Soc. Rev.* **2012***, 41*, 5102.
97. Colombo, P.; Mera, G.; Riedel, R.; Soraru, G. D. *J. Am. Ceram. Soc.* **2010***, 93*, 1805.
98. Bernardo, E.; Fiocco, L.; Parcianello, G.; Storti, E.; Colombo, P. *Materials* **2014***, 7*, 1927.

Chapter Two: A New Family of Dendrimers[†]

Abstract

This *Chapter* focuses on the design of a new family of dendrimers that incorporates the redox active η^6-arene-η^5-cyclopentadienyliron(II) complex in its structure and can be functionalized to give a multifunctional dendrimer. The objective is to design dendrimers that exploit the intrinsic functionality of the redox active iron center in the complex and can potentially incorporate other functional molecules to impart additional properties. Towards this, η^6-dichlorobenzene-η^5-cyclopentadienyliron(II) complex was selected as the building block, providing the intrinsic functionality. The chloro groups in the arene ligand are susceptible to nucleophilic aromatic substitution, mediating the facile functionalization of the dendrimer periphery. To demonstrate this, a readily available photoactive nucleophile, β-naphthol, was selected to substitute the chloro groups. The resulting dendrimers were bifunctional, being redox- and photo-active as evidenced by data from cyclic voltammetry and fluorescence spectroscopy. Irradiation of $CH_3CN/CHCl_3$ solutions of the dendrimers cleaved the redox active iron moieties, yielding organic photoactive dendrimers. The reported synthesis approach is a general route to a new family of functional dendrimers.

2.1. Introduction

There is continuing interest in the synthesis of functional materials as they have useful applications in science, technology, and medicine.[1-16] The synthesis of functional dendrimers represents a part

[†] This chapter is published as Abd-El-Aziz, A. S.; Agatemor, C.; Etkin, N.; Bissessur, R. *Macromol. Chem. Phys.* **2015**, *216*, 369 and is reproduced by permission of WILEY-VCH Verlag GmbH & Co. KGaA, Weinheim.

of the ongoing quest for functional materials. Dendrimers are an attractive type of polymer that feature a unique topology, offering the opportunity for multi-functionalization since the termini, branches, core, or all three microstructures can be precisely functionalized. This possibility is well-exploited to rationally design functional dendrimers for specialty applications in sensing, catalysis, molecular electronics and photonics, medicine, and drug delivery.[17-19] Accordingly, the synthesis of dendrimers remains attractive among polymer scientists.

Dendrimers are synthesized *via* a divergent or convergent synthesis route, which has resulted in a broad spectrum of families that include Tomalia-type poly(amidoamine)s, Fréchet-type polyethers, Newkome-type polyamides, Meijer-type poly(propyleneimine)s, and Astruc-type organometallic dendrimers.[20-22] Organometallic dendrimers are an important family of dendrimers because the presence of a metal center has broad implications for medicine, catalysis, sensing, and photonics. As an example, an alkynylbis(bidentate phosphine)-ruthenium dendrimer exhibits a multiphoton absorption property,[23] a clue to the potential applications of organometallic dendrimers as multiphoton absorption materials. Further, the use of organometallic dendrimers, such as the η^6-arene-η^5-cyclopentadienyliron(II)-containing dendrimers, in redox sensing of cations and anions,[24,25] as well as redox reagents,[26] is established.

In addition to their redox property, η^6-arene-η^5-cyclopentadienyliron(II) ([η^6-arene-η^5-CpFe]$^+$) complexes are reactive towards a wide range of nucleophiles that include alcohols, thiols, and amines,[27-29] mediating the facile synthesis of small molecules[30] as well as polymers.[27,28] As an example, Abd-El-Aziz *et al*. used [η^6-dichloroarene-η^5-CpFe]$^+$ to mediate the facile polymerization of different types of polymers including linear polymers,[31-33] hyperbranched polymers,[34] star polymers,[35-38] as well as redox active polymers.[39-41] Despite the rich chemistry of [η^6-dichloroarene-η^5-CpFe]$^+$ complexes, their use in the synthesis of functional dendrimers is

limited. Here, the hypothesis is that through rational design, the electrophilicity of these complexes mediates the facile synthesis of intrinsically functional dendrimers that are reactive towards nucleophilic functional molecules yielding bifunctional dendrimers under mild conditions. This study tested the hypothesis through the facile synthesis of a new family of redox-, photo-active dendrimers using $[\eta^6$-dichloroarene-η^5-CpFe$]^+$ as a building block and redox active moiety, and β-naphthol, as a photoactive moiety.

Distinctively, this new family of dendrimers incorporates the redox-active moieties within the branches and the photoactive moieties at the periphery. The photoactivity of the dendrimers was ascertained using UV-vis absorption as well as fluorescence spectroscopy, while the redox activity was confirmed using cyclic voltammetry. Studies on the thermal properties, crystallinity and surface morphology of the dendrimers were also carried out.

2.2 Results and discussion

2.2.1. Synthesis and characterization of dendrimers

Here, the objective is to exploit the chemistry of $[\eta^6$-dichloroarene-η^5-CpFe$]^+$ complexes in the facile synthesis of a new family of functional dendrimers. These complexes are building blocks in the synthesis of redox-active organometallic polymers, where they are incorporated into the backbone of linear polymers, or as pendent moieties in branched polymers or as terminal groups in dendrimers. Uniquely, the dendrimers in this present work incorporated the redox-active complexes in the dendrimer branches and photoactive naphthyl groups in the termini.

The dendrimers were synthesized in good yield (52–96%) under mild conditions. As illustrated in Schemes 2.1 and 2.2, the synthesis of the zeroth generation (G_0), bifunctional naphthyl-capped dendrimer (**G_0 naphthyl-dendrimer**) proceeded *via* a convergent or divergent route. Either route involves the initial synthesis of the building block $[\eta^6$-dichlorobenzene-η^5-

$CpFe]^+$ (**2.2**), *via* ligand exchange reaction of ferrocene with dichlorobenzene and subsequent nucleophilic aromatic substitution (S_NAr) reaction of **2.2** with 4,4′-bis(4-hydroxyphenyl)valeric acid to obtain the bimetallic complex (**2.3**) (Scheme 2.1). The divergent route involved the Steglich esterification reaction of **2.3** with the tetrahydroxy core, pentaerythritol, to give the G_0 chloro-capped dendrimer (**G_0 Cl-dendrimer**), which in a subsequent step, reacts with β-naphthol to afford **G_0 naphthyl-dendrimer** (Scheme 2.2). **G_0 naphthyl-dendrimer** was also synthesized *via* the convergent route, where **2.3** reacts with β-naphthol to give **2.4** (Scheme 2.1), which reacts with pentaerythritol, to give the target dendrimer (Scheme 2.2). In this study, both routes afforded perfect dendrimers, but the convergent route is preferred because it saves time.

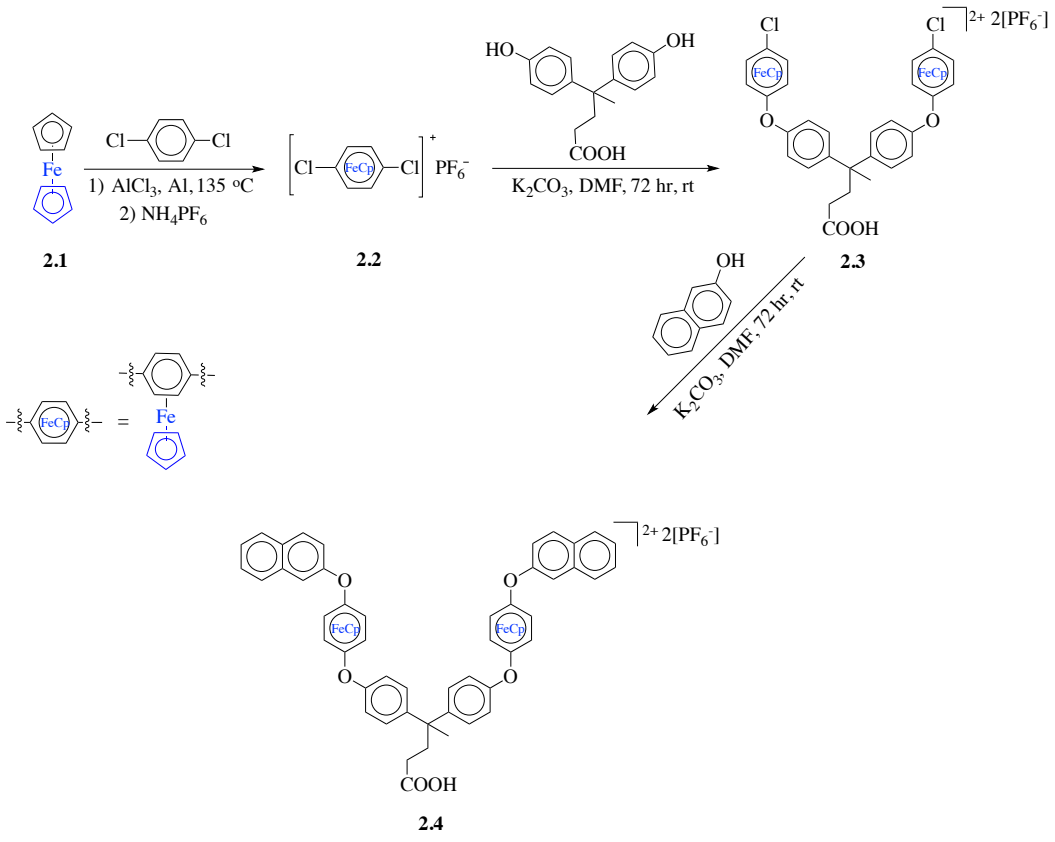

Scheme 2.1. Schematic representation of the synthesis of bimetallic complexes, **2.3** and **2.4**.

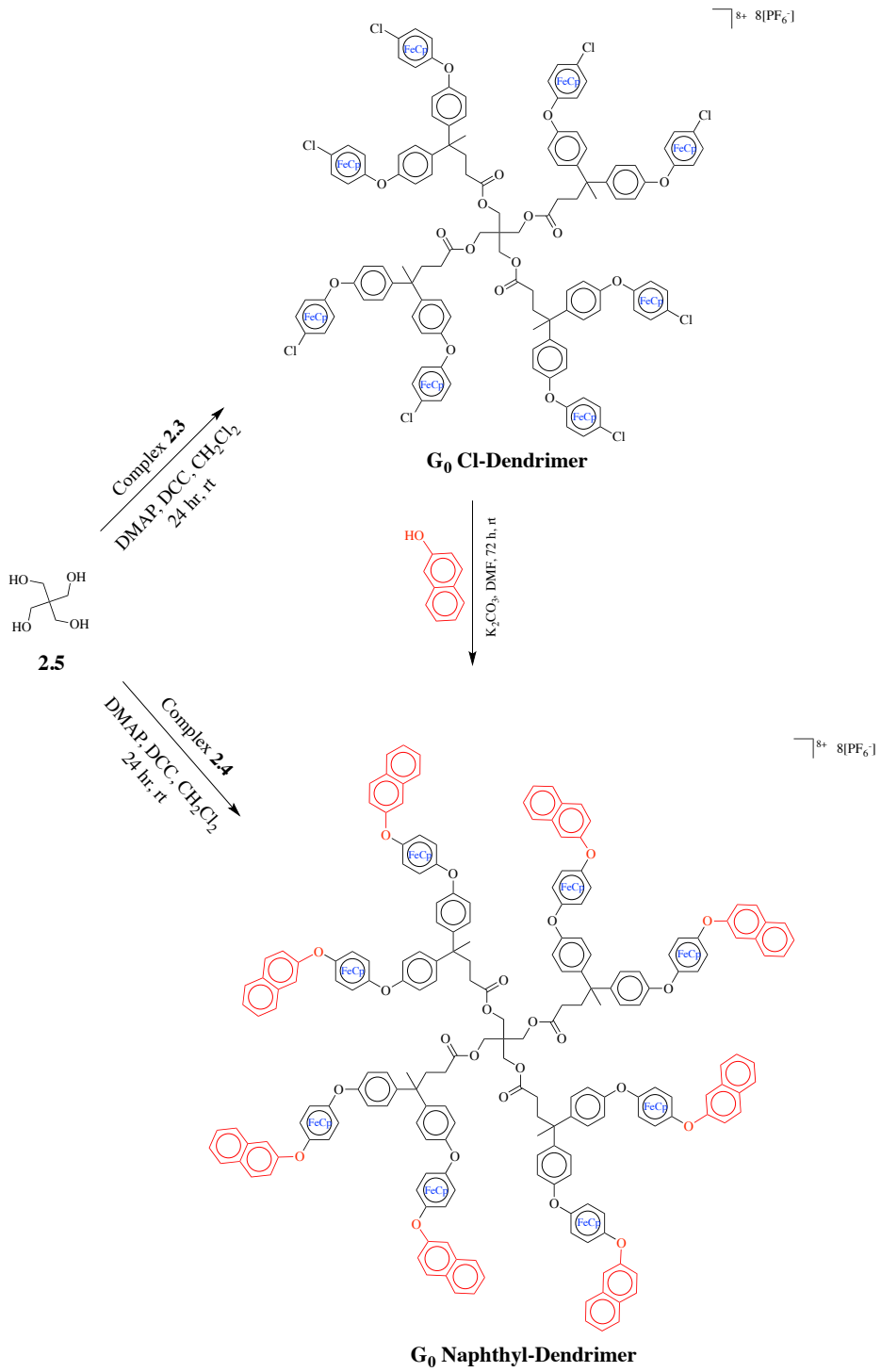

Scheme 2.2. Schematic representation of the synthesis of **G_0 naphthyl-dendrimer**.

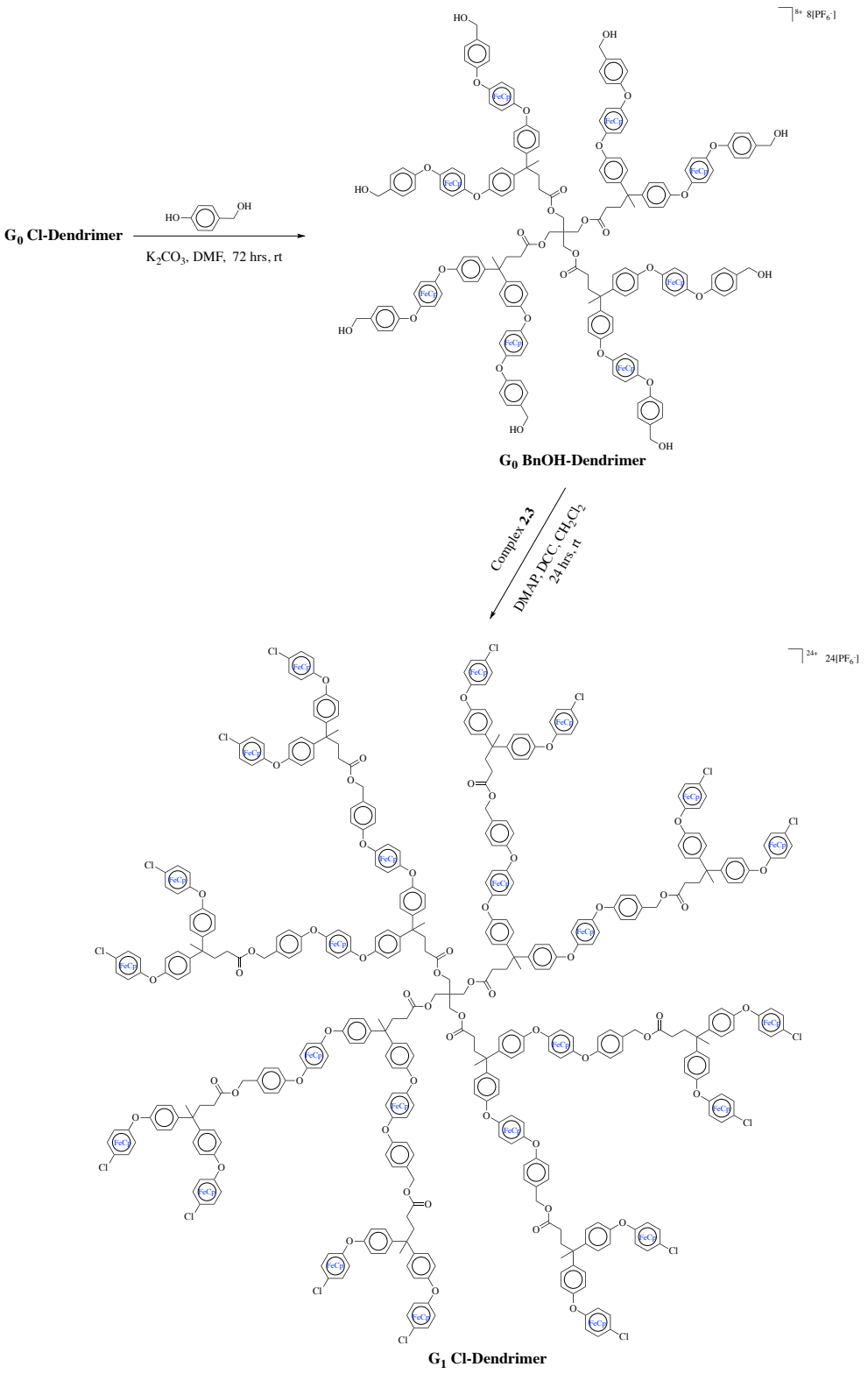

Scheme 2.3. Schematic representation of the synthesis of **G_1 Cl-dendrimer**.

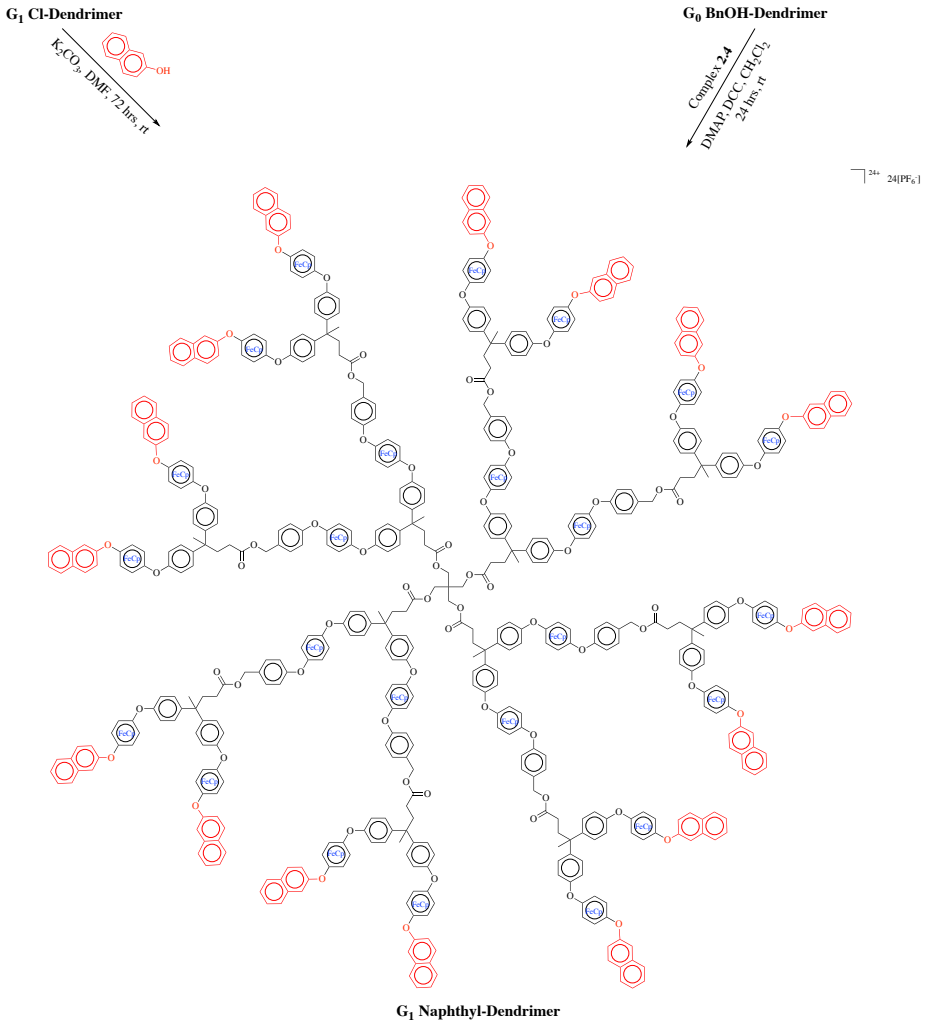

Scheme 2.4. Schematic representation of the synthesis of **G_1 naphthyl-dendrimer**.

The first generation (G_1) dendrimer (**G_1 naphthyl-dendrimer**) was obtained *via* synthesis route that involved S_NAr reaction of **G_0 Cl-dendrimer** with 4-hydroxybenzyl alcohol to give the hydroxyl-terminated dendrimer, (**G_0 BnOH-dendrimer**) (Scheme 2.3). In a subsequent step, **G_0 BnOH-dendrimer** underwent Steglich esterification reaction with complex **2.3** or **2.4**, yielding **G_1 Cl-dendrimer** or **G_1 naphthyl-dendrimer**, respectively (Scheme 2.4). Also, *via* a divergent route, **G_1 naphthyl-dendrimer** was synthesized by reacting **G_1 Cl-dendrimer** with β-naphthol

(Scheme 2.4). Similar iterative steps starting with **G_1 Cl-dendrimer** afforded the second generation (G_2) bifunctional dendrimer (**G_2 naphthyl-dendrimer**) (Schemes 2.5–2.7). The organic photoactive dendrimers were obtained *via* a 24-hour UV irradiation of the $CH_3CN/CHCl_3$ solutions of **G_0 naphthyl-dendrimer**, **G_1 naphthyl-dendrimer** or **G_2 naphthyl-dendrimer** to break-off the redox-active cyclopentadienyliron moieties as evidenced by the disappearance of the cyclopentadienyl ligand peak in the ^{1}H NMR (Figure 2.1).

The ^{1}H NMR spectra of these dendrimers support their successful synthesis. Changes in peak positions as the sequence of reactions progressed especially from the chloro-capped dendrimers to the naphthyl-capped dendrimers, also serve as a spectroscopic tool to confirm the successful

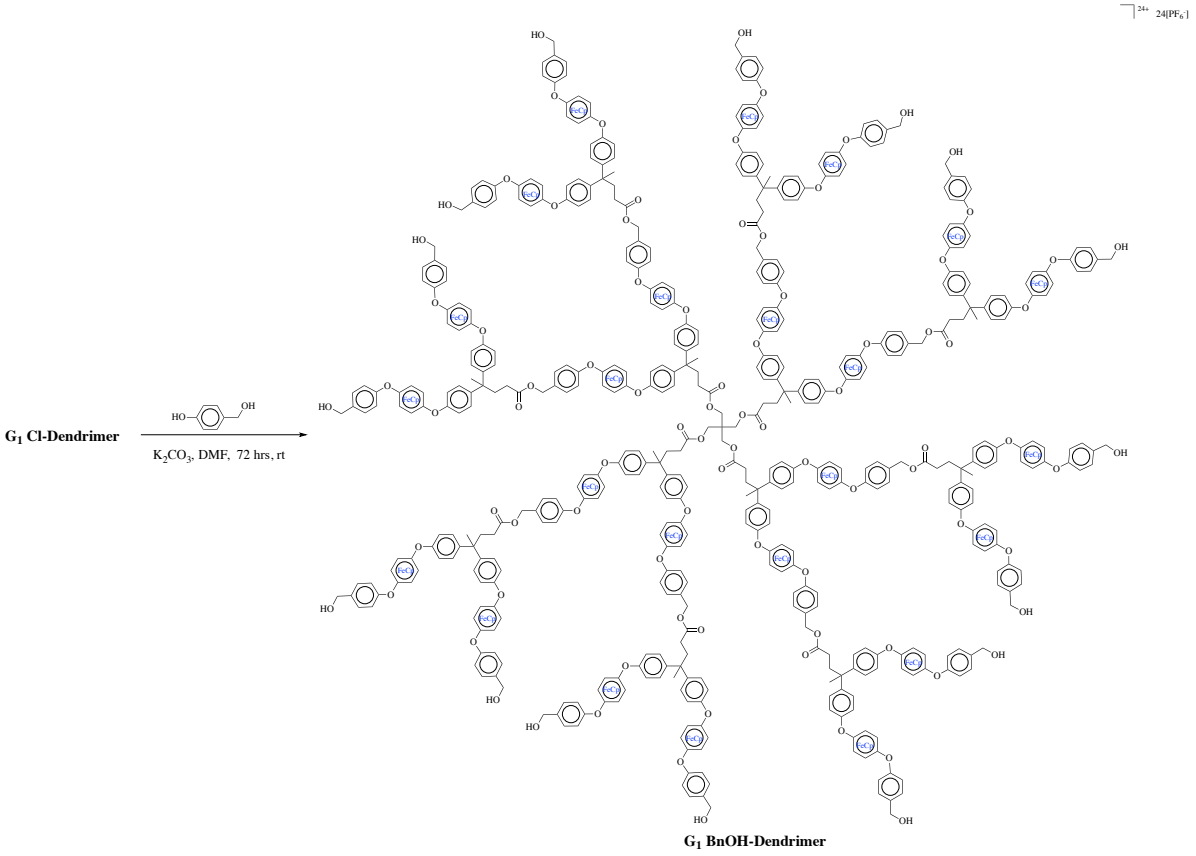

Scheme 2.5. Schematic representation of synthesis of **G_1 BnOH-dendrimer**.

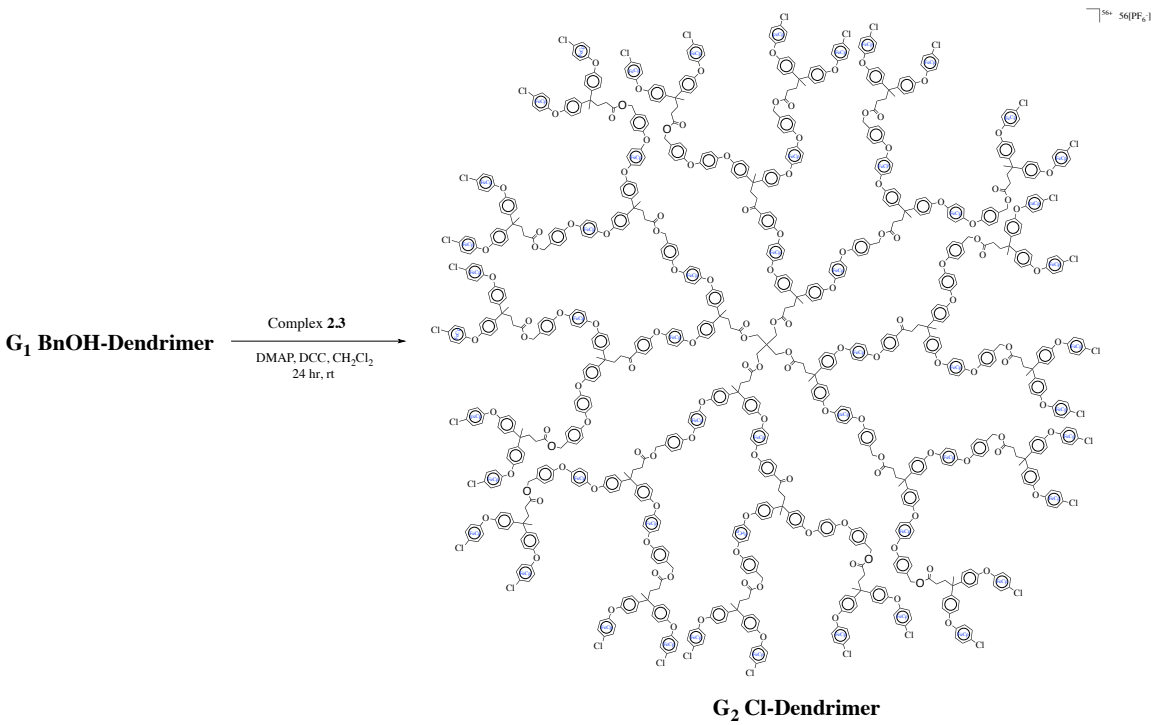

Scheme 2.6. Schematic representation of the synthesis of **G_2 Cl-dendrimer**.

syntheses of these dendrimers. For instance, in the ^{1}H NMR spectrum of **G_0 Cl-dendrimer**, two singlets at 6.72 and 6.42 ppm, each corresponding to 32 protons of the eight iron-complexed arene ligand were found (Experimental section). The protons of the iron-complexed arene ligand resonate at different frequencies since they were non-equivalent due to the chloro group and the etheric oxygen at the para position. After reaction of **G_0 Cl-dendrimer** with β-naphthol to give **G_0 naphthyl-dendrimer**, these protons resonated at 6.45 and 6.40 ppm, respectively (Experimental section). Also, the peaks corresponding to the cyclopentadienyl ligand were also insightful, distinguishing the various generations of dendrimers. For instance, in **G_1 naphthyl-dendrimer**, two peaks that corresponded to the inner 40 and outer 80 cyclopentadienyl protons were found at 5.27 and 5.21 ppm, respectively (Experimental section). Whereas in **G_0 naphthyl-**

dendrimer only one peak corresponding to the 40 cyclopentadienyl protons was found at 5.36 ppm (Experimental section). At the second generation, the peaks broadened as is typical of some

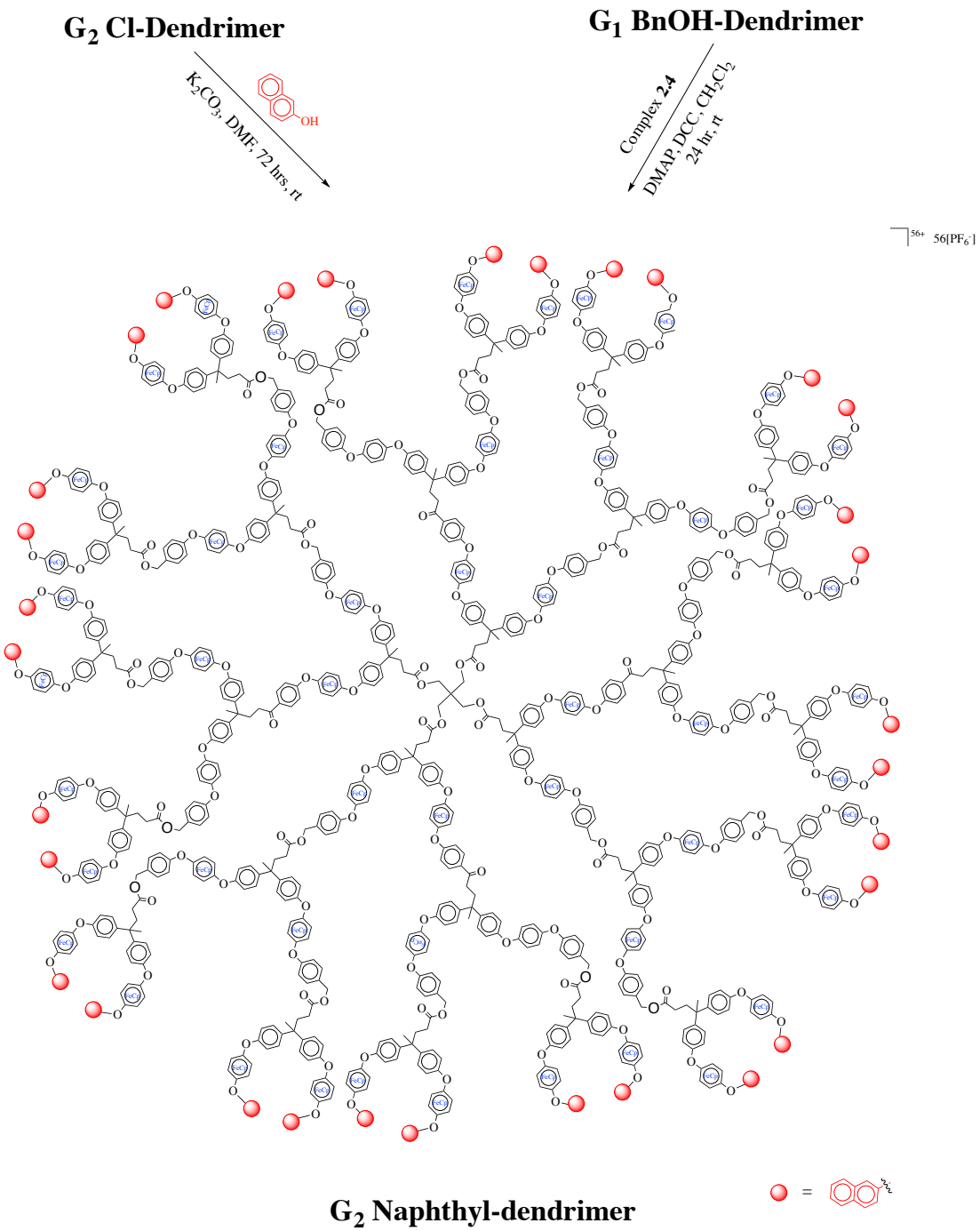

Scheme 2.8. Schematic representation of the synthesis of **G_2 naphthyl-dendrimer**.

polymers.[38,42] Attempts to characterize the dendrimers using mass spectrometry failed because of the insolubility of the dendrimers in solvents that are compatible with the instruments or lack of a suitable matrix. Elemental analyses, specifically carbon and hydrogen (CH) analyses further confirm that the syntheses were successful because the experimental percentages of carbons and hydrogens in the dendrimers agreed with calculated values. Additionally, ATR-FTIR absorption spectra revealed the presence of the expected functional groups in all dendrimers. The characteristic bands of ester and ether groups were found around 1700 cm^{-1} and 1220 cm^{-1}, respectively.

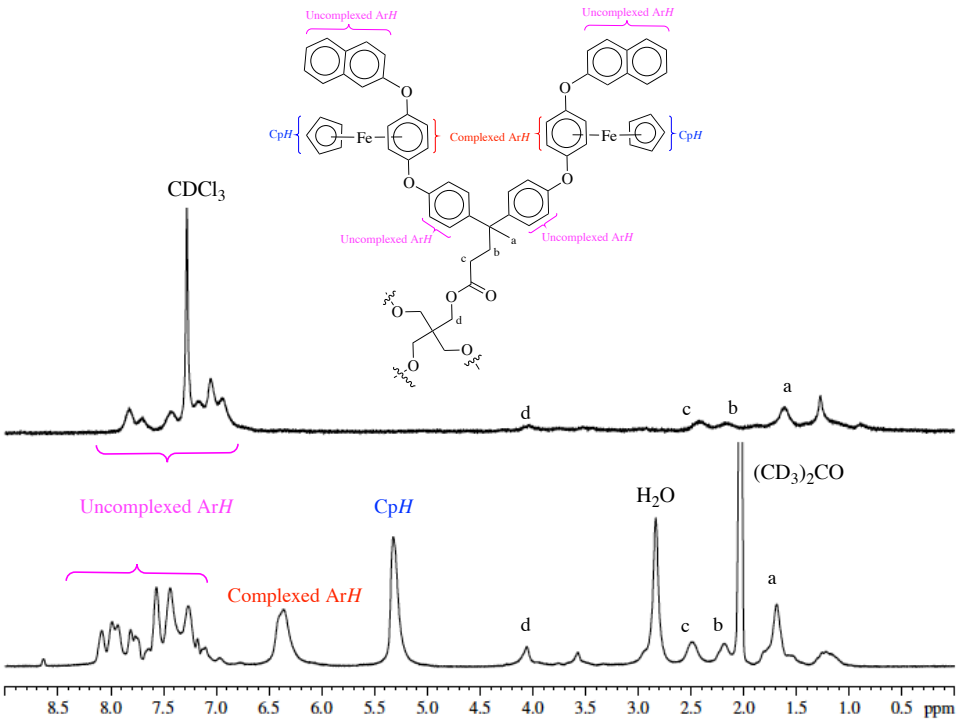

Figure 2.1. Representative ^{1}H NMR of dendrimers illustrating demetallation of dendrimers. Top spectrum; demetallated **G_1 naphthyl-dendrimer** in $CDCl_3$. Bottom spectrum; **G_1 naphthyl-dendrimer** in $(CD_3)_2CO$. Complexed Ar*H*: protons on arene ligand coordinated to Fe; uncomplexed Ar*H*: protons on arene nuclei not coordinated to Fe; Cp*H*, protons on cyclopentadienyl ligand. The Cp*H* and the complexed Ar*H* shifted upfield due to shielding effect of electrons back donated by the iron.

2.2.2. Thermal properties of dendrimers

From an application perspective, it is important to understand the thermal properties of materials. Thus, the thermal stability of these dendrimers was investigated by means of thermogravimetric analysis (TGA). Typical of [η^6-dichloroarene-η^5-CpFe]$^+$-derived polymers,[27,31,34,35,43,44] the dendrimers exhibited good thermal stability. Two thermal degradation processes were observed

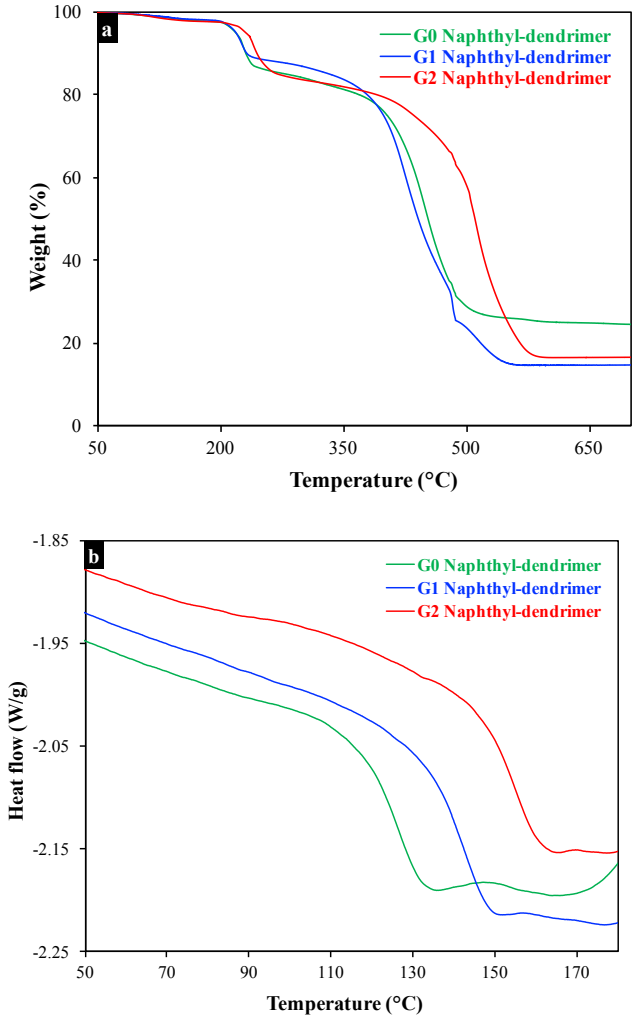

Figure 2.2. Thermal properties of bifunctional dendrimers. (a) Thermogravimetric analysis profiles, and (b) differential scanning calorimetry profiles of dendrimers. Green: **G_0 naphthyl-dendrimer**; blue: **G_1 naphthyl-dendrimer**; red: **G_2 naphthyl-dendrimer**.

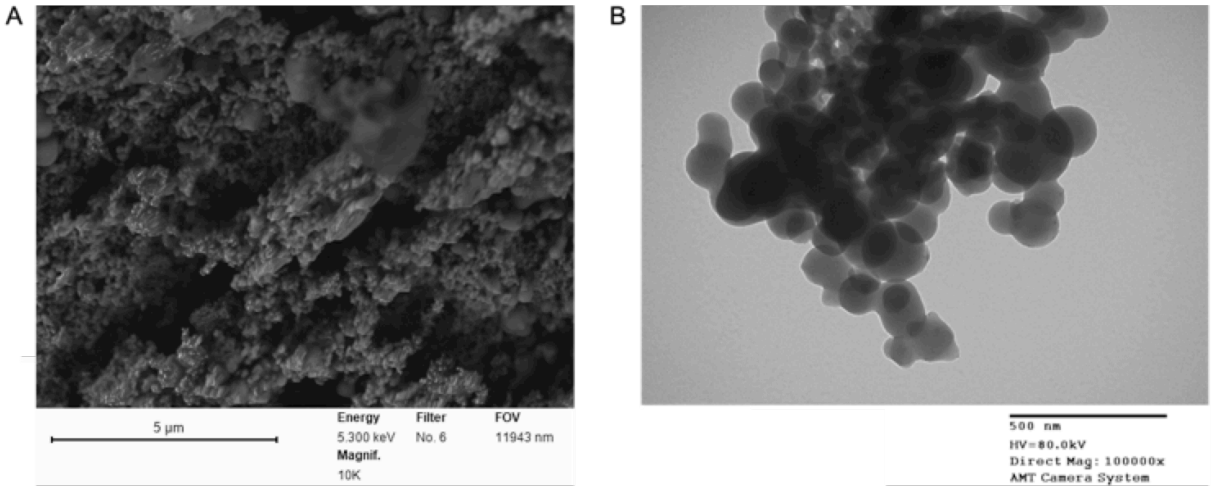

Figure 2.3. Morphology of bifunctional dendrimers. (a) Scanning and (b) transmission electron microscope images of **G_0 naphthyl-dendrimer**.

(Figure 2.2a), which is consistent with previous reports on $[\eta^6$-dichloroarene-η^5-CpFe$]^+$-derived polymers.[27,31,34,35,44] With **G_0 naphthyl-dendrimer** and **G_1 naphthyl-dendrimer**, the first onset of rapid degradation, attributed to the cleavage of the cyclopentadienyliron(II) moieties and thermolysis of the cyclopentadienyl ligand,[31]occurred at 215 °C in **G_0 naphthyl-dendrimer** and **G_1 naphthyl-dendrimer**, but increased to 230 °C in **G_2 naphthyl-dendrimer**. This positive dendritic effect is consistent with a previous report, where the thermal stability of pyrene-capped, Frèchet-type benzyl ether dendrimers increases with generation.[45] A plausible explanation for this effect is the increase in molecular weight or aromatic-aromatic interactions, as the generation increases. Evidently, this effect was more noticeable during the second onset of rapid degradation that involves the breakdown of the dendrimer backbone. In **G_0 naphthyl-dendrimer** and **G_1 naphthyl-dendrimer**, the second onset commenced around 360 °C, whereas it was delayed till 400 °C in **G_2 naphthyl-dendrimer** (Figure 2.2a).

Fundamental to polymer processing and application are the glass transition (T_g) and melting (T_m) temperatures. The dendrimers featured high T_gs, which is characteristic of previously reported [η^6-dichloroarene-η^5-CpFe]$^+$-derived polymers.[31] As evident from the DSC data (Figure 2.2b), **G_0 naphthyl-dendrimer**, **G_1 naphthyl-dendrimer** and **G_2 naphthyl-dendrimer** had T_gs of 130, 147, and 160 °C, respectively; a positive dendritic effect that may be due to increasing molecular weight or increasing *pi* interactions that restrict molecular motion at higher generation. Expectedly, the dendrimers lack a T_m, an observation that supports the amorphous nature of dendrimers.[21] The DSC data were supported by powder X-ray diffractograms, which showed the dendrimers possess a low degree of crystallinity that ranged between 16–19%. Scanning and transmission electron microscope imaging further confirmed the amorphous character of these dendrimers, as revealed by their irregular surface morphologies (Figure 2.3). The micrographs also suggest a globular morphology, characteristic of dendrimers (Figure 2.3).

2.2.3. Photophysical properties of dendrimers

β-Naphthol was arbitrarily chosen as the photoactive nucleophile to demonstrate the susceptibility of the dendrimers toward bi-functionalization. UV-vis absorption and fluorescence spectroscopy provided information on the photophysical properties of the dendrimers. The UV-vis absorption spectrum of β-naphthol in degassed DMF showed the typical bands at 320 and 335 nm (Figure 2.4a). Similarly, DMF solution of **G_0 naphthyl-dendrimer**, **G_1 naphthyl-dendrimer** or **G_2 naphthyl-dendrimer** exhibited these bands, although a blue shift as well as an absorption tail that was similar in intensity for **G_0 naphthyl-dendrimer** and **G_1 naphthyl-dendrimer**, but noticeably higher in intensity for **G_2 naphthyl-dendrimer**, was observed (Figures 2.4a and b). Interactions between electron-rich and electron-deficient aromatic rings in the dendrimers could be responsible

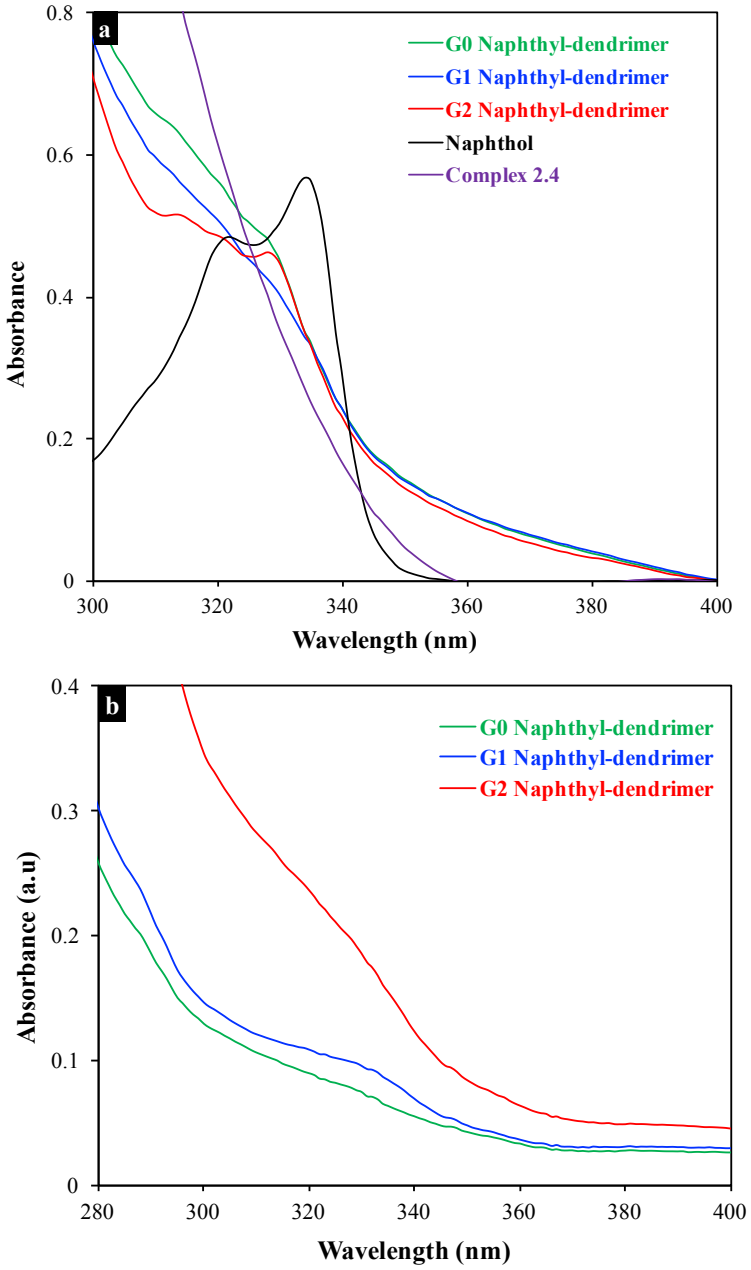

Figure 2.4. UV-vis absorption spectra of bifunctional dendrimers in DMF. (a) Spectra of **G_0 naphthyl-dendrimer**, **G_1 naphthyl-dendrimer**, **G_2 naphthyl-dendrimer**, β-naphthol, and **2.3** at similar absorbance; (b) Evidence of tailing in dendrimers. Green: **G_0 naphthyl-dendrimer**; blue: **G_1 naphthyl-dendrimer**; red: **G_2 naphthyl-dendrimer**; purple: **2.3**; black: β-naphthol.

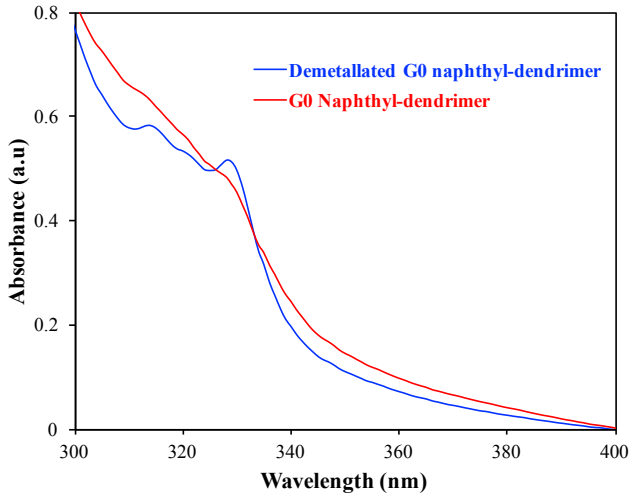

Figure 2.5. Effect of demetallation on UV-vis absorption of bifunctional dendrimers. Red: **G_0 naphthyl-dendrimer**; blue: demetallated **G_0 naphthyl-dendrimer**.

for the absorption tail.[46-48] Although these interactions are typically weak, they can result in a charge transfer absorption band at longer wavelength.[48-51] For instance, aromatic donor-acceptor interactions can occur between the electron-rich, uncomplexed aromatic ring and the electron-deficient, iron-complexed aromatic ring. The presence of similar absorption tail in the UV-Vis spectrum of chloro-capped dendritic branch (**2.3**), which lacks naphthyl groups, suggests that these electrostatic interactions result from the dendrimer branches (Figure 2.4a).

The contribution of the dendrimer structure, especially the iron, to the absorption profile is shown by the apparent difference in the shape of the absorption spectra of **G_0 naphthyl-dendrimer**, **G_1 naphthyl-dendrimer** and **G_2 naphthyl-dendrimer** and their demetallated organic analogs (Figure 2.5). These results suggest that the iron interfered with the absorption, as demetallation modified the absorption band of naphthyl groups in the dendrimer (Figure 2.5. In addition to aromatic donor-acceptor interactions, other aromatic interactions, could have influenced the absorption profile, as the demetallated dendrimers also featured a tail that was like that of their parent dendrimers at a longer wavelength (Figure 2.5). The presence of an absorption

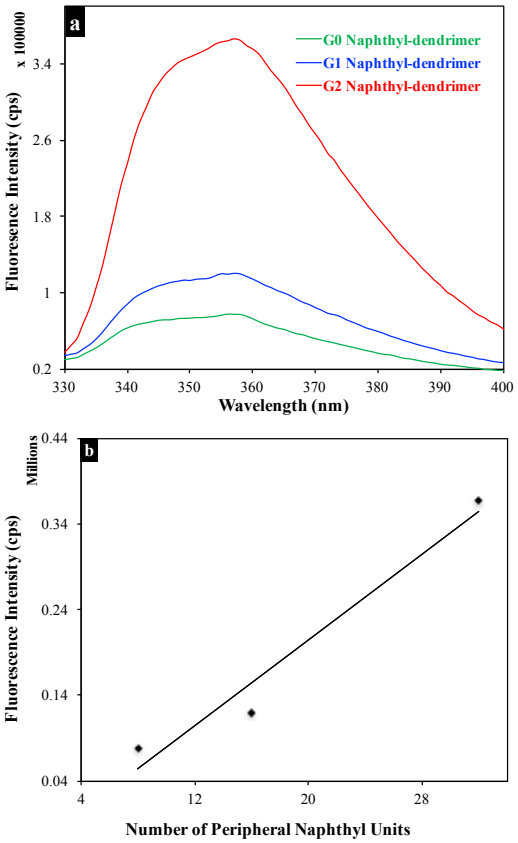

Figure 2.6. Fluorescence intensity of bifunctional dendrimers at equal concentrations. (a) Fluorescence intensity of 2 × 10^{-6} M DMF solutions of **G_0 naphthyl-dendrimer** (green); **G_1 naphthyl-dendrimer** (blue); and **G_2 naphthyl-dendrimer** (red). (b) Relationship of intensity with number of naphthyl units in dendrimer periphery.

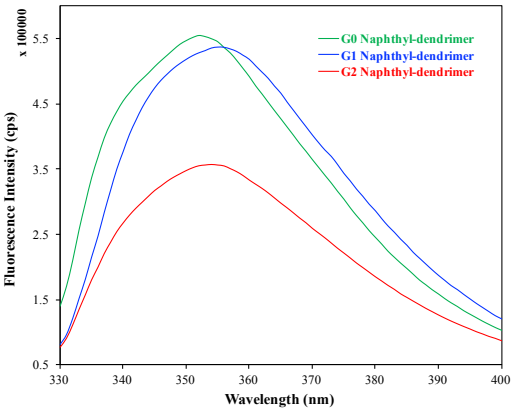

Figure 2.7. Fluorescence intensity of dendrimers at equal absorbance. Green: **G_0 naphthyl-dendrimer**; blue: **G_1 naphthyl-dendrimer**; red: **G_2 naphthyl-dendrimer**.

tail and blue shift suggests ground state electrostatic interactions that involve the dendrimer backbone and the terminal naphthyl groups. While this finding contrasts with those in previous reports,[46-48,52,53] where no measurable ground state interactions were found between terminal fluorophores and dendrimer backbone, it is consistent with the findings of Ceroni *et al*., where charge transfer between terminal groups and dendrimer core results in a broad absorption tail.[49] It is worth mentioning that the dendrimers in the present study featured flexible aliphatic segments, which differs considerably from the Frèchet-type poly(aromatic ether), where no ground state interactions between terminal fluorophores and dendrimer backbones were found. The presence of such flexible segment may result in appreciable back folding of the terminal groups into the dendrimer cavity as is typical of dendrimers.[19]

Degassed DMF solutions of the dendrimers show an emission band with λ_{max} at 360 nm after excitation at 320 nm (Figure 2.6a). The intensity of the emission band increased with generation due to an increase in the number of naphthyl groups. An acceptable, positive linear correlation (R^2 = 0.9611) of the intensity of the emission band at 360 nm with the number of naphthyl groups was found (Figure 2.6b). However, this correlation falls below expectations, and the ground state electrostatic interactions between terminal naphthyl groups and dendrimer branch might account for the low correlation.[49] Although this result did provide information on the emission intensity of the entire terminal naphthyl groups in the dendrimers, it yielded no information on the emission intensity of individual naphthyl groups. The latter information will be relevant to gaining deeper understanding of the interactions in the dendrimers as well as the effects of these interactions on the emission of each naphthyl group.

To gain insight into the emission of an individual naphthyl group, DMF solutions of **G_0 naphthyl-dendrimer**, **G_1 naphthyl-dendrimer** and **G_2 naphthyl-dendrimer** at equal absorbance

(A = ~0.4) were similarly excited, and their emission recorded. The respective solutions of **G_0 naphthyl-dendrimer**, **G_1 naphthyl-dendrimer** and **G_2 naphthyl-dendrimer** at equal absorbance were expected to exhibit equal emission intensity if the dendrimer structure does not influence the fluorescence of the naphthyl groups. The results of these experiments showed that emission intensity decreased with increase in dendrimer generation (Figure 2.7). This negative dendritic effect suggests that the fluorescence of each naphthyl group is quenched with increasing dendrimer generation. In addition, the spectra shape of **G_0 naphthyl-dendrimer** was clearly different from those of **G_1 naphthyl-dendrimer** and **G_2 naphthyl-dendrimer** (Figure 2.7) probably due to

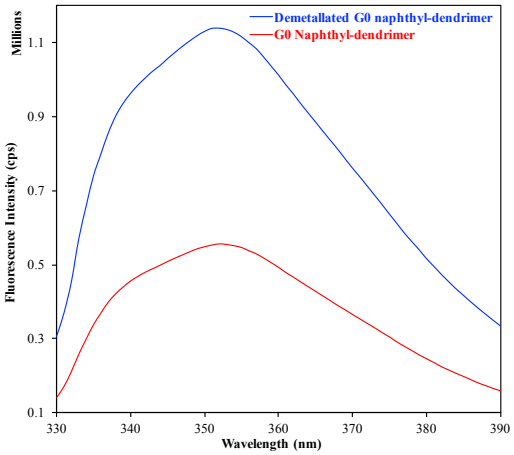

Figure 2.8. Effect of demetallation on emission intensity. Red: **G_0 naphthyl-dendrimer**, and blue: demetallated **G_0 naphthyl-dendrimer**.

changes in the topology of the dendrimers as the generation changes. Such change in topology can induce variation in the steric and electronic environment of the terminal naphthyl groups and ultimately affect the spectra shape. Demetallation increased the emission intensity (Figure 2.8), conclusively indicating that the presence of the iron quenched the fluorescence. Data from steady-state fluorescent measurements support those from UV-vis experiments, that the naphthyl groups

backfolded into the dendrimer, or were overcrowded at the periphery. Overall, it is obvious that the peripheral groups interacted with other parts of the dendrimer structure. Also, energy transfer-induced quenching was probable, as the absorption tail in the UV-vis spectra overlapped with the emission band at 360 nm (Figures 2.5-2.7).

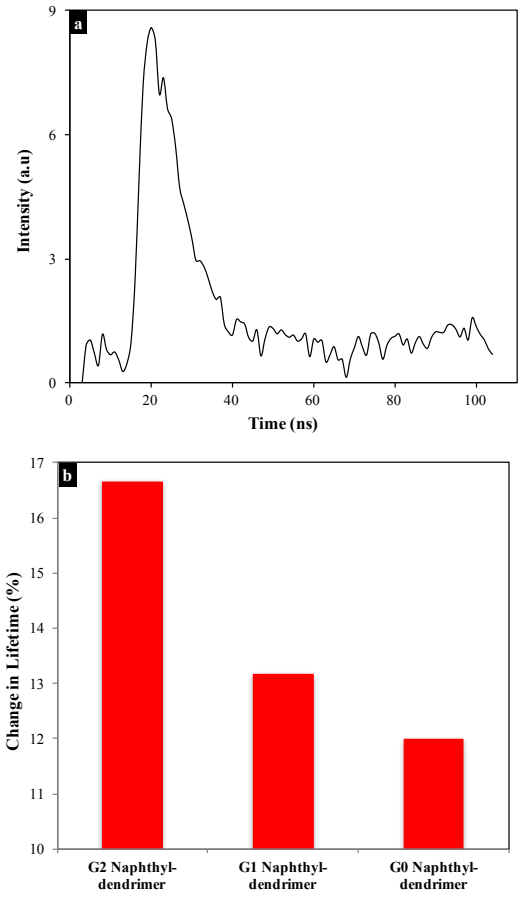

Figure 2.9. Fluorescence lifetime decay profile of dendrimer. (a) Lifetime decay profile of **G_2 naphthyl-dendrimer**; (b) Effect on demetallation on lifetime of bifunctional dendrimers.

To further probe the quenching, time-resolved fluorescence spectroscopic measurements of fluorescence lifetime (τ) of **G_0 naphthyl-dendrimer**, **G_1 naphthyl-dendrimer**, **G_2 naphthyl-dendrimer** and β-naphthol in degassed DMF was conducted. Like β-naphthol, all the dendrimers

exhibited monoexponential lifetime decay process (Figure 2.9); however, **G_0 naphthyl-dendrimer**, **G_1 naphthyl-dendrimer** and **G_2 naphthyl-dendrimer** had τ = 6.08, 6.15, and 5.16 ns, respectively that were shorter than that of β-naphthol with τ = 7.28 ns. With demetallation, τ of the dendrimers increased, although they were still lower than that of β-naphthol. The change in τ after demetallation was more pronounced for **G_2 naphthyl-dendrimer** than for **G_0 naphthyl-dendrimer** and **G_1 naphthyl-dendrimer** (Figure 2.9b). These results further implicate the presence of iron in the quenching process and suggest a dynamic quenching mechanism, which involves excited state processes. Further, the dynamic quenching mechanism involved aromatic donor-acceptor interactions as well as other aromatic-aromatic interactions, as lifetimes of the demetallated dendrimers were still lower than that of β-naphthol. These interactions were stronger in **G_2 naphthyl-dendrimer** given that the change in lifetime after demetallation (Figure 2.9b) was markedly higher than those of **G_0 naphthyl-dendrimer** and **G_1 naphthyl-dendrimer** (Figure 2.9b). Taken together, the photophysics of the **G_2 naphthyl-dendrimer** was noticeably distinct from those of **G_0 naphthyl-dendrimer** and **G_1 naphthyl-dendrimer**, probably, due to increasing back folding or overcrowding of the naphthyl groups at higher generation.

2.2.4. Redox activity of dendrimers

Like η^6-arene-η^5-cyclopentadienyliron(II) complexes, which are redox-active,[26,35,36,54-58] these dendrimers were expected to be redox active. The redox activity of **G_0 naphthyl-dendrimer**, **G_1 naphthyl-dendrimer** and **G_2 naphthyl-dendrimer** was investigated using cyclic voltammetry. It is established that the reversibility of redox activity of the $[\eta^6$-arene-η^5-CpFe$]^+$ complexes depends on experimental conditions.[54,55,57] In these studies, **G_0 naphthyl-dendrimer**, **G_1 naphthyl-dendrimer** and **G_2 naphthyl-dendrimer** exhibited irreversible redox process at room

temperature, which agreed with a previous report.[31] However, at 0 °C, the redox processes became quasi-reversible (Figure 2.10). The dendrimers had a single redox wave with cathodic peak (E_{pc}) and anodic peak (E_{pa}) values that agreed with previous reports[57] (Table 2.1). A positive dendritic effect on the half-wave potential ($E_{1/2}$) was also observed (Table 2.1), which suggest increasing difficulty in reducing the iron at higher generation. The presence of a single redox wave for **G_1 naphthyl-dendrimer** and **G_2 naphthyl-dendrimer**, contrasts with a previous report on an [η^6-arene-η^5-CpFe]$^+$ complex derived star polymer, where two distinct redox waves that corresponded to iron centers in two different locations within the polymer were found.[35]

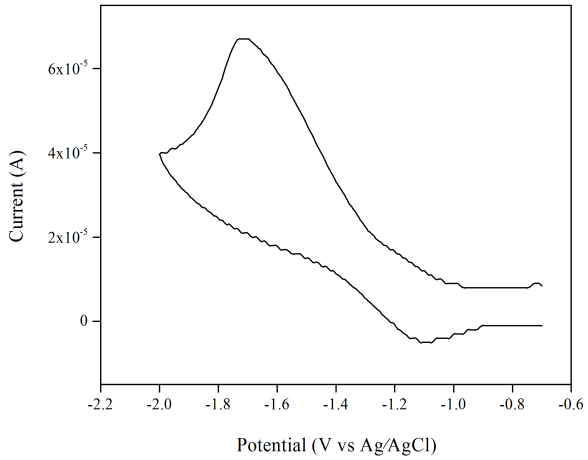

Figure 2.10. Cyclic voltammogram of **G_1 naphthyl-dendrimer** in 0.1 M Bu_4NPF_6 in DMF, scan rate = 100 mV/s, at 0 °C.

Table 2.1. Electrochemical data[a] of bifunctional dendrimers.

	E_{pc} (V)	E_{pa} (V)	$E_{1/2}$ (V)
G_0 Naphthyl-dendrimer	–1.63	–1.14	–1.39
G_1 Naphthyl-dendrimer	–1.66	–1.16	–1.41
G_2 Naphthyl-dendrimer	–1.61	–1.31	–1.49
Iron complex polymer[57]	–1.61	–1.18	–1.40

[a]quasi-reversible redox process. Cyclic voltammogram at glassy carbon of dendrimers in 0.1 M Bu_4NPF_6 in DMF, scan rate = 100 mV/s, at 0 °C.

It is worth noting that the reduction wave in **G_1 naphthyl-dendrimer** and **G_2 naphthyl-dendrimer** were broad relative to **G_0 naphthyl-dendrimer**. The broadness could be attributed to overlapped cathodic currents that result from the reduction of iron at different locations in these higher generation dendrimers. Although the rate of electron transfer between the electrodes and iron at different locations may be approximately the same to preclude apparent splitting of the reduction wave, it is possible that the rate differs slightly to initiate broadening of the wave. The CV data suggest that electron transfer at the redox centers was influenced by the dendrimer structure.

2.3. Conclusion

It is evident that $[\eta^6$-dichloroarene-η^5-CpFe$]^+$ complex is a versatile building block for the facile synthesis of functional dendrimers. This is demonstrated with the successful synthesis of three generations of bifunctional dendrimers with redox and photoactive properties. Indeed, the photophysical properties were evidenced by UV-vis and fluorescence studies, while CV experiments revealed that the dendrimers were redox active. Importantly, the synthesis route shown here can be extended to design a broad range of redox active, bifunctional dendrimers with emissive, biomedical, and magnetic properties as will be shown in subsequent chapters.

2.4. Experimental section

2.4.1 Materials

All chemicals and reagents were obtained from Sigma-Aldrich and were used without further purification unless stated otherwise. Dimethyl sulfoxide (DMSO), *N*,*N*′-dimethylformamide (DMF) were dried, and stored over activated 3 Å molecular sieve before being used. Dichloromethane (DCM) was purified by passing the solvent through an Innovative Technology

solvent purification system that consists of columns of alumina and copper catalyst. The synthesis of the organoiron complexes (**2.2** and **2.3**) followed previously reported procedures.[59]

2.4.2. Instrumentation

A Bruker Avance NMR spectrometer (^{1}H, 300 MHz and ^{13}C, 75 MHz) was used to characterize all synthesized compounds in DMSO-d_6 or acetone-d_6 with the chemical signals referenced to solvent residual proton signal in ppm. Attenuated total reflection Fourier transform IR (ATR-FTIR) spectroscopy data were acquired on a Bruker Alpha FTIR spectrometer Alpha-P. Differential scanning calorimetry (DSC) was carried out in sealed aluminium pans under nitrogen using a heat/cool/heat cycle at a heating and cooling rate of 10 °C/minute on a TA Instruments DSC Q100. Thermogravimetric analysis (TGA) were conducted in platinum pans under nitrogen at a heating rate of 10 °C/minute on a TA Instruments TGA Q500. A Bruker AXS Advance D8 diffractometer equipped with a graphite monochromator, variable divergence, antiscatter slits, and a scintillation detector was used to acquire powder X-ray diffractograms from fine powders of the dendrimers. Steady-state and time-resolved fluorescence data were acquired on Photon Technology International LS-100 luminescence spectrophotometer and Photon Technology International Timemaster spectrophotometer, respectively. UV-vis absorption measurements were performed using a Cary 50 Bio UV-visible spectrophotometer. The fluorescence and UV-vis absorption spectroscopic measurements were carried out using degassed DMF solutions of the dendrimers. Cyclic voltammetry was carried out on a Princeton Applied Research/EG&G Model 283 potentiostat/galvanostat using glassy carbon working electrode, Pt counter electrode, and Ag reference electrode. The experiments, which were carried out at a scan rate of 0.1 V/s and at a temperature of 0 °C under nitrogen atmosphere in degassed DMF as solvent and tetrabutyl-

ammonium hexafluorophosphate as supporting electrolyte. Scanning electron microscopic images of the dendrimers were obtained on a LVEM5 Delong Instruments operated at 5 kV. The powdered samples were sprinkled on carbon-coated SEM stubs, sputter-coated with Au/Pd for 10 seconds (SPI Sputter Coater) before being imaged. Transmission electron microscopic images were acquired on a Hitachi BioTEM 7500 (Nissei-Sangyo, Rexdale, ON, Canada) operated at 80 kV, with a digital camera: AMT XR40 side mount, (Advance Microscopy Techniques, Danvers, Ma USA), and AMT Image Capture Engine software version 600.149. The dendrimer samples were dispersed in deionized water, pipetted onto a carbon-coated copper grid, and allowed to dry before being imaged. Elemental analyses, specifically, carbon and hydrogen (CH) analyses, were performed on CE-440 Elemental Analyzer, Exeter Analytical, Inc.

2.4.3. Synthesis of 2.4

The synthesis of bimetallic complex (**2.4**) followed the well-established S_NAr reaction.[31] In brief, a 50-mL round-bottom flask was charged with β-naphthol (1.02 g, 7.06 mmol), **2.3** (3.67 g, 3.53 mmol), K_2CO_3 (4.87 g, 35.3 mmol), and 10 mL of DMF. The reaction mixture was flushed with nitrogen for one hour, then stirred at room temperature for 72 hours. Subsequently, the reaction mixture was added dropwise to 300 mL of 10% HCl solution, followed by the addition of NH_4PF_6 (1.15 g, 7.06 mmol) to precipitate the product. The product was filtered, and dried under vacuum. Yield: 93%. ^{1}H NMR data (300 MHz; DMSO-d_6): δ (ppm) 8.13 (2H, d, J = 8.7 Hz, naphthyl *H*), 8.01 (4H, m, naphthyl *H*), 7.86 (2H, s, naphthyl *H*), 7.61 (4H, m, naphthyl *H*), 7.49 (2H, d, J = 8.4 Hz, naphthyl *H*), 7.38 (4H, d, J = 7.8 Hz, uncomplexed Ar*H*), 7.27 (4H, d, J = 7.2 Hz, complexed Ar*H*), 6.36 (4H, br s, complexed Ar*H*), 6.30 (4H, br s, complexed Ar*H*), 5.26 (10, s, Cp*H*), 2.43 (2H, br s, CH_2), 2.08 (2H, br s, CH_2), 1.69 (3H, s, CH_3). ^{13}C NMR (75 MHz, DMSO-d_6): δ (ppm)

174.9 (*C*=O), 155.8, 152, 151.5, 146.6, 134.2, 131.4, 131.3, 130.5, 129.6, 128.2, 128, 127.5, 126.5, 120.3, 117.4, 109, 75.7, 75.5 (Ar*C*), 78.3 (Cp*C*), 45.4 (quat *C*), 36.6, 30.4 (CH_2), 27.4 (CH_3). ATR-FTIR: ν_{max} (cm^{-1}) 3461 (COOH), 3097 (Ar CH), 2969 (Cp CH), 1722 (CO), 1223 (C-O-C). Elemental analyses: calculated for C, 56.48; H, 3.86; found for C, 56.65; H, 3.83.

2.4.4. Synthesis of G_0 Cl-dendrimer

The dendrimer, **G_0 Cl-dendrimer**, was synthesized using the Steglich esterification method.[60] In brief, a 50 mL round-bottom flask was charged with pentaerythritol (0.170 g, 1.27 mmol), **2.3** (5.28 g, 5.08 mmol), 4-(dimethylamino)pyridine (DMAP) (0.500 g, 4.08 mmol), and 10 mL of 3:1 DCM/DMSO solution. The solution was stirred and cooled in an ice bath to 0 °C under nitrogen atmosphere while *N*,*N*′-dicyclohexylcarboiimide (DCC) (1.15 g, 5.59 mmol) was added over a 5-minute period. Thereafter, the ice-bath was removed and the reaction mixture stirred under nitrogen for 24 hours at room temperature. Precipitated dicyclohexylurea (DCU) was removed by filtration through a Büchner funnel and the filtrate was hydrolyzed in 50 mL of ice water to which NH_4PF_6 (1.66 g, 10.2 mmol) was added. The product was extracted with three 50-mL portions of 5:1 DCM/DMF mixture. The extracts were washed with two 50-mL portions of 5% HCl and subsequently with two 50-mL portions of Na_2CO_3, dried over $MgSO_4$, filtered, and the solvent removed with a rotary evaporator. The crude product was dissolved in $(CH_3)_2CO$, cooled to –25 °C in a freezer for one hour, filtered to remove more DCU and precipitated from $(C_2H_5)_2O$. The resulting yellow-green solid was collected by suction filtration and dried under vacuum at room temperature. Yield: 76%. ^{1}H NMR data (300 MHz, acetone-d_6): δ (ppm) 7.44 (16H, br s, uncomplexed Ar*H*), 7.29 (16H, br s, uncomplexed Ar*H*), 6.72 (16H, br s, complexed Ar*H*), 6.42 (16H, br s, complexed Ar*H*), 5.31 (40H, s, Cp*H*), 4.20 (8H, br s, CH_2), 2.51 (8H, br s, CH_2), 2.22

(8H, br s, CH_2), 1.70 (12H, br s, CH_3). ^{13}C NMR (75 MHz, acetone-d_6): δ (ppm) 174.14 (*C*=O), 152.5, 148.4, 134.4, 131.1, 121.8, 105.3, 88.3, 77.5 (Ar*C*), 80.9 (Cp*C*), 63.5 (*C*H$_2$), 46.8, 44.8 (quat *C*), 37.7 (*C*H$_2$), 28.4 (*C*H$_3$) (a *C*H$_2$ peak overlapped with the acetone peak). ATR-FTIR: ν_{max} (cm^{-1}) 3096 (Ar CH), 2979 (Cp CH), 1732 (CO), 1243 (C-O-C). Elemental analyses: calculated for C, 45.81; H, 3.34; found for C, 45.98; H, 3.35.

2.4.5. Synthesis of G_0 naphthyl-dendrimer

In a procedure, similar to that used in the synthesis of **G_0 Cl-dendrimer**, **G_0 naphthyl-dendrimer** was synthesized from **2.4** (100 mg, 0.0800 mmol), pentaerythritol (2.70 mg, 0.0200 mmol), DMAP (7.80 mg, 0.0640 mmol), and DCC (18 mg, 0.0880 mmol) in 5 mL of 3:1 DCM/DMSO. Yield: 82%. ^{1}H NMR data (300 MHz, acetone-d_6): δ (ppm) 8.11 (8H, d, J = 6.6 Hz, naphthyl *H*), 7.99 (16H, br m, naphthyl *H*), 7.84 (8H, br s, naphthyl *H*), 7.58 (16H, br s, naphthyl *H*), 7.50 (8H, br s, naphthyl *H*), 7.47 (16H, br s, uncomplexed Ar*H*), 7.31 (16H, br s, uncomplexed Ar*H*), 6.45 (16H, br s, complexed Ar*H*), 6.40 (16H, br s, complexed Ar*H*), 5.36 (40H, s, Cp*H*), 4.07 (8H, br d, J = 11.1 Hz, CH_2), 2.52 (8H, br s, CH_2), 2.23 (8H, br s, CH_2), 1.72 (12H, br s, CH_3). ^{13}C NMR (75 MHz, DMSO-d_6): δ (ppm) 171.2 (*C*=O), 152.1, 151.9, 151.4, 146.5, 134.2, 130.4, 131.4, 131.3, 129.6, 128.3, 128, 127.5, 126.5, 120.3, 120.1, 117.4, 75.7 (Ar*C*), 78.3 (Cp*C*), 60.4 (*C*H$_2$), 47.7, 45.5 (quat *C*), 36.4, 32.8 (*C*H$_2$), 27.2 (*C*H$_3$). ATR-FTIR: ν_{max} (cm^{-1}) 3097 (Ar CH), 2933 (Cp CH), 1729 (CO), 1224 (C-O-C). Elemental analyses: calculated for C, 56.95; H, 3.89; found for C, 57.13; H, 4.05.

2.4.6. Synthesis of G_0 BnOH-dendrimer

In a procedure, similar to that used in the synthesis of **2.4**, **G_0 BnOH-dendrimer** was synthesized from **G_0 Cl-dendrimer** (1.17 g, 0.270 mmol), 4-hydroxybenzyl alcohol (0.270 g, 2.16 mmol), and

K_2CO_3 (1.49 g, 10.8 mmol) in 10 mL DMF. Yield: 96%. ^{1}H NMR (300 MHz, DMSO-d_6): δ (ppm) 7.47 (16H, br s, Bn*H*), 7.35 (16H, br s, Bn*H*), 7.26 (32H, br s, uncomplexed Ar*H*), 6.25 (32H, br s, complexed Ar*H*), 5.40 (4H, br s, BnO*H*), 5.21 (40H, s, Cp*H*), 4.55 (16H, br s, CH_2), 3.95 (8H, br s, CH_2), 2.42 (8H, br s, CH_2), 1.65 (12H, br s, *C*H_3) (A CH_2 overlapped with DMSO-d_6 residue proton peak). ^{13}C NMR (75 MHz, DMSO-d_6): δ (ppm) 173.1 (*C*=O), 152.2, 152, 146.5, 146.1, 141.1, 130.9, 129.6, 129, 120.7, 120.3, 75.6, 75 (Ar*C*) 78.2 (Cp C), 62.5 (Bn*C*H_2), 60.9 (*C*H_2), 45.3, 44.3 (quat *C*), 39.2, 30.2, (*C*H_2) 27.4 (*C*H_3). ATR-FTIR: ν_{max} (cm^{-1}) 3389 (OH), 3090 (Ar CH), 2967 (Cp CH), 1732 (CO), 1224 (C-O-C). Elemental analyses: calculated for C, 52.95; H, 4.01; found for C, 52.73; H, 4.05.

2.4.7. Synthesis of G_1 Cl-dendrimer

In a procedure, similar to that used in the synthesis of **G_0 Cl-dendrimer**, **G_1 Cl-dendrimer** was synthesized from **G_0 BnOH-dendrimer** (750 mg, 0.150 mmol), **2.3** (1.26 g, 1.22 mmol), DMAP (120 mg, 0.980 mmol), and DCC (276 mg, 1.34 mmol) in 10 mL of 1:3 DCM/DMSO solvent mixture. Yield: 74%. ^{1}H NMR data (300 MHz, DMSO-d_6): δ (ppm) 7.51-7.24 (96H, m, uncomplexed Ar*H*); 6.99-6.97 (32H, br m, Bn*H*), 6.78 (32H, br s, complexed Ar*H*), 6.40 (32H, br s, complexed Ar*H*), 6.24 (32H, br s, complexed Ar*H*), 5.26, (80H, s, Cp*H*), 5.20 (40H, s, Cp*H*), 4.53 (16H, s, CH_2), 3.93 (8H, br s, CH_2), 2.53 (16H, br s, CH_2), 2.38 (16H, br s, CH_2), 2.27 (16H, br s, CH_2), 1.66 (24H, br s, CH_3), 1.61 (12H, br s, CH_3). ^{13}C NMR (75 MHz, DMSO-d_6): δ (ppm) 174.8, 173.1 (*C*=O), 152.2, 151.4, 146.8, 146.6, 141.4, 141.1, 139.4, 129.7, 129.6, 129.1, 129, 120.7, 120.5, 120.3, 118.7, 104, 87.1, 78.2, 78.1, 76.7 (Ar*C*), 79.7 (Cp*C*), 75.4, 74.9 (*C*H_2) 65.3, 62.6, 45 (quat *C*), 36.5, 36.2, 31.2, 31 (*C*H_2), 27.3, 26.6 (*C*H_3). ATR-FTIR: ν_{max} (cm^{-1}) 3099 (Ar

CH), 2970 (Cp CH), 1722 (CO), 1226 (C-O-C). Elemental analyses: calculated for C, 48.53; H, 3.48; found for C, 48.49; H, 3.53.

2.4.8. Synthesis of G_1 naphthyl-dendrimer

In a procedure, similar to that used in the synthesis of **G_0 naphthyl-dendrimer**, **G_1 naphthyl-dendrimer** was synthesized from **G_0 BnOH-dendrimer** (0.900 g, 0.180 mmol), **2.4** (1.82 g, 1.45 mmol), DMAP (0.140 g, 1.17 mmol), and DCC (0.320 g, 1.60 mmol) in 5 mL of 3:1 DCM/DMSO mixture. Yield: 72%. ^{1}H NMR (300 MHz, acetone-d_6): δ (ppm) 8.12 (16H, br dd, J = 8.4 Hz, naphthyl *H*), 8.01 (32H, br m, naphthyl *H*), 7.85 (16H, br s, naphthyl *H*), 7.59 (32H, br s, naphthyl *H*), 7.49, 7.46 (32H, br s Bn*H*) (16H of the naphthyl units overlapped with the Bn*H* peak at 7.49 and 7.46)), 7.40 (32H, br m, uncomplexed Ar*H*), 7.29 (64H, br m, uncomplexed Ar*H*), 6.37–6.31 (96H, br m, complexed Ar*H*), 5.30, 5.28 (120H, br s, Cp*H*), 4.60 (16H, br s, CH_2), 4.00 (8H, br dd, J = 8.1 Hz, CH_2), 2.65 (16H, br s, CH_2), 2.54 (16H, br s, CH_2), 2.40 (16H, br s, CH_2), 1.78 (12H, br s, CH_3), 1.69 (24H, br s, CH_3). ^{13}C NMR (75 MHz, DMSO-d_6): δ (ppm) 174.8, 172.3 (*C*=O), 152.1, 152, 151.5, 148.5, 146.6, 146.5, 146.4, 146.2, 134.4, 134.2, 133.7, 130.5, 131.4, 131.3, 130, 129.7, 129.6, 129, 128.2, 128, 127.8, 127.5, 127.1, 126.5, 126.2, 122, 120.7, 120.3, 118.8, 117.4, 75.6, 75.5 (Ar*C*), 78.3 (Cp*C*), 62.6, 53 (*C*H$_2$), 45.5, 45.4, 45.2 (quat *C*), 36.5, 36.3, 30.3, 30.2 (*C*H$_2$) 27.5, 27.4 (*C*H$_3$). ATR-FTIR: ν_{max} (cm^{-1}) 3090 (Ar CH), 2976 (Cp CH), 1751 (CO), 1224 (C-O-C). Elemental analyses: calculated for C, 55.96; H, 3.88; found for C, 55.97; H, 3.89.

2.4.9. Synthesis of G_1 BnOH-dendrimer

In a procedure, similar to that used in the synthesis of **G_0 BnOH-dendrimer**, **G_1 BnOH-dendrimer** was synthesized from **G_1 Cl-dendrimer** (0.520 g, 0.0390 mmol), 4-hydroxybenzyl

alcohol (78 mg, 0.630 mmol), and K_2CO_3 (0.430 g, 3.15 mmol) in 10 mL of DMF. Yield: 82%. ^{1}H NMR data (300 MHz, DMSO-d_6): δ (ppm) 7.49 (32H, dd, J = 8.1 Hz, Bn*H*), 7.38-7.23 (160H, m, Bn*H* and uncomplexed Ar*H*), 6.25 (64H, dd, J = 5.7 Hz, complexed Ar*H*), 6.22 (32H, s, complexed Ar*H*), (16H, 5.33 (br s, BnO*H*), 5.22 (120H, s, Cp H), 4.56 (48H, s, CH_2), 3.98 (8H, br dd, J = 16.2 Hz, CH_2), 2.64 (16H, br s, CH_2), 2.53 (br s, 16H, CH_2), 2.32 (br s, 16H, CH_2), 1.66, and 1.62 (br s, 36H, CH_3). ^{13}C NMR (75 MHz, DMSO-d_6): δ (ppm) 174.8, 173.1 (*C*=O), 156, 153.5, 152, 152.2, 152.1, 146.7, 146.5, 146.3, 141.1, 134.4, 130.3, 129.6, 129, 128.6, 120.8, 120.7, 120.5, 120.3, 118.7, 118.4, 75.5, 75 (Ar*C*), 78.3, 78.2 (Cp*C*), 65.3, 62.8, 62.6 (*C*H$_2$), 47.7, 45.5, 45.4 (quat *C*), 37.1, 36.5, 36.1, 32.8 (*C*H$_2$), 30.2, 27.3 (*C*H$_3$). ATR-FTIR: ν_{max} (cm^{-1}) 3395 (OH), 3102 (Ar CH), 2977 (Cp CH), 1725 (CO), 1224 (C-O-C). Elemental analyses: calculated for C, 53.12; H, 3.92; found for C, 52.93; H, 3.80.

2.4.10. Synthesis of G_2 Cl-dendrimer

In a procedure, similar to that used in the synthesis of **G_1 Cl-dendrimer**, **G_2 Cl-dendrimer** was obtained from **G_1 BnOH-dendrimer** (0.25 g, 0.017 mmol), **2.3** (0.28 g, 0.27 mmol), DMAP (26 mg, 0.21 mmol), and DCC (62 mg, 0.30 mmol) in 10 mL of 3:1 DCM/DMSO mixture. Yield: 52%. ^{1}H NMR (300 MHz, DMSO-d_6): δ (ppm) 7.51 (64H, br m, Bn*H*), 7.28, 7.25 (224H, br s, uncomplexed Ar*H*), 6.78, 6.40, 6.26 (224H, br s, complexed Ar*H*), 5.26, (240H, br s, Cp*H*) 5.21 (40H, br s, Cp*H*), 4.55 (48H, br s, CH_2), 3.94 (8H, br s, CH_2), 2.43-2.24, (112H, br s, CH_2), 1.69 (84H, br s, CH_3). ^{13}C NMR (75 MHz, DMSO-d_6): δ (ppm) 174.8, 173.1 (*C*=O), 162.7, 157.0, 153.5, 152.0, 151.5 146.8, 146.6, 146.3, 146.0, 134.4, 131.2, 130.8, 130.5, 129.7, 129.5, 129.2, 128.0, 120.8, 120.5, 120.3 119.7, 118.7, 118.2, 118.0, 104.0, 87.2, 76.7, 75.4 (Ar*C*), 79.7, 78.3,

77.4 (Cp*C*), 65.3, 62.5 (*C*H_2), 47.9, 45.4, 45.2, 45.1 (quat *C*), 36.5, 31.9, 30.7, 30.2, (*C*H_2), 27.5, 27.3 (*C*H_3). Elemental analyses: calculated for C, 49.31; H, 3.51; found for C, 49.74; H, 3.38.

2.4.11. Synthesis of G_2 naphthyl-dendrimer

In a procedure, similar to that used in the synthesis of **G_1 naphthyl-dendrimer**, **G_2 naphthyl-dendrimer** was synthesized from **G_1 BnOH-dendrimer** (0.28 g, 0.0190 mmol), **2.4** (0.39 g, 0.310 mmol), DMAP (32 mg, 0.260 mmol), and DCC (70 mg, 0.340 mmol) in 10 mL of 3:1 DCM/DMSO mixture. Yield: 64%. ^{1}H NMR (300 MHz, DMSO-d_6): δ (ppm) 8.11 (32H, br dd, *J* = 8.7 Hz, naphthyl *H*), 7.99 (64H, br m, naphthyl *H*), 7.84 (32H, br s, naphthyl *H*), 7.58 (64H, br s, naphthyl *H*), 7.47 (96H, br m, Bn*H* (32H of naphthyl units overlapped with the Bn protons at 7.31 ppm)), 7.35, 7.26 (224H, br s, uncomplexed Ar*H*), 6.34, 6.28 (224H, br s, complexed Ar*H*), 5.25, (240H, br s, Cp*H*) 5.21 (40H, br s, Cp*H*), 4.56 (48H, br s, CH_2), 3.94 (8H, br s, CH_2), 2.44-2.24, (112H, br s, CH_2), 1.71 (84H, br s, CH_3). ^{13}C NMR (75 MHz, DMSO-d_6): δ (ppm) 174.8, 169.8 (*C*=O), 152.2, 152.1, 152, 151.5, 146.5, 146.4, 146.3, 146.1, 141.1, 134.3, 134.2, 131.4, 131.3, 130.5, 130.4, 130, 129.6, 129.4, 129.6, 128.2, 128, 127.8 127.5 127.1, 126.5, 120.6, 119.7, 118.8, 117.3, 75.6, 75.5 (Ar*C*), 78.3, 78.2 (Cp*C*), 65.0, 62.5 (*C*H_2), 45.5, 45.4, 45.2, 45.1 (quat *C*), 36.5, 31.9, 30.7, 30.2, (*C*H_2), 27.5, 27.3 (*C*H_3). ATR-FTIR: ν_{max} (cm^{-1}) 3093 (Ar CH), 2964 (Cp CH), 1752 (CO), 1223 (C-O-C). Elemental analyses: calculated for C, 55.52; H, 3.82; found for C, 55.48; H, 3.74.

2.4.12. Demetallation of dendrimers

The demetallation was carried out as previously reported.[61-63] A 0.0003 mmol of the sample was placed in a Pyrex test tube, to which 5 mL of 5:1 $CH_3CN/CHCl_3$ mixture was added. The test tube was sealed with a septum and degassed with nitrogen for 10 minutes. The mixture was irradiated

for 24 hours in a Rayonett photochemical reactor equipped with a 300 nm UV lamp. Subsequently, the solvent was removed under vacuum and the residue washed with $(C_2H_5)_2O$ to remove the side product, ferrocene. The residue was extracted with $CHCl_3$, the extract was washed with water, dried with $MgSO_4$, and the concentrated under vacuum. The product was obtained by adding the concentrate into hexane. The product was characterized using 1H NMR spectrum. For photophysical characterizations, the extract was dissolved in DMF.

References

1. Yang, B.; Zhao, Y.; Wang, S.; Zhang, Y.; Fu, C.; Wei, Y.; Tao, L. *Macromolecules* **2014**, *47*, 5607.
2. Niu, J.; Lunn, D. J.; Pusuluri, A.; Yoo, J. I.; O'Malley, M. A.; Mitragotri, S.; Soh, H. T.; Hawker, C. J. *Nat. Chem.* **2017**, doi: 10.1038/nchem.2713.
3. Kubo, T.; Figg, C. A.; Swartz, J. L.; Brooks, W. L.; Sumerlin, B. S. *Macromolecules* **2016**, *49*, 2077.
4. Zhao, J.; Ma, L.; Millians, W.; Wu, T.; Ming, W. *ACS Appl. Mater. Interfaces* **2016**, *8*, 8737.
5. Jiang, B.; Nykypanchuk, D.; Endoh, M. K.; Chen, X.; Qian, B.; Kisslinger, K.; Koga, T.; Parise, J. B.; Grubbs, R. B. *Macromolecules* **2016**, *49*, 853.
6. Fuchs, S.; Pla-Quintana, A.; Mazeres, S.; Caminade, A.; Majoral, J. *Org. Lett.* **2008**, *10*, 4751.
7. Caminade, A.; Majoral, J. *Molecules* **2016**, *21*, 538.
8. Caminade, A.; Hameau, A.; Majoral, J. *Dalton Trans.* **2016**, *45*, 1810.
9. Khandare, J.; Calderón, M.; Dagia, N. M.; Haag, R. *Chem. Soc. Rev.* **2012**, *41*, 2824.
10. De, S.; Stelzer, C.; Khan, A. *Polym. Chem.* **2012**, *3*, 2342.
11. Behl, M.; Razzaq, M. Y.; Lendlein, A. *Adv. Mater.* **2010**, *22*, 3388.
12. Zeng, H.; Little, H. C.; Tiambeng, T. N.; Williams, G. A.; Guan, Z. *J. Am. Chem. Soc.* **2013**, *135*, 4962.
13. Persano, L.; Camposeo, A.; Pisignano, D. *Prog. Polym. Sci.* **2015**, *43*, 48.
14. Persano, L.; Camposeo, A.; Pisignano, D. *J. Mater. Chem. C* **2013**, *1*, 7663.
15. Hirao, A.; Hayashi, M.; Loykulnant, S.; Sugiyama, K.; Ryu, S. W.; Haraguchi, N.; Matsuo, A.; Higashihara, T. *Prog. Polym. Sci.* **2005**, *30*, 111.
16. Zhao, Y.; Higashihara, T.; Sugiyama, K.; Hirao, A. *J. Am. Chem. Soc.* **2005**, *127*, 14158.
17. Juris, A. *Annu. Rep. Section C (Phys. Chem.)* **2003**, *99*, 177.
18. Balzani, V.; Campagna, S.; Denti, G.; Juris, A.; Serroni, S.; Venturi, M. *Acc. Chem. Res.* **1998**, *31*, 26.
19. Astruc, D.; Boisselier, E.; Ornelas, C. *Chem. Rev.* **2010**, *110*, 1857.
20. Svenson, S.; Tomalia, D. A. *Adv. Drug Deliv. Rev.* **2012**, *64*, 102.

21. Tomalia, D. A.; Christensen, J. B.; Boas, U. *Dendrimers, dendrons, and dendritic polymers: discovery, applications, and the future;* Cambridge University Press: 2012.
22. Menjoge, A. R.; Kannan, R. M.; Tomalia, D. A. *Drug Discov. Today* **2010***, 15*, 171.
23. Samoc, M.; Morrall, J. P.; Dalton, G. T.; Cifuentes, M. P.; Humphrey, M. G. *Angew. Chem. Int. Ed.* **2007***, 119*, 745.
24. Casado, C. M.; González, B.; Cuadrado, I.; Alonso, B.; Morán, M.; Losada, J. *Angew. Chem. Int. Ed.* **2000***, 112*, 2219.
25. Djeda, R.; Rapakousiou, A.; Liang, L.; Guidolin, N.; Ruiz, J.; Astruc, D. *Angew. Chem Int. Ed.* **2010***, 49*, 8152.
26. Djeda, R.; Ornelas, C.; Ruiz, J.; Astruc, D. *Inorg. Chem.* **2010***, 49*, 6085.
27. Abd-El-Aziz, A. S.; Todd, E. K. *Coord. Chem. Rev.* **2003***, 246*, 3.
28. Abd-El-Aziz, A. S. Overview of Organoiron Polymers. In *Macromolecules Containing Metal and Metal-like Elements*; Abd-El-Aziz, A. S., Carraher Jr., C. E., Pittman Jr., C. U., Sheats, J. E., Zeldin, M., Eds.; John Wiley & Sons: New York, **2004**; Vol. 2, pp 1-27.
29. Astruc, D.; Wang, Y.; Rapakousiou, A.; Diallo, A.; Djeda, R.; Ruiz, J.; Ornelas, C. Polyhedron **2015**, 86, 24.
30. Sutherland, R. G.; Zhang, C.; Piórko, A.; Lee, C. C. *Can. J. Chem.* **1989***, 67*, 137.
31. Abd-El-Aziz, A. S.; Todd, E. K.; Okasha, R. M.; Shipman, P. O.; Wood, T. E. *Macromolecules* **2005***, 38*, 9411.
32. Abd-El-Aziz, A. S.; Todd, E. K.; Okasha, R. M. *Macromol. Symp*. **2003**, *196*, 77.
33. Abd-El-Aziz, A. S.; Pilfold, J. L.; Momeni, B. Z.; Proud, A. J.; Pearson, J. K. *Polym. Chem.* **2014***, 5*, 3453.
34. Abd-El-Aziz, A. S.; Carruthers, S. A.; Aguiar, P. M.; Kroeker, S. *J. Inorg. Organomet. Polym. Mater.* **2005***, 15*, 349.
35. Abd-El-Aziz, A. S.; Todd, E. K.; Afifi, T. H. *Macromol. Rapid Commun.* **2002***, 23*, 113.
36. Abd-El-Aziz, A. S.; Strohm, E. A.; Ding, M.; Okasha, R. M.; Afifi, T. H.; Sezgin, S.; Shipley, P. R. *J. Inorg. Organomet. Polym. Mater.* **2010***, 20*, 592.
37. Abd-El-Aziz, A. S.; Carruthers, S. A.; Todd, E. K.; Afifi, T. H.; Gavina, J. *J. Polym. Sci. Part A: Polym. Chem.* **2005***, 43*, 1382.
38. Abd-El-Aziz, A. S.; Pereira, N. M.; Winram, D. J.; Sidhu, P.; Kroeker, S. *J. Inorg. Organomet. Polym. Mater.* **2007***, 17*, 275.
39. Abd-El-Aziz, A.; Dalgakiran, S. S.; Bichler, L. *Eur. Polym. J.* **2012***, 48*, 1901.
40. Abd-El-Aziz, A.; Dalgakiran, S. S. *J. Inorg. Organomet. Polym. Mater.* **2013***, 23*, 126.
41. Abd-El-Aziz, A. S.; Winram, D. J.; Shipman, P. O.; Rock, C. L.; Vandel, M. S.; Patrick, B. O. *Macromol. Chem. Phys.* **2012***, 213*, 2136.
42. Wang, Y.; Rapakousiou, A.; Astruc, D. *Macromolecules* **2014***, 47*, 3767.
43. Abd-El-Aziz, A. S.; Schriemer, D. C.; de Denus, C. R. *Organometallics* **1994***, 13*, 374.
44. Abd-El-Aziz, A.; Todd, E.; Ma, G. *J. Polym. Sci. Part A: Polym. Chem.* **2001***, 39*, 1216.
45. Vanjinathan, M.; Lin, H.; Nasar, A. S. *Macromol. Chem. Phys.* **2011**, *212*, 849.
46. Albrecht, K.; Yamamoto, K. *J. Am. Chem. Soc.* **2009**, *131*, 2244.
47. Schlutter, F.; Wild, A.; Winter, A.; Hager, M. D.; Baumgaertel, A.; Friebe, C.; Schubert, U. S. *Macromolecules*, **2010**, *43*, 2759.
48. Martinez, C. R.; Iverson, B. L. *Chem. Sci.* **2012**, *3*, 2191.
49. Ceroni, P.; Vicinelli, V.; Maestri, M.; Balzani, V.; Müller, W. M.; Müller, U.; Hahn, U.; Osswald, F.; Vögtle, F. *New J. Chem.* **2001**, *25*, 989.

50. Sisido, M.; Inai, Y.; Imanishi, Y. *Macromolecules*, **1990**, *23*, 1665.
51. Tan, L.; Curtis, M. D.; Francis, A. *Macromolecules*, **2002**, *35*, 4628.
52. Li, M.; Li, Y.; Zeng, Y.; Chen, J.; Li, Y. *J. Phys. Chem. C*, **2009**, *113*, 11554.
53. Li, Y.; Han, L.; Chen, J.; Zheng, S.; Zen, Y.; Li, Y.; Li, S.; Yang, G. *Macromolecules* **2007**, *40*, 9384.
54. Abd-El-Aziz, A. S.; Baranski, A. S.; Piorko, A.; Sutherland, R. G. *Inorg. Chim. Acta* **1988**, *147*, 77.
55. Abd-El-Aziz, A. S.; Winkler, K.; Baranski, A. S. *Inorg. Chim. Acta* **1992**, *194*, 207.
56. Ruiz, J.; Astruc, D. *C. R. Acad. des Sci. IIc: Chem*. **1998**, *1*, 21.
57. de Denus, C. R.; Baker, P.; Toner, J.; McKevitt, S.; Todd, E. K.; Abd-El-Aziz, A. S. *Macromol. Symp.* **2003**, *196*, 113.
58. Aranzaes, J. R.; Daniel, M.; Astruc, D. *Can. J. Chem.* **2006**, *84*, 288.
59. Abd-El-Aziz, A. S.; May, L.; Hurd, J.; Okasha, R. *J. Polym. Sci. Part A: Polym Chem.* **2001**, *39*, 2716.
60. Neises, B.; Steglich, W. *Angew Chem. Int. Ed.* **1978**, *17*, 522.
61. Abd-El-Aziz, A. S.; Todd, E. K.; Okasha, R. M.; P. O. Shipman, P. O.; T. E. Wood, T. E. *Macromolecules* **2005**, *38*, 9411.
62. Abd-El-Aziz, A. S.; Armstrong, D. A.; Bernardin, S.; Hutton, H. M. *Can J. Chem.* **1996**, *74*, 2073.
63. Gill, T. P.; Mann, K. R. *Inorg. Chem.* **1983**, *22*, 1986.

Chapter Three: Towards Functional Materials[†]

Abstract

Chapter Two reports a synthesis route to bifunctional dendrimers capped with β-naphthol, a randomly selected photoactive terminal unit. Here, a bulkier group is incorporated into the dendrimers to demonstrate the versatility of the synthesis route and to access a functional dendrimer for real applications. Tetraphenylethylene (TPE) is bulkier than β-naphthol, and features a photochemistry that is yet-to-be-exploited in the design of photoactive, dual-emissive dendrimer. Therefore, the TPE-based nucleophile, 1-(4′-hydroxyphenyl)-1,2,2-triphenylethylene, was designed and reacted with the zeroth- and first-generation chloro-capped dendrimers (**G_0 Cl-dendrimer** and **G_1 Cl-dendrimer**) to obtain photoactive dendrimers. A UV light irradiation was used as a facile photochemical tool to convert some of the TPE moieties to photoactive 9,10-diphenylphenanthrene (DPP) moieties. The result is the first dual-emissive TPE-based dendrimers that emit in the solution and aggregate state with tunable dual emissions at 368 nm and 469 nm. Also, the dendrimers can function as oxygen sensor since the DPP emission at 368 nm is turned-on after UV irradiation in the presence of oxygen. Indeed, the dendrimers successfully screened degassed solvents from aerated ones.

3.1. Introduction

Functional materials drive innovations that are improving human condition.[1,2] These materials find application as sensors,[3-5] imaging platforms, stimuli-responsive materials,[6-9] and optoelectronic

[†] This chapter is published as Abd-El-Aziz, A. S.; Agatemor, C.; Etkin, N.; Wagner, B. *Macromol. Rapid Commun.* **2016**, *37*, 1235 and is reproduced by permission of WILEY-VCH Verlag GmbH & Co. KGaA, Weinheim.

systems.[10-12] Thus, new approaches, and phenomena are pursued with the aim of developing the next-generation of functional materials. The synthesis route developed in *Chapter Two* is further explored to design a functional, specifically photoactive, material with the objective of demonstrating the versatility of the route. Tetraphenylethylene (TPE), a much bulkier photoactive molecule than β-naphthol, was selected to cap the dendrimers as terminal groups. Recently, the photophysical phenomenon of aggregation-induced emission (AIE) was discovered in TPE leading to breakthroughs that are both fundamental and applied.[13]

TPE is an easily accessible AIE fluorophore with turn-on fluorescence induced by restricted intramolecular rotation (RIR), especially, in the aggregate state. Various aggregate state applications of TPE-based systems are explored, and research in this area enjoys exciting times.[1,2,14] While most of these studies exploit the photophysics of TPE in the design of photoactive materials,[1] the photochemistry, which involves photo-induced conversion of TPE to 9,10-diphenylphenanthrene (DPP), is not fully explored.[15] Although largely under-investigated, the photochemistry of TPE influences the mesomorphic properties of TPE-derived liquid crystals by increasing *pi*-interactions, and enhancing crystallization tendency.[16] Recently, the fluorescence property of a TPE-based system was modified by manipulating its photochemistry, and host-guest complexation, transforming the AIE emission at ~ 480 nm to DPP emission at ~ 385 nm.[17] Molecules that emit at two different wavelengths, a phenomenon known as dual emission,[18,19] are in demand, for instance in the design of sensors.[3,5,20-22] TPE is a dual emissive fluorophore,[19,23] featuring the familiar AIE emission at ~ 480 nm, and another emission at ~ 540 nm.[24] As the two emissions overlap,[24] it is challenging to apply the dual emissive property.

An attractive challenge is to position TPE-based systems as a practically useful dual emissive system, broadening their scope of application. Interest in these systems is emerging, and a recent

report featured a dual emissive, TPE-based enzyme sensing system designed by blending the fluorescent properties of a positively charged TPE derivative with those of a positively charged anthracene derivative.[22] Incorporating two fluorophores into a sensing system to realize dual emission is classic;[18,22] but synthetically complicated.[22] Circumventing this synthetic complexity by using a single fluorophore is therefore worthwhile, and is an objective of these studies.

To tackle this challenge, the synthesis route reported in *Chapter Two* was used to design dendrimers that were multi-functionalized at their termini with TPE and, in a simple photochemical reaction, convert some of the TPE to DPP units. The main objective was to demonstrate the versatility of the synthesis strategy to bulkier groups and to access functional materials for real application. Thus, TPE is a perfect choice. The fundamentals of photo-induced conversion of TPE to DPP is well established,[15-17,25-27] and is controlled by irradiation time and solvent. Here, irradiation time was used to control the conversion of TPE to DPP to obtain hetero-functional dendrimers that were dual emissive. The two emissions from the dendrimers were resolved, allowing their use in a real application, for instance, the qualitative detection of oxygen.

3.2. Results and discussion

3.2.1. Synthesis and characterization of TPE- and TPE/DPP-dendrimers

Most often, constructing a dual emissive system is a challenge that involves incorporating two fluorophores into the system.[22] It is, therefore, attractive to exploit the photochemistry of TPE to realize these systems using a single fluorophore. Here, the strategy involved constructing a TPE-functionalized polymer and irradiating this polymer with UV light, eventually transforming it into a hetero-functional TPE/DPP system.

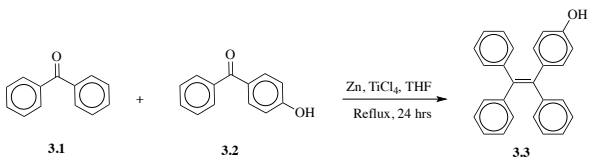

Scheme 3.1. Schematic representation of the synthesis of 1-(4′-hydroxyphenyl)-1,2,2-triphenylethylene (**3.3**).

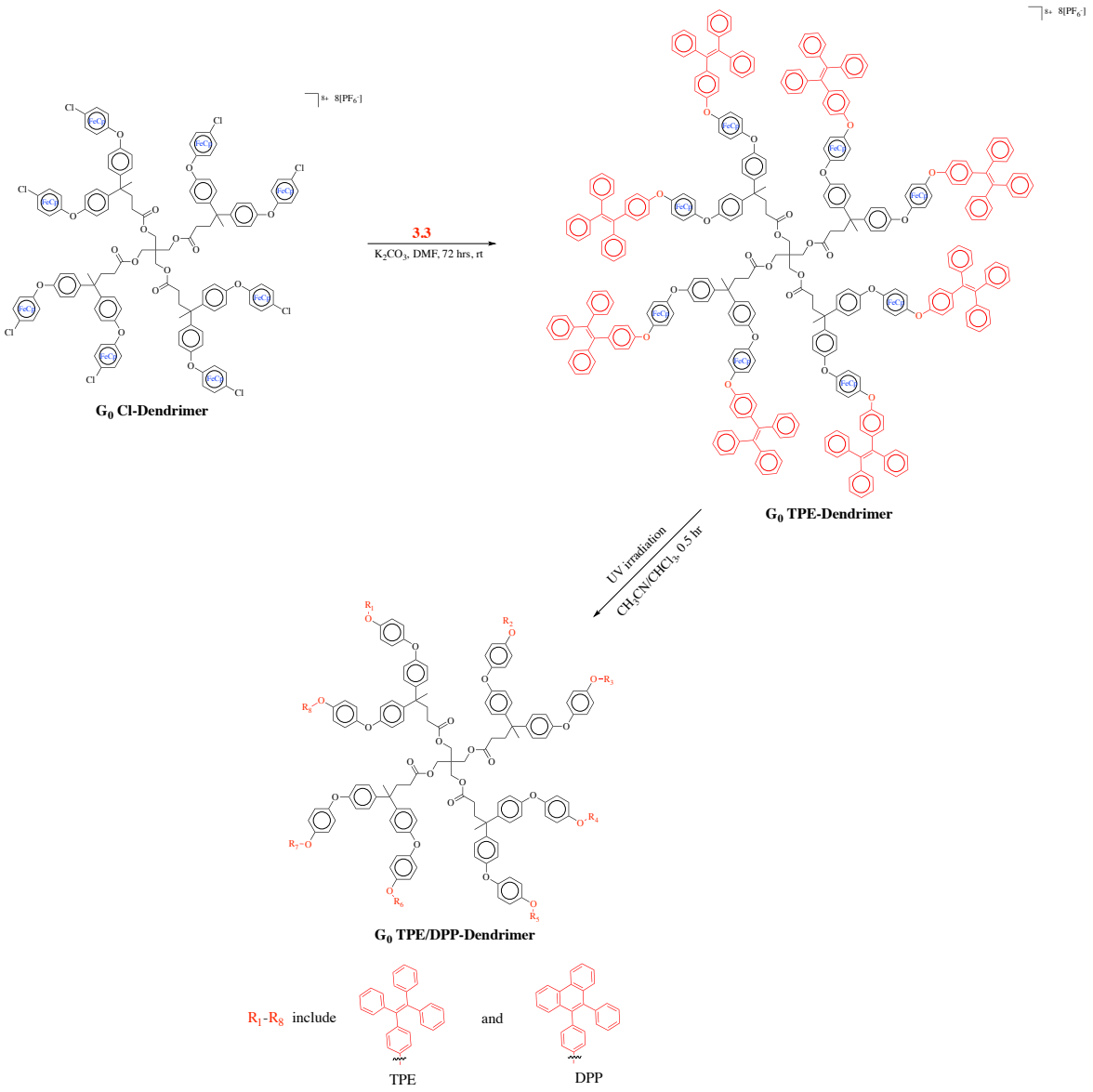

Scheme 3.2. Schematic representation of the synthesis of **G_0 TPE-dendrimer** and **G_0 TPE/DPP-dendrimer**.

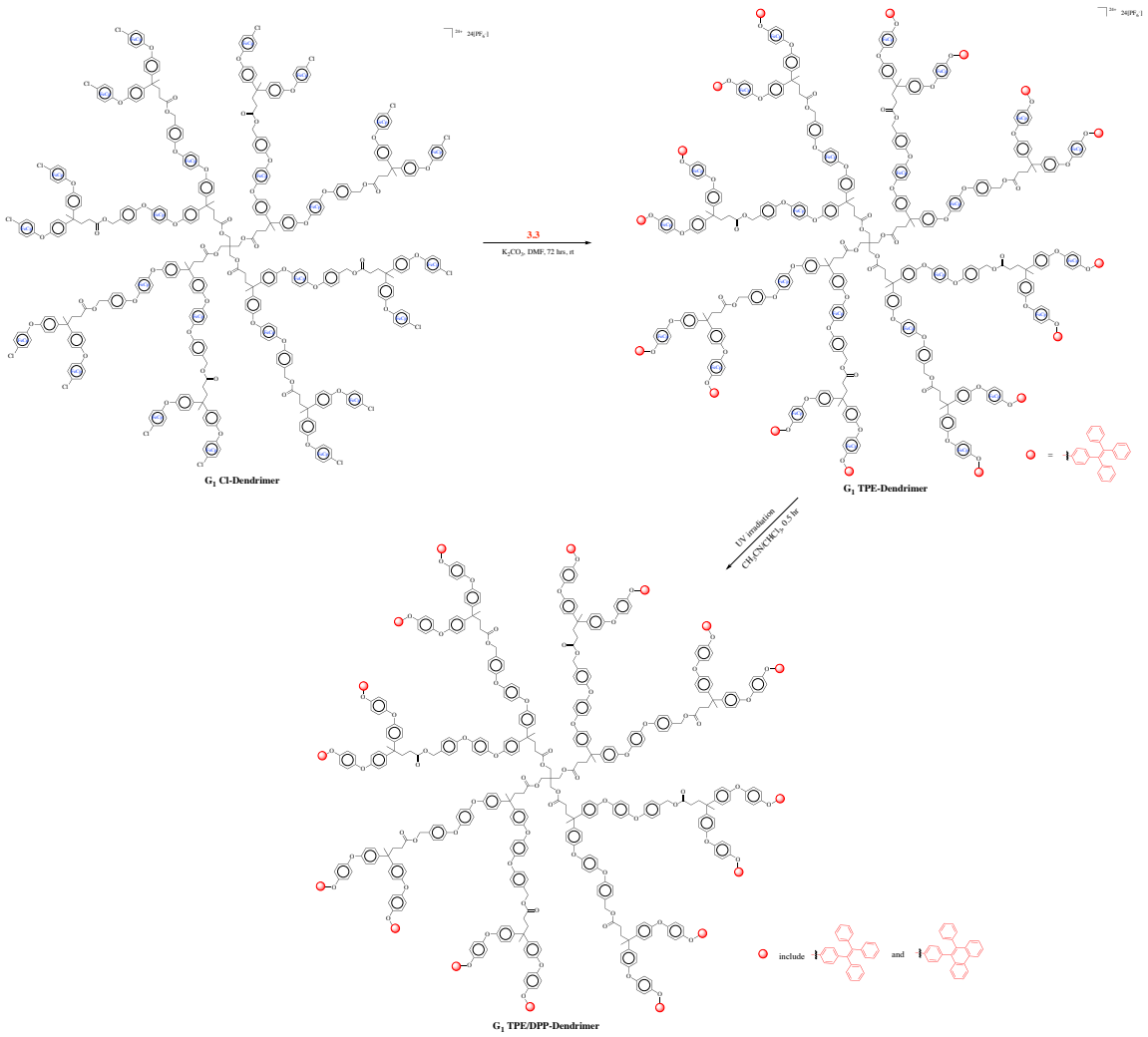

Scheme 3.3. Schematic representation of the synthesis of **G_1 TPE-dendrimer** and **G_1 TPE/DPP-dendrimer**.

The synthesis route to the dendrimers exploits the reactivity of $[\eta^6$-dichloroarene-η^5-CpFe$]^+$ towards many nucleophiles. The photoactive TPE-based nucleophile, 1-(4-hydroxyphenyl)-1,2,2-triphenylethylene (**3.3**), was synthesized using a previously reported procedure (Scheme 3.1)[28] and reacted with **G_0 Cl-dendrimer** or **G_1 Cl-dendrimer** *via* S_NAr reaction to obtain the TPE-capped organometallic dendrimers (**G_0 TPE-dendrimer** and **G_1 TPE-dendrimer**) (Schemes 3.2 and 3.3). UV irradiation of $CH_3CN/CHCl_3$ solution **G_0 TPE-dendrimer** or **G_1 TPE-dendrimer** in a

photochemical reactor converted some TPE to DPP moieties, yielding the hetero-functional **G_0 TPE/DPP-dendrimer** or **G_1 TPE/DPP-dendrimer**, respectively. Photoinduced conversion of TPE to DPP involved cyclization of the former to *trans*-4a,4b-dihydrodiphenylphenanthrene, followed by oxidation to DPP.[15] Here, oxygen in the solvent was enough to oxidize the TPE to DPP. The photochemical reaction also demetallates the organometallic dendrimers, converting them to organic dendrimers.

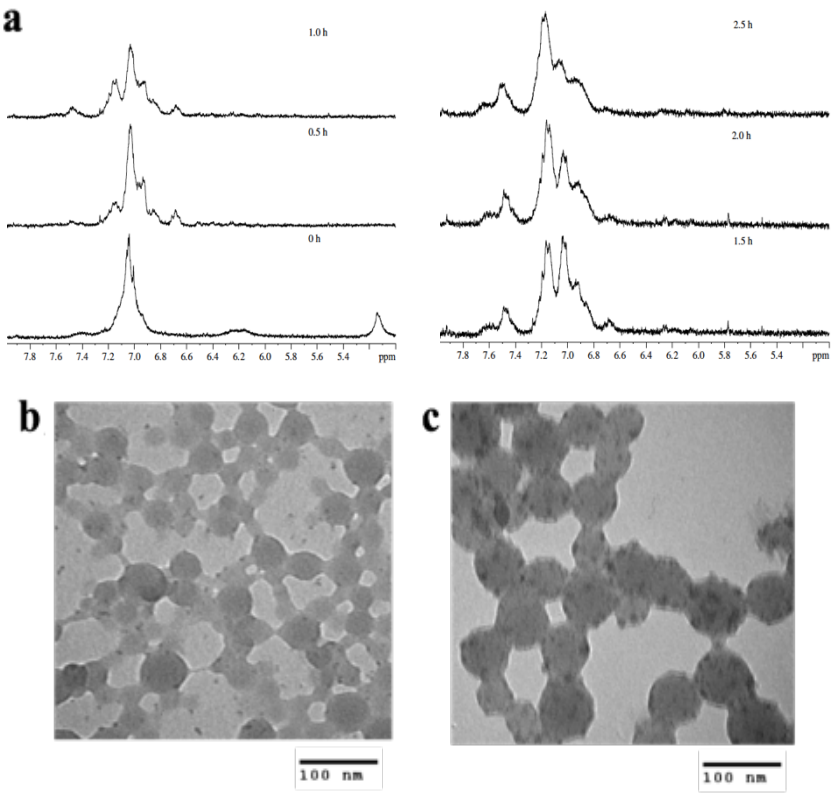

Figure 3.1. Photoinduced structural and morphological changes in TPE-dendrimers. Top, a) Representative ^{1}H NMR depicting the photochemical transformation of 10 μM of **G_0 TPE-dendrimer** in 100% THF-d_8. Bottom) Transmission electron micrographs depicting photoinduced change in size of nanoaggregates of 10 μM of **G_0 TPE-dendrimer** in THF/H_2O (10%:90%) mixture. b) before UV irradiation; c) after UV irradiation for 0.5 h.

The successful synthesis of the dendrimers was implied from their ^{1}H and ^{13}C NMR spectra, where characteristic peaks were observed to shift, disappear, or broaden after a reaction. For instance, the peak at 9.24 ppm corresponding to the hydroxyl proton of **3.3** disappeared after S_NAr reaction with **G_0 Cl-dendrimer** or **G_1 Cl-dendrimer**. Also, the progress of the photochemical reaction was monitored over time using ^{1}H NMR spectroscopy, which show the protons of the cyclopentadienyl ligand at 5.13 ppm and those of the iron-complexed arene ligand at 6.15 and 6.26 ppm disappeared after one hour irradiation (Figures 3.1a) suggesting demetallation as previously proved.[29-32] For instance, in **G_0 TPE-dendrimer**, the broad aromatic peak at 7.03 corresponding to overlapped peaks of aromatic protons decreased while new peaks appeared at 6.95 and 7.15 ppm (Figure 3.1a). Again, the intensity of the peak at 7.03 ppm decreased with time with a concurrent increase in the intensity of the peak at 7.15 ppm (Figure 3.1a), suggesting gradual conversion of TPE to DPP. Therefore, the peak at 7.03 ppm was assigned to TPE aromatic protons, and that at 7.15 ppm to DPP protons. As both peaks were present in **G_0 TPE/DPP-dendrimer** and **G_1 TPE/DPP-dendrimer**, it was assumed that the dendrimers were hetero-functional. Carbon and hydrogen analyses data support NMR spectroscopy results, further suggesting the successful synthesis of the organometallic dendrimers because the experimental percentages of carbons and hydrogens agreed with the calculated values for the **G_0 TPE-dendrimer** and **G_1 TPE-dendrimer**. Again, attempts to use mass spectrometry to quantitatively determine the TPE/DPP ratio in **G_0 TPE/DPP-dendrimer** and **G_1 TPE/DPP-dendrimer** was unsuccessful.

The dendrimers formed nanoaggregates in THF/H_2O solvent mixture. The photochemical reaction changed the size of these aggregates with transmission electron microscopic imaging showing an increase in the size of the aggregates from ~ 46 ± 7 nm to ~ 69 ± 8 nm (Figure 3.1b and c) after irradiation for 30 minutes in 10:90% THF/H_2O solvent mixture. This increase in size

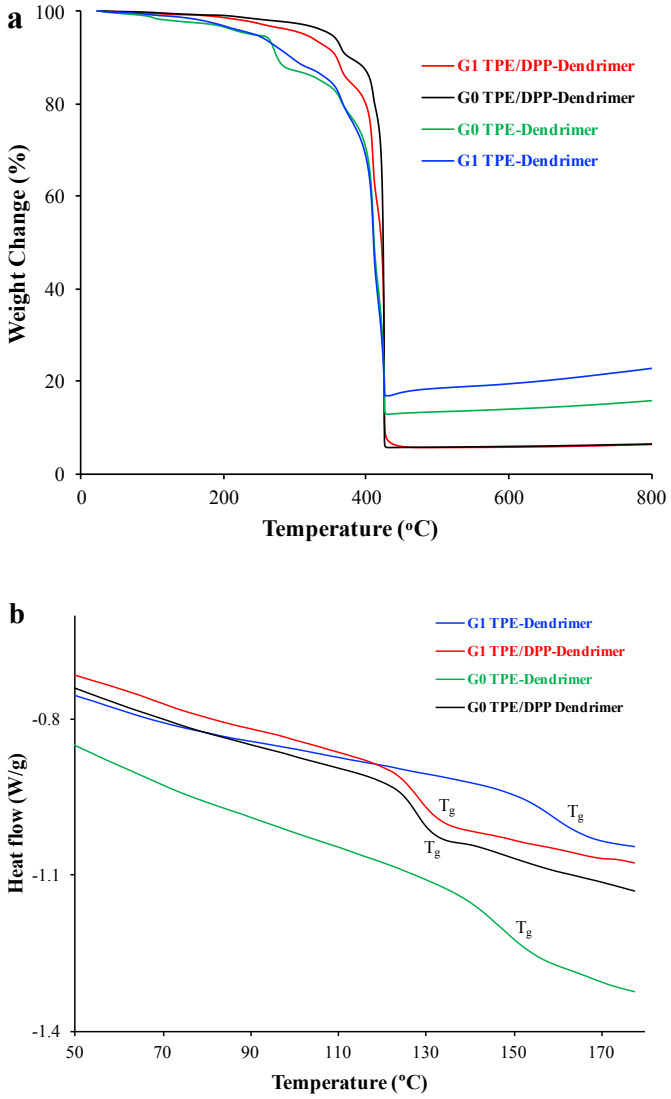

Figure 3.2. Thermal properties of TPE-containing dendrimers. (a) Thermal stability determined using thermogravimetric analysis; (b) glass transition temperatures (T_g) determined using differential scanning calorimetry. Blue: **G_1 TPE-dendrimer**; red: **G_1 TPE/DPP-dendrimer**; green: **G_0 TPE-dendrimer**; black: **G_0 TPE/DPP-dendrimer**.

is attributed to the hetero-functional nature of the dendrimers because a homo-functional TPE-dendrimer should be relatively more crystalline, leading to more compact packing, and eventually smaller size as observed in the TEM micrographs. Of fundamental interest were the glass transition temperatures (T_gs) and thermal stability of the homo-functional TPE-capped and hetero-functional

TPE/DPP-capped dendrimers. These thermal properties were markedly different, with the former dendrimers exhibiting higher T_gs but lower thermal stability compared to the latter (Figures 3.2).

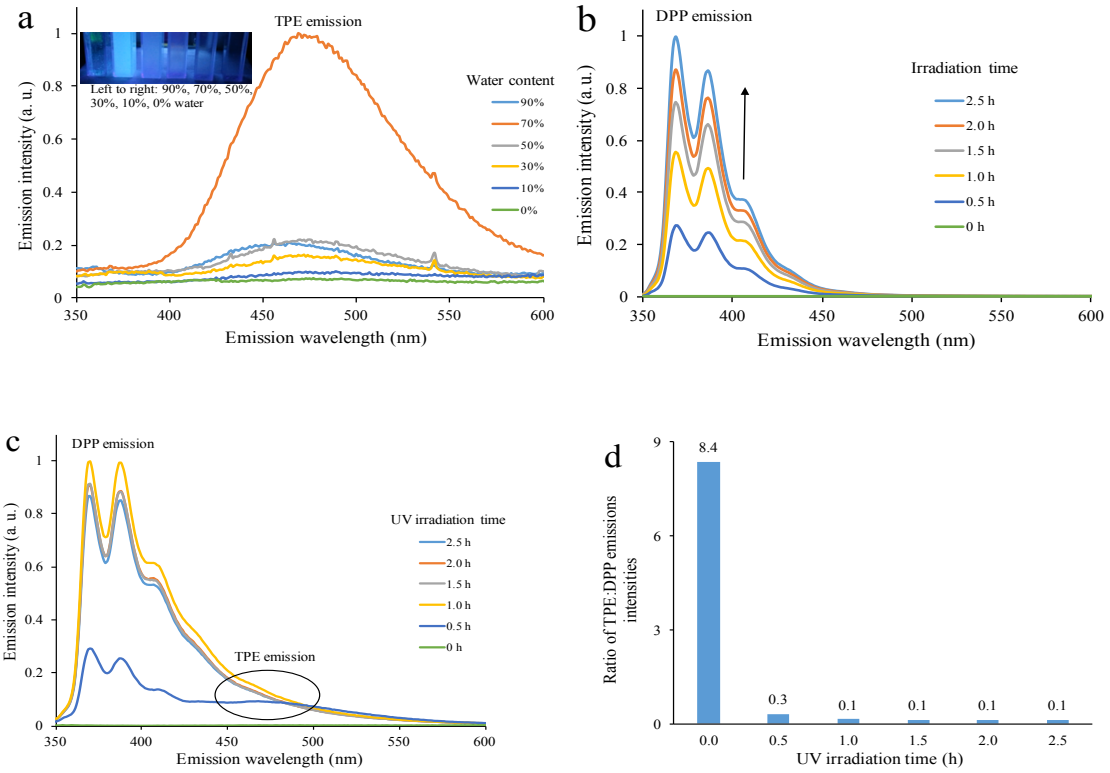

Figure 3.3. Fluorescence properties of 10 µM of dual-emissive organometallic TPE dendrimers excited at 320 nm. (a) Aggregation-induced emission (insert: photograph of **G_0 TPE-dendrimer** illuminated at 365 nm in THF/H_2O); (b) emission of DPP in 100% THF; (c) dual emission in THF/H_2O (30%:70%); d) ratio of TPE and DPP emissions intensities in THF/H_2O (30%:70%).

3.2.2. Photophysical and photochemical properties of dendrimers

The photophysics of the organometallic **G_0 TPE-dendrimer** and **G_1 TPE-dendrimer** was studied in 100% THF, and in THF/H_2O mixtures using fluorescence spectroscopy. Typical of TPE-systems,[1,2,14] the dendrimers did not emit in 100% THF, but emitted as aggregation was induced by the addition of water (Figure 3.3a). Emission intensity of TPE at 469 nm increased with

increasing water content in the THF/water mixture until the water content was increased above 70% when a noticeable decrease, as well as a blue shift from 469 nm to 464 nm, occurred. This quenching was also evident from visual inspection of 10 μM of THF/H_2O solutions of the dendrimers illuminated at 365 nm (Figure 3.3a insert). The emission quenching and the blue shifting are attributed to changes in the topology of the dendrimers at higher water content, possibly, leading to an interaction of the TPE units with other structures in the dendrimer, which eventually quenches the fluorescence. Indeed, with the naphthyl-capped dendrimers in *Chapter Two*, fluorescence was quenched by the dendrimer structure, and a report from another research group confirm this possibility.[26]

A key challenge in this study was imparting the dual emissive property on TPE-based systems by exploiting its photochemistry as well as the dendrimers' unique architecture. A 10 μM THF solution of the organometallic **G_0 TPE-dendrimer** and **G_1 TPE-dendrimer** was irradiated at 300 nm in a photochemical reactor, and the photophysics of the resulting solution probed using fluorescence spectroscopy. Before irradiation, **G_0 TPE-dendrimer** and **G_1 TPE-dendrimer** were not emissive but became emissive after 30 minutes irradiation (Figure 3.3b), featuring the characteristic DPP emission at 368 nm.[15,17,26] The intensity of the peak depends on irradiation time (Figure 3.3b), indicating that TPE was gradually transformed to DPP over time.[15,26] The photochemistry of the aggregates was also probed in THF/H_2O (30%:70%) mixture to understand the effect of UV irradiation on the AIE phenomenon and to modulate the dendrimer photo property to realize dual emissive behavior. There was a noticeable increase in the emission intensity of DPP with increasing irradiation time (Figure 3.3c). The ratio of TPE and DPP emissions intensity, which was higher than unity before irradiation, dropped below unity after UV irradiation (Figure 3.3d), suggesting transformation of TPE to DPP. Nonetheless, the dendrimers were dual emissive

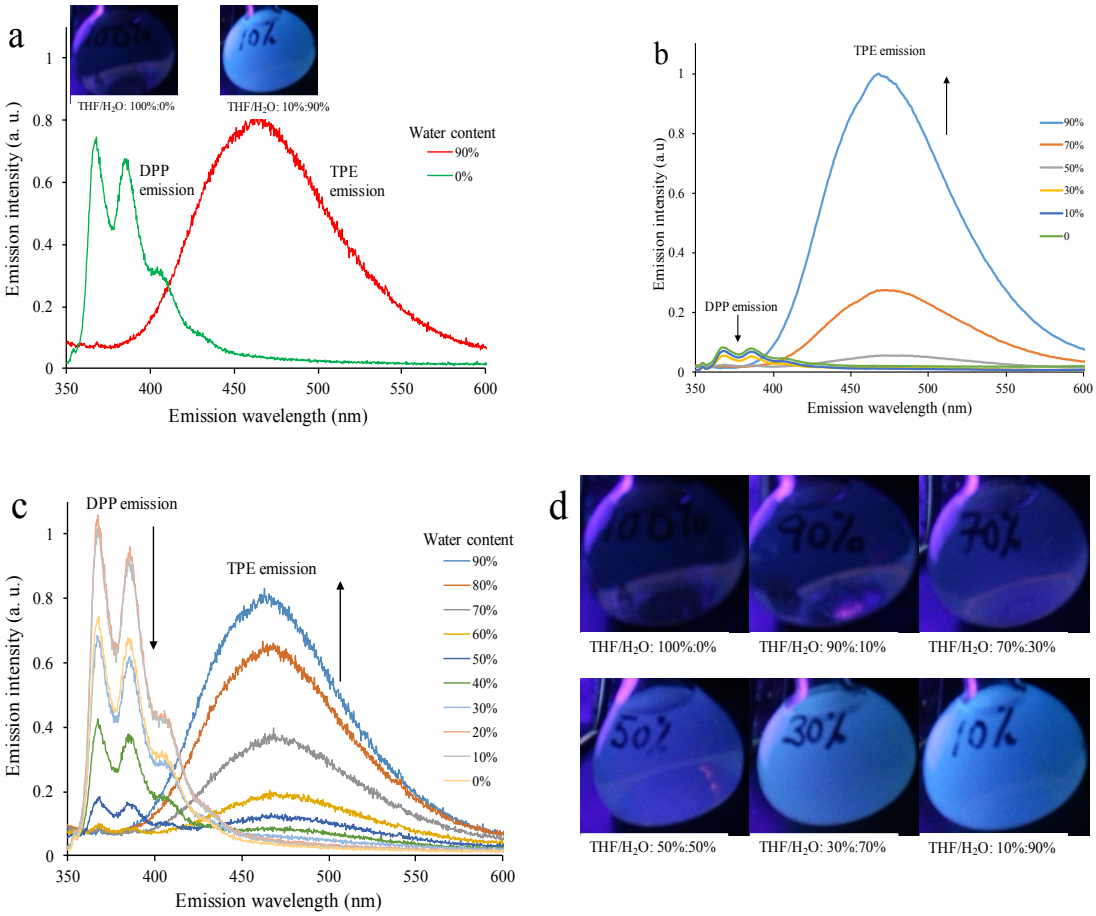

Figure 3.4. Fluorescence of hetero-functional TPE/DPP dendrimers excited at 320 nm. (a) Dual emission in 100% THF and in THF/H_2O (10%:90%). Dual emission tuned by photochemical reaction time for (b) 0.5 h; and (c) 5 h. (d) Photograph of 10 μM **G_0 TPE/DPP-dendrimer** in THF/H_2O mixture excited at 365 nm.

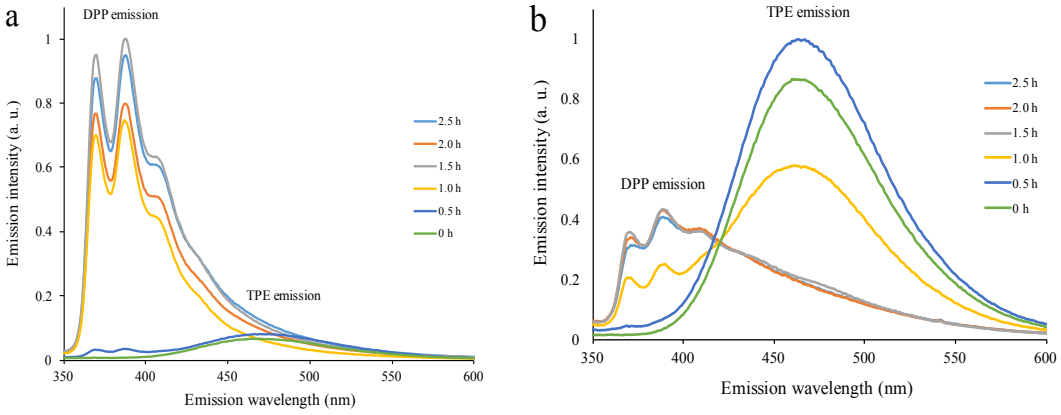

Figure 3.5. Fluorescence of dendrimers depicting dual emission of nanoaggregates. Dual emission in (a) 70%:30%; (b) 10%:90% THF/H_2O mixture.

in THF/H_2O (30%:70%) even after irradiation for 2.5 hours although the intensity of the TPE emission was weak compared with that of DPP (Figure 3.3c).

The AIE of **G_0 TPE-dendrimer** and **G_1 TPE-dendrimer** quenched at higher water content (Figure 3.3a). To circumvent this problem, the dendrimers were demetallated to obtain their organic analogs that were expected to feature enhanced emission. As previously demonstrated,[29-32] irradiating [η^6-arene-η^5-CpFe]$^+$- derived polymers with UV light, removes the cyclopentadienyliron(II) moieties. Demetallation was confirmed as the peak at 5.13 ppm corresponding to protons of the cyclopentadienyl ligand disappeared after photo-irradiation (Figures 3.1a). More importantly, this photochemical reaction aimed at photo-transforming the homo-functional **G_0 TPE-dendrimer** and **G_1 TPE-dendrimer**, to hetero-functional, **G_0 TPE/DPP-dendrimer**, and **G_1 TPE/DPP-dendrimer**, respectively.

The photophysical properties of the **G_0 TPE/DPP-dendrimer** and **G_1 TPE/DPP-dendrimer** were probed in THF and THF/H_2O mixture. Unlike **G_0 TPE-dendrimer** and **G_1 TPE-dendrimer**, in 100% THF, **G_0 TPE/DPP-dendrimer** and **G_1 TPE/DPP-dendrimer** emitted at 368 nm due to the presence of DPP moieties and at 469 nm due to AIE of TPE moieties (Figure 3.4a). In THF/H_2O, the intensity of the DPP emission decreased as the water content increased due to aggregation-caused quenching (ACQ) of DPP emission (Figures 3.4b-d). Conversely, increasing the water fraction of THF/H_2O mixture increased the emission intensity at 469 nm due to AIE of TPE (Figures 3.4b-d). Evidently, **G_0 TPE/DPP-dendrimer** and **G_1 TPE/DPP-dendrimer** were dual emissive as they emitted at two spectrally resolved wavelengths: 368 and 469 nm. (Figures 3.4a and b). The AIE of **G_0 TPE/DPP-dendrimer** and **G_1 TPE/DPP-dendrimer** was neither quenched nor blue shifted at high water fraction (Figures 3.4a and b), implicating the iron moieties with the quenching and blue shifting observed in **G_0 TPE-dendrimer** and **G_1 TPE-**

dendrimer. Also, the relative intensity of the emissions was tuned by the irradiation time of the photochemical reaction (Figures 3.4b and c), probably, due to change in the ratio of TPE and DPP moieties in the dendrimers. Specifically, increasing the irradiation time from 0.5 h to 5 h decreased the ratio of TPE and DPP emission intensities from ~ 12 to ~ 1, suggesting that the dual emissive behavior is tunable. Remarkably, the aggregates irradiated in THF/H_2O (70%:30%) for 0–0.5 h, and in THF/H_2O (10%:90%) for one hour were dual emissive, simultaneously emitting at 368 nm and 469 nm (Figures 3.5a and b).

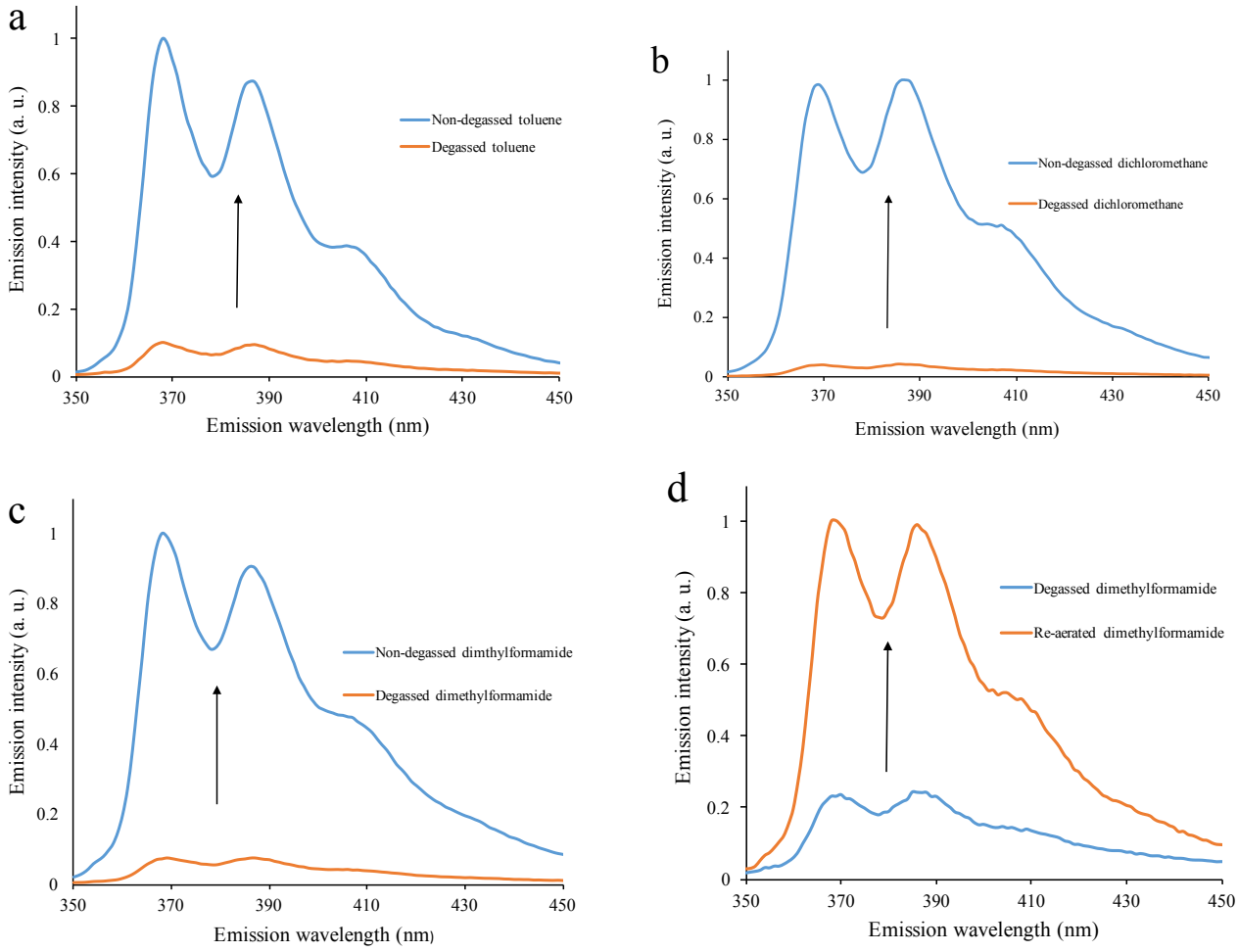

Figure 3.6. Fluorescent screening of degassed and non-degassed solvents (a) toluene; (b) dimethylformamide; (c) dichloromethane; (d) dimethylformamide using 10 μM **G_1 TPE/DPP-dendrimer** in the respective solvent.

3.2.3. Qualitative detection of dissolved oxygen in organic solvents

Dissolved oxygen in organic solvents create problems in many laboratory reactions as well as in many industrial processes.[33-35] For instance, dissolved oxygen in hydrocarbon feedstocks fouls and corrodes refinery units,[33,35] as well as shortens the shelf life of refinery products.[33] Detection of oxygen in organic solvents is, therefore, essential for the optimum performance of industrial plants, and ultimately, in reducing maintenance cost. The photoinduced conversion of TPE to DPP involved an oxidation step, which depends on oxidants such as oxygen,[14] and could be exploited in the detection of oxygen in organic solvents. This concept was tested by irradiating the solubilized dendrimers in representative degassed and non-degassed solvents for 0.5 hour. The dendrimers successfully screened degassed from non-degassed solvents as evidenced by the increased DPP emission intensity in the latter compared to the former solvent (Figures 3.6a-c). The turn-on optical method also successfully screened degassed and re-aerated solvents (Figure 3.6d). Turn-on optical techniques are emerging as alternatives to turn-off techniques, such as pyrene-based systems, which are less selective,[36] therefore, indicating the potential usefulness of these dendrimers.

3.3. Conclusion.

The first dual emissive TPE-based polymer was successfully synthesized using the synthesis route developed in *Chapter Two*. This demonstrates the versatility of the synthesis route in accessing other functional dendrimers. The dual emissive dendrimers emitted the typical DPP and TPE emissions at 368 nm and 469 nm, respectively. Control of irradiation time tuned the dual emissive property. The dependence of the photochemical conversion of TPE to DPP on oxygen was explored to screen degassed from non-degassed solvents, highlighting the possibility to use these hetero-functional dendrimers as turn-on sensors for oxygen.

3.4. Experimental section

3.4.1. Materials

All chemicals were reagent grade, and were used without further purification, unless otherwise stated. Toluene, dichloromethane, and tetrahydrofuran were purchased from Caledon Laboratories, and were purified by passing the solvents through an Innovative Technologies solvent purification system equipped with columns of alumina and copper catalysts. Other organic solvents except THF-d_8 were dried over activated 3 Å molecular sieves before use. The synthesis of **G_0 Cl-dendrimer** and **G_1 Cl-dendrimer** is detailed in *Chapter Two*.

3.4.2. Instrumentation

^{1}H and ^{13}C NMR spectra were recorded on a Bruker Avance NMR spectrometer (^{1}H, 300 MHz; ^{13}C, 75 MHz). For ^{1}H, and ^{13}C NMR experiments, DMSO-d_6, $CDCl_3$, THF-d_8, or D_2O was used as solvent with the chemical shifts internally referenced to DMSO-d_6, $CDCl_3$, or THF-d_8 residual proton peak in ppm. Elemental analyses, differential scanning calorimetry, and thermogravimetric analysis, UV-vis absorption measurements, transmission electron microscopy were carried out as described in *Chapter Two*. Steady-state fluorescence spectra were acquired on Photon Technology International QuantaMaster^{TM} 400 spectrophotometer.

3.4.3. Synthesis of 3.3

To synthesize **3.3**, a 250 mL two-necked round-bottom flask fitted with a reflux condenser was charged with 3.48 g (19.1 mmol) of benzophenone (**3.1**), 3.79 g (19.1 mmol) of 4-hydroxylbenzophenone (**3.2**), and 76.5 g (76.5 mmol) of zinc dust. The flask was evacuated under vacuum, and flushed with nitrogen thrice. Then 100 mL of dry tetrahydrofuran was added under an atmosphere of nitrogen. The mixture was stirred and maintained at –78 °C while 7.20 g (38.2

mmol) of $TiCl_4$ was added dropwise. The reaction mixture was warmed to room temperature, stirred for 0.5 hours, then refluxed for 24 hours. The reaction was quenched with 10% aqueous K_2CO_3 solution, and extracted with DCM three times. The extracts were washed with water, dried with $MgSO_4$, and concentrated under vacuum. The crude product was purified using silica gel column chromatography, and C_6H_{14}/DCM/$(CH_3)_2CO$/ (20:5:1) eluent to give **3.3**. Yield: 73%. ^{1}H NMR (300 MHz, DMSO-d_6): δ (ppm) 8.31 (1 H, s, ArO*H*), 7.09 (15 H, m, Ar*H*), 6.79 (2 H, d, J = 8.4 Hz, Ar*H*), 6.54 (2 H, d, J = 8.4 Hz, Ar*H*). ^{13}C {^{1}H} NMR (75 MHz, DMSO-d_6): δ (ppm) 157.97, 145.59, 145.46, 142.46, 140.88, 135.48, 133.58, 132.45, 132.40, 132.35 129.20, 129.13 127.95, 127.79. 127.65, 116.17.

3.4.4. Synthesis of G_0 TPE-dendrimer

To synthesize the dendrimer, a 50-mL round-bottom flask was charged with 1.00 g (0.24 mmol) of **G_0 Cl-dendrimer**, 0.66 g (1.90 mmol) of **3.3**, 0.66 g (4.74 mmol) of K_2CO_3 and 3 mL of DMF. The flask was flushed with dry nitrogen gas for 0.5 hour, afterward, the reaction mixture was stirred at 65 ºC overnight in the dark. To obtain the product, the reaction mixture was added to100 mL of 10% HCl solution, followed by the addition of 0.31 g (1.92 mmol) of NH_4PF_6. The precipitated product was filtered, and dried under vacuum. Yield: 89%. ^{1}H NMR (300 MHz, DMSO-d_6): δ (ppm) 7.33 (16 H, br s, Ar*H*), 7.07 (168 H, m, Ar*H*), 6.29 (16 H, br, s, complexed Ar*H*) 6.18 (16 H, br s, complexed Ar*H*), 5.17 (40 H, s, Cp*H*), 4.04 (8 H, br s, CH_2), 2.41 (8 H, br s, CH_2), 2.13 (8 H, br s, CH_2), 1.63 (12 H, br s, CH_3); ^{13}C{^{1}H} NMR (75 MHz, DMSO-d_6): δ (ppm) 173.21, 162.70, 152.20, 152.17, 146.32, 143.52, 143.36, 143.20, 143.04, 141.73, 141.58, 140.94, 139.82, 133.22, 131.09, 130.97, 130.33, 129.53, 128.32, 128.23, 128.17, 127.10, 126.89,

120.26, 120.15, 78.23, 75.58, 75.49, 45.34, 36.15, 31.09, 27.34. Elemental analyses: calculated for C, 65.83; H, 4.61; found for C, 66.19; H, 4.52.

3.4.5. Synthesis of G_1 TPE-dendrimer

To synthesize the dendrimer, a 50-mL round-bottom flask was charged with 1.44 g (0.11 mmol) of **G_1 Cl-dendrimer**, 0.61 g (1.76 mmol) of **3.3**, 0.61 g (4.40 mmol) of K_2CO_3, and 3 mL of DMF. The flask was flushed with dry nitrogen gas for 0.5 hour. Next, the reaction mixture was stirred in the dark at 65 ºC overnight. The product was obtained using work-up procedure similar to that used to obtained **G_0 TPE-dendrimer**. ^{1}H NMR (300 MHz, DMSO-d_6): δ (ppm) 7.36 (432 H, m, Ar*H*), 6.30 (64 H, br s, complexed Ar*H*), 6.19 (32 H, br s, complexed Ar*H*), 5.20 (40 H, s, Cp*H*), 5.17 (80 H, s, Cp*H*), 5.01 (16 H, br s, CH_2), 3.99 (8 H, br s, CH_2), 2.42 (16 H, br s, CH_2), 2.15, (32 H, br s, CH_2), 1.63 (36 H, br s, CH_3); ^{13}C{^{1}H} NMR (75 MHz, DMSO-d_6): δ (ppm) 173.09, 171.07, 162.67, 157.46, 152.22, 152.12, 146.28, 144.71, 143.94, 143.49, 143.36, 143.19, 143.00, 141.73, 141.53, 140.93, 139.83, 133.18, 131.07, 130.97, 130.53, 130.47, 130.34, 130.27, 129.58, 128.57, 128.31, 128.22, 128.15, 127.08, 126.86, 121.01, 120.83, 120.27, 120.16, 118.18, 117.96, 115.04, 78.24, 77.42, 75.61, 75.50, 75.46, 45.35, 36.31, 36.12, 31.13, 30.07, 27.34, 27.25. Elemental analyses: calculated for C, 62.77; H, 4.21; found for C, 62.59; H, 4.41.

3.4.6. Synthesis of G_0 TPE/DPP-dendrimer and G_1 TPE/DPP-dendrimer

A 7-mM $CH_3CN/CHCl_3$ (7:3) solution of the appropriate organometallic dendrimer, **G_0 TPE-dendrimer** or **G_1 TPE-dendrimer**, was placed in a Pyrex test tube, sealed, and degassed. The mixture was irradiated for 0.5 hour or 5 hours at 300 nm in a Rayonett photochemical reactor. The solvent was then removed under vacuum, and the residue washed with $(C_2H_5)_2O$ to remove the side product, ferrocene. The residue was dissolved in chloroform, washed with water three times,

dried with $MgSO_4$, and concentrated under vacuum. The product was precipitated from $(C_2H_5)_2O$ or C_6H_{14}. The demetallation of the dendrimer to give its organic analog was confirmed with ^1H NMR spectroscopy. The progress of the photochemical synthesis was also monitored with ^1H NMR spectroscopy.

3.4.7. Photophysical and photochemical characterizations

To probe the aggregation-induced emission, and dual emission of these dendrimers, a 100 μM stock THF solutions of the dendrimers was prepared. An aliquot (1 mL) of this stock solution was pipetted into a 10-mL volumetric flask, followed by the addition of an appropriate volume of THF, and dropwise addition of an appropriate volume of deionized water with vigorous agitation to furnish a 10 μM solution of specific THF/H_2O mixture. The water content was varied from 0–90 %. Immediately after sample preparation, the solutions were excited at 320 nm to probe their dual emission and AIE properties. For photochemical studies, 10 μM dendrimer solutions were irradiated for a specific time (0–150 min) at 300 nm in Rayonett photochemical reactor, and the emission, and ^1H NMR spectra as well as TEM images were taken immediately.

Reference

1. Mei, J.; Leung, N. L.; Kwok, R. T.; Lam, J. W.; Tang, B. Z. *Chem. Rev.* **2015**, *115*, 11718.
2. Zhao, Z.; He, B.; Tang, B. Z. *Chem. Sci.* **2015***, 6,* 5347.
3. Ding, Y.; Li, J.; Enterina, J. R.; Shen, Y.; Zhang, I.; Tewson, P. H.; Mo, G. C.; Zhang, J.; Quinn, A. M.; Hughes, T. E.; Maysinger, D.; Alford, S. C.; Zhang, Y.; Campbell, R. E. *Nat. Methods* **2015***, 12,* 195.
4. Zhuang, Y.; Xu, Q.; Huang, F.; Gao, P.; Zhao, Z.; Lou, X.; Xia, F. *ACS Sensors* **2016**, 1, 572.
5. Han, K.; Wang, S.; Lei, Q.; Zhu, J.; Zhang, X. *ACS Nano* **2015***, 9,* 10268.
6. Zhang, Y.; Song, Q.; Wang, K.; Mao, W.; Cao, F.; Sun, J.; Zhan, L.; Lv, Y.; Ma, Y.; Zou, B.; Zhang, C. *J. Mater. Chem. C* **2015***, 3,* 3049.
7. Zhang, X.; Xie, T.; Cui, M.; Yang, L.; Sun, X.; Jiang, J.; Zhang, G. *ACS Appl. Mater. Interfaces* **2014***, 6,* 2279.
8. Yuan, H.; Wang, K.; Yang, K.; Liu, B.; Zou, B. *J. Phys. Chem. Lett.* **2014***, 5,* 2968.

9. Chang, Z.; Jing, L.; Wei, C.; Dong, Y.; Ye, Y.; Zhao, Y. S.; Wang, J. *Chem. Eur. J.* **2015***, 21,* 8504.
10. Huang, Y.; Jiang, Y.; Yang, J.; Tang, R.; Xie, N.; Li, Q.; Kwok, H. S.; Tang, B. Z.; Li, Z. *J. Mater. Chem. C* **2014***, 2,* 2028.
11. Schelkle, K. M.; Bender, M.; Beck, S.; Jeltsch, K. F.; Stolz, S.; Zimmermann, J.; Weitz, R. T.; Pucci, A.; Müllen, K.; Hamburger, M.; Uwe, H. F. B. *Macromolecules* **2016**, *49*, 1518.
12. Ingrosso, C.; Bianco, G. V.; Corricelli, M.; Comparelli, R.; Altamura, D.; Agostiano, A.; Striccoli, M.; Losurdo, M.; Curri, M. L.; Bruno, G. *ACS Appl. Mater. Interfaces* **2015***, 7,* 4151.
13. Luo, J.; Xie, Z.; Lam, J. W. Y.; Cheng, L.; Chen, H.; Qiu, C.; Kwok, H. S.; Zhan, X.; Liu, Y.; Zhuc, D.; Tang, B. Z. *Chem.Commun.* **2001**, 1740.
14. Ma, Y.; Zeng, Y.; Liang, H.; Ho, C-L.; Zhao, Q. Z.; Huang, W.; Wong, W-Y. *J. Mater. Chem. C* **2015**, 11850.
15. Aldred, M. P.; Li, C.; Zhu, M. *Chem. Eur. J.* **2012***, 18,* 16037.
16. Schultz, A.; Laschat, S.; Diele, S.; Nimtz, M. *Eur. J. Org. Chem.* **2003***,* 2829.
17. Jiang, B.; Guo, D.; Liu, Y.; Wang, K.; Liu, Y. *ACS Nano* **2014***, 8,* 1609.
18. Zhang, G.; Palmer, G. M.; Dewhirst, M. W.; Fraser, C. L. A. *Nat. Mater.* **2009***, 8,* 747.
19. Grabowski, Z. R.; Rotkiewicz, K.; Rettig, W. *Chem. Rev.* **2003***, 103,* 3899.
20. Xiang, H.; Zhou, L.; Feng, Y.; Cheng, J.; Wu, D.; Zhou, X. *Inorg. Chem.* **2012***, 51,* 5208.
21. Guo, T.; Cui, L.; Shen, J.; Wang, R.; Zhu, W.; Xu, Y.; Qian, X. *Chem. Commun.* **2013***, 49,* 1862.
22. Xie, H.; Zeng, F.; Wu, S. *Biomacromolecules* **2014***, 15,* 3383.
23. Zijlstra, R. W.; van Duijnen, P. T.; Feringa, B. L.; Steffen, T.; Duppen, K.; Wiersma, D. A. *J. Phys. Chem. A* **1997***, 101,* 9828.
24. Schuddeboom, W.; Jonker, S. A.; Warman, J. M.; de Haas, M. P.; Vermeulen, M. J.; Jager, W. F.; de Lange, B.; Feringa, B. L.; Fessenden, R. W. *J. Am. Chem. Soc.* **1993***, 115,* 3286.
25. Mallory, F. B.; Wood, C. S.; Gordon, J. T. *J. Am. Chem. Soc.* **1964***, 86,* 3094.
26. Huang, G.; Ma, B.; Chen, J.; Peng, Q.; Zhang, G.; Fan, Q.; Zhang, D. *Chem. Eur. J.* **2012***, 18,* 3886.
27. Schreivogel, A.; Sieger, M.; Baro, A.; Laschat, S. *Helv. Chim. Acta* **2010***, 93,* 1912.
28. Hu, R.; Maldonado, J. L.; Rodriguez, M.; Deng, C.; Jim, C. K. W.; Lam, J. W. Y.; Yuen, M. M. F.; Ramos-Ortiz, G.; Tang, B. Z. *J. Mater. Chem*. **2012**, 232.
29. Abd-El-Aziz, A. S.; Todd, E. K.; Okasha, R. M.; Shipman, P. O.; Wood, T. E. *Macromolecules* 2005, 38, 9411.
30. Abd-El-Aziz, A. S.; Armstrong, D. A.; Bernardin, S.; Hutton, H. M. *Can J. Chem.* **1996**, *74*, 2073.
31. Gill, T. P.; Mann, K. R. *Inorg. Chem.* **1983**, *22*, 1986.
32. Martinez, V.; Blais, J.; Astruc, D. *Angew. Chem. Int. Ed.* **2003***, 42,* 4366.
33. Sato, T.; Hamada, Y.; Sumikawa, M.; Araki, S.; Yamamoto, H. *Ind. Eng. Chem. Res.* **2014***, 53,* 19331.
34. Wu, X.; Chung, K. H. *Energy Fuels* **2007***, 21,* 1212.
35. Wu, X. A.; Chung, K. H. *Ind. Eng. Chem. Res.* **2006***, 45,* 3707.
36. Germain, M. E.; Knapp, M. J. *Chem. Soc. Rev*. **2009**, *38*, 2543.

Chapter Four: Antimicrobial Organometallic Dendrimers[†‡]

Abstract

Examining the biological activity of η^6-arene-η^5-cyclopentadienyliron(II) ([η^6-arene-η^5-CpFe]$^+$) complexes is central to this research. This *Chapter* focuses on the biological, precisely the antimicrobial activity, of these complexes against drug-resistant microorganisms. In a preliminary study, a series of [η^6-arene-η^5-CpFe]$^+$ complexes were synthesized and evaluated for their activity against a panel of infection-causing microorganisms. A structure-activity relationship investigation revealed critical parameters that control the activity of these complexes. The demonstrated activity of these complexes provided the motivation to synthesize a series of [η^6-arene-η^5-CpFe]$^+$-derived dendrimers using the synthesis route established in *Chapter Two*. These dendrimers exerted potent activity against drug-resistant Gram-positive bacteria. To improve the activity, known antimicrobial agents were incorporated into the dendrimers' termini, yielding hybrid antimicrobial agents with enhanced activity. The studies also examined the cytotoxicity, and mechanism of activity of these dendrimers. These complexes induced oxidative stress and disrupted the cell membrane of Gram-positive bacteria, contributing to the overall activity. In vitro, these complexes were non-cytotoxic to human epidermal cell lines.

[†] This chapter is published as Abd-El-Aziz, A. S.; Agatemor, C.; Etkin, N.; Overy, D. P.; Kerr, R. G. *RSC Adv*. **2015**, *5*, 86421 and is reproduced by permission of The Royal Society of Chemistry. Another part is published as Abd-El-Aziz, A. S.; Agatemor, C.; Etkin, N.; Overy, D. P.; Lanteigne, M.; McQuillan, K.; Kerr, R. G. *Biomacromolecules* **2015**, *16*, 3694 and is reproduced by permission of The American Chemical Society. Another part is published as Abd-El-Aziz, A. S.; Agatemor, C.; Etkin, N.; Bissessur, R.; Overy, D. P.; Lanteigne, M.; McQuillan, K.; Kerr, R. G. *Macromol. Biosci.* **2017**, DOI: 10.1002/mabi.201700020 and is reproduced by permission of WILEY-VCH Verlag GmbH & KgaA, Weinheim.

[‡] All biological assay experiments were recommended by Agatemor, C. under the supervision of Professors Abd-El-Aziz, A. S. and Etkin, N. The experiments were run by Overy, D. P.; Lanteigne, M.; McQuillan, K. in Professor Kerr R. G. Laboratory and the results interpreted by Agatemor, C. under the supervision of Abd-El-Aziz, A. S. and Etkin, N.

4.1. Introduction

Drug-resistant infections pose an enormous threat to our society, as an annual 10 million losses in human lives and a 100 trillion USD cost to the global economy is projected by 2050.[1] Consequently, there is an accelerated interest in the discovery of new antimicrobial agents that curb the virulence of drug-resistant microorganisms. Recently, attention is focused on organometallic antimicrobial agents,[2-10] with the assumption that the functionality offered by the presence of a metal in the antimicrobial agent will, possibly, provide a new mechanism of action that bypass resistance mechanisms in the drug-resistant microorganisms. This attention is stirred by the established biological activity of cisplatin, an anticancer platinum-containing drug, and ferroquine, an antimalarial iron-containing compound. Indeed, ferroquine is effective against chloroquine-resistant strains of *Plasmodium falciparum*.[11] A subcellular probe of *P. falciparum* after treatment with the ferroquine indicates increased reactive oxygen species (ROS), which were implicated in causing oxidative damage to the cells, ultimately killing the parasite.[11] This mechanism of action is linked to the redox chemistry of ferrocene, which under physiological conditions oxidizes to the 17-electron ferrocenium cation that catalyzes the in vivo generation of ROS.[7,11]

The redox-active monocation η^6-arene-η^5-cyclopentadienyliron(II) ([η^6-arene-η^5-CpFe]$^+$) complex is a derivative of ferrocene. Unlike ferrocene, which is at the forefront of organometallic medicinal chemistry, interest in the biological activity of these complexes is low despite its rich redox chemistry. Like ferrocene, [η^6-arene-η^5-CpFe]$^+$ oxidizes to the 17-electron dication complex, [η^6-arene-η^5-CpFe]$^{2+}$, a stronger oxidizing agent than ferrocene.[12] While the redox chemistry of ferrocene differs from that of [η^6-arene-η^5-CpFe]$^+$ complex, it is still reasonable to assume that under physiological conditions, the complex could also be oxidized to its 17-electron

$[\eta^6$-arene-η^5-CpFe$]^{2+}$ analog, which could catalyze the generation of ROS, eventually inducing oxidative stress. While oxidative stress damages cells, it is a cellular defense strategy employed against a broad spectrum of microorganisms.[13-16] Thus, the hypothesis that $[\eta^6$-arene-η^5-CpFe$]^+$ is an antimicrobial agent. The present work tests this hypothesis by evaluating the antimicrobial activity of these complexes as molecules and as functional moieties in organometallic polymers. Interest in antimicrobial organometallic polymers is emerging,[8] with organometallic dendrimers, a special type of polymer, yet-to-be-explored. As it is acknowledged that dendrimers have immense potentials in the biomedical field, developing an antimicrobial organometallics dendrimer is, therefore, attractive and is a key objective in this study.

The synthesis route developed in *Chapter Two* was slightly modified to afford a series of $[\eta^6$-arene-η^5-CpFe$]^+$-derived dendrimers. The presence of redox-active $[\eta^6$-arene-η^5-CpFe$]^+$ in the dendrimers is expected to cause oxidative damage to microorganisms. Also, as cationic polymers are known to exert antimicrobial activity by disrupting the microbial cell membrane, the cationic charge on the complex is expected to act in a similar manner to enhance the antimicrobial activity. The presence of two different mechanisms of action in a single antimicrobial agent is posit as an effective treatment for drug-resistant infections.[1] This postulation further inspired the design of a series of hybrid antimicrobial dendrimers by functionalizing the dendrimers with known antimicrobial agents, specifically, quaternary ammonium groups or 2-mercaptobenzothiazole. The dendrimers were evaluated for their activity against infection-causing microorganisms that included *Candida albicans*, *Pseudomonas aeruginosa*, *Proteus vulgaris*, methicillin-resistant *Staphylococcus aureus* (MRSA), vancomycin-resistant *Enterococcus faecium* (VRE) and *Staphylococcus warneri*. Structure-activity relationship investigation was conducted to understand critical parameters that affect the activity of these complexes as molecule and as moieties in the

dendrimers. The dendrimers were also screened for their activity against human epidermal keratinocytes cells (HEka), human foreskin BJ fibroblast cells and mammalian, specifically, sheep red blood cells.

4.2. Results and discussion

4.2.1. Synthesis and characterization of $[\eta^6$-arene-η^5-CpFe$]^+$complexes

The increasing prevalence of antimicrobial resistance coupled with the decreasing number of effective antibiotics stresses a need for new treatment options. To identify new antimicrobial agents, organometallic compounds are explored[2-5,7,8,17-19] and metallocenes such as ferrocene (**4.1a**) (Figure 4.1) are emerging as effective candidates.[5,7] Here, a series of ferrocene derivatives, $[\eta^6$-arene-η^5-CpFe$]^+$ complexes (Scheme 4.1), were synthesized and assessed for their activity against representative infection-causing microorganisms with the objective of understanding the biological activity of these complexes and introducing new antimicrobial agents. These complexes (**4.1**–**4.4**) were obtained *via* the well-established ligand exchange reaction of the appropriate arene with ferrocene (Scheme 4.1).[20-25] Through nucleophilic aromatic substitution (S_NAr) reaction of the appropriate $[\eta^6$-arene-η^5-CpFe$]^+$ with 4,4′-bis(4-hydroxyphenyl)valeric acid or 4,4′-thiobisbenzenethiol, bimetallic complexes (**4.5** and **4.6**) were also synthesized (Scheme 4.2).[26] The NMR spectra of these complexes agreed with previous reports.[20-26]

4.2.2. Synthesis and characterization of dendrimers

The G_0 dendrimers were synthesized from $[\eta^6$-1,4-dichlorobenzene-η^5-CpFe$]^+$, $[\eta^6$-1-chloro-4-methylbenzene-η^5-CpFe$]^+$ or $[\eta^6$-chlorobenzene-η^5-CpFe$]^+$ complex using the general synthesis route established in *Chapter Two* and illustrated in Schemes 4.3 and 4.4. The synthesis route was

slightly modified to afford a series of dendrimers with tetrafluoroborate (BF_4^-) counteranion in addition to a hexafluorophosphate (PF_6^-) series. The change in counteranion was designed

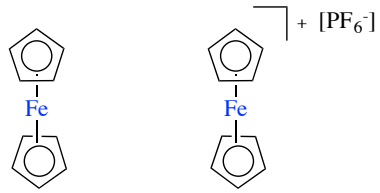

4.1a **4.1b**

Figure 4.1. Schematic representation of complexes **4.1**

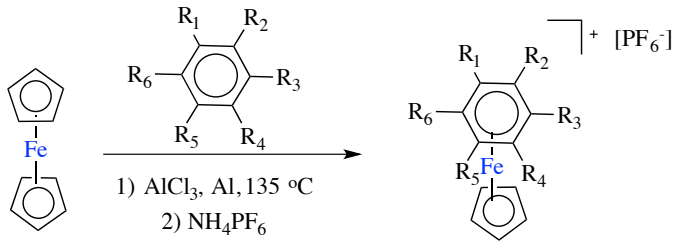

4.1a **4.2 - 4.4**

	R_1	R_2	R_3	R_4	R_5	R_6
4.2a	H	H	H	H	H	H
4.2b	CH_3	H	H	H	H	H
4.2c	CH_3	H	H	CH_3	H	H
4.2d	CH_3	CH_3	H	CH_3	CH_3	H
4.2e	CH_3	CH_3	CH_3	CH_3	CH_3	CH_3
4.2f	H	H	H	H	H	CH_2CH_3
4.3a	Cl	H	H	H	H	H
4.3b	Cl	H	H	CH_3	H	H
4.3c	Cl	H	H	Cl	H	H
4.4a	NH_2	H	H	H	H	H
4.4b	CHO	H	H	H	H	H

Scheme 4.1. Schematic representation of the synthesis of complexes **4.2**–**4.4**.

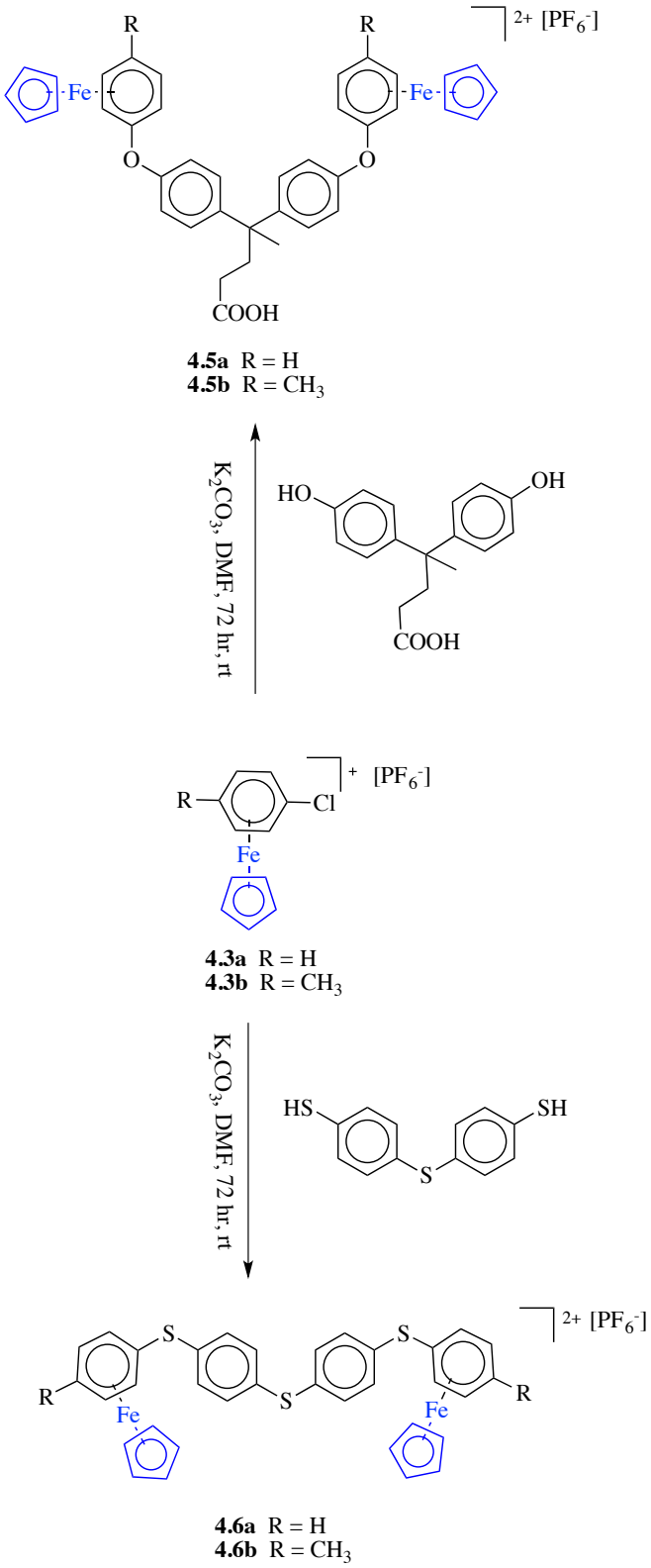

Scheme 4.2. Schematic representation of the synthesis of **4.5** and **4.6**.

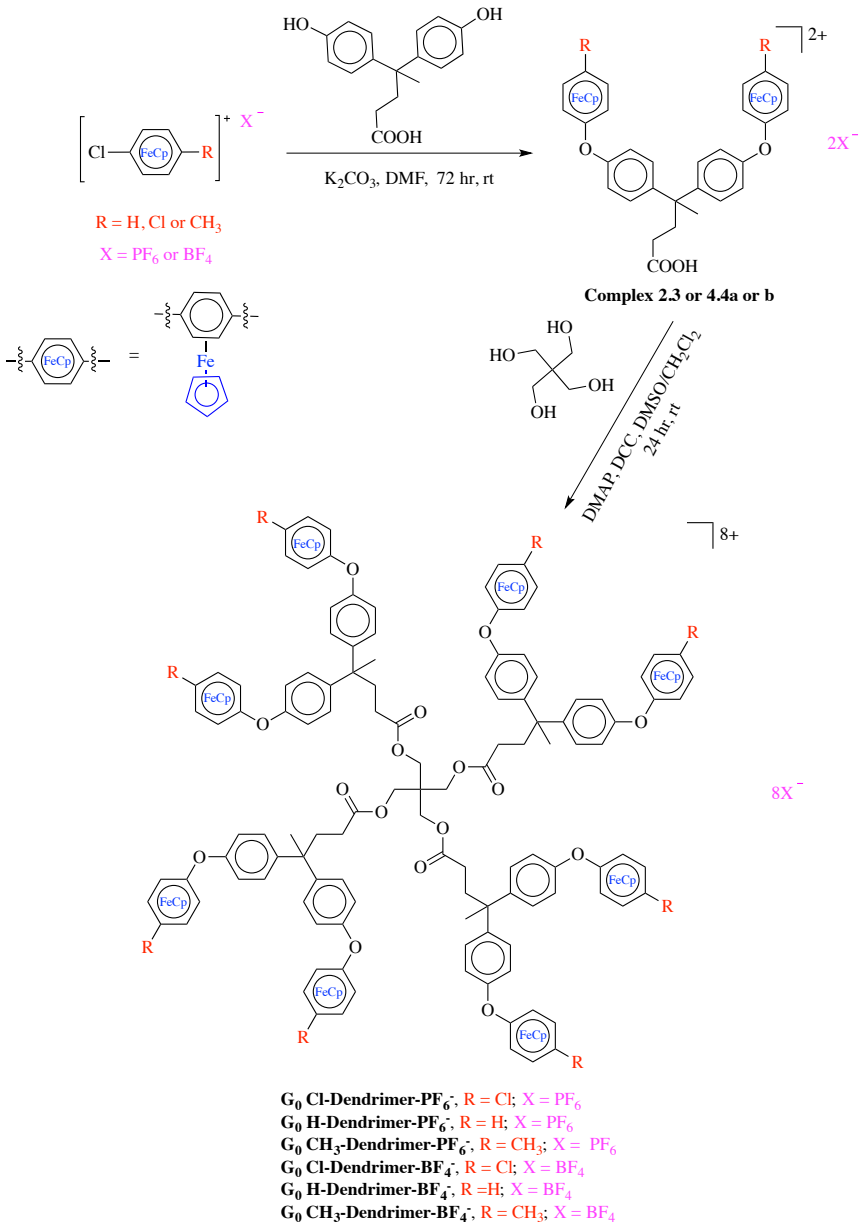

Scheme 4.3. Schematic representation of the synthesis of G_0 antimicrobial organometallic dendrimers.

to modify the solubility of the dendrimers in aqueous media as previously reported.[27] Further, changing the substitution on the arene ligand by using different arenes, 1,4-dichlorobenzene, 1-chloro-4-methylbenzene, or chlorobenzene, we expect to tune the redox activity of the iron, and ultimately the antimicrobial activity. As previously proved,[28-30] the substitution on the arene ligand

was also designed to modulate the lipophilicity of the dendrimers. A set of G_1 dendrimers were synthesized (Scheme 4.4) to gain insight into the influence of dendritic effect on antimicrobial activity. The dendrimers were characterized using ^{1}H, ^{13}C, ^{11}B, and ^{31}P NMR as well as CH analyses. The expected characteristic NMR peaks were found (Experimental section) and suggest the successful synthesis of the dendrimers. Data from elemental analyses (Experimental section), which complemented NMR data, also suggest successful syntheses.

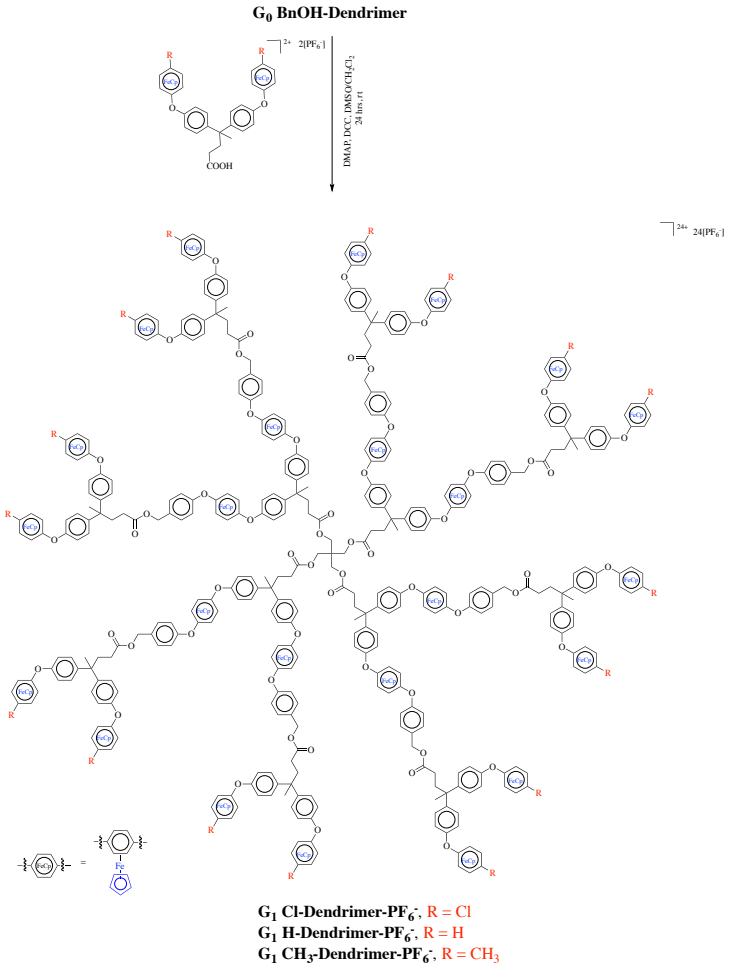

Scheme 4.4. Schematic representation of the synthesis of G_1 antimicrobial organometallic dendrimers.

The redox activity of $[\eta^6$-arene-η^5-CpFe$]^+$ complexes is well documented[23-25,31,32], and this activity was confirmed in these dendrimers using cyclic voltammetry (Table 4.1). The cyclic voltammetry was carried out at room temperature in propylene carbonate solution of the dendrimers. Changing the substitution on the arene ligand affected the redox activity of the dendrimers (Table 4.1) as expected. For instance, the reduction potential (E_{pc}) differed noticeably between dendrimers derived from the 1,4-dichlorobenzene (**G_0 Cl-dendrimer-PF_6^-** and **G_0 Cl-dendrimer-BF_4^-**) and those from the chlorobenzene ligand (**G_0 H-dendrimer-PF_6^-** and **G_0 H-dendrimer-BF_4^-**) (Table 4.1). Of course, the chloro groups in **G_0 Cl-dendrimer-PF_6^-** and **G_0 Cl-dendrimer-BF_4^-** are electron withdrawing, decreasing the electron density at the iron centre, and ultimately increasing susceptibility of the iron to reduction. As previously shown,[33] exchanging PF_6^- with BF_4^- did not change the redox property of the dendrimers (Table 4.1); however, the counteranion exchange affected the aqueous solubility of the dendrimers. Counteranion exchange is a demonstrated strategy for controlling the aqueous solubility of cationic polymers.[27] Here, the BF_4^- series of dendrimers were relatively more water-soluble than the PF_6^- series, as suggested by their lower percent yield, ~57% for BF_4^- *vs* ~74% for PF_6^- series. It is also worth noting that the BF_4^- series were tedious to work with due to their enhanced aqueous solubility. As demonstrated in previous reports,[34,35] the counteranion exchange affected the glass transition temperature (T_g) of the dendrimers with the PF_6^- series exhibiting slightly higher T_g than the BF_4^- series (Table 4.1). In these previous reports,[34,35] the trend in T_g was attributed to the presence of hydrogen bonding interactions in PF_6^- polymers. With these dendrimers, hydrogen bonding between the fluorine atoms in the counteranions and the aromatic hydrogens is probable. Indeed, a previous report on density functional theory calculations provided evidence of hydrogen bonding interactions between the fluorine atoms in these counteranions and the hydrogens of thiophenes.[36]

As there are more fluorine atoms in PF_6^- than in BF_4^-, it may be reasonable to assume that the interactions will be slightly stronger in the PF_6^- series of dendrimers, accounting for their slightly higher T_g.

Table 4.1. Reduction potential, glass transition temperature, diffusion coefficient, and hydrodynamic radii of dendrimers.

dendrimer	E_{pc} (V)[a]	T_g (°C)[b]	R_h (nm)[c]
G_0 Cl-Dendrimer-PF_6^-	–1.25	136	1.28
G_0 H-Dendrimer-PF_6^-	–1.49	122	1.28
G_0 CH_3-Dendrimer-PF_6^-	–1.49	126	1.46
G_0 Cl-Dendrimer-BF_4^-	–1.19	122	nd[d]
G_0 H-Dendrimer-BF_4^-	–1.48	118	1.18
G_0 CH_3-Dendrimer-BF_4^-	–1.50	116	1.22
G_1 Cl-Dendrimer-PF_6^-	–1.23	178	1.77
G_1 H-Dendrimer-PF_6^-	–1.41	144	1.69
G_1 CH3-Dendrimer-PF_6^-	–1.41	142	1.89

[a]Reduction potential obtained from cyclic voltammetry (CV). CV experiments were carried out on nitrogen purged, 6 mM solution of dendrimer in propylene carbonate at room temperature. Scan rate, 0.1 V/s; supporting electrolyte, 0.1 M [n-Bu_4N][PF_6] or [n-Bu_4N][BF_4]. [b]Glass transition temperature determined from differential scanning calorimetry. [c]Hydrodynamics radii determined from diffusion-order spectroscopy. [d]Not determined.

Further, diffusion-order spectroscopy (DOSY) NMR was used to gain insight into the size of the dendrimers in solution, as size is a parameter that influences the diffusion of chemotherapeutics through the cell wall.[37] The diffusion coefficient obtained from the DOSY NMR experiments is related to the hydrodynamic radii of the dendrimers by the Stokes–Einstein equation.[38] Typical of dendrimers,[39,40] these dendrimers were nanoscopic with the hydrodynamic radii increasing with generation (Table 4.1). The results also show that the dendrimer with methyl

groups had larger radii than the other dendrimers. In addition, the counteranion also affected the radii of the dendrimers with the BF_4^- series being smaller than the PF_6^- series (Table 4.1).

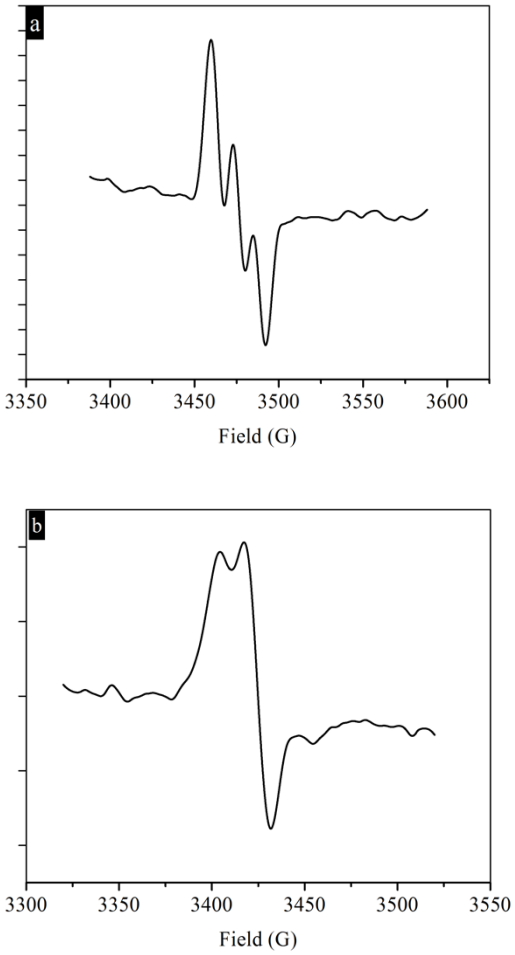

Figure 4.2. Electron spin resonance spectra of nitroxyl radical generated by reaction of **G_0 Cl-dendrimer-PF_6^-** with nitrosobenzene spin trap. At (a) room temperature, (b) 77 K. Experimental settings: microwave power = 15 mW, frequency = 9768.84 MHz.

It is assumed that the biological activity of ferrocene depends on its redox activity, which catalyzes the generation of free radicals that eventually cause oxidative damage to cells.[41] Driven by this assumption, electron spin resonance (ESR) spectroscopy was used to probe the dendrimers

for their ability to form radicals. With nitrosobenzene (PhNO) as a spin trap, evidence of free radicals in DMSO/H_2O solution of the **G_0 Cl-dendrimer-PF_6^-** was found. At room temperature, **G_0 Cl-dendrimer-PF_6^-**/PhNO in DMSO/H_2O solvent mixture gave an EPR resonance at g_{iso} = 2.008, which is typical of nitroxyl radicals,[41,42] (Figure 4.2a). Further, characteristic of nitroxyl radicals at 77 K,[41] the **G_0 Cl-dendrimer-PF_6^-**/PhNO mixture gave an anisotropic nitrogen-split triplet EPR resonance at $g_{1,2,3}$ = 2.010, 2.005, 1.998 (Figure 4.2b). This finding is exciting as it demonstrates for the first time that 18-electron iron sandwich complex, $[\eta^6$-arene-η^5-CpFe$]^+$, could initiate the generation of free radicals. Indeed, its counterparts, the 19-electron, and 17-electron iron sandwich complexes are well-known to form radicals, which account for their well-explored biological activity.[41-48] Here, the mechanistic scenario leading to the formation of these radicals and their exact nature are yet to be understood and could be a goal of a future study. Nonetheless, this finding hints a free radical-dependent biological activity for this family of dendrimers.

4.2.3. Synthesis and characterization of hybrid antimicrobial dendrimers

The chemistry of the complex allows functionalization of **G_0 Cl-dendrimer-PF_6^-** and **G_1 Cl-dendrimer-PF_6^-** with a nucleophilic antimicrobial agent to obtain hybrid antimicrobial organometallic dendrimers. Two hybrids, **G_0 thiazole-dendrimer-PF_6^-** and **G_1 thiazole-dendrimer-PF_6^-**, were obtained by functionalizing **G_0 Cl-dendrimer-PF_6^-** and **G_1 Cl-dendrimer-PF_6^-** with 2-mercaptobenzothiazole, respectively (Schemes 4.5). Through a series of reactions, **G_0 Cl-dendrimer-PF_6^-** and **G_1 Cl-dendrimer-PF_6^-** were also functionalized with quaternary ammonium groups to afford **G_0 R_4N^+-dendrimer-PF_6^-** and **G_1 R_4N^+-dendrimer-PF_6^-**, respectively (Schemes 4.6). The objective was to obtain antimicrobial dendrimers with superior activity over their constituent bioactive parts, **G_0 Cl-dendrimer-PF_6^-**, **G_1 Cl-dendrimer-PF_6^-** or

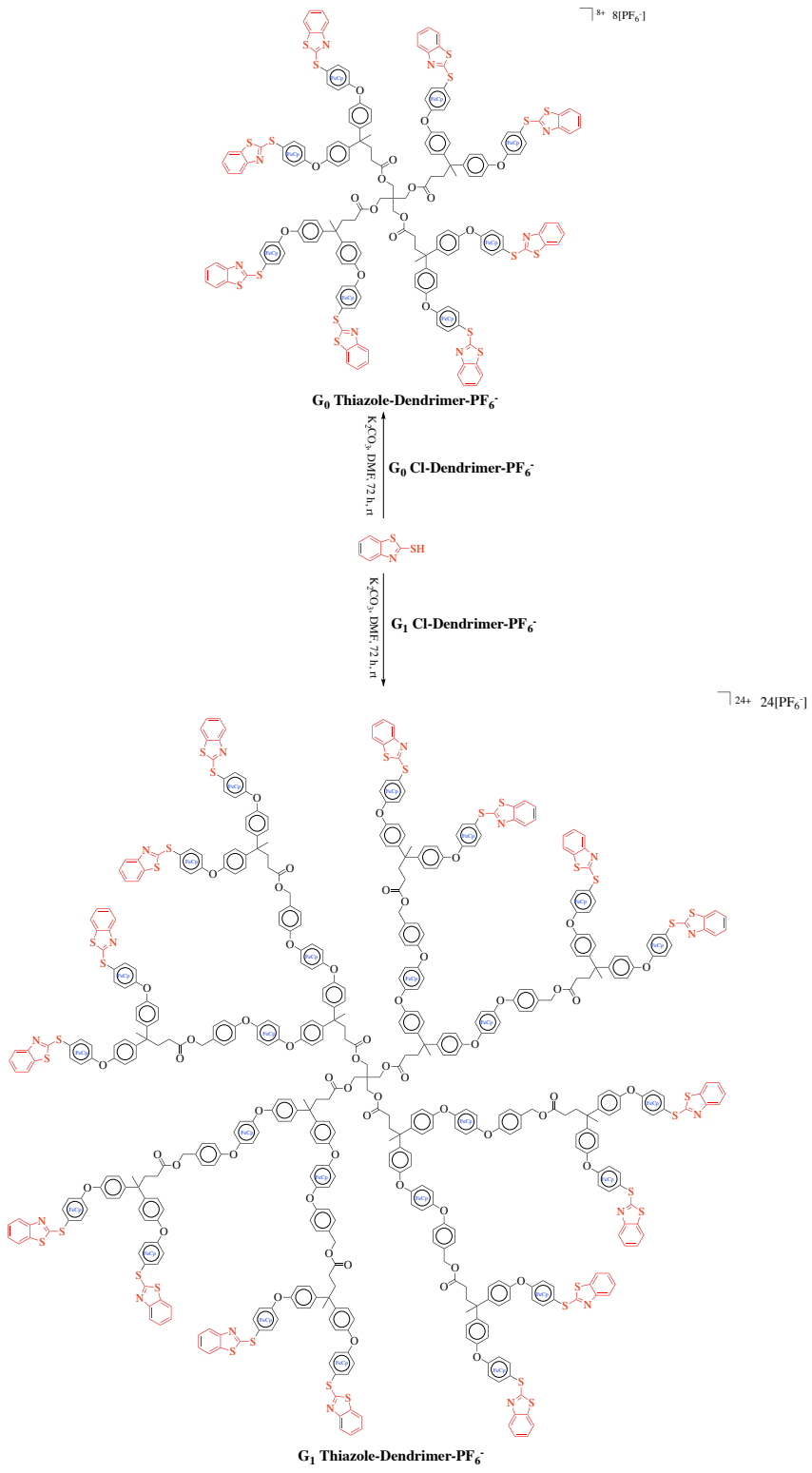

Scheme 4.5. Schematic representation of the synthesis of thiazole-functionalized hybrid antimicrobial dendrimers.

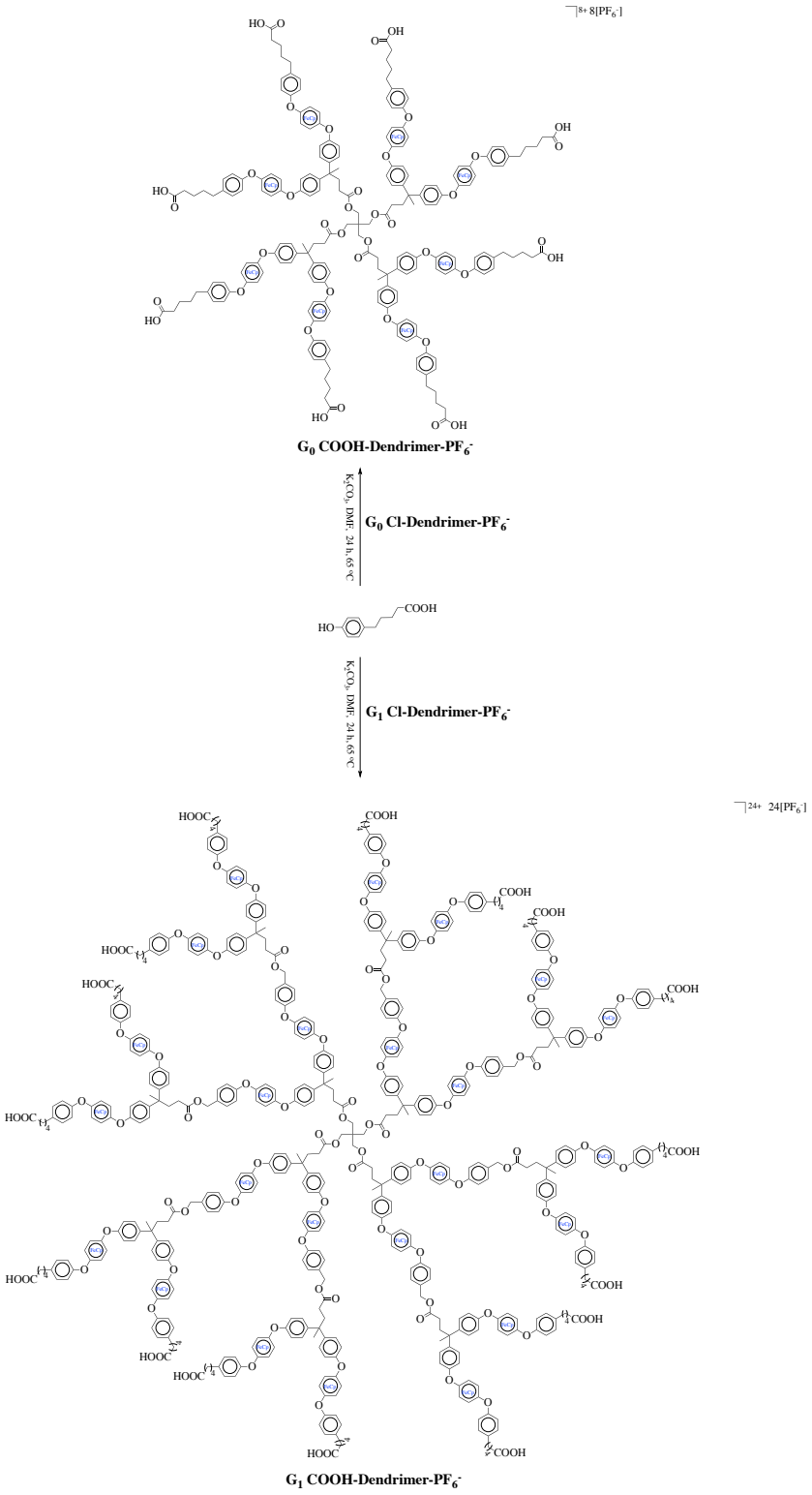

Scheme 4.6. Schematic representation of the synthesis of **G_0 COOH-dendrimer-PF_6^-** and **G_1 COOH-dendrimer-PF_6^-**.

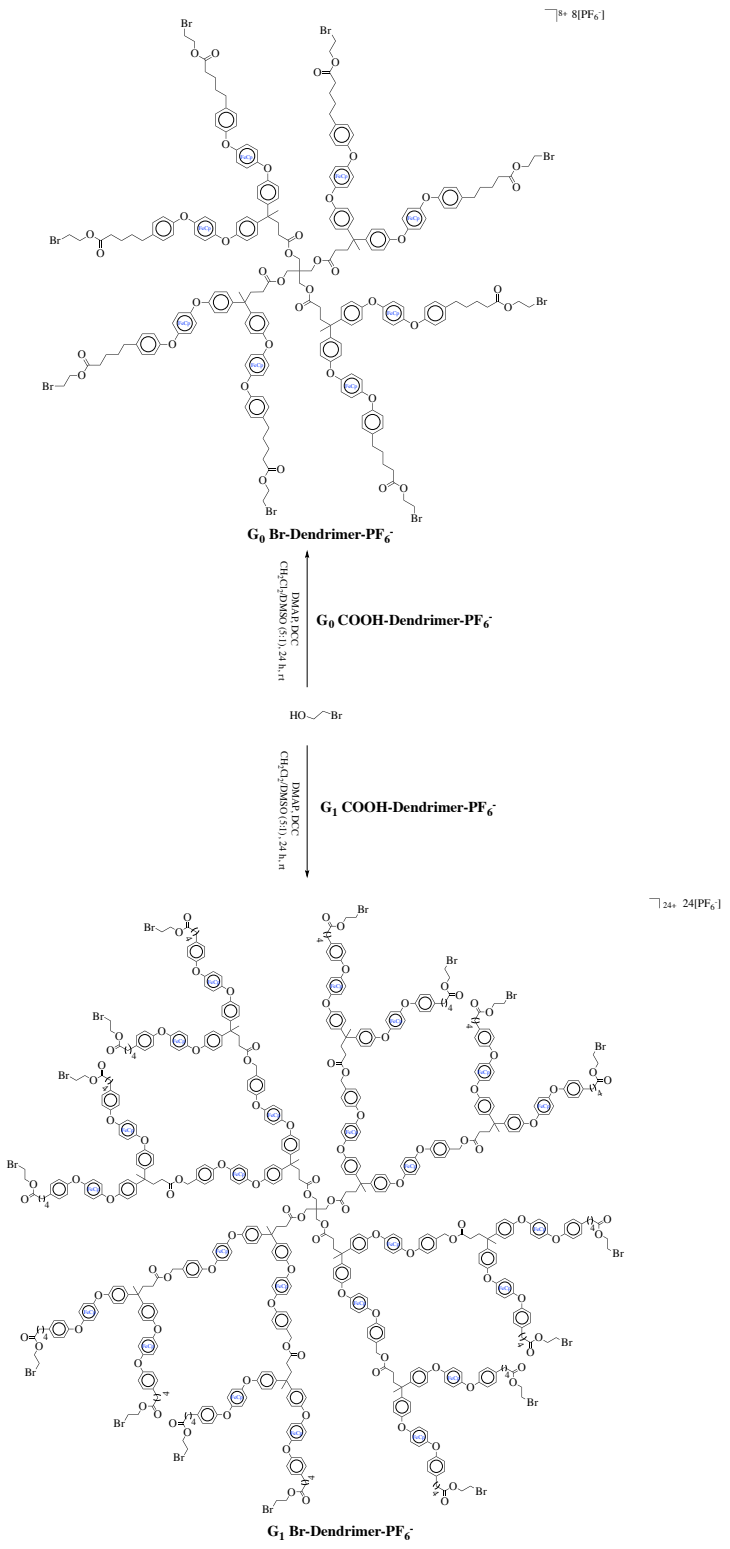

Scheme 4.7. Schematic representation of the synthesis of **G_0 Br-dendrimer-PF_6^-** and **G_1 Br-dendrimer-PF_6^-**.

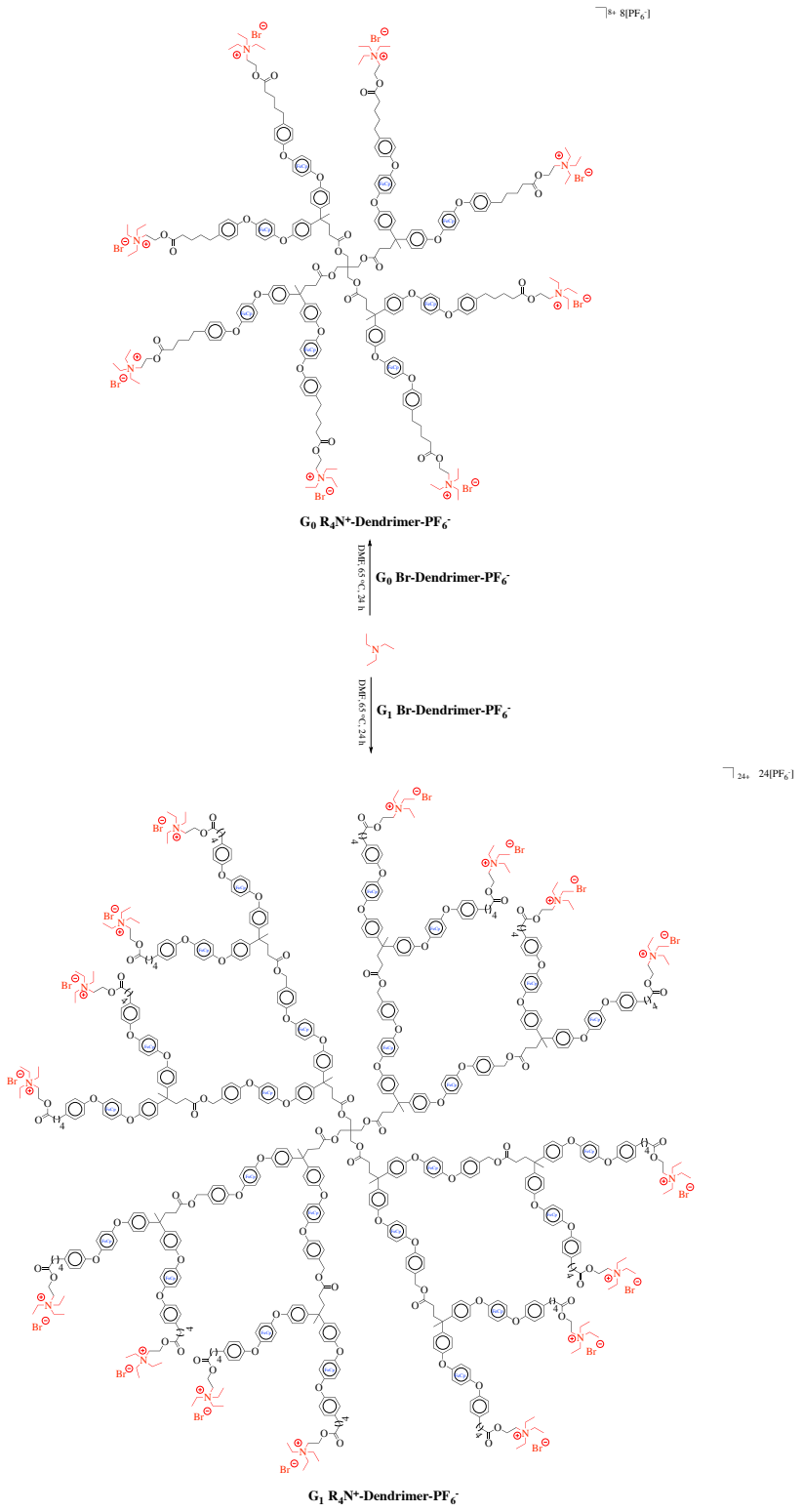

Scheme 4.8. Schematic representation of the synthesis of quaternized hybrid antimicrobial dendrimers, **G_0 R_4N^+-dendrimer-PF_6^-** and **G_1 R_4N^+-dendrimer-PF_6^-**. The degree of quaternization was determined from ^1H NMR to be approximately 75% for both dendrimers.

2-mercaptobenzothiazole. The expected improved performance of the hybrids is possible since the dendrimer structure will offer a high local concentration of quaternary ammonium groups or 2-mercaptobenzothiazole, which may amplify activity or act in synergy with the redox-active, cationic $[\eta^6$-arene-η^5-CpFe$]^+$ moieties in **G_0 Cl-dendrimer-PF_6^-** and **G_1 Cl-dendrimer-PF_6^-** to improve overall activity.

The synthesis of **G_0 R_4N^+-dendrimer-PF_6^-** or **G_1 R_4N^+-dendrimer-PF_6^-** involved S_NAr reaction of **G_0 Cl-dendrimer-PF_6^-** or **G_1 Cl-dendrimer-PF_6^-** with 5(4-hydroxyl)phenylpentanoic acid to give **G_0 COOH-dendrimer-PF_6^-** or **G_1 COOH-dendrimer-PF_6^-**, respectively, in high yield after precipitation from 10% (v/v) aqueous HCl (Scheme 4.6). Subsequently, Steglich esterification reaction of **G_0 COOH-dendrimer-PF_6^-** or **G_1 COOH-dendrimer-PF_6^-** with 2-bromoethanol at room temperature yielded **G_0 Br-dendrimer-PF_6^-** or **G_1 Br-dendrimer-PF_6^-** (Scheme 4.7), which on quaternization with triethylamine produced the G_0 hybrid dendrimer, **G_0 R_4N^+-dendrimer-PF_6^-**, or its G_1 analog, **G_1 R_4N^+-dendrimer-PF_6^-**, respectively, (Scheme 4.8). The S_NAr reaction of **G_0 Cl-dendrimer-PF_6^-** or **G_1 Cl-dendrimer-PF_6^-** with 2-mercaptobenzothiazole afforded the G_0 or G_1 hybrid dendrimer, **G_0 thiazole-dendrimer-PF_6^-** or **G_1 thiazole-dendrimer-PF_6^-**, respectively (Scheme 4.5).

As usual, ^{1}H NMR, ^{13}C NMR, and elemental analyses were used to characterize the dendrimers (Experimental section). Notably, changes in resonance frequencies and splitting pattern of proton and carbon environments in reactants and products offer insights on the success of the syntheses. As an example, functionalization of **G_0 Cl-dendrimer-PF_6^-** with 5(4-hydroxyl)phenylpentanoic acid resulted in the non-equivalent protons of the iron-complexed chlorophenoxyl ligand in **G_0 Cl-dendrimer-PF_6^-** resonating as a single broad peak in the ^{1}H NMR

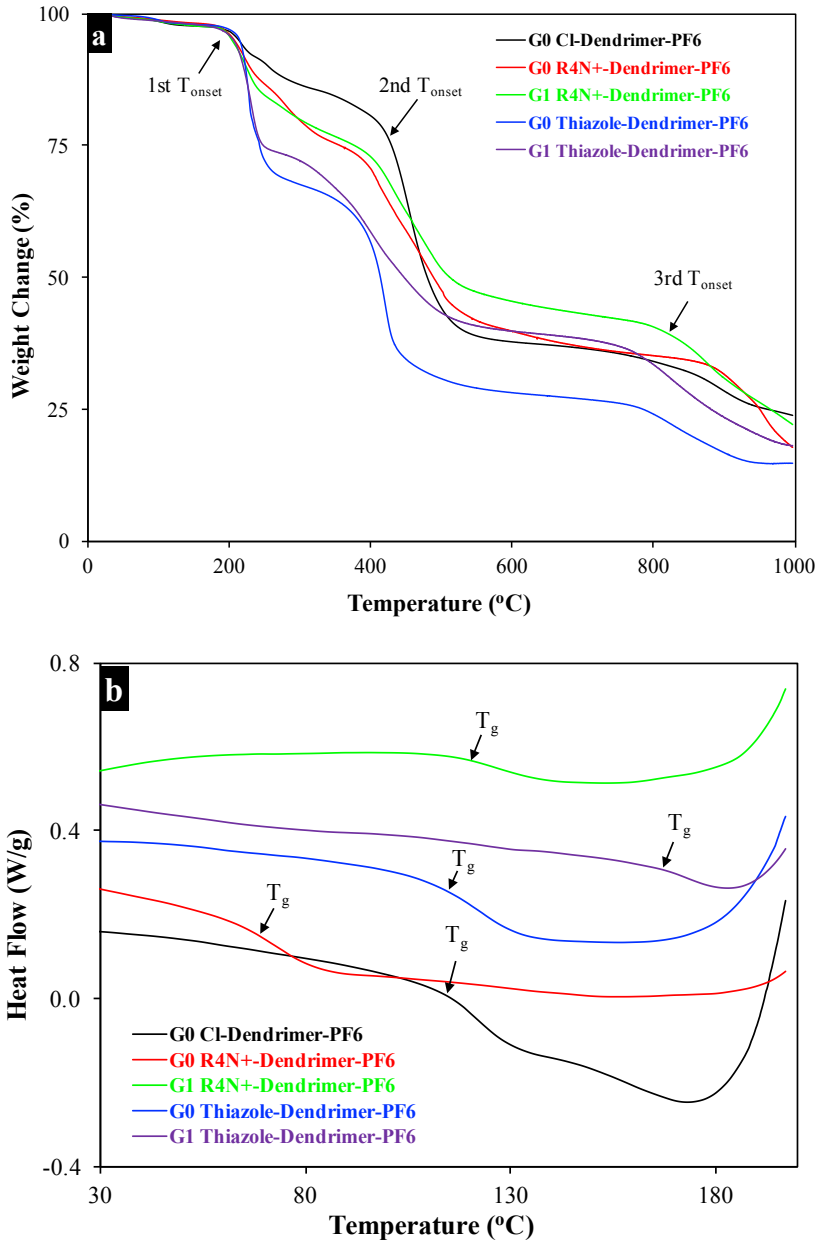

Figure 4.3. Effect of functionalization on the thermal properties of antimicrobial dendrimers. Functionalization did not noticeably change the thermal stability, onset of rapid decomposition, of the dendrimers but drastically changed the glass transition temperature (T_g) of the dendrimers. (a) Thermogravimetric analysis profiles of dendrimers showing the onset temperatures (T_{onset}). (b) Differential scanning calorimetry profiles of the dendrimers showing the T_g. Black: **G_0 Cl-dendrimer-PF_6^-**; red: **G_0 R_4N^+-dendrimer-PF_6^-**; green: **G_1 R_4N^+-dendrimer-PF_6^-**; blue: **G_0 thiazole-dendrimer-PF_6^-**; purple: **G_1 thiazole-dendrimer-PF_6^-**.

spectrum of the product, **G_0 COOH-dendrimer-PF_6^-**. Previously, Abd-El-Aziz *et al*. proved that the splitting pattern and resonance frequencies of the iron-complexed chlorophenoxyl change after S_NAr reaction of the chloro group.[49] Moreover, the appearance and disappearance of peaks attributed to functional groups were diagnostic tools to monitor the success of the synthesis steps. On functionalization of **G_0 Cl-dendrimer-PF_6^-** with 5(4-hydroxyl)phenylpentanoic acid to give carboxylic acid-terminated **G_0 COOH-dendrimer-PF_6^-**, carboxylic acid protons' peak was observed at 12.06 ppm in the ^{1}H NMR spectrum. This peak completely disappeared after Steglich esterification reaction of **G_0 COOH-dendrimer-PF_6^-** with 2-bromoethanol, suggesting successful esterification between the ethanolic hydroxyl and the carboxylic acid functional groups. Further, as previously demonstrated in a report,[50] ^{1}H NMR spectra indicated successful quaternization. Expectedly, after quaternization, the peripheral bromo-bonded methylene protons (CH_2CH_2Br) that transformed into nitrogen-bonded methylene protons ($CH_2CH_2N^+$) resonated downfield. The degree of quaternization in both dendrimers was obtained from ^{1}H NMR by integrating the downfield-shifted modified nitrogen-bonded methylene protons ($CH_2CH_2N^+$) to those of the unmodified bromo-bonded methylene protons (CH_2CH_2Br). Data from elemental analyses further suggest that the dendrimers were successfully synthesized.

Functionalization alters the thermal properties of materials.[51-57] It is, therefore, informative to understand how functionalization affects the thermal properties of these hybrids as this fundamental knowledge hints at their scope of application. Thermogravimetric analysis (TGA) data reveal that functionalization did not remarkably change the thermal stability, which is characterized by the onset of rapid degradation of the dendrimers (Figure 4.3a). Typical of polymers derived from $[\eta^6\text{-arene-}\eta^5\text{-CpFe}]^+$ complexes, all the dendrimers were thermally stable up to 200 °C and degraded in three steps (Figure 4.3a). The first onset of rapid degradation (T_{onset})

Table 4.2. Reduction potential and antimicrobial activity of complexes.

Complex	E_{pc} (V)[b]	IC_{50} /MIC (μM)[a]					
		MRSA	VRE	*S. warnerii*	*P.aeruginosa*	*P.vulgaris*	*C.albicans*
4.2a	−1.59	294	161/186	-	-	-	-
4.2b	−1.64	176/358	165/357	307/358	-	-	-
4.2c	−1.70	95/172	201/344	93.4/172	-	-	-
4.2d	−1.72	6.6/10.0	161/320	7.27/10.0	-	-	-
4.2e	−1.79	174/299	34.4/74.7	257/299	-	299	63.9
4.2f	−1.65	76.8/172	108/172	139/172	-	-	342
4.3a	−1.38	10.5/21.1	-	10.3/21.1	-	-	-
4.3b	−1.44	46.3/81.5	-	25.9/81.5	-	-	-
4.3c	−1.21	28.9/77.5	-	38.8/77.5	-	-	-
4.4a	−1.75	11.6/22.3	-	10.1/22.3	-	-	-
4.4b	−1.64	53.0/86.0	257/344	68.4/86.0	-	-	-
4.5a	−1.56	93.2/132	-	51.8/132	-	-	-
4.5b	−1.57	18.0/32.1	122	17.1/32.1	-	-	-
4.6a	−1.47	29.8/68.5	-	23.7/68.5	72.9	19.3	13.0/17.1
4.6b	−1.50	11.4/16.6	-	11.3/16.6	-	-	7.04/16.6

[a]The compounds were tested at 12 different concentrations obtained by serial dilution of the initial concentration, 128 μg/mL, to a final concentration, 0.0625 μg/mL, in 2% DMSO. Non-active compounds (-) did not show activity at ≤ 128 μg/mL. [b]Cyclic voltammetry was conducted using nitrogen-purged 6 mM solution of compound in propylene carbonate at room temperature; working electrode, glassy carbon; reference electrode, Ag; counter electrode, Pt; scan rate, 0.1 V/s; supporting electrolyte, 0.1 M $[n\text{-}Bu_4N][PF_6]$.

corresponds to cleavage of the $CpFe^{2+}$ moieties and the subsequent thermal degradation of the cyclopentadienyl ligands as previously proved.[26] The resulting organic dendrimer-iron composite

was stable up to 380 °C, after which rapid weight loss and volatilization occurred at the second and third T_{onset}, respectively (Figure 4.3a).

To further understand how functionalization affect the thermal property, the glass transition temperatures (T_gs), a fundamentally important thermal property of materials, were examined. Here, the functionalization noticeably changed the T_g (Figure 4.3b). The T_g increased in the 2-mercaptobenzothiazole-functionalized dendrimers, **G_0 thiazole-dendrimer-PF_6^-** and **G_1 thiazole-dendrimer-PF_6^-**, but decreased in the quaternary ammonium groups-functionalized dendrimers, **G_0 R_4N^+-dendrimer-PF_6^-** and **G_1 R_4N^+-dendrimer-PF_6^-** (Figure 4.3b). These findings are reasonable since aromatic systems, such as the thiazole, ensure close packing, which decrease free volume, and ultimately increase T_g.[58] In contrast, flexible aliphatic chains, such as the linker in **G_0 R_4N^+-dendrimer-PF_6^-** and **G_1 R_4N^+-dendrimer-PF_6^-**, hinders close packing, and eventually decrease T_g[58] as observed in this study.

4.2.4. Antimicrobial activity of $[\eta^6$-arene-η^5-CpFe$]^+$ complexes

In vitro antimicrobial activity of the complexes (**4.2**–**4.6**) was evaluated using two drug-resistant Gram-positive bacteria, MRSA and VRE, as well as other infection-causing microorganisms, *S. warneri*, *P. aeruginosa*, *P. vulgaris*, and *C. albicans*. As a reference, the antimicrobial activity of ferrocene (**4.1a**), its cationic 17-electron species (**4.1b**), and an arene, dichlorobenzene, was also evaluated in vitro. Under the test conditions, **4.1a** and **b** as well as the arene were inactive against all tested microorganisms. Previously, ferrocene was reported to be inactive against microorganisms but shown to enhance antimicrobial activity *via* oxidative damage caused by reactive oxygen species (ROS).[7] In contrast to ferrocene, the $[\eta^6$-arene-η^5-CpFe$]^+$ complexes were

mostly active against the Gram-positive bacteria, with some exhibiting activity against the Gram-negative bacteria and the fungus (Table 4.2).

A structure-activity relationship (SAR) investigation was conducted to gain insight into critical parameters that control the activity of these complexes. Towards this, electron-donating alkyl groups were introduced into the arene ligand to alter properties such as the redox chemistry of the iron as well as the hydrophilic/lipophilic balance of the complex. Previously, the addition of alkyl groups was shown to change the hydrophilic/lipophilic balance of molecules with increasing alkyl groups resulting in increased lipophilicity.[28-30] Cyclic voltammetry measurements indicated that the addition of methyl groups decreased the E_{pc} (Table 4.2). Also, increasing the number of methyl substituents on the arene ligand increased activity until all the hydrogens on the ligand were replaced with methyl groups (Table 4.2). Perhaps, an interplay of several parameters, which include hydrophilic/lipophilic balance and redox chemistry affected the antimicrobial activity because activity decreased after all hydrogens were substituted with methyl groups. Further, the ethyl-substituted complex, **4.2f**, (IC_{50} = 76.8 μM) had better activity against MRSA than its methyl-substituted analog, **4.2b**, (IC_{50} = 176 μM). Again, complexes **4.2e** and **4.2f** with six methyl groups and an ethyl group, respectively, in the arene ligand, had broader spectra of activity, being active against the Gram-negative bacterium, *P. vulgaris*, as well as the fungus, *C. albicans* (Table 4.2). In another SAR investigation, the methyl group of **4.2b** was replaced with a chloro group, giving **4.3a** (Scheme 4.1). This substitution increased the E_{pc} from −1.64 V in **4.2b** to −1.38 V in **4.3a** and led to a noticeable improvement in the antimicrobial activity against MRSA and *S. warneri* (Table 4.2). Similarly, **4.3b** and **4.3c** exhibited increased activity against MRSA and *S. warneri* compared with **4.2a** and **4.2c** (Table 4.2). Further, substituting polar groups (CHO

and NH_2) resulted in increased activity against MRSA and *S. warneri* compared with the methyl-substituted analog (Table 4.2).

Table 4.3. Antimicrobial activity of dendrimers.

Dendrimer	IC_{50}/MIC (μM)		
	MRSA	VRE	*S. warnerii*
G_0 Cl-Dendrimer-PF_6^-	3.6/7.6	6.6/15	6.9/7.6
G_0 H-Dendrimer-PF_6^-	3.3/4.1	2.5/4.1	3.5/4.1
G_0 CH_3-Dendrimer-PF_6^-	1.8/3.9	2.2/3.9	2.5/3.9
G_0 Cl-Dendrimer-BF_4^-	15/17	16/34	12/17
G_0 H-Dendrimer-BF_4^-	6.1/9.2	22/37	9.6/18
G_0 CH_3-Dendrimer-BF_4^-	10/18	13/36	11/18
G_1 Cl-Dendrimer-PF_6^-	-	-	-
G_1 H-Dendrimer-PF_6^-	3.5/5.1	5.9/-	2.2/2.6
G_1 CH_3-Dendrimer-PF_6^-	2.2/5.0	3.3/5.0	2.1/2.5

[a]The compounds were tested at twelve different concentrations obtained by serial dilution of the initial concentration, 128 μg/mL, to a final concentration, 0.0625 μg/mL, in 2% DMSO. Inactive compounds (-) did not show activity at ≤ 128 μg/mL. The dendrimers were also inactive against tested Gram-negative bacteria, fungus, human epidermal keratinocytes (HEka) and BJ fibroblast cell lines at ≤ 128 μg/mL.

4.2.5. Antimicrobial activity of organometallic dendrimers

The activity of the complexes against drug-resistant microorganisms was exciting and inspired the synthesis of series of $[\eta^6$-arene-η^5-CpFe$]^+$-derived dendrimers for antimicrobial functions. The microbroth dilution protocol[59,60] was used to assay these dendrimers against MRSA, VRE, *S. warneri*, *P. aeruginosa*, *P. vulgaris* and *C. albicans*. At the tested concentrations, these cationic,

redox active dendrimers were inactive against the Gram-negative bacteria, *P. aeruginosa* and *P. vulgaris*, and the fungus *C. albicans*. While most cationic antimicrobial agents, such as cationic peptides, exhibit activity against Gram-positive and Gram-negative bacteria, some reports,[3,7] which corroborate these present results, show that some cationic organometallic antimicrobial agents are active only against Gram-positive bacteria. The inactivity towards Gram-negative bacteria may be due to the presence of an outer membrane structure that is absent in Gram-positive bacteria,[27,61] or to structural differences between these dendrimers and the other broad spectrum cationic antimicrobials agents.[62,63] Excitedly, most of the dendrimers were active against the Gram-positive bacteria with the concentration that inhibited 90% growth of the microorganisms (IC_{90}) being in the low micromolar range (Table 4.3).

The results further show that the nature of the counteranion tuned the activity of the dendrimers because the PF_6^- dendrimers were more active than their BF_4^- analogs (Table 4.3). Although the finding is explicable, it is still paradoxical, because the BF_4^- series had smaller hydrodynamic radii and better aqueous solubility, parameters that could favor enhanced systemic assimilation of the dendrimer, and could ultimately, result in improved activity.[28,37] Indeed, it was previously demonstrated that BF_4^--containing cationic polymers are more active than their PF_6^- analogs and this activity correlates with the aqueous solubility of the polymers.[27] Perhaps, the lower activity of the BF_4^- series of dendrimers is due to the relatively more coordinating ability of their counteranions than those of the PF_6^- series.[67] With a stronger coordinating counteranion, the cationic charge is less likely to interact with the cell membrane to kill the microorganisms. Nonetheless, the present findings agreed with those of others[64-66] where more coordinating counteranions decease antimicrobial activity of cationic antimicrobial agents. The results also show the absence of dendritic effect in the hydrido and methyl-substituted PF_6^- series of

dendrimers since no appreciable difference in antimicrobial activity was found between the G_0 dendrimers, **G_0 H-dendrimer-PF_6^-** and **G_0 CH_3-dendrimer-PF_6^-**, and the G_1, **G_1 H-dendrimer-PF_6^-** and **G_1 CH_3-dendrimer-PF_6^-** (Table 4.3). However, with chloro-substituted dendrimers, **G_0 Cl-dendrimer-PF_6^-** and **G_1 Cl-dendrimer-PF_6^-**, a noticeable dendritic effect on activity was evident because the latter dendrimer was inactive against all microorganisms (Table 4.3).

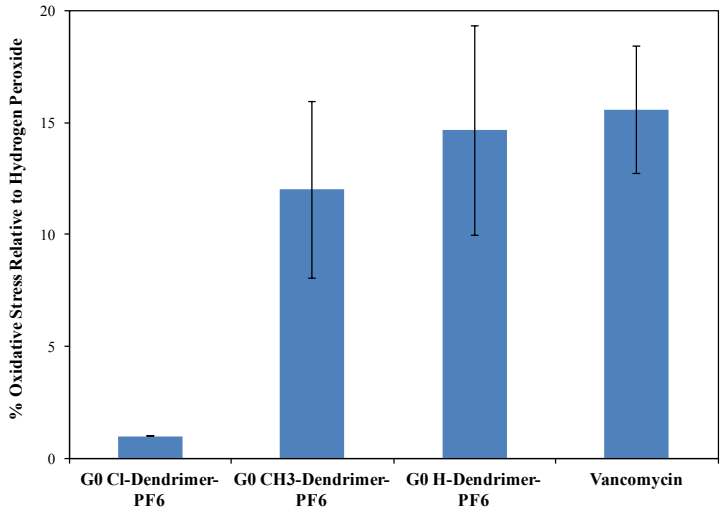

Figure 4.4. Percentage of oxidative stress induced on MRSA by **G_0 Cl-dendrimer-PF_6^-**, **G_0 H-dendrimer-PF_6^-** and **G_0 CH_3-dendrimer-PF_6^-**. Hydrogen peroxide was positive control (100% oxidative stress) and vancomycin, known to induce oxidative stress, was reference.

The antimicrobial activity of organometallic antimicrobial agents is influenced by an interplay of several parameters that include free radicals-induced oxidative stress.[7] As these organometallic dendrimers initiated the generation of free radicals (Figure 4.2), they are likely to induce oxidative stress. Using the dichlorodihydrofluorescein (H_2DCF) oxidative assay,[68,69] the induction of cellular oxidative stress by **G_0 Cl-dendrimer-PF_6^-**, **G_0 H-dendrimer-PF_6^-** and **G_0 CH_3-dendrimer-PF_6^-** on MRSA was evaluated. The dendrimers induced oxidative stress on

MRSA with the chloro-substituted dendrimer, **G_0 Cl-dendrimer-PF_6^-**, being the least efficient (Figure 4.4). The oxidative stress induced by **G_0 H-dendrimer-PF_6^-** and **G_0 CH_3-dendrimer-PF_6^-** was comparable to that of vancomycin, which is reported to improve its antimicrobial activity by inducing cellular oxidative stress on bacteria.[70,71]

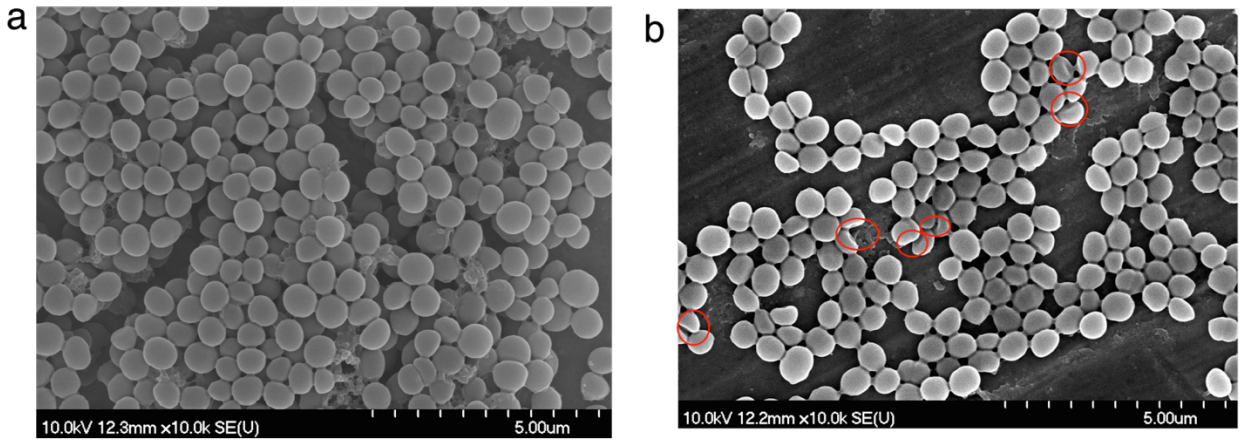

Figure 4.5. The dendrimers disrupted cell membrane of MRSA as evidenced by field emission scanning electron micrographs of MRSA. (a) MRSA cells without treatment with **G_0 CH_3-dendrimer-PF_6^-**. (b) MRSA cells treated with **G_0 CH_3-dendrimer-PF_6^-** at the antimicrobial IC_{50}.

The cationic charge on the dendrimers offers another mechanism of activity. Indeed, cationic polymers function as antibacterial agents by interacting with the negatively charged bacterial cell membrane, disrupting cellular integrity, and eventually leading to fatal processes that include depolarization of membrane, disruption of cellular processes, modification of membrane lipid composition and/or leakage of cell content.[72] To confirm the membrane-interacting property of the dendrimers, field emission scanning electron microscope (FE-SEM) was used to visually assess the integrity of the cell membrane of MRSA before and after treatment with the most active dendrimer, **G_0 CH_3-dendrimer-PF_6^-**, at its antimicrobial IC_{50}. This technique is used to

qualitatively confirm a membrane-disrupting mechanism of action of cationic antimicrobial agents.[73] Here, the FE-SEM images revealed that the untreated MRSA had intact morphology whereas evidences of ruptured and shrunken membranes were found in **G_0 CH_3-dendrimer-PF_6^-**-treated MRSA cells (Figure 4.5).

Table 4.4. Antimicrobial activity of hybrid dendrimers.[a]

dendrimer	IC_{50}/IC_{90} (μM)				
	MRSA	VRE	*S. warneri*	*B. subtilis*	*C. albicans*
2-Mercaptobenzothiazole	178/383	630/765	446/765	-/-	-/-
G_0 R_4N^+-Dendrimer-PF_6^-	1.37/2.29	2.04/2.29	1.05/2.29	3.20/4.57	11.86/-
G_1 R_4N^+-Dendrimer-PF_6^-	0.71/0.84	1.44/6.76	0.71/0.84	2.85/3.38	-/-
G_0 Thiazole-Dendrimer-PF_6^-	4.05/-	5.07/-	1.81/3.04	3.84/6.08	17.6/-
G_1 Thiazole-Dendrimer-PF_6^-	1.63/2.11	2.96/-	0.90/1.05	1.84/2.11	-/-

[a]The compounds were tested at twelve different concentrations obtained by serial dilution of the initial concentration, 128 μg/mL, to a final concentration, 0.0625 μg/mL, in 2% DMSO. Inactive compounds (-) did not show activity at ≤ 128 μg/mL. The dendrimers were also inactive against tested Gram-negative bacteria, human epidermal keratinocytes (HEka) and BJ fibroblast cell lines at ≤ 128 μg/mL.

4.2.6. Antimicrobial activity of hybrid dendrimers

Aiming to improve the activity of the dendrimers, their peripheries were functionalized with known antimicrobial agents to afford hybrid antimicrobial dendrimers. The CLSI microbroth dilution antimicrobial assay protocol was also used to evaluate the in vitro antimicrobial activity of these hybrid dendrimers to gain insight into their IC_{50}s and IC_{90}s. Like the parent dendrimers, **G_0 Cl-dendrimer-PF_6^-** and **G_1 Cl-dendrimer-PF_6^-**, these hybrids were active against the Gram-positive MRSA, VRE, and *S. warneri*, but inactive against the Gram-negative bacteria, *P. aeruginosa* and *P. vulgaris*, (Tables 4.3 and 4.4). These hybrid dendrimers especially the

quaternary ammonium group-functionalized series, **G_0 R_4N^+-dendrimer-PF_6^-** and **G_1 R_4N^+-dendrimer-PF_6^-**, were expected to be broad in the spectrum of activity, inhibiting the growth of the Gram-positive and Gram-negative bacteria like some cationic peptides. This finding suggest that the lesser susceptibility of Gram-negative bacteria to these cationic organometallic dendrimers is most probably due to their structure, which is markedly different from those of other cationic antimicrobials agents that are active against Gram-negative bacteria.

Comparatively, the thiazole-functionalized dendrimers, **G_0 thiazole-dendrimer-PF_6^-** and **G_1 thiazole-dendrimer-PF_6^-**, were broader in their spectrum of activity than one of their constituent bioactive moiety, 2-mercaptobenzthiazole (Table 4.4). Also, **G_0 thiazole-dendrimer-PF_6^-** and **G_1 thiazole-dendrimer-PF_6^-** were more potent than the 2-mercaptobenzthiazole as evidenced by their lower IC_{90} and IC_{50} (Table 4.4). As an example, the IC_{50} of **G_1 thiazole-dendrimer-PF_6^-** against MRSA was more than five times lower than that of the 2-mercaptobenzthiazole (Table 4.4), implying more potent activity. Further, the thiazole-functionalized dendrimer, **G_1 thiazole-dendrimer-PF_6^-**, was more active against the tested microorganisms than its constituent bioactive agents, **G_1 Cl-dendrimer-PF_6^-**, and 2-mercaptobenzthiazole, (Tables 4.3 and 4.4). Functionalization with quaternary ammonium groups drastically improved the activity. Indeed, **G_0 R_4N^+-dendrimer-PF_6^-** and **G_1 R_4N^+-dendrimer-PF_6^-** were highly potent, exhibiting activities that were in most cases superior to those of the parent dendrimers, **G_0 Cl-dendrimer-PF_6^-** and **G_1 Cl-dendrimer-PF_6^-** (Tables 4.3 and 4.4). For instance, **G_0 R_4N^+-dendrimer-PF_6^-** was more active against MRSA and *C. albicans* than its parent **G_0 Cl-dendrimer-PF_6^-** as evidenced by the lower IC_{50} values of the former dendrimer (Tables 4.3 and 4.4). Again, G_1 hybrid dendrimers, **G_1 thiazole-dendrimer-PF_6^-** and **G_1 R_4N^+-dendrimer-**

PF_6^-, were superior in activity to the inactive **G_1 Cl-dendrimer-PF_6^-** (Tables 4.3 and 4.4). A positive dendritic effect was evident in the series of hybrid dendrimers. For instance, the activity of the hybrid dendrimers against the Gram-positive bacteria increased at higher generation, which contrasts with the findings on **G_0 Cl-dendrimer-PF_6^-** and **G_1 Cl-dendrimer-PF_6^-**, with negative dendritic effects on activity (Tables 4.3 and 4.4). This dendritic effect is attributed to the increase in local concentration of peripheral antimicrobial agents at higher generation. In contrast, a negative dendritic effect was found in the activity against the fungus as evidenced by high activity of G_0 hybrids compare with their G_1 analogs (Table 4.4).

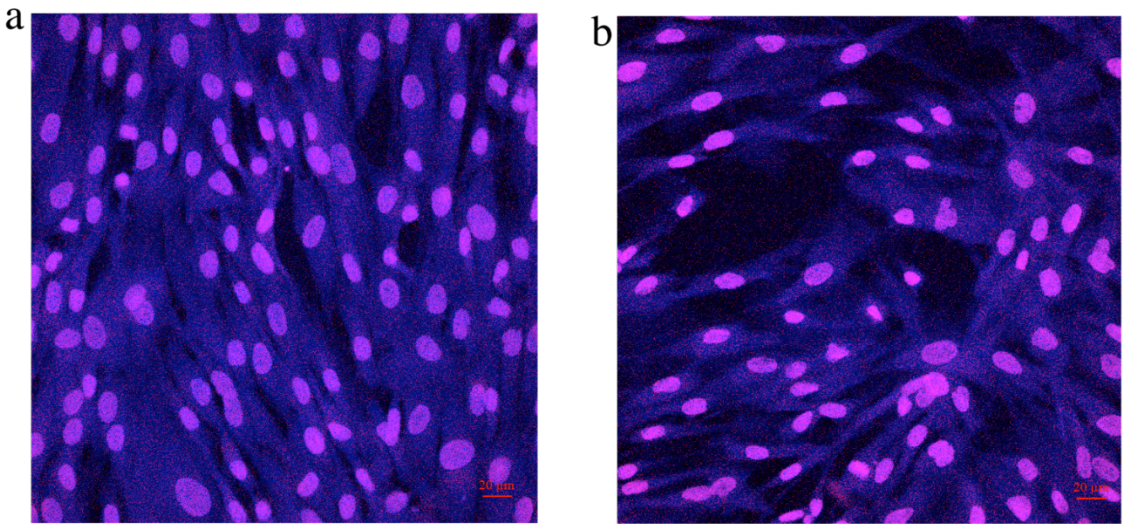

Figure 4.6. Cytotoxicity of dendrimers to human BJ fibroblast cells. Human skin cells remained viable after 24 hours exposure to the dendrimers in vitro. Confocal laser fluorescence micrographs showing autofluorescence of cell membrane and DAPI-stained nuclei of human BJ fibroblast cells. a) Without treatment with **G_0 CH_3-dendrimer-PF_6^-**; b) treated with **G_0 CH_3-dendrimer-PF_6^-** at 128 μg/mL).

4.2.7. Cytotoxicity of dendrimers

Membrane-active antimicrobial agents can also interact with mammalian cell membranes, causing harm, a development that could limits their clinical applications.[8,74] The toxicity of these cationic

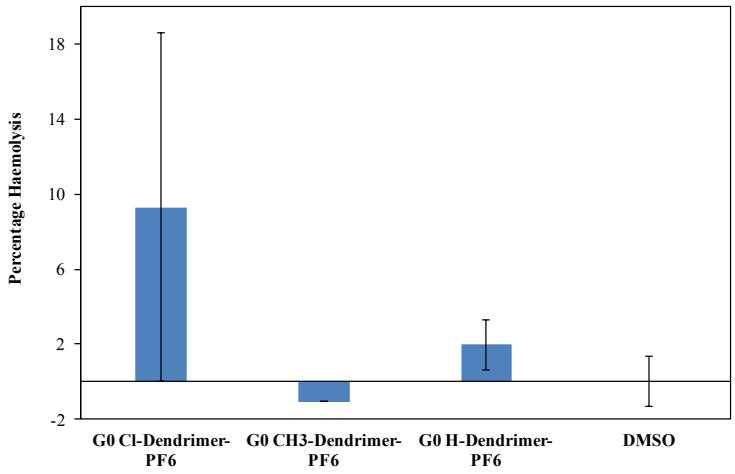

Figure 4.7. Cytotoxicity of **G_0 Cl-dendrimer-PF_6^-**, **G_0 H-dendrimer-PF_6^-** and **G_0 CH_3-dendrimer-PF_6^-** to sheep red blood cells. Percentage haemolysis of sheep red blood cells treated with 128 μg/mL of G_0 dendrimers.

dendrimers against human epidermal keratinocytes cells (HEka) and human foreskin BJ fibroblast cells was evaluated. In vitro, these dendrimers were non-toxic to HEka and BJ fibroblast cells under assay conditions. For instance, the human cells were viable after 24 hours' stress with **G_0 CH_3-dendrimer-PF_6^-** at concentration eight times the antimicrobial IC_{90} against MRSA. Indeed, examination of the BJ fibroblast cells using confocal laser fluorescence microscopy revealed no treatment-induced changes in morphology of the cell membrane as visualized from intracellular autofluorescence of the cell membrane as well as from the DAPI-stained cell nuclei (Figures 4.6). To gain deeper insight into the toxicity of these dendrimers to mammalian cells, their haemolytic activity was evaluated using defibrinated sheep whole blood. Specifically, the harvested sheep blood cells were treated with 128 μg/mL of **G_0 Cl-dendrimer-PF_6^-**, **G_0 H-dendrimer-PF_6^-**, or **G_0 CH_3-dendrimer-PF_6^-**, incubated at pH = 7.4 for 2 hours, and the absorbance of heme released due to haemolysis was measured. Compared to a positive control, these dendrimers did not

remarkably disrupt red blood cells membrane under these conditions (Figure 4.8), which include concentrations that are higher than their IC_{90} (Figure 4.7).

4.3. Conclusion

Here, the antimicrobial activity of $[\eta^6\text{-arene-}\eta^5\text{-CpFe}]^+$ complexes is demonstrated. This inspires the synthesis of the first organometallic antimicrobial dendrimers with activity against drug-resistant Gram-positive bacteria. These dendrimers incorporated $[\eta^6\text{-arene-}\eta^5\text{-CpFe}]^+$ complex as the active moiety, and can be functionalized with known antimicrobial agents to afford hybrid antimicrobial dendrimers. Comparatively, the hybrids had improved activities at the higher generation compared with the parent dendrimers. By changing the nature of the counteranion, the activities of the dendrimers were tuned as evidenced by the higher activities of the PF_6^- series of dendrimers compared with the BF_4^- series. Electron spin resonance spectroscopy indicated that the dendrimers initiated the formation of free radicals. Also, the dendrimers disrupted the microbial cell membrane and induced oxidative stress on MRSA, processes that could contribute to their activity. Interestingly, the dendrimers were non-toxic to human skin cell lines, suggesting possible use in dermal formulations.

4.4. Experimental section

4.4.1. Materials

All chemicals were purchased from Sigma-Aldrich or Alfa Aesar. Unless otherwise stated, the chemicals were used without further purification. Deuterated solvents, dimethyl sulfoxide (DMSO), and dimethylformamide (DMF) were dried over molecular sieves before use. The synthesis of **G_0 Cl-dendrimer-PF_6^-** and **G_1 Cl-dendrimer-PF_6^-**, which are the same as **G_0 Cl-dendrimer** and **G_1 Cl-dendrimer**, respectively, are described in *Chapter Two*. Also, complex **2.3**

and **G_0 BnOH-dendrimer** were synthesized as described in *Chapter Two*. Complexes **4.2**–**4.6** were synthesized as described in reported procedures.[20-26]

4.4.2. Instrumentation

A Bruker Avance NMR spectrometer (^{1}H, 300 MHz; ^{13}C, 75 MHz; ^{11}B, 96 MHz; and ^{31}P, 122 MHz) was used to record the ^{1}H, ^{13}C, ^{11}B, and ^{31}P NMR spectra of all synthesized compounds. For ^{1}H and ^{13}C, the chemical shifts were internally referenced to the DMSO-d_6 residual proton peak while for ^{11}B and ^{31}P, the chemical shifts were externally referenced to boron trifluoride diethyl etherate in $CDCl_3$ and phosphoric acid in D_2O, respectively. Elemental analyses, differential scanning calorimetry and room temperature cyclic voltammetry were performed as described in *Chapter Two*. The ^{31}P NMR spectroscopy of the PF_6^- series of dendrimer gave a septet at −125 to −161 ppm while ^{11}B NMR spectroscopy of the BF_4^- series gave a singlet at −1 ppm.

4.4.3. Synthesis of G_0 H-dendrimer-PF_6^-, G_0 CH_3-dendrimer-PF_6^-, G_0 Cl-dendrimer-BF_4^-, G_0 H-dendrimer-BF_4^- and G_0 CH_3-dendrimer-BF_4^-

The synthesis of these dendrimers were carried out using the general procedure described in *Chapter Two* for the synthesis of **G_0 Cl-dendrimer-PF_6^-**. In brief, in a 50-mL round-bottom flask, was added pentaerythritol (0.170 g, 1.25 mmo), complex **2.3**, **4.5a** or **4.5b** (5.00 mmol), 4-(dimethylamino)pyridine (DMAP) (0.470 g, 3.85 mmol), and 10 mL of 3:1 DCM/DMSO solution. The resulting solution was cooled to 0 °C using ice bath, and stirred under nitrogen atmosphere while *N*,*N*'-dicyclohexylcarboiimide (DCC) (1.13 g, 5.50 mmol) was added over 5 minutes. Next, the ice bath was removed, and the mixture was stirred at room temperature for 24 hours under nitrogen. Afterwards, precipitated dicyclohexylurea (DCU) was removed by filtration. The filtrate was added to 50 mL of ice water, extracted twice with 20-mL portions of DCM/$(CH_3)_2CO$ mixture,

and the organic extract was washed twice with 50-mL portions of 5% HCl. The organic extract was added to 10 mL of water to which NH_4PF_6 or NH_4BF_4 (10.0 mmol) was dissolved, and allowed to stand for 30 minutes. The aqueous layer was separated, the organic portion dried over $MgSO_4$, filtered under gravity, and solvent removed using rotary evaporator. The residue was dissolved in acetone, cooled in a freezer for one hour, filtered to remove precipitated DCU, and precipitated from $(C_2H_5)_2O$. The yellow-green solid was collected, and dried at room temperature to give corresponding dendrimer.

Characterization of G_0 H-dendrimer-PF_6^- and G_0 H-dendrimer-BF_4^-: Yield: **G_0 H-dendrimer-PF_6^-**, 74%; **G_0 H-dendrimer-BF_4^-**, 49%. ^{1}H NMR (300 MHz, DMSO-d_6): δ (ppm) 7.41 (16 H, br s, Ar*H*), 7.28 (16 H, br s, Ar*H*), 6.33 (32 H, br s, complexed Ar*H*), 6.19 (8 H, br s, complexed Ar*H*), 5.16 (40 H, s, Cp*H*), 4.04 (8 H, br s, CH_2), 2.45 (8 H, br s, CH_2), 2.16 (8 H, br s, CH_2), 1.69 (12 H, br s, CH_3). ^{13}C{^{1}H} NMR (75 MHz, DMSO-d_6): δ (ppm) 172.6, 151.0, 145.9, 132.5, 129.1, 120.2, 118.6, 86.6, 76.8, 76.9, 64.8, 45.0, 35.9, 29.8, 27.0. Elemental analyses: **G_0 H-dendrimer-PF_6^-**: calculated for C, 49.01; H, 3.78; found for C, 49.67; H, 3.96; **G_0 H-dendrimer-BF_4^-**: calculated for C, 55.57; H, 4.29; found for C, 55.86; H, 4.65.

Characterization of G_0 CH_3-dendrimer-PF_6^- and G_0 CH_3-dendrimer-BF_4^-: Yield: **G_0 CH_3-dendrimer-PF_6^-**, 77%; **G_0 CH_3-dendrimer-BF_4^-**, 56%. ^{1}H NMR (300 MHz, DMSO-d_6): δ (ppm) 7.34 (16 H, br s, Ar*H*), 7.23 (16 H, br s, Ar*H*), 6.23 (32 H, s, complexed Ar*H*), 5.12 (40 H, s, Cp*H*), 4.10 (8 H, br s, CH_2), 2.36, (32 H, br s, CH_2 and CH_3 (CH_2 overlapped CH_3), 2.15 (8H, br s, CH_2), 1.65 (12 H, br s, CH_3). ^{13}C{^{1}H} NMR (75 MHz, DMSO-d_6): δ (ppm) 172.5, 151.4, 145.8, 131.3, 129.1, 120.2, 100.7, 86.9, 75.7, 77.4, 64.9, 44.4, 35.9, 30.6, 26.7, 20.1. Elemental analyses: **G_0 CH_3-dendrimer-PF_6^-**: calculated for C, 50.03; H, 4.07; found for C, 50.31; H, 4.13; **G_0 CH_3-dendrimer-BF_4^-**: calculated for C, 56.51; H, 4.60; found for C, 57.03; H, 4.83.

Characterization of G_0 Cl-dendrimer-BF_4^-: Yield: 57%. ^{1}H NMR (300 MHz, DMSO-d_6): δ (ppm) 7.35 (16 H, br s, Ar*H*), 7.24 (16 H, br s, Ar*H*), 6.77 (16 H, br, s, complexed Ar*H*) 6.39 (16 H, br s, complexed Ar*H*), 5.25 (40 H, s, Cp*H*), 4.01 (8 H, br s, CH_2), 2.40 (8 H, br s, CH_2), 2.13 (8 H, br s, CH_2), 1.64 (12 H, br s, CH_3). ^{13}C{^{1}H} NMR (75 MHz, DMSO-d_6): δ (ppm) 172.9, 151.0, 146.5, 132.3, 129.6, 120.5, 118.8, 86.6, 76.7, 79.7, 65.3, 45.4, 36.3, 30.1, 27.3. Elemental analyses: calculated for C, 51.49; H, 3.76; found for C, 51.87; H, 4.07.

4.4.4. Synthesis of G_1 H-dendrimer-PF_6^- and G_1 CH_3-dendrimer-PF_6^-

The syntheses of these dendrimers followed the general procedure described in *Chapter Two* for the synthesis of **G_1 Cl-dendrimer-PF_6^-**. These dendrimers were synthesized from **4.5a** or **4.5b** (1.22 mmol), **G_0 BnOH-dendrimer** (0.750 g, 0.152 mmol), DMAP (0.115 g, 0.940 mmol), and DCC (0.276 g, 1.34 mmol) in 10 mL of 1:3 DCM/DMSO mixture.

Characterization of G_1 H-dendrimer-PF_6^-: Yield: 68%. ^{1}H NMR (300 MHz, DMSO-d_6): δ (ppm) 7.39 (48 H, br s, Ar*H*), 7.30 (48 H, br s, Ar*H*), 7.00 (32 H, br s, Bn*H*), 6.33 (96 H, br s, complexed Ar*H*), 6.19 (16 H, br s, complexed Ar*H*), 5.20 (40 H, s, Cp*H*), 5.16 (80 H, s, Cp*H*), 4.55 (16 H, br s, CH_2), 4.03 (8H, br s, CH_2), 2.43 (24 H, br s, CH_2), 2.11 (24 H, br s, CH_2), 1.68 (36 H, s, CH_3). ^{13}C{^{1}H} NMR (75 MHz, DMSO-d_6): δ (ppm) 174.2, 172.7, 152.1, 151.6, 151.1, 146.1, 145.9, 145.8, 133.9, 132.5, 132.4, 129.9, 129.1, 128.5, 120.5, 120.3, 120.1, 119.7, 86.6, 84.7, 74.9, 74.4, 77.7, 76.7, 64.8, 62.1, 45.0, 44.9, 44.7, 36.0, 35.8, 29.7, 29.6, 27.1, 26.8. Elemental analyses: calculated for C, 50.66; H, 3.76; found for C, 50.38; H, 3.67.

Characterization of G_1 CH_3-dendrimer-PF_6^-: Yield: 71%. ^{1}H NMR (300 MHz, DMSO-d_6): δ (ppm) 7.35 (48 H, br s, Ar*H*), 7.26 (48 H, br s, Ar*H*), 6.98 (32 H, br s, Bn*H*), 6.25 (96 H, br s, complexed Ar*H*), 5.21 (40 H, s, Cp*H*), 5.12 (80 H, s, Cp*H*), 4.56 (16 H, br s, CH_2), 4.03 (8 H,

br s, CH_2), 2.37, (64 H, br s, CH_3 and CH_2 (the CH_2 overlapped with CH_3), 1.67 (36 H, br s, CH_3). ^{13}C{^{1}H} NMR (75 MHz, DMSO-d_6): δ (ppm) 174.3, 172.6, 151.7, 151.5, 151.2, 146.1, 145.9, 145.8, 131.3, 130.3, 129.8, 129.7, 129.1, 128.5, 127.9 120.3, 120.1, 100.1, 86.6, 76.1, 75.0, 74.4, 77.7, 77.2, 64.8, 62.1, 45.0, 44.9, 44.6, 36.7, 35.8, 29.7, 29.6, 27.1, 26.9, 19.1. Elemental analyses: calculated for C, 51.28; H, 3.95; found for C, 51.60; H, 4.18.

4.4.5. Synthesis of G_0 thiazole-dendrimer-PF_6^-

The hybrid dendrimer was obtained as follow: **G_0 Cl-dendrimer-PF_6^-** (520 mg, 0.123 mmol), 2-mercaptobenzothiazole (166 mg, 0.984 mmol), K_2CO_3 (340 mg, 2.46 mmol), and 3 mL of DMF were added to a 25-mL round-bottomed flask. The reaction mixture was stirred at room temperature for 72 hours under nitrogen. Subsequently, the reaction mixture was added dropwise to 150 mL of 10% (v/v) aqueous HCl. Next, NH_4PF_6 (160 mg, 0.984 mmol) was added to precipitate the product, which was filtered and dried at room temperature to give the final product. Yield: 81%. ^{1}H NMR (300 MHz, DMSO-d_6): δ (ppm) 7.34 (32 H, br s, Ar*H*), 7.25 (32 H, br s, Ar*H*), 6.78 (16 H, br s, complexed Ar*H*), 6.38 (16 H, br s, complexed Ar*H*), 5.24 (40 H, s, Cp*H*), 4.09 (8 H, br s, CH_2), 2.40 (8 H, br s, CH_2), 2.15 (8 H, br s, CH_2), 1.66 (12 H, br s, CH_3). ^{13}C{^{1}H} NMR (75 MHz, DMSO-d$_6$): δ (ppm) 172.3 (*C*=O), 152.1, 150.9, 145.9, 134.7, 131.7, 131.6 (Ar*C*), 129.6, 128.4 (complexed Ar*C*), 129.0, 126.8, 124.6, 123.9, 121.5, 119.8 (Ar*C*H), 86.5, 76.6 (complexed Ar*C*H) 79.1 (Cp *C*), 62.2, 44.7, 42.2, 35.5, 29.3, 26.3. Elemental analyses: calculated for: C, 49.48; H, 3.29, N, 2.13; found for C, 49.57; H, 3.41; N, 1.94.

4.4.6. Synthesis of G_1 thiazole-dendrimer-PF_6^-

The dendrimer was obtained using a procedure similar to that used in synthesizing **G_0 thiazole-dendrimer-PF_6^-**. In brief, **G_1 Cl-dendrimer-PF_6^-** (217 mg, 0.0166 mmol), 2-

mercaptobenzothiazole (44.5 mg, 0.266 mmol), K_2CO_3 (91.9 mg, 0.665 mmol) was used to synthesize **G_1 thiazole-dendrimer-PF_6^-**. Yield: 83%. ^{1}H NMR (300 MHz, DMSO-d_6): δ (ppm) 7.39, 7.27 (192 H, m, Ar*H*), 6.80 (32 H, br s, complexed Ar*H*), 6.43 (32 H, br s, complexed Ar*H*), 6.27 (32 H, br s, complexed Ar*H*), 5.30 (80 H, s, Cp*H*), 5.22 (40 H, s, Cp*H*) 5.12 (16 H, br s, CH_2), 4.02 (8H, br s, CH_2), 2.44, 2.23 (48 H, br s, CH_2), 1.68, (24 H, br s, CH_3) 1.63 (12 H, br s, CH_3). ^{13}C{^{1}H} NMR (75 MHz , DMSO-d_6): δ (ppm) 174.2, 172.6 (*C*=O), 162.2, 155.5, 153.0, 151.5, 151.0, 146.3, 146.1, 134.0, 133.9, 131.8, 130.7, 130.3 (Ar*C*), 130.1, 129.9, 129.8, 129.7 (complexed Ar*C*) 129.2, 129.1, 120.5, 120.2, 120.0, 119.8, 118.2 (Ar*C*), 79.2, 77.8 (Cp*C*), 86.7, 76.3, 75.0 (complexed Ar*C*), 64.8, 44.9, 44.7, 44.4, 35.8, 30.6, 30.5, 29.7, 29.6, 26.9, 26.8. Elemental analyses: calculated for C, 50.79; H, 3.44; N, 1.48; found for C, 51.17; H, 3.55; N, 1.24.

4.4.7. Synthesis of G_0 COOH-dendrimer-PF_6^-

The dendrimer was synthesized as follow: **G_0 Cl-dendrimer-PF_6^-** (500 mg, 0.12 mmol), 5-(4-hydroxyphenyl)pentanoic acid (186 mg, 0.96 mmol), K_2CO_3 (332 mg, 2.40 mmol), and 3 mL of DMF were placed in a 25-mL round-bottomed flask. The reaction mixture was heated at 65 °C for 24 hours. Subsequently, the reaction mixture was cooled to room temperature. To precipitate the product, the mixture was added dropwise to 10% (v/v) HCl, followed by the addition of NH_4PF_6 (156 mg, 0.96 mmol). The product was isolated by filtration and dried at room temperature. Yield: 75%. ^{1}H NMR (300 MHz, DMSO-d_6): δ (ppm) 12.06 (8 H, br s, COO*H*), 7.36 (32 H, br s, Ar*H*), 7.23 (32 H, br s, Ar*H*), 6.21 (32 H, br s, complexed Ar*H*), 5.19 (40 H, s, Cp*H*), 4.06 (8 H, br s, CH_2), 2.63 (32 H, br s, CH_2), 2.41 (8 H, br s, CH_2), 2.26, (32 H, br s, CH_2), 2.14 (8 H, br s, CH_2), 1.58 (12 H, br s, CH_3). ^{13}C{^{1}H} NMR (75 MHz, DMSO-d_6): δ (ppm) 174.3, 172.4 (*C*=O), 151.6, 151.1, 146.0, 140.2, 130.3, 129.1, 120.3, 119.8 (Ar*C*), 129.8, 120.7 (complexed Ar*C*), 77.7 (Cp*C*),

75.0, 74.5 (complexed Ar*C*H), 54.7, 44.8, 44.2, 35.8, 34.0, 33.4, 30.7, 30.2, 26.8, 24.0. Elemental analyses: calculated for C, 54.54; H, 4.49; found for C, 54.00; H, 4.35.

4.4.8. Synthesis of G_1 COOH-dendrimer-PF_6^-

The synthesis of the dendrimer followed a procedure similar to that used in synthesizing **G_0 COOH-dendrimer-PF_6^-**. In brief, **G_1 Cl-dendrimer-PF_6^-** (521 mg, 0.040 mmol), 5-(4-hydroxyphenyl)pentanoic acid (124 mg, 0.640 mmol), K_2CO_3 (221 mg, 1.60 mmol), and 3 mL of DMF were used in the synthesis. The product was obtained after a work-up procedure similar to that of **G_0 COOH-dendrimer-PF_6^-**. Yield: 81%. ^{1}H NMR (300 MHz, DMSO-d_6): δ (ppm) 12.01 (16 H, br s, COO*H*), 7.51 (16 H, br s, Ar*H*), 7.35 (80 H, br s, Ar*H*), 7.23 (80 H, br s, Ar*H*), 6.98 (16 H, br s, Ar*H*) 6.23 (96 H, br s, complexed Ar*H*), 5.21 (80 H, s, Cp*H*), 5.11 (16H, br s, CH_2)) 5.05 (40 H, s, Cp*H*), 4.02 (8 H, br s, CH_2), 2.64, 2.41 2.25, 2.07 (176 H, CH_2), 1.65, 1.57 (36 H, CH_3). ^{13}C{^{1}H} NMR (75 MHz, DMSO-d_6): δ (ppm) 172.8, 172.6, 172.5 (*C*=O), 155.5, 155.3, 151.7, 151.6, 151.2, 146.1, 145.9, 140.2, 130.5, 130.3 (Ar*C*), 130.1, 129.9, 129.8, 129.7 (complexed Ar*C*) 129.1, 129.0, 120.3, 120.2, 119.7, 119.5 (Ar*C*), 77.7, 77.0 (Cp*C*), 75.5, 75.4, 75.3, 75.2 (complexed Ar*C*), 64.9, 45.0, 44.7, 44.4, 36.1, 36.0, 35.7, 34.0, 33.4, 30.7, 30.3, 29.8, 29.7, 26.9, 24.0. Elemental analyses: calculated for C, 54.22; H, 4.26; found for C, 53.68; H, 4.20.

4.4.9. Synthesis of G_0 Br-dendrimer-PF_6^-

The dendrimer was synthesized as follow: **G_0 COOH-dendrimer-PF_6^-** (490 mg, 0.09 mmol), 2-bromoethanol (270 mg, 2.16 mmol), DMAP (67 mg, 0.55 mmol), and 10 mL of 5:1 DCM/DMSO solvent mixture were added to a 25-mL round-bottomed flask. The reaction mixture was cooled to 0 °C using ice bath. Next, DCC (163 mg, 0.79 mmol) was added to the reaction mixture over 30 minutes while stirring. The reaction mixture was warmed to room temperature and stirred under

nitrogen for 24 hours. Afterwards, the reaction was stopped, filtered to removed precipitated DCU, and the filtrate added to 50 mL of ice water. A work-up procedure similar to that of **G_0 H-dendrimer-PF_6^-** afforded the product. Yield: 78%. ^{1}H NMR (300 MHz, DMSO-d_6): δ (ppm) 7.35 (32 H, br s, Ar*H*), 7.23 (32 H, br s, Ar*H*), 6.23 (32 H, br s, complexed Ar*H*), 5.20 (40 H, s, Cp*H*), 4.34 (16 H, t, CH_2) 4.02 (8 H, br s, CH_2), 3.67 (16 H, t, CH_2), 2.63 (32 H, br s, CH_2), 2.59 (8 H, br s, CH_2), 2.38, (32 H, br s, CH_2), 2.12 (8 H, br s, CH_2), 1.62 (12 H, br s, CH_3). ^{13}C{^{1}H} NMR (75 MHz, DMSO-d_6): δ (ppm) 172.6, 172.5 (*C*=O), 151.8, 151.2, 145.8, 140.1, 130.5, 129.1, 120.4, 120.0 (Ar*C*), 129.8, 129.7 (complexed Ar*C*), 77.8 (Cp*C*), 75.5, 75.1 (complexed Ar*C*), 63.5, 55.5, 44.8, 44.3, 35.9, 34.0, 33.3, 33.1, 30.7, 30.1, 26.9, 24.0. Elemental analyses: calculated for C, 50.21; H, 4.26; found for C, 49.89; H, 4.33.

4.4.10. Synthesis of G_1 Br-dendrimer-PF_6^-

The synthesis of the dendrimer followed a procedure similar to that used in synthesizing **G_0 Br-dendrimer-PF_6^-**. In brief, **G_1 COOH-dendrimer-PF_6^-** (513 mg, 0.033 mmol), 2-bromoethanol (197 mg, 1.58 mmol), DMAP (49.7 mg, 0.407 mmol), DCC (120 mg, 0.581 mmol), and 10 mL of 3:1 DCM/DMSO solvent mixture were used. The product was isolated using a work-up procedure similar to that of **G_0 H-dendrimer-PF_6^-**. Yield: 77%. ^{1}H NMR (300 MHz, DMSO-d_6): δ (ppm) 7.52 (16 H, br s, Ar*H*), 7.36 (80 H, br s, Ar*H*), 7.25 (80 H, br s, Ar*H*), 7.03 (16 H, br s, Ar*H*) 6.24 (96 H, br s, complexed Ar*H*), 5.21 (80 H, s, Cp*H*), 5.12 (16H, br s, CH_2)) 5.06 (40 H, s, Cp*H*), 4.36 (32 H, br s, CH_2), 4.02 (8 H, br s, CH_2), 3.65 (32 H, br s, CH_2), 2.65, 2.39 2.18 (176 H, CH_2), 1.67, 1.62 (36 H, CH_3). ^{13}C{^{1}H} NMR (75 MHz, DMSO-d_6): δ (ppm) 172.8, 172.5, 172.4 (*C*=O), 155.3, 155.2, 151.9, 151.7, 151.2, 146.1, 145.8, 140.1, 130.5, 130.4 (Ar*C*), 130.0, 129.9, 129.8, 129.7 (complexed Ar*C*) 129.1, 129.0, 120.2, 120.1, 119.8, 119.7 (Ar*C*), 77.8, 77.0 (Cp*C*), 75.4,

75.3, 75.1, 75.0 (complexed Ar*C*), 64.9, 63.7, 45.0, 44.8, 44.4, 36.0, 35.7, 34.0, 33.2, 33.1, 30.8, 30.7, 30.1, 29.7, 29.6, 26.9, 24.0. Elemental analyses: calculated for C, 51.09; H, 4.12; found for C, 50.57; H, 4.13.

4.4.11. Synthesis of G_0 R_4N^+-dendrimer-PF_6^-

The hybrid dendrimer was obtained as follow: **G_0 Br-dendrimer-PF_6^-** (200 mg, 0.032 mmol), triethylamine (777 mg, 7.68 mmol), and 3 mL of DMF were charged into a 25-mL round-bottomed flask. The reaction mixture was stirred at 65 °C under nitrogen for 24 hours. Thereafter, the reaction mixture was cooled to room temperature, added dropwise to $(C_2H_5)_2O$, filtered, washed with copious amount of $(C_2H_5)_2O$, and dried at room temperature to give the product. Yield: 66%. ^{1}H NMR (300 MHz, DMSO-d_6): δ (ppm) 7.35, (32 H, br s, Ar*H*) 7.22 (32 H, br s, Ar*H*), 6.23 (32 H, br s, complexed Ar*H*), 5.19 (40 H, s, Cp*H*), 4.39 (12 H, br s, CH_2), 4.33 (4 H, br s, CH_2) 4.00 (20 H, br s, CH_2), 3.66 (4H, br s, CH_2) 3.10 (36 H, q, CH_2), 2.64 (32 H, br s, CH_2), 2.59 (8 H, br s, CH_2), 2.38, (32 H, br s, CH_2), 2.12 (8 H, br s, CH_2), 1.59 (12 H, br s, CH_3) 1.19 (54 H, t, CH_3). ^{13}C{^{1}H} NMR (75 MHz, DMSO-d_6): δ (ppm) 172.8, 172.7, 172.6, 172.5, 172.4, 172.3 (*C*=O), 151.7, 151.6, 151.2, 151.1, 142.4, 140.1, 130.4, 129.1, 129.0 120.3, 120.1, 119.9, 119.8 (Ar*C*), 129.8, 129.6 (complexed Ar*C*), 77.8 (Cp*C*), 75.1, 75.0 (complexed Ar*C*), 65.5, 63.7, 58.9, 55.4, 54.4, 52.7, 44.9, 44.7, 42.6, 35.9, 34.0, 33.9, 33.2, 33.1, 33.0, 30.2, 30.1, 30.0, 29.7, 29.6, 29.5, 26.9, 23.8, 8.5, 7.1. Elemental analyses calculated for C, 52.06; H, 5.17; N, 1.21 found for C, 51.68; H, 5.23; N, 1.37.

4.4.12. Synthesis of G_1 R_4N^+-dendrimer-PF_6^-

The hybrid dendrimer was obtained using a procedure similar to that used in synthesizing **G_0 R_4N^+-dendrimer-PF_6^-**. In brief, **G_1 Br-dendrimer-PF_6^-** (200 mg, 0.0115 mmol), triethylamine (559

mg, 5.52 mmol), and 3 mL of DMF were used. Yield: 76%. ^{1}H NMR (300 MHz, DMSO-d_6): δ (ppm) 7.52 (16 H, br s, Ar*H*), 7.35 (80 H, br s, Ar*H*), 7.23 (80 H, br s, Ar*H*), 7.04 (16 H, br s, Ar*H*) 6.25 (96 H, br s, complexed Ar*H*), 5.21 (80 H, s, Cp*H*), 5.12 (16H, br s, CH_2)) 5.06 (40 H, s, Cp*H*), 4.39 (24 H, br s, CH_2), 4.30 (8 H, br s, CH_2), 4.03 (32 H, br s, CH_2), 3.68 (8 H, br s, CH_2), 3.54 (72 H, br s, CH_2), 2.64, 2.40 2.18 (176 H, CH_2), 1.67, 1.62 (36 H, CH_3), 1.19 (108 H, t, CH_3). ^{13}C{^{1}H} NMR (75 MHz, DMSO-d_6): δ (ppm) 172.8, 172.6, 172.5, 172.4, 172.3, 172.2 (*C*=O), 155.5, 155.4, 155.3, 155.2, 151.9, 151.6, 151.5, 151.2, 145.8, 145.7, 140.1, 130.4, 130.3 (Ar*C*), 130.0, 129.9, 129.8, 129.7, 129.6 (complexed Ar*C*) 129.1, 129.0, 120.5, 120.3, 119.8, 119.6 (Ar*C*), 77.8, 77.7, 77.0 (Cp*C*), 75.4, 75.3, 75.2, 75.1, 75.0, 74.5 (complexed Ar*C*), 65.4, 64.8, 63.7, 63.5, 44.9, 44.8, 44.7, 42.6, 42.4, 36.0, 35.7, 33.9, 33.2, 32.9, 30.8, 30.7, 30.2, 30.1, 29.7, 29.6, 29.5, 26.9, 23.8, 8.4, 7.1. Elemental analyses: calculated for C, 52.41; H, 4.83; N, 0.91 found for C, 52.62; H, 4.90; N, 0.98.

4.4.13. DOSY NMR spectroscopy

Diffusion-order spectroscopy (DOSY) measurements were carried using a Bruker Avance III 600 MHz NMR spectrometer (Bruker Corporation, East Milton, ON) equipped with a 1.7 mm Bruker gradient triple resonance inverse (TXI) probe. Dendrimer samples (2.5 mM) were dissolved in DMSO-d_6 ($\eta_s = 1.99 \times 10^{-3}$ Pa s at 25 °C) and the DOSY experiments conducted at 25.0 ± 0.1 °C. Each sample was auto-locked on DMSO-d_6, auto-tuned at 600.28 MHz and shimmed. The Bruker DOSY pulse program "dstebpgp3s", which included bipolar gradients and double stimulated echo for compensating for gradient errors and convection, respectively, was used. The pulsed gradient strength of 56 G/cm in the z-direction (GPZ) was calibrated using water. For all spectra, the diffusion time (d20) and the eddy current delay (d21) were set to 200 ms and 5 ms,

respectively. The duration of the pulse gradient (p30) was optimized for each sample (ranging from 1550-2050 μs) to ensure that about 10% of the original signal remained after linear ramping from 5–90% of the maximum gradient strength GPZ (Bruker gradient shaped pulse SMSQ10.100) with 18 data points (gradient ramp in 5% increments). Other operating parameters were 16k/18 F2/F1 time domain sizes, 6s relaxation delay, 8 dummy scans, and 16 or 64 acquisition scans. All peaks were referenced to DMSO-d_6 residual peak at 2.50 ppm. After acquisition, the data was zero filled to 64 K, Fourier transformed and baseline corrected in F2. The Bruker Dynamics Center Software was used to fit the data and to provide diffusion coefficients. For each sample, the cyclopentadienyl peak at ~ 5.20 ppm was used to extract individual diffusion coefficients. The hydrodynamic radius was calculated from the diffusion coefficient using the Stokes-Einstein relationship:[75]

$$D_0 = \frac{k_B T}{6\pi\eta_s R_h}$$

where D_0 is the diffusion coefficient, k_B the Boltzmann constant, T the absolute temperature, η_s the viscosity, and R_h the hydrodynamic radius.

4.4.14. Electron spin resonance (EPR) spectroscopy

A 128 mg/mL DMSO/H_2O (70%:30%) solution of dendrimer containing 1.2 molar equivalent of nitrosobenzene spin trap per iron center was prepared under ambient conditions. The EPR spectra were acquired at room temperature and 77 K using 2.0 mm internal diameter EPR tubes. The spectra were acquired on Active Spectrum Micro-ESR™ instrument immediately after sample preparation. As a control, EPR spectra of the same equivalent of nitrosobenzene in DMSO/H_2O (70%:30%) were also acquired at 298 K and 77 K.

4.4.15. Evaluation of antimicrobial activity

Antimicrobial activity of the complexes or dendrimers against methicillin-resistant *Staphylococcus aureus* ATCC 33591 (MRSA), *Staphylococcus warneri* ATCC 17917, vancomycin-resistant *Enterococcus faecium* EF379 (VRE), *Bacillus subtilis* ATCC 9466, *Pseudomonas aeruginosa* ATCC 14210, *Proteus vulgaris* ATCC 12454, and *Candida albicans* ATCC 14035 were carried out in 96-well plates using the Clinical Laboratory Standards Institute (CLSI) microbroth dilution antimicrobial testing protocol.[59,60] The microorganisms were grown according to the CLSI protocol[60] and overnight seed cultures of assay microorganisms were diluted in their respective growth medium to a concentration of 6.5×10^5 cfu/mL and dispensed into assay plates. Assays were carried out in triplicate against each microorganism at twelve different concentrations obtained by serial dilution of the initial concentration, 128 μg/mL, to give the final concentration, 0.0625 μg/mL, in 2% DMSO. Each plate also contained eight uninoculated positive controls (media + 2% DMSO), eight untreated negative controls (media + 2% aqueous DMSO + microorganism), and one column containing a concentration range of a control antibiotic (vancomycin for MRSA and *S. warneri*; rifampicin for VRE; gentamycin for *P. aeruginosa*; ciprofloxacin for *P. vulgaris*; or nystatin for *C. albicans*). The optical density of the plate was recorded using a Thermo Scientific Varioskan Flash plate reader at 600 nm before and after incubation of the plates at 37 °C for 22 hours. After subtracting the initial OD_{600} reading from the final, the percentages of microorganisms' survival relative to the positive control wells were calculated, the concentrations that inhibited 90% and 50% of the microorganisms, IC_{90} and IC_{50}, respectively, were determined and reported in μM.

4.4.16. Evaluation of cytotoxicity

The toxicity of the complexes or dendrimers against adult human epidermal keratinocytes (HEKa) (Invitrogen#C-005-5C) and human foreskin BJ fibroblast cells (ATCC CRL-2522) was carried out as previously reported.[59] Prior to the cytotoxicity assays, the cells were grown as follows: human foreskin BJ fibroblast cells were grown and maintained in 15 mL of Eagle's minimal essential medium supplemented with 10% fetal bovine serum and 100 μU penicillin and 0.1 mg/mL streptomycin in T75 cm^2 cell culture flasks at 37 ^oC in a humidified atmosphere of 5% CO_2. Culture medium was refreshed every 2-3 days and cells were not allowed to exceed 80% confluency. The adult human epidermal keratinocytes (HEKa) isolated from skin were grown in 15 mL of EpiLife medium supplemented with human keratinocyte growth supplements in T75 cm^2 cell culture flasks, and incubated at 37 ^oC in a humidified atmosphere of 5% CO_2. Growth medium was refreshed every 2 days until the cells reached 50% confluency and then the medium was refreshed every day until 80% confluency was obtained.

At 80% confluency, the cells were counted, diluted and plated into 96 well-treated cell culture plates. The cells were plated at a cell density of 10,000 cells per well in 90 μL of respective growth medium, which were the same as those described above except antibiotics were not added. The plates were incubated at 37 ^oC in a humidified atmosphere of 5% CO_2 to allow cells to adhere to the plates for 24 hours before treatment. DMSO was used as the vehicle at a final concentration of 1% in the wells. The complexes or dendrimers were resolublized in sterile DMSO and a dilution series was prepared for each cell line using the respective cell culture growth medium of which 10 μL were added to the respective assay plate well to give eight final concentrations that ranged from 128 μg/mL to 1 μg/mL per well that had a final volume of 100 μL. Each plate also contained four uninoculated positive controls (media + 1% DMSO), four untreated negative controls (media +

1% DMSO + cells), and one column containing a concentration range of zinc pyrithione or doxorubicin as standard. Next, the plates were incubated at 37 ^{o}C in a humidified atmosphere of 5% CO_2 for 24 hours. After 24 hours, AlamarBlue was added to each well at 10% of the culture volume (11 µL in 100 µL). Fluorescent emission at 590 nm was monitored using a Thermo Scientific Varioskan Flash plate reader after excitation at 560 nm. The emission was monitored before AlamarBlue was added and 4 hrs later. After subtracting the initial emission reading from the final, the inferred percentage of cell viability relative to positive control wells were calculated, the IC_{50} was determined and reported in µM. Assays were conducted in triplicate.

4.4.17. Oxidative stress assay

Using a previously reported protocol,[68] the oxidative stress assay was carried out in 96 well plates with the same inoculum density generated using the antimicrobial assay protocol described above. Prior to plate inoculation, the MRSA inoculum was split by transferring equal volumes into two 50-mL conical centrifuge tubes and both tubes were centrifuged at 19,040 g-force for 5 minutes. The supernatant was discarded and the bacterial pellets resuspended in 10 mL of assay buffer (4.2 g MOPS, 80 mg NH_4NO_3, 4 mg K_2HPO_4 in 1 L sterile deionized H_2O) one of which included dichlorodihydrofluorescein (H_2DCF, 4.87 mg/L), and incubated for 30 minutes at room temperature. Bacterial cells were then centrifuged at 19,040 g-force. The cells pellet was washed twice with assay buffer, and then suspended to the original volume in pre-warmed CAMHB media (37°C). A 90 µL of the H_2DCF treated and untreated bacterial cells were dispensed into 96-well assay plates containing test compounds, a vancomycin dilution series (reference), and a 200–25 µM dilution series of H_2O_2 (positive control). Fluorescent emission at 535 nm was monitored using a Thermo Scientific Varioskan Flash plate reader after excitation at 485 nm. Plates were incubated

at 37°C and fluorescence measurements were taken at 0, 0.5, 4 and 24 hours. The assay results were corrected for baseline fluorescence (measurements of untreated controls were subtracted from treated controls) and expressed as a percentage of maximal oxidative stress response relative to H_2O_2 positive control.

4.4.18. Evaluation of haemolytic activity

The haemolytic activity of the dendrimers was tested using defibrinated sheep whole blood. To pellet the blood cells, 1 mL of defibrinated sheep whole blood was centrifuged at 1680 g-force for 5 min and the pellet was washed four times with 0.9% saline. The red blood cells pellet was suspended in red blood cell buffer that consists of 0.5999 g of 5 mM sodium phosphate and 8.766 g of 150 mM NaCl in deionized H_2O maintained at pH 7.4. A 20 µL aliquot of dendrimer (6.40 mg/mL) in 2% sterilized DMSO was added to 980 µL of red blood cells buffer. Then, 25 µL of blood cell suspension was added to 1 mL of dendrimer solution prepared in the buffer. A vehicle control (20 µL of 2% DMSO in 980 µL RBC buffer), positive control (25 µL of cell suspension in 1 mL of deionized H_2O), and negative control (25 µL of cell suspension in 1 mL the buffer) were also assayed. Tubes that contained test samples and assay controls were incubated for 2 hrs at room temperature. Afterwards, the tubes were centrifuged at 1680 g-force for five minutes, and 200 µL of the supernatant was transferred into a 96-well plate. The absorbance was measured at 540 nm after shaking for 10 seconds. All measurements were blanked with the negative and vehicle control and were taken in triplicate. The haemolysis percentage was determined relative to the positive control.

4.4.19. Field emission scanning electron microscopy (FE-SEM)

A 20 μL of MRSA was cultured in 20 mL of cation adjusted Mueller Hinton (CAMH) broth supplemented with 12.5 μg/mL of penicillin G. The microorganisms were inoculated at 37 ^{o}C for 18 hours under constant shaking at 3.25 g-force. The inoculum was transferred into a 50-mL flacon tube with beads, vortexed for one minute and allowed to sit for five minutes to allow aerosols to settle. Then, the inoculum was diluted to give 6.5×10^5 or 6.5×10^7 cfu/mL. Using the same antibacterial testing protocol described above, the diluted inoculum was treated with the antimicrobial IC_{50} of the appropriate dendrimer in DMSO, and incubated for 22 hours. A negative control, which consisted of untreated inoculum, was also prepared using the above protocol. Afterwards, the inoculum was centrifuged at 1075 g-force for five minutes. The supernatant was collected, washed twice with 1 mL of 2.5% glutaraldehyde/phosphate-buffered saline, centrifuged at 1075 g-force, and the supernatant removed. The bacterial cells were fixed with 500 μL of 2.5% glutaraldehyde/phosphate-buffered saline for 60 minutes, pelleted and washed twice with phosphate-buffered saline. Dehydration was carried out in a series of ethanol solutions (25%, 35%, 50%, 75%, 90%, 95%, and 100%). The bacterial cells were suspended in 100% ethanol, dripped on copper tape, and dried at room temperature for 2 days. The dried samples were sputtered coated with gold/palladium layer before SEM imaging using Hitachi S-4700 FE-SEM.

4.4.20. Confocal laser fluorescence microscopy

The BJ fibroblast cells were grown to 80% confluency using the cytotoxicity assay protocol.[28] At 80% confluency, the cells were counted, diluted, and plated into 4-chamber culture slides. The cells were plated at a cell density of 50,000 cells per chamber in 540 μL of the growth medium. All media used in the preparation of the slides was the same as those used to grow the cells except antibiotics were absent. The culture slides were incubated at 37 ^{o}C in a humidified atmosphere of

5% CO_2 to allow cells to adhere to the slides for 24 hours before treatment. Dendrimers were solubilized in sterile DMSO and diluted to 1.28 mg/mL using the cell culture growth medium. The diluted dendrimer solution (60 µL) was added to the respective chamber well to give a final concentration of 128 µg/mL with a final DMSO concentration of 1% per chamber. Each culture slide included an untreated negative control chamber that contained cells, growth media and 1% DMSO. The cells were incubated at 37 ^{o}C in a humidified atmosphere of 5% CO_2 for 24 hours. Next, the growth medium was removed from the culture slide chambers by vacuum. The chambers were washed twice with a pH 7.5, phosphate-buffered saline solution. The upper plastic chambers of the slides were removed. The slides were transferred to a glass-staining dish, fixed with cold acetone for 10 minutes at 4 ^{o}C, air-dried in a fumehood for two minutes, and washed twice with phosphate-buffered saline solution. A fluorescent dye, 4',6-diamidino-2-phenylindole (DAPI), diluted to 1:500 in deionized H_2O was added to the slides to stain the nuclei of the cells. The slides were then incubated at room temperature for one minute, and were washed twice with phosphate-buffered saline solution. A mounting medium of 30% glycerol and 70% phosphate-buffered saline was prepared and was used to mount coverslips onto the slides before confocal laser fluorescence microscopic imaging using Carl Zeiss Confocal Laser Fluorescence Microscope.

Reference

1. Shallcross, L. J.; Howard, S. J.; Fowler T.; Davies, S. C. *Philos. Trans. R. Soc. B.* **2015**, *370*, 20140082.
2. Patra, M.; Gasser, G.; Metzler-Nolte, N. *Dalton Trans.,* **2012**, *41*, 6350.
3. Patra, M.; Wenzel, M.; Prochnow, P.; Pierroz, V.; Gasser, G.; Bandow J. E.; Metzler-Nolte, N. *Chem. Sci.,* **2015**, *6*, 214.
4. Lam, P.; Lu, G.; Hon, K.; Lee, K.; Ho, C.; Wang, X.; Tang, J.; Lam, K.; Wong, R.; Kok, S. *Dalton Trans.,* **2014**, *43*, 3949.
5. Chen, W.; Ou, W.; Wang, L.; Hao, Y.; Cheng, J.; Li, J.; Liu, Y. *Dalton Trans.,* **2013**, *42*, 15678.

6. Albada, H. B.; Prochnow, P.; Bobersky, S.; Bandow, J. E.; Metzler-Nolte, N. *Chem. Sci.,* **2014**, *5*, 4453.
7. Wenzel, M.; Patra, M.; Senges, C. H. R.; Ott, I.; Stepanek, J. J.; Pinto, A.; Prochnow, P.; Vuong, C.; Langklotz, S.; Metzler-Nolte, N. *ACS Chem. Biol.,* **2013**, *8*, 1442.
8. Zhang, J.; Chen, Y. P.; Miller, K. P.; Ganewatta, M. S.; Bam, M.; Yan, Y.; Nagarkatti, M.; Decho, A. W.; Tang, C. *J. Am. Chem. Soc.,* **2014**, *136*, 4873.
9. Nguyen, D.; Nguyen, T.; Rice, S. A.; Boyer, C. *Biomacromolecules,* **2015**, *16*, 2776.
10. Paladini, F.; Pollini, M.; Sannino, A.; Ambrosio, L. *Biomacromolecules,* **2015**, *16*, 1873.
11. Dubar, F.; Slomianny, C.; Khalife, J.; Dive, D.; Kalamou, H.; Guérardel, Y.; Grellier, P.; Biot, C. *Angew. Chem. Int. Ed.,* **2013**, *52*, 7690.
12. Astruc, D. *Acc. Chem. Res*. **2000**, *33*, 287.
13. Deffert, C.; Cachat, J.; Krause, K. *Cell. Microbiol.,* **2014**, *16*, 1168.
14. Kim, H. J.; Kim, C.; Ryu, J.; Kim, M.; Park, C. Y.; Lee, J. M.; Holtzman, M. J.; Yoon, J. *Am. J. Respir. Cell Mol. Biol.,* **2013**, *49*, 855.
15. Rada, B.; Leto, T. L. *Contrib. Microbiol.,* **2008**, *15*, 164.
16. West, A. P.; Shadel, G. S.; Ghosh, S. *Nat. Rev. Immunol.,* **2011**, *11*, 389.
17. Peacock, A. F.; Sadler, P. J. *Chem Asian J.,* **2008**, *3*, 1890.
18. Li, F.; Collins, J. G.; Keene, F. R. *Chem. Soc. Rev.,* **2015**, *44*, 2529.
19. Li, F.; Harry, E. J.; Bottomley, A. L.; Edstein, M. D.; Birrell, G. W.; Woodward, C. E.; Keene, F. R.; Collins, J. G. *Chem. Sci.,* **2014**, *5*, 685.
20. Khand, I.; Pauson, P.; Watts, W. *J. Chem. Soc.: C,* **1968**, 2257.
21. Khand, I.; Pauson, P.; Watts, W. *J. Chem. Soc.: C* **1968**, 2261.
22. Khand, I.; Pauson, P.; Watts, W. *J. Chem. Soc.: C* **1969**, 116.
23. Abd-Ei-Aziz, A. S.; Denus, C. R. D.; Epp, K. M.; Smith, S.; Jaeger, R. J.; Pierce, D. T. *Can. J. Chem.,* **1996**, *74*, 650.
24. Abd-El-Aziz, A. S.; Winkler, K.; Baranski, A. S. *Inorg. Chim. Acta,* **1992**, *194*, 207.
25. Abd-El-Aziz, A. S.; Baranski, A.; Piorko, A.; Sutherland, R. *Inorg. Chim. Acta,* **1988**, *147*, 77.
26. Abd-El-Aziz, A. S.; Todd, E. K.; Okasha, R. M.; Shipman, P. O.; Wood, T. E. *Macromolecules, 2005*, *38*, 9411.
27. Kenawy, E.; Worley, S.; Broughton, R. *Biomacromolecules* **2007***, 8*, 1359.
28. Patrick, G. L. *An Introduction to Medicinal Chemistry;* Oxford University Press: **2013**.
29. Marchal, E.; Uddin, M. I.; Smithen, D.; Hawco, C.; Lanteigne, M.; Overy, D.; Kerr, R.; Thompson, A. *RSC Adv.* **2013***, 3*, 22967.
30. Mallavadhani, U.V.; Sahoo, L.; Kumar, K. P.; Murty, U. S. *Med. Chem. Res.* **2014**, *23*, 2900.
31. Astruc, D.; Ruiz, J. *J. Inorg. Organomet. Polym. Mater.* **2015***, 25*, 330.
32. Rapakousiou, A.; Wang, Y.; Ciganda, R.; Lasnier, J.; Astruc, D. *Organometallics* **2014***, 33*, 3583.
33. Astruc, D.; Dabard, R.; Laviron, E. *C. R. Acad. Sci., Ser. C* **1969***, 269*, 608.
34. Hunley, M. T.; England, J. P.; Long, T. E. *Macromolecules* **2010***, 43*, 9998.
35. Narayanan, A.; Bauri, K.; Ruidas, B.; Pradhan, G.; Banerjee, S.; De, P. *Langmuir* **2014***, 30*, 13430.
36. Lu, R.; Qu, Z.; Yu, H., Wang, F.; Wang, S., *J. Mol. Graph. Model*. **2012**, *36*, 36.
37. Savjani, K. T.; Gajjar, A. K.; Savjani, J. K. *ISRN Pharm.* **2012***, 2012*.
38. Bogdan, A. R.; Davies, N. L.; James, K. *Org. Biomol. Chem.* **2011***, 9*, 7727.

39. Wong, S.; Appelhans, D.; Voit, B.; Scheler, U. *Macromolecules* **2001***, 34*, 678.
40. van Dongen, M. A.; Orr, B. G.; Banaszak Holl, M. M. *J. Phys. Chem. B* **2014***, 118*, 7195.
41. Neidlinger, A.; Kienz, T.; Heinze, K. *Organometallics,* **2015**, *34*, 5310.
42. Barclay, L. R. C.; Dust, J. M. *Can. J. Chem.,* **1982**, *60*, 607.
43. Djeda, R.; Ornelas, C.; Ruiz, J.; Astruc, D. *Inorg. Chem.,* **2010**, *49*, 6085.
44. Rajasekharan, M.; Giezynski, S.; Ammeter, J.; Oswald, N.; Hamon, J.; Astruc, D.; Michaud, P. *J. Am. Chem. Soc.,* **1982**, *104*, 2400.
45. Ruiz, J.; Pradet, C.; Varret, F.; Astruc, D. *Chem. Commun.,* **2002**, 1108.
46. Astruc, D.; Hamon, J. R.; Roman, E.; Michaud, P. *J. Am. Chem. Soc.,* **1981**, *103*, 7502.
47. Hamon, J. R.; Astruc, D.; Michaud, P. *J. Am. Chem. Soc.,* **1981**, *103*, 758.
48. Cais, M.; Ashkenazi, P.; Dani, S.; Gottlieb, J. *J. Organomet. Chem.,* **1977**, *124*, 49.
49. Abd-El-Aziz, A. S.; Afifi, T. H.; Budakowski, W. R.; Friesen, K. J.; Todd, E. K. *Macromolecules,* **2002**, *35*, 8929.
50. Patil, M. L.; Zhang, M.; Taratula, O.; Garbuzenko, O. B.; He, H.; Minko, T. *Biomacromolecules*, **2009**, *10*, 258.
51. Maitra, P.; Wunder, S. L. *Chem. Mater*. **2002**, *14*, 4494.
52. Kathi, J.; Rhee, K-Y.; Lee, J. H. *Composites: Part A*, **2009**, *40*, 800.
53. Tang, X-Z.; Li, W.; Yu, Z-Z.; Rafiee, M. A.; Rafiee, J.; Yavari, F.; Koratkar, N. *Carbon*, **2011**, *49*, 1258.
54. Wu, D.; Wu, L.; Zhang, M.; Zhao, Y. *Polym. Degrad. Stab*., **2008**, *93*, 1577.
55. Gulotty, R.; Castellino, M.; Jagdale, P.; Tagliaferro, A.; Balandin, A. A. *ACS Nano*, **2013**, *7*, 5114.
56. Yang, K.; Gu, M.; Guo, Y.; Pan, X.; Mu, G. *Carbon*, **2009**, *47*, 1723.
57. Velasco-Santos, C.; Martínez-Hernández, A. L.; Fisher, F. T.; Ruoff, R.; Castano, V. M. *Chem. Mater*., **2003**, *15*, 4470.
58. Stevens, M. P. *Polymer Chemistry an Introduction*, Oxford University Press, New York, USA **1999**.
59. Overy, D. P.; Berrue, F.; Correa, H.; Hanif, N.; Hay, K.; Lanteigne, M.; Mquilian, K.; Duffy, S.; Boland, P.; Jagannathan, R. *Mycology* **2014***, 5*, 130-144.
60. National Committee for Clinical Laboratory Standards, Approved standard M7–A6 6th ed.
61. Dahl, T. A.; Midden, W. R.; Hartman, P. E. *J. Bacteriol.,* **1989**, *171*, 2188.
62. Herzog, I. M.; Fridman, M. *Med. Chem. Commun.* **2014**, *5*, 1014.
63. Yin, L. M.; Edwards, M. A.; Li, J.; Yip, C. M.; Deber, C. M. *J. Biol. Chem.* **2012**, *287*, 7738.
64. Chen, C. Z.; Beck-Tan, N. C.; Dhurjati, P.; Van Dyk, T. K.; LaRossa, R. A.; Cooper, S. L. *Biomacromolecules* **2000**, *1*, 473.
65. Sharma, S. K.; Chauhan, G. S.; Gupta, R.; Ahn, J.-H. *J. Mater. Sci. Mater. Med*. **2010**, *21*, 717.
66. Shadil, Y.; Chauhan, G. S.; Ahn, J.-H., Sharma, R. K. *Anti-Infective Agents* **2015**, *13*, 78.
67. Diaz-Torres, R.; Alvarez, S. *Dalton Trans*. **2011**, *40*, 10742.
68. Choi, O.; Hu, Z. *Environ. Sci. Technol*. **2008**, *42*, 4583.
69. Wang, H.; Joseph, J. A. *Free Radic. Biol. Med.* **1999***, 27*, 612.
70. Ahmida, M. H. *Exp. Toxicol. Pathol.* **2012***, 64*, 149.
71. Bizzini, A.; Zhao, C.; Auffray, Y.; Hartke, A. *J. Antimicrob. Chemother.* **2009***, 64*, 1196.
72. Straus, S. K.; Hancock, R. E. W. *Biochim. Biophys. Acta* **2006**, *1758*, 1215.

73. Pascual, A.; Tan, J. P.; Yuen, A.; Chan, J. M.; Coady, D. J.; Mecerreyes, D.; Hedrick, J. L.; Yang, Y. Y.; Sardon, H. *Biomacromolecules* **2015***, 16*, 1169.
74. Hurdle, J. G.; O'Neill, A. J.; Chopra, I.; Lee, R. E. *Nat. Rev. Microbiol.* **2011***, 9*, 62.
75. Bogdan, A. R.; Davies, N. L.; James, K. *Org. Biomol. Chem*. **2011**, *9*, 7727.

Chapter Five: Magnetoceramics from Organometallic Dendrimers[†]

Abstract

Magnetic materials drive many innovative technologies. Several approaches that include pyrolysis of linear and hyperbranched polymer precursors are developed to generate these magnetic materials. Inspired by the continuing demand for magnetic materials, $[\eta^6$-arene-η^5-CpFe$]^+$-derived dendrimers were explored. Indeed, dendrimer unique topology offers means to control magnetic properties *via* dendritic effects and functionalization with various ferromagnetic metals. Here, the magnetic properties of ceramics obtained from $[\eta^6$-arene-η^5-CpFe$]^+$-derived dendrimers were tuned *via* dendritic effects. Specifically, the saturation magnetization (M_s) and coercivity (H_c) decreased as the dendrimer generation increased. Aiming to tune the magnetic property *via* another approach, the dendrimers periphery was functionalized with cobalt (Co) to obtain a heterometallic dendrimer. Incorporating Co into the dendrimers noticeably changes the magnetic properties of the ceramics. M_s and H_c increased in ceramics derived from the G_2 dendrimer but these properties decreased in ceramics derived from G_0 and G_1 dendrimers. Also, the magnetism in the homometallic and heterometallic ceramics differs in their response to change in temperature. Overall, the results present dendrimers as a new type of precursor for magnetoceramics and expand the parameter space towards understanding magnetism in ceramics, allowing for the development of ceramics with tunable magnetism.

[†] This chapter is published as Abd-El-Aziz, A. S.; Agatemor, C.; Etkin, N.; Bissessur, R. *J. Mater. Chem. C* **2017**, *5*, 2268 and reproduced by permission of The Royal Society of Chemistry.

5.1. Introduction.

Magnetic materials continue to attract attention because of their importance in many areas of fundamental and applied sciences ranging from medicine to information technology.[1-5] Indeed, the design of new magnetic materials remains an attractive research goal.[1] A persistently explored strategy to develop these materials, pyrolytic ceramization, involves the high-temperature transformation of an organometallic polymer precursor into magnetic ceramics.[6,7] It is desirable that the structure, as well as the number of magnetic species in unit volume of the precursor, be controlled to tune the magnetic property. Indeed, many reports feature the effect of structure on the saturation magnetization (M_s). As an example, magnetic ceramics derived from linear polymers are characterized by relatively low M_s, usually in the range of 6–55 emu g^{-1},[1,7,8] whereas those derived from hyperbranched polymers exhibit M_s values that are high, up to 120 emu g^{-1}.[9,10] The high M_s of ceramics derived from hyperbranched polymers is attributed to the "cage effect" of the 3D structure of these precursors, which better retain pyrolyzed species, and grow the magnetic crystallites.[9-11] It is, therefore, logical to assume that 3D organometallic polymers are a promising class of precursors of magnetic ceramics.

Dendrimers, a type of 3D perfectly branched polymers, features some acknowledged advantages over hyperbranched polymers. For instance, the step-by-step, iterative synthesis of dendrimers results in perfectly branched and well-defined structures with dispersity that approaches unity, properties that are desirable in many applications.[12-17] Further, through a well implemented synthesis strategy, dendrimers with "inner nanocavities" that mimic "cages" that trap pyrolyzed species and grow magnetic crystallite can be designed by choosing appropriate core or generation. Also, the well-known "dendritic effects," where a functional property is tuned by changing the dendrimer generation, can open new frontiers in many fields.[13] Indeed, although these

attractive properties of dendrimers are well explored in catalysis and biology, they are currently used to a lesser extent in material science.[13] As an example, literature search reveals that while 3D hyperbranched polymers are at the forefront, advancing the design of magnetic ceramics, dendrimers remain unexplored in this regard. To promote the potentials of dendrimers, especially, in the field of materials science, it is attractive to use them as precursors for magnetic ceramics.

To design magnetic ceramic precursors, it is critical to incorporate magnetic species into the polymer framework. Most precursors incorporate ferromagnetic metals such as iron,[6,7,8,10,11,19-28] cobalt[1,7,9,10,11,28-32] and nickel[33] as magnetic species. For instance, Manners *et al*.[6,7,33] developed magnetic ceramics from nickel-, iron- or cobalt-containing linear and cross-linked polymers while Tang *et al*.[11,25] focused on iron- or cobalt-containing hyperbranched polymers as precursors. In the previous *Chapters*, it is evident that $[\eta^6$-arene-η^5-CpFe$]^+$ complex in the dendrimers impart redox activity and bioactivity. In this *Chapter*, the objective is to derive magnetic materials from the dendrimers given that iron, which is present in $[\eta^6$-arene-η^5-CpFe$]^+$ complex, is ferromagnetic. Further, the presence of the iron induces the chloro groups in **G_0 Cl-dendrimer-PF_6^-**, **G_1 Cl-dendrimer-PF_6^-** and **G_2 dendrimer-PF_6^-** (*Chapter Two*) towards S_NAr reactions at the periphery, allowing the functionalization of these dendrimers with other ferromagnetic species to, possibly, manipulate the magnetic property. Given the objective and the fact that dendrimers are yet-to-be-explored as a preceramic precursor, it is rational to use $[\eta^6$-arene-η^5-CpFe$]^+$-derived dendrimers to demonstrate the potential of dendrimers as precursors of magnetic ceramics.

Bulk pyrolysis of the homometallic, chloro-capped dendrimers, hereafter coded **G_0 Fe-dendrimer**, **G_1 Fe-dendrimer** and **G_2 Fe-dendrimer**, yielded room temperature ferromagnetic ceramics. The susceptibility of these chloro-capped dendrimers towards S_NAr reactions, allows their functionalization with cobalt to obtain heterometallic dendrimers (**G_0 Co/Fe-dendrimer**, **G_1**

Co/Fe-dendrimer, **G_2 Co/Fe-dendrimer**), which on pyrolysis, also yielded magnetic ceramics. This study enriches the current portfolio of ceramic precursors and introduces new parameters to control magnetism in ceramics.

5.2. Results and discussion

5.2.1. Synthesis of dendrimers

Previously, efforts in accessing magnetic ceramics from polymers focused on linear and hyperbranched polymers precursors.[6,7,11,24,33] Here, three generations of a heterometallic dendrimer, **G_0 Co/Fe-dendrimer**, **G_1 Co/Fe-dendrimer**, and **G_2 Co/Fe-dendrimer**, were synthesized, pyrolyzed, and investigated for their magnetic property. The magnetic property of homometallic ceramics derived from **G_0 Fe-dendrimer**, **G_1 Fe-dendrimer** and **G_2 Fe-dendrimer** was also investigated.

The synthesis of the heterometallic dendrimers, **G_0 Co/Fe-dendrimer**, **G_1 Co/Fe-dendrimer** and **G_2 Co/Fe-dendrimer**, proceeded *via* a three-step synthesis route, involving well-established chemistries. As an example, **G_0 Co/Fe-dendrimer** was synthesized *via* a sequence of reaction steps that included S_NAr reaction of **G_0 Cl-dendrimer** with 5-(4-hydroxyphenyl)-pentanoic acid in the presence of the weak base, potassium carbonate, to obtain **G_0 COOH-dendrimer**, which on Steglich esterification reaction with 2-butyne-1,4-diol yielded the alkyne-containing **G_0 alkyne-dendrimer** (Scheme 5.1). The cobalt moieties were coordinated into **G_0 alkyne-dendrimer** in a step that exploited the reactivity of the alkyne bonds with cobalt octacarbonyl (Scheme 5.1). The G_1 and G_2 dendrimers, **G_1 Co/Fe-dendrimer** and **G_2 Co/Fe-dendrimer**, respectively**,** were synthesized using similar procedures. The synthesis routes to **G_0 Fe-dendrimer**, **G_1 Fe-dendrimer** and **G_2 Fe-dendrimer** are detailed in *Chapter Two*.

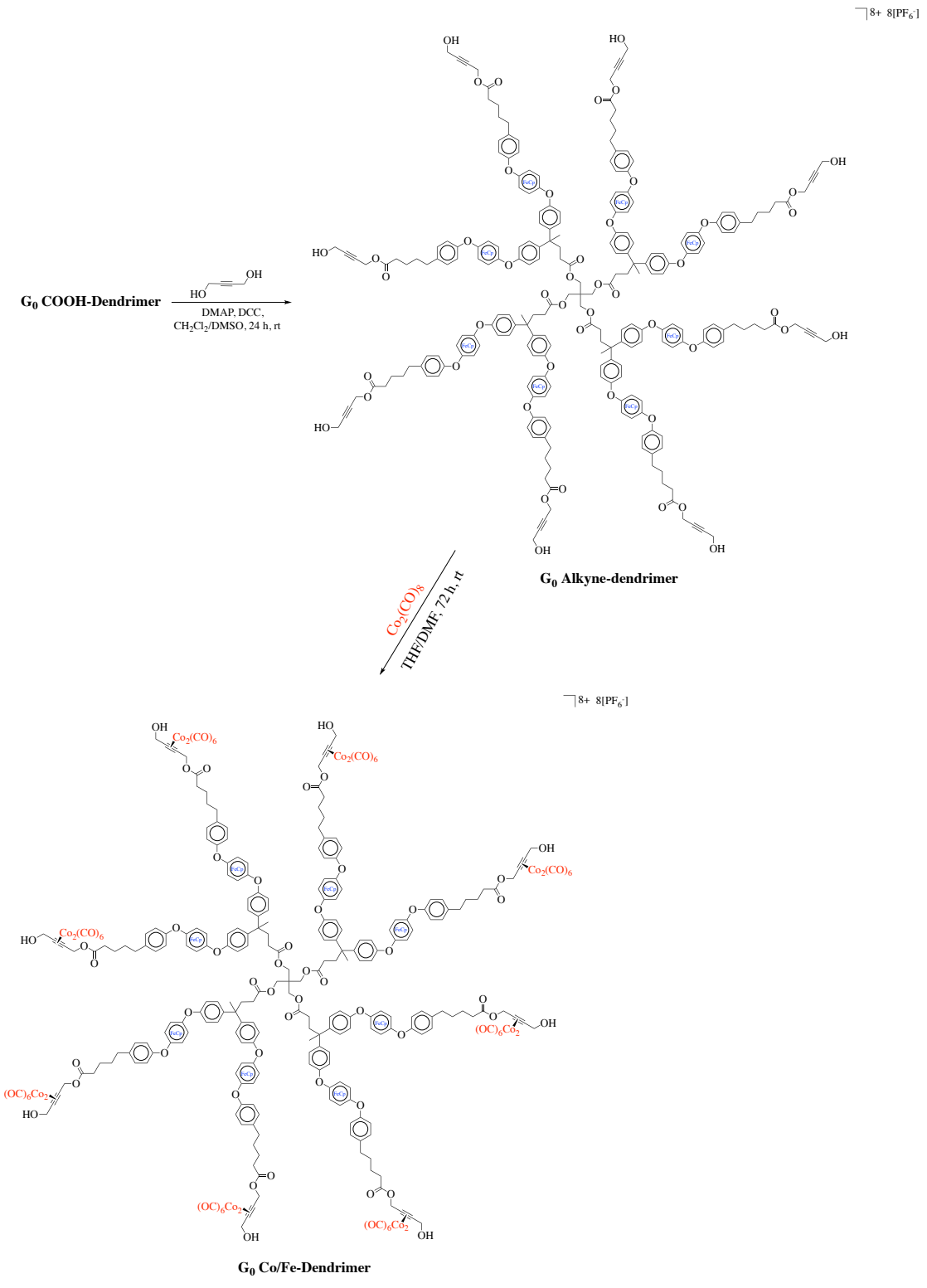

Scheme 5.1. Schematic representation of the synthesis of heterometallic dendrimer, **G_0 Co/Fe-dendrimer**. The structure of **G_0 COOH-dendrimer** is the same as **G_0 COOH-dendrimer-PF_6^-** in *Chapter Four*.

Scheme 5.2. Schematic representation of the synthesis of heterometallic dendrimer, **G_1 Co/Fe-dendrimer**. The structure of **G_1 COOH-dendrimer** is the same as **G_1 COOH-dendrimer-PF_6^-** in *Chapter Four*.

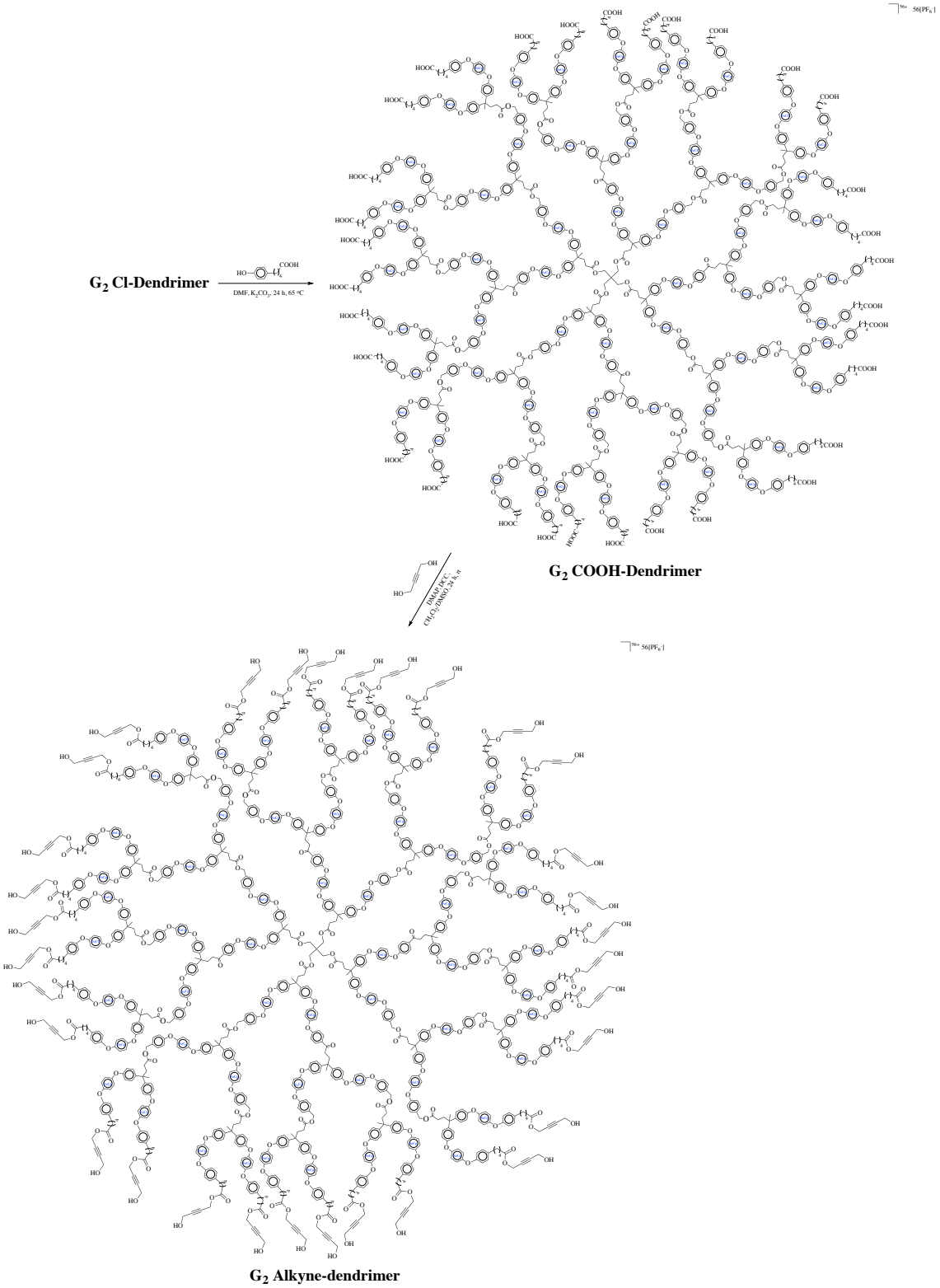

Scheme 5.3. Schematic representation of the synthesis of **G_2 alkyne-dendrimer**.

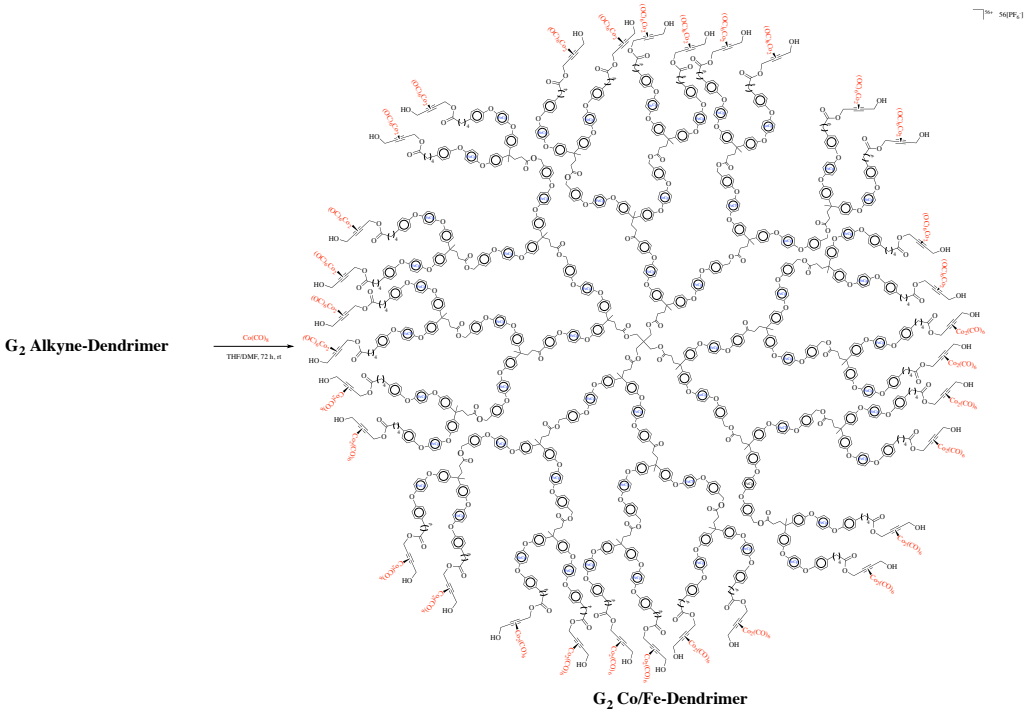

Scheme 5.4. Schematic representation of the synthesis of heterometallic dendrimer, **G_2 Co/Fe-dendrimer-PF_6^-**.

The success of the reactions was monitored using ^{1}H and ^{13}C NMR spectroscopies, ATR-FTIR spectroscopy and elemental analyses (Experimental section). For instance, the carboxylic acid protons in **G_0 COOH-dendrimer**, which resonated at 12.06 ppm, disappeared in the ^{1}H NMR spectrum of the **G_0 alkyne-dendrimer**, suggesting successful esterification reaction between the 2-butyne-1,4-diol and the **G_0 COOH-dendrimer**. Again, as shown in previous reports,[1,7,32,34] the carbonyl carbons of the $Co_2(CO)_6$ moieties were observed at 196.8 ppm in the ^{13}C NMR spectrum of **G_0 Co/Fe-dendrimer** (Experimental section). Again, after coordination of cobalt hexacarbonyl to the triple bonds, the methylene protons of butyne downshifted in the ^{1}H NMR spectra of the heterometallic dendrimers. These observations suggested that $Co_2(CO)_6$ was coordinated into the

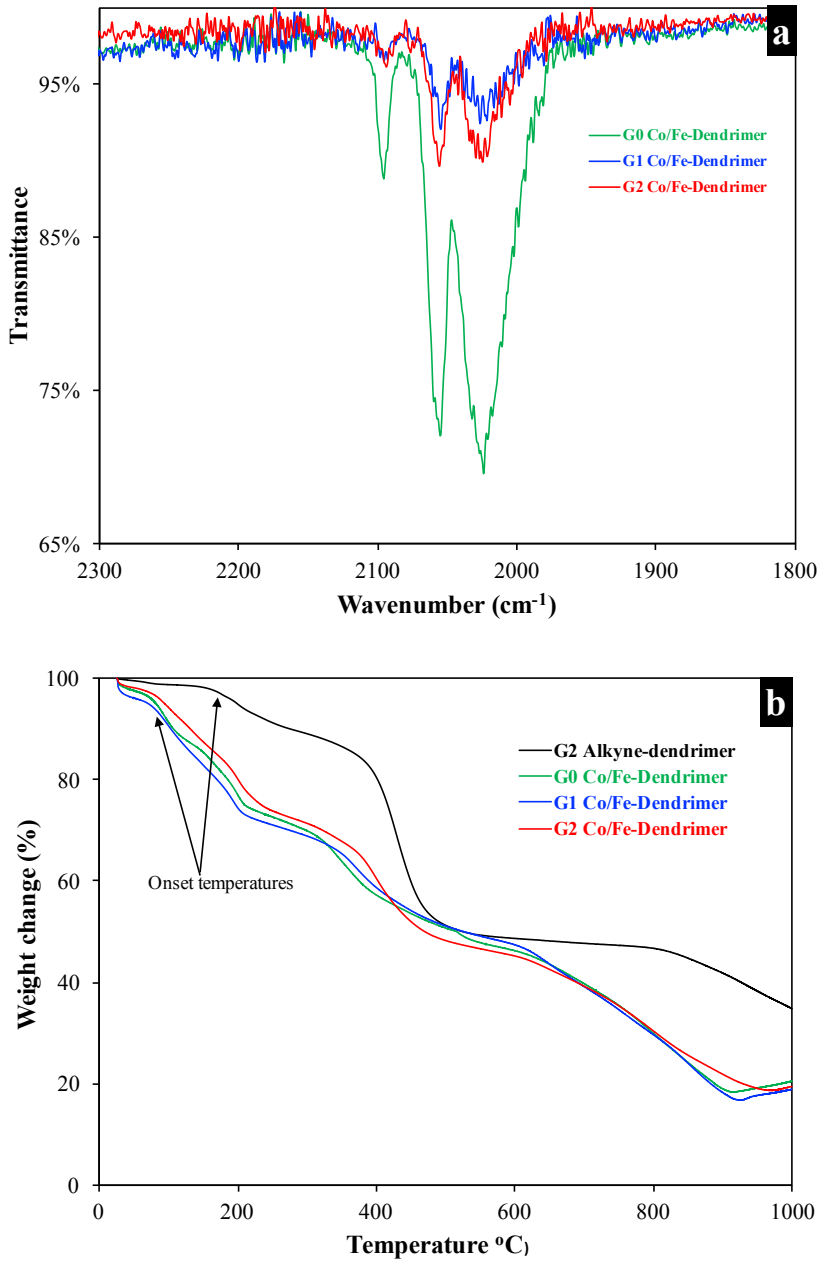

Figure 5.1. ATR-FTIR and TGA of preceramic dendrimers. (a) ATR-FTIR spectra of heterometallic dendrimers showing the characteristic C≡O stretch bands at 2095, 2057, and 2024 cm^{-1} due to coordinated $Co(CO)_6$. (b) TGA thermograms of heterometallic dendrimers showing the thermolysis of $Co_2(CO)_6$ (onset = ~77 ºC) in contrast with typical member of this class of dendrimer without $Co_2(CO)_6$ (**G_2 alkyne-dendrimer**) (onset at ~200 ºC). Black: **G_2 alkyne-dendrimer**; green: **G_0 Co/Fe-dendrimer**; blue: **G_1 Co/Fe-dendrimer**; red: **G_2 Co/Fe-dendrimer**.

dendrimers. It is worth mentioning that **G_1 Co/Fe-dendrimer** and **G_2 Co/Fe-dendrimer** were partially soluble in common laboratory solvents, limiting their characterization to ATR-FTIR spectroscopy and elemental analyses, which confirm their successful syntheses. For instance, ATR-FTIR spectroscopy clearly suggest that the $Co_2(CO)_6$ was coordinated to the dendrimers as evidenced by the characteristic CO stretch bands at 2095, 2057, and 2024 cm^{-1} (Figure 5.1a). Also, thermogravimetric analyses (TGA) of **G_0 Co/Fe-dendrimer**, **G_1 Co/Fe-dendrimer** and **G_2 Co/Fe-dendrimer** reveal the thermolysis of $Co_2(CO)_6$ at onset temperatures (~77 ºC), which are notably lower than the typical onset of ~200 ºC that is characteristic of these dendrimers without $Co_2(CO)_6$ (Figure 5.1b).

5.2.2. Formation and characterization of ceramics

Laboratory-scale pyrolysis of the dendrimers in a tube furnace at 900 °C in nitrogen atmosphere transformed **G_0 Fe-dendrimer**, **G_1 Fe-dendrimer**, **G_2 Fe-dendrimer**, **G_0 Co/Fe-dendrimer**, **G_1 Co/Fe-dendrimer** and **G_2 Co/Fe-dendrimer** to ceramics in 20–44 % yield. Ceramic yield is critical in choosing a precursor, and the obtained yield agrees reasonably well with those obtained for some hyperbranched polymers.[18] Further, the low yield is explicable; obviously, a significant portion of dendrimer consist of flexible aliphatic segments, which contrast with previously reported rigid crosslinked[7] or hyperbranched[9] polymers that afforded better yields. To gain insight into the morphology and bulk composition of these ceramics, electron microscopies (TEM and SEM), atomic absorption spectroscopy (AAS), energy dispersive X-ray analysis (EDX), and powder X-ray diffraction (p-XRD) were used to characterize the ceramics.

The ceramics, in contrast with the amorphous dendrimer precursors, were polycrystalline, consisting of several nanocrystallites embedded within an amorphous matrix. A powder X-ray technique[35] reveal degrees of crystallinity that ranged from 37–56%, with the heterometallic dendrimers yielding more crystalline ceramics (Table 5.1). The crystallites were large as evidenced by several sharp peaks around $2\theta = 40–45°$ in the diffractograms and the crystallite sizes were greater than 15 nm as determined by the Scherrer equation[36] (Table 5.1, and Figures 5.2). For the homometallic ceramics, the size of the Fe_3O_4 crystallite increased with dendrimer generation (Table 5.1). The presence of Fe_3O_4 crystallite, a product of oxidation, although unexpected since the pyrolysis was conducted under an inert atmosphere is likely since oxygen is present in the dendrimer scaffold. Also, oxidation is possible during sample handling if the Fe species are not completely embedded in the amorphous matrix. More interesting is the gradual increase in the size of the crystallite with an increase in dendrimer generation, a dendritic effect that implies the possibility of tuning crystallites size by changing dendrimer generation (Table 5.1). Previously, by changing pyrolysis conditions, Manners *et al*. tuned the crystallites size of α-Fe nanoparticle ($2\theta \sim 45°$), and eventually the magnetic property of their ceramics.[6] Here, the size of the α-Fe nanoparticle was uncontrolled as evidenced by the reflection peak near $2\theta \sim 45°$ (Table 5.1). However, the size of the Fe_3O_4 crystallites ($2\theta \sim 40°$) was altered by changing the dendrimer generation (Figure 5.2 and Table 5.1). Further, p-XRD also revealed that in the heterometallic ceramics, the iron and cobalt species formed different crystalline domains as evidenced by the presence of {111} Co, {200} Co, {400} Co_3O_4, {311} Fe_3O_4 and {110} α-Fe reflection peaks in the diffractograms (Figure 5.2). This finding contrasts with reports on iron-cobalt linear polymer-derived ceramics, where cobalt and iron were localized in the same crystalline domains, forming an alloy.[7] It is, therefore, reasonable to conclude that the dendrimer structure controls crystallite

growth because unlike some heterometallic Fe-Co ceramics with Fe-Co alloy crystallites,[7] these dendrimers formed ceramics with separate Fe and Co crystalline domains. Indeed, the structures of these dendrimers differs from those of preceramic linear polymers that yielded Fe-Co alloy crystallites. The proximity of Co and Fe in the linear polymers was much closer than in these dendrimers, which localized the Fe at the inner cavity and the Co at the periphery. Such localized concentration of distinct regions of Fe and Co could favor formation of separate Fe and Co nanocrystallites. The presence of oxides of cobalt in the ceramics even when the pyrolysis was conducted in an inert atmosphere, as with Fe_3O_4, may be due to oxygen atoms in the dendrimer structures which can facilitate the oxidation of cobalt during pyrolysis, in addition to possible oxidation during sample storage and handling. Indeed, EDX data revealed the presence of oxygen in these ceramics.

Table 5.1. Yield and bulk composition of ceramics.[a]

Ceramics precursor	Metallic content (%)		C (%)	Crystallinity (%)	Crystallite size (nm)	
	Fe/Co[b]	Fe[c]			$2\theta = \sim 40°$ (Fe_3O_4)	$2\theta = \sim 45°$ (α-Fe/Co_3O_4)
G_0 Fe-Dendrimer[d]	24.6/0	35.0	63.0	41.2	29.6	41.5/-
G_1 Fe-Dendrimer[d]	30.0/0	25.2	64.0	47.7	35.4	24.4/-
G_2 Fe-Dendrimer[d]	16.6/0	16.3	75.8	37.9	41.0	38.0/-
G_0 Co/Fe-Dendrimer	6.90/21.3	9.09	56.7	56.2	26.6	15.4/31.2
G_1 Co/Fe-Dendrimer	6.18/10.3	8.47	78.4	51.3	35.0	51.4/22.7
G_2 Co/Fe-Dendrimer	11.6/21.2	9.30	54.6	56.2	28.6	26.8/25.7

[a]Ceramics were obtained by pyrolysis of dendrimers under nitrogen atmosphere at 900 ºC in a tube furnace.
[b]Determined using EDX.
[c]Determined using AAS.
[d]The structures of **G_0 Fe-dendrimer**, **G_1 Fe-dendrimer**, and **G_2 Fe-dendrimer** are the same as **G_0 Cl-dendrimer**, **G_1 Cl-dendrimer**, and **G_2 Cl-dendrimer**, respectively, in *Chapter Two*.

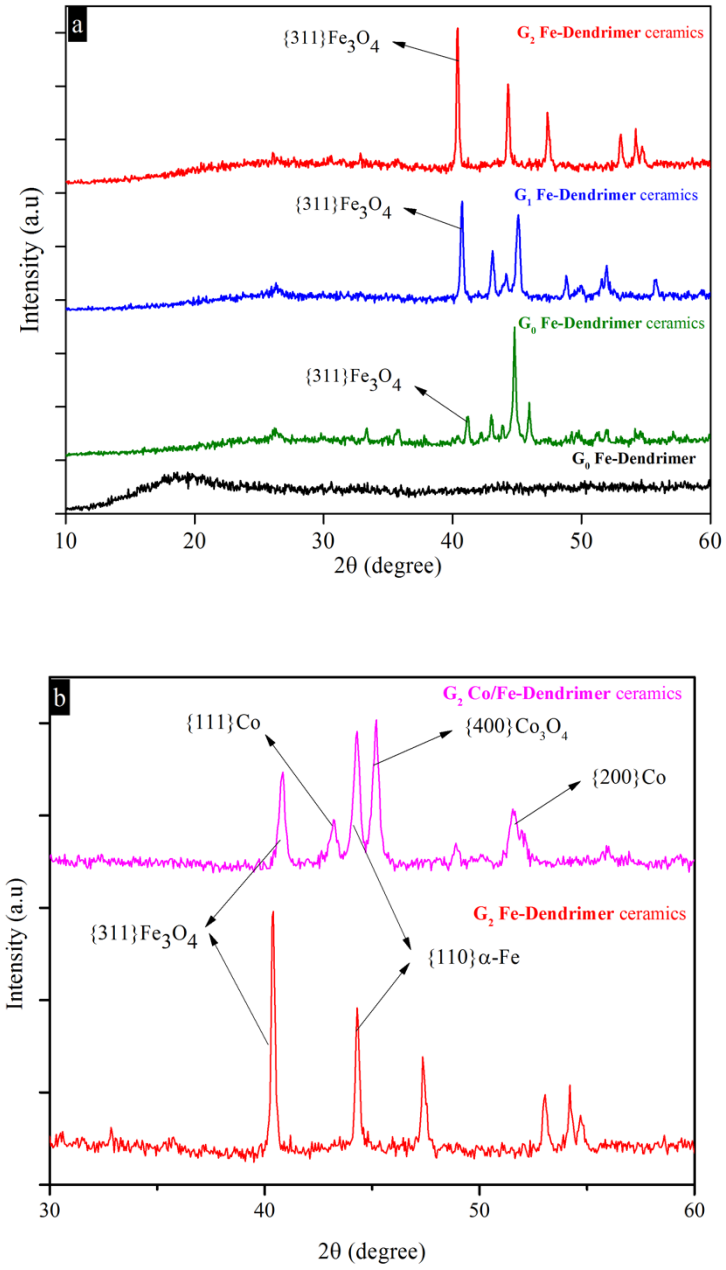

Figure 5.2. Powder X-ray diffractograms of preceramic dendrimer and ceramics derived from dendrimers. (a) Powder X-ray diffractograms of **G_0 Fe-dendrimer** (black) and ceramics derived from **G_0 Fe-dendrimer** (green), **G_1 Fe-dendrimer** (blue), **G_2 Fe-dendrimer** (red) showing that the ceramics were polycrystalline compare to the amorphous dendrimer precursors. (b) powder X-ray diffractograms of homometallic ceramics derived from **G_2 Fe-dendrimer** (red) and heterometallic ceramic derived from **G_2 Co/Fe-dendrimer** (purple) showing that Fe and Co were in separate crystalline domains.

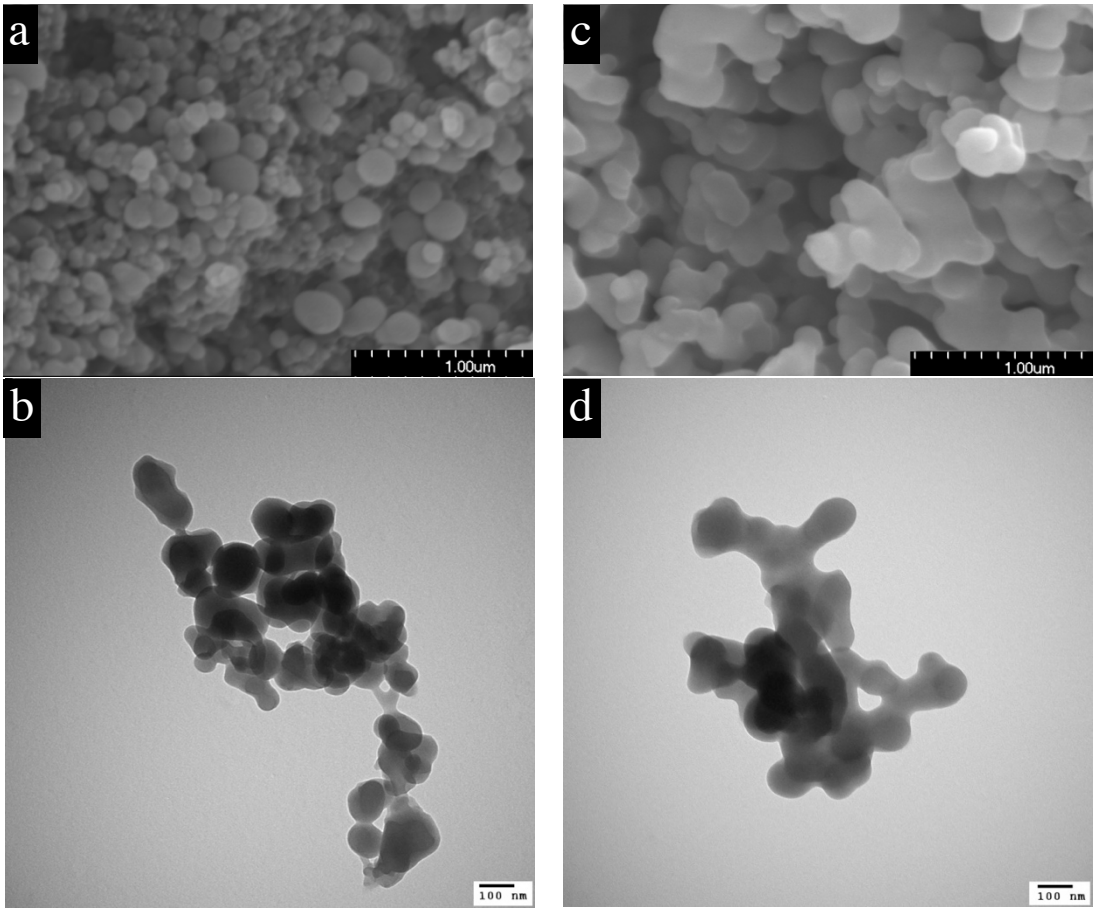

Figure 5.3. Morphology of preceramic dendrimers. Top: SEM images of (a) **G_0 Fe-dendrimer** and (c) **G_0 Co/Fe-dendrimer**. Bottom: TEM images of (b) **G_0 Fe-dendrimer** and (d) **G_0 Co/Fe-dendrimer**.

To further probe the bulk composition of the ceramics, EDX and AAS were used as analytical tool. The results reveal that homometallic ceramics had higher iron content than the heterometallic ceramics, a finding that agreed with theoretical calculations. Also, EDX data show that carbon constituted over 50% of the ceramic (Table 5.1), providing the amorphous matrix in which the metallic nanoparticles are embedded. Also, EDX data reveal that the ceramics contained compounds of phosphorus and fluorine, which originated from the PF_6^- counteranion in the dendrimers. Visual inspection of the bulk dendrimers and their ceramics using SEM and TEM

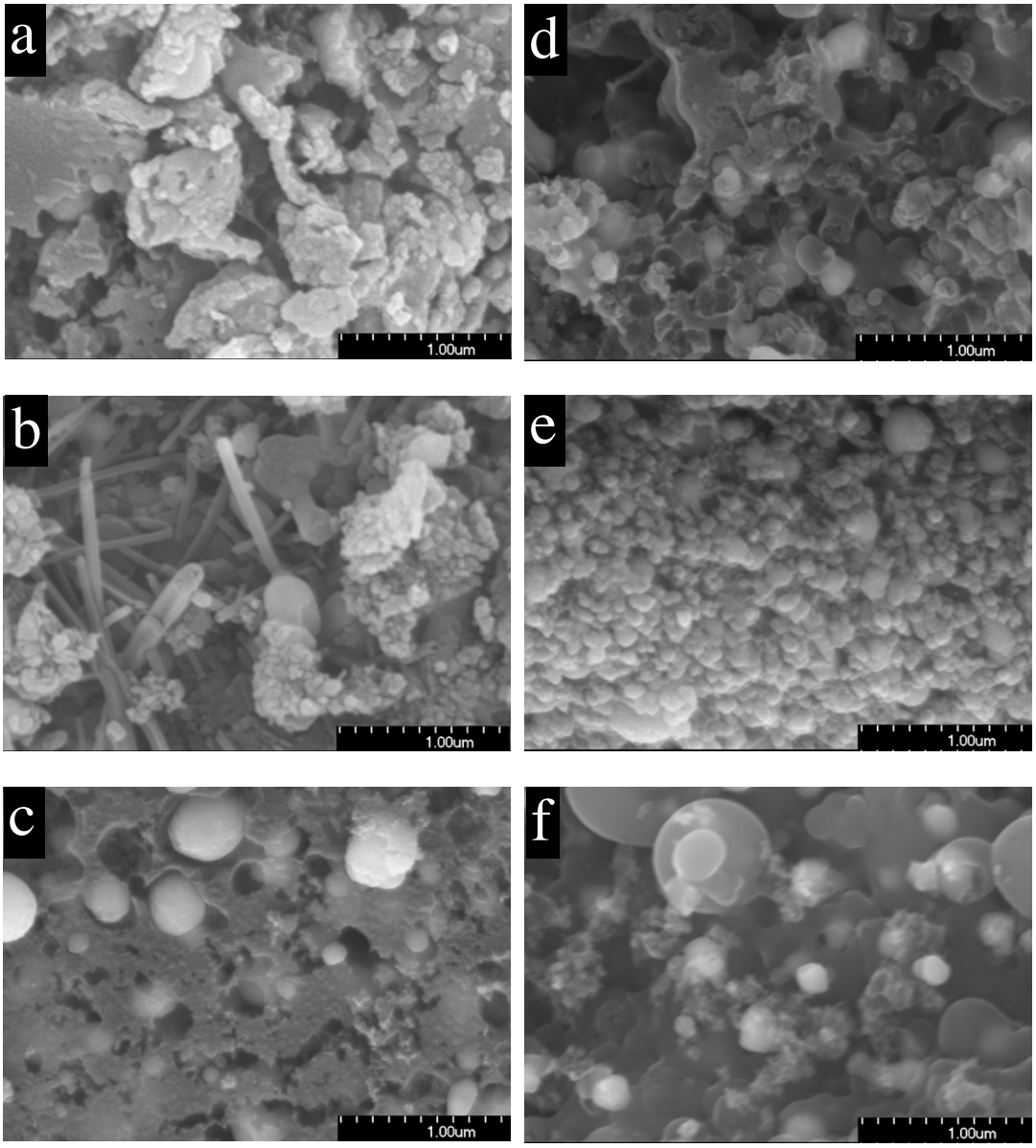

Figure 5.4. SEM images of ceramics. Left: homometallic ceramics (a) **G_0 Fe-dendrimer**, (b) **G_1 Fe-dendrimer** (c) **G_2 Fe-dendrimer**; right heterometallic ceramics (d) **G_0 Co/Fe-dendrimer** (e) **G_1 Co/Fe-dendrimer** (f) **G_2 Co/Fe-dendrimer** showing magnetic crystallites embedded with amorphous matrix.

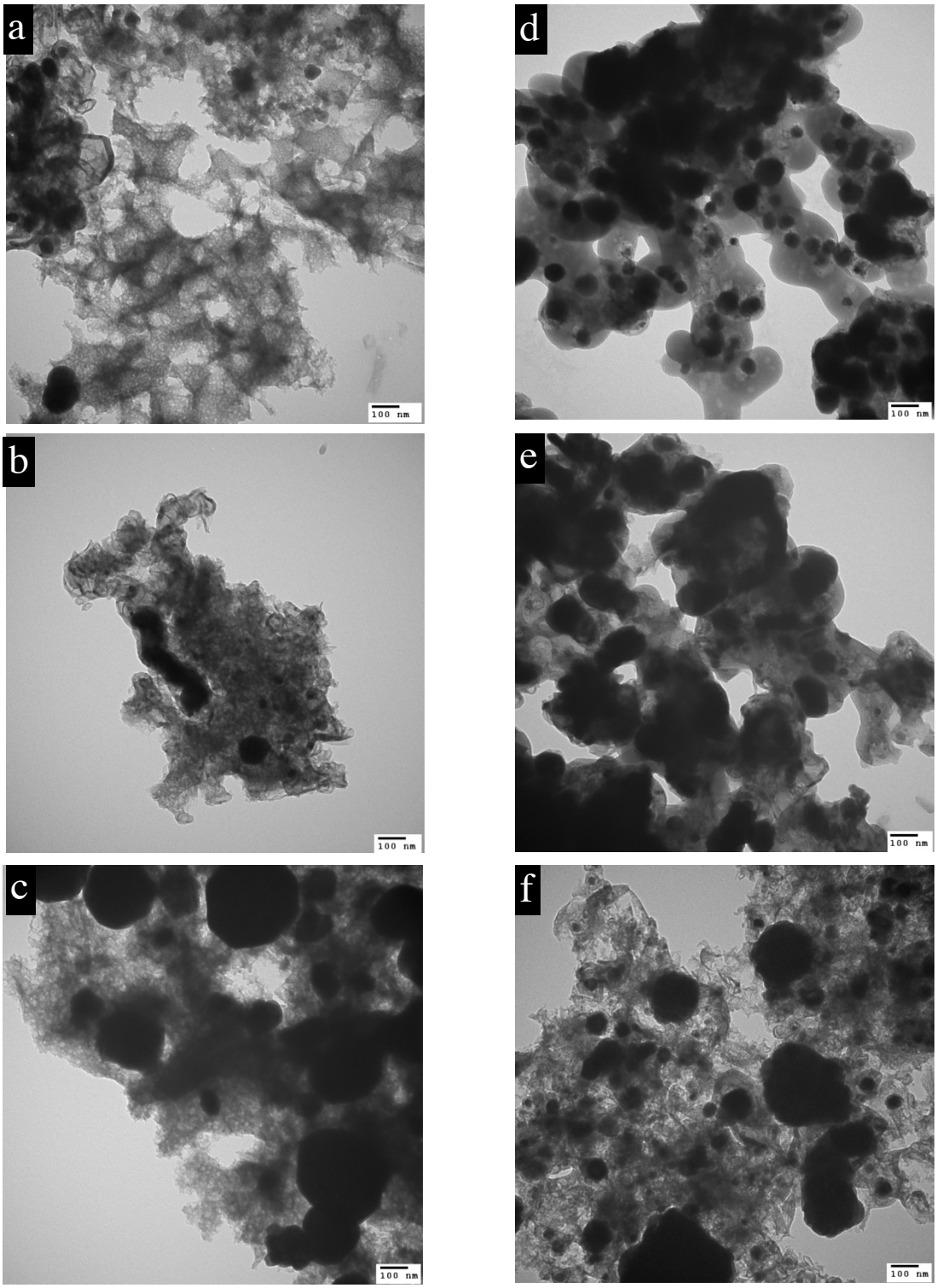

Figure 5.5. TEM images of ceramics. Left: homometallic ceramics (a) **G_0 Fe-dendrimer**, (b) **G_1 Fe-dendrimer** (c) **G_2 Fe-dendrimer**; right heterometallic ceramics (d) **G_0 Co/Fe-dendrimer** (e) **G_1 Co/Fe-dendrimer** (f) **G_2 Co/Fe-dendrimer** showing magnetic crystallites embedded with amorphous matrix.

clearly showed that the precursors differed from the ceramics and that in the ceramics, the metallic crystallites were embedded within the amorphous carbon matrix (Figures 5.3-5.5). Also, the SEM and TEM images validated results from p-XRD, where the size of some of the crystallites was found to increase with increase in dendrimer generation for the homometallic ceramics (Figures 5.4a-c and 5.5a–c).

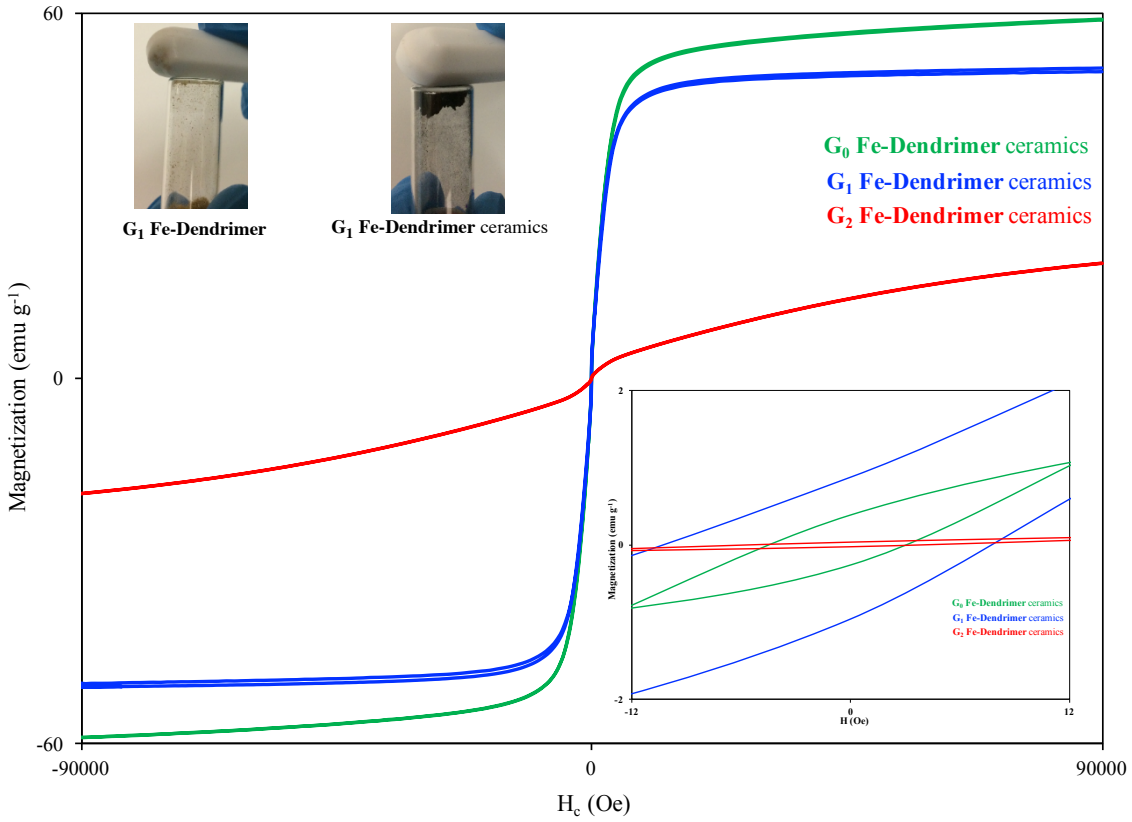

Figure 5.6. Room temperature magnetization curves of homometallic ceramics. Response to magnetic stir bar (inserted picture) and magnetization curves for ceramics derived from **G_0 Fe-dendrimer** (green) **G_1 Fe-dendrimer** (blue), and **G_2 Fe-dendrimer** (red). Inserted Figure: the ceramics exhibits soft ferromagnetism as shown by their hysteresis loops**.**

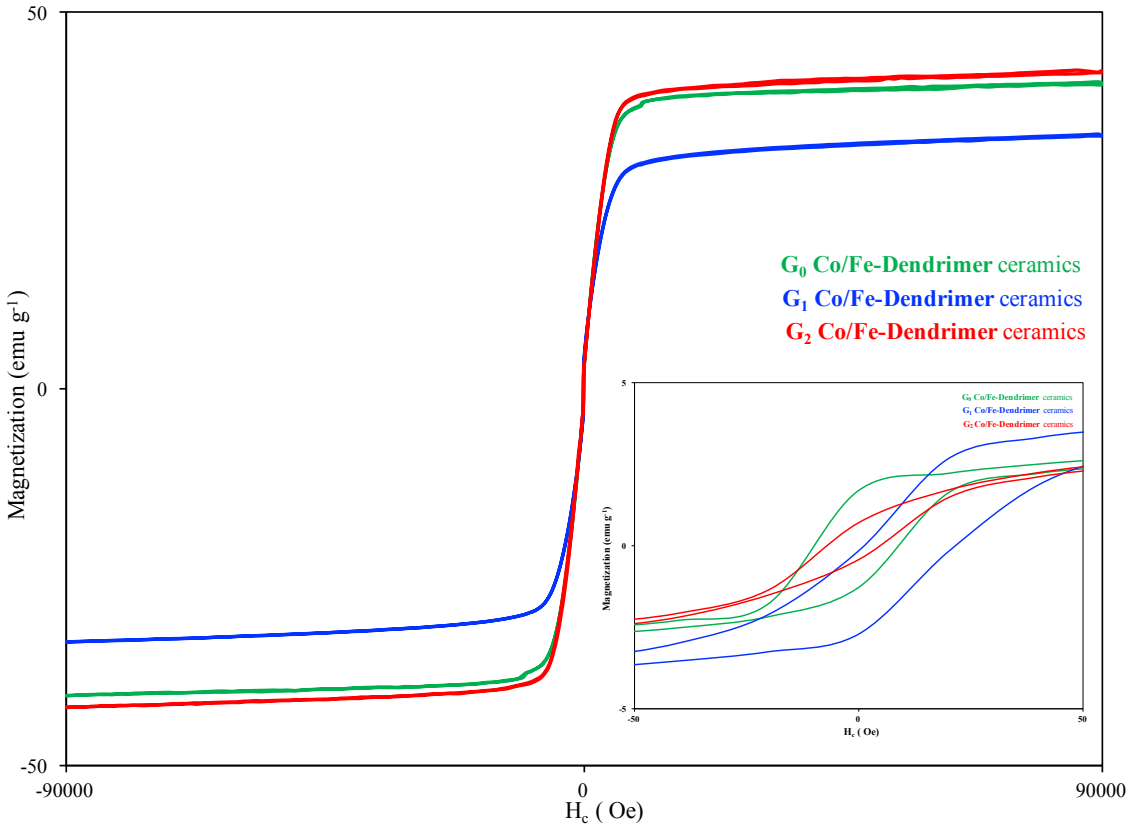

Figure 5.7. Room temperature magnetization curves of heterometallic ceramics. **G_0 Co/Fe-dendrimer** (green) **G_1 Co/Fe-dendrimer** (blue), and **G_2 Co/Fe-dendrimer** (red). Inserted Figure: the ceramics exhibit soft ferromagnetism evidenced by their hysteresis loops.

Table 5.2. Saturation magnetization (M_s), remanent magnetization (M_r), and coercivity (H_c) of ceramics.

Ceramic precursor	M_s (emu g^{-1})	M_r (emu g^{-1})	H_c (Oe)
G_0 Fe-Dendrimer	59	–0.4	28
G_1 Fe-Dendrimer	51	0.9	18
G_2 Fe-Dendrimer	19	0.03	10
G_0 Co/Fe-Dendrimer	41	1.7	18
G_1 Co/Fe-Dendrimer	34	–0.05	25
G_2 Co/Fe-Dendrimer	42	0.72	13

5.2.3. Magnetic properties

Preliminary examination of the magnetic property of the ceramics using a magnetic stir bar indicated magnetism because the ceramics were attracted to the magnetic bar (Figure 5.7 inserted picture). To further understand this magnetic property, a Quantum Design 9T-PPMS DC magnetometer/AC susceptometer was used to obtain magnetization curves (Figures 5.6 and 5.7). At room temperature, all ceramics were ferromagnetic as evidenced by the presence of hysteresis loops (Figures 5.6 and 5.7 inserts), and the magnetism was soft as suggested by the low coercivity (H_c) (Table 5.2).[37,38] Also, the result show that saturation magnetization (M_s) and remanent magnetization (M_r) were low (Table 5.2). The homometallic ceramics exhibited dendritic effects on magnetic property, specifically on H_c and M_s, which decreased with increased in dendrimer generation (Table 5.2). Usually, the magnetic property of nanoparticles is controlled by many parameters including the size, concentration, interparticle distance, and degree of oxidation of the nanoparticles.[32,39-41] Here, it is evident that with the homometallic ceramics, the concentration of iron, the magnetic species, decreased and the size of the Fe_3O_4 crystallite increased with the dendrimer generation (Table 5.1), changes that could contribute to the observed trend in H_c and M_s (Table 5.2). As Fe_3O_4 results from oxidation, it is logical to assume that the degree of oxidation increases with generation. The degree of oxidation is shown to affect the overall magnetic response of magnetic nanoparticles,[32,39] specifically decreasing magnetic response of cobalt nanoparticles.[42,43] Thus, it is logical to assume that the negative correlation between the size of Fe_3O_4 crystallite and magnetic properties, specifically H_c and M_s, is suggestive of the effect of oxidation on the magnetic property of this series of dendrimers. Further, it was previously proved that as the concentration of magnetic species increases to a critical point, interparticle distance decreases, leading to increase in dipolar interaction and ultimately increase in H_c.[32,44,45] It is,

therefore, reasonable to conclude that changes in the concentration of the Fe nanoparticles in the ceramics tuned the H_c and M_s, leading to the observed trend. As the pyrolysis, storage and handling conditions were the same for all ceramics; it is the dendrimer generation that ultimately determines the overall crystallite size of the Fe_3O_4 and concentration of Fe nanoparticles. Thus, the conclusion that dendrimer generation is critical to the overall magnetic property of the ceramics. It is worth noting that the effect of crystallite size of α-Fe on the magnetic behavior of the homometallic ceramics was less obvious as no trend was observed (Tables 5.2).

Incorporating cobalt into the dendrimer noticeably changed the magnetic responses of derived ceramics. For instance, it was found that heterometallic ceramics derived from **G_2 Co/Fe-dendrimer** had higher H_c and M_s compared with its homometallic analog, ceramics derived from **G_2 Fe-dendrimer**. In contrast, heterometallic ceramics derived from **G_0 Co/Fe-dendrimer** and **G_1 Co/Fe-dendrimer** had lower H_c and M_s compared with their homometallic analogs, ceramics derived from **G_0 Fe-dendrimer** and **G_1 Fe-dendrimer** (Tables 5.2). This seemingly contradictory finding suggests that incorporating cobalt into preceramic polymer does not necessarily increase these magnetic properties (M_s, M_r, and H_c) as previously reported[11] but could also decrease these properties depending on the structure of the polymer. The observed decrease in these magnetic properties in the ceramics derived from the lower generation dendrimers, **G_0 Co/Fe-dendrimer** and **G_1 Co/Fe-dendrimer**, is attributed to the formation of paramagnetic Co_3O_4 and CoO, which may be less likely formed in ceramics derived from the higher generation dendrimer, **G_2 Co/Fe-dendrimer**. Typical of dendrimers, surface groups back-fold into the dendrimer inner cavity at higher generation.[16] Thus, at higher dendrimer generation, for instance, in **G_2 Co/Fe-dendrimer**, it is possible that the peripheral $Co_2(CO)_6$ backfolded into the dendrimer cavity, protecting the cobalt moieties from oxidation. Indeed, heterometallic ceramics derived from the G_0

heterometallic dendrimer, **G_0 Co/Fe-dendrimer**, had the largest Co_3O_4 crystallite size compared with the other heterometallic ceramics (Table 5.1). Therefore, although other factors may play a role in modulating the overall magnetic property of the ceramics, the dendrimer structure was critical.

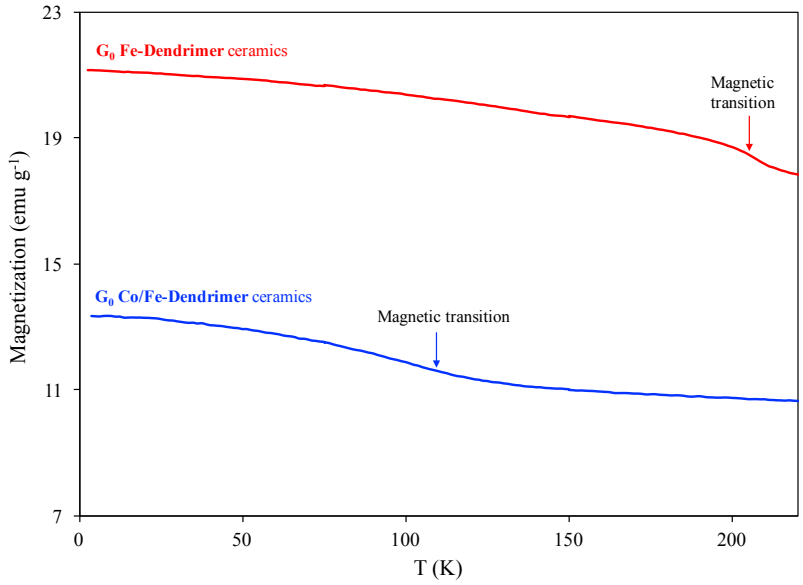

Figure 5.8. Temperature-dependent magnetization curves of ceramics. The ferromagnetism in homometallic and heterometallic ceramics were different. The homometallic ceramics exhibited a magnetic phase transition at higher temperature than heterometallic ceramics. Red: **G_0 Fe-dendrimer**; blue: **G_0 Co/Fe-dendrimer**.

Again, in contrast with the homometallic ceramics, no structure-property relationship was found in the heterometallic series of ceramics. Further, ferromagnetism in these two series of ceramics differs in their response to temperature as revealed by temperature-dependent magnetization measurements (Figure 5.8). Indeed, the ferromagnetism of the homometallic ceramics was less susceptible to the influence of temperature because a magnetic phase transition

was observed at about 210 K, whereas the heterometallic ceramics had a transition at about 110 K (Figure 5.8).

5.3. Conclusion.

Magnetic materials remain attractive because of their importance in many advanced applications. This *Chapter* reports the synthesis of three generations of $[\eta^6\text{-arene-}\eta^5\text{-CpFe}]^+$-derived dendrimers, which on pyrolysis yielded room temperature, soft ferromagnetic ceramics. Powder X-ray diffraction, SEM, and TEM revealed that these magnetic ceramics were polycrystalline. In the heterometallic ceramics, Fe and Co existed in separate crystalline domains probably due to the unique topology that localized these magnetic species in distinct regions. Dendritic effects on ferromagnetism in the homometallic ceramics were evident as the M_s and H_c decreased with increase in dendrimer generation. Incorporating Co into the dendrimers dramatically changed the magnetism in these ceramics, increasing M_s and H_c in ceramics derived from second-generation dendrimers whereas decreasing these properties in ceramics derived from G_0 and G_1 dendrimers. Concluding, the studies demonstrated that the iron in $[\eta^6\text{-arene-}\eta^5\text{-CpFe}]^+$ complex imparts magnetism on the ceramics and that the structure of the dendrimer is critical to the magnetic properties.

5.4. Experimental section

5.4.1. Materials

All chemicals were purchased from Sigma-Aldrich or Alfa Aesar. The chemicals, unless otherwise stated, were used without purification. THF obtained from Sigma-Aldrich was purified by passing the solvent through an Innovative Technologies solvent purification system that consisted of columns of alumina and copper catalyst. DMSO, DMF and DMSO-d_6 were dried and stored over

activated 3 Å molecular sieves before use. The structures of **G_0 Fe-dendrimer**, **G_1 Fe-dendrimer**, **G_2 Fe-dendrimer** are the same as **G_0 Cl-dendrimer**, **G_1 Cl-dendrimer**, **G_2 Cl-dendrimer**, respective, and their syntheses procedures are described in *Chapter Two* while those of **G_0 COOH-dendrimer** and **G_1 COOH-dendrimer** are described in *Chapter Four*.

5.4.2. Instrumentation

All NMR spectra were acquired on a Bruker Avance NMR spectrometer (^{1}H, 300 MHz and ^{13}C, 75 MHz). The spectra were acquired from a DMSO-d_6 solution of the compounds with the chemical shifts in ppm referenced to the solvent residual proton peak. Elemental analyses, attenuated total reflection Fourier transform IR (ATR-FTIR) spectroscopic measurements and powder X-ray diffraction were performed as described in *Chapter Two*. Thermogravimetric analysis (TGA) was carried out under nitrogen at a heating rate of 1 °C/minute on a TA Instruments TGA Q500.

5.4.3. Electron microscopy

Dendrimer or ceramic samples for transmission electron microscopic measurements were dispersed and vortexed in C_6H_{14}, pipetted onto a carbon-coated copper grid, and allowed to dry in air before imaging. The microscopic images were acquired on a Hitachi BioTEM 7500 fitted with a digital camera, Advanced Microscopy Techniques (AMT) XR40 side mount, an AMT Image Capture Engine software version 600.149, and operated at 80 kV. For field emission scanning electron microscopy (FE-SEM) and energy-dispersive X-ray (EDX) analysis, fine powders of dendrimers or ceramics were sprinkled on double-sided copper tape adhered on aluminum SEM stubs, sputter-coated with Pd for 10 seconds before imaging. The FE-SEM images and EDX data were acquired using a Hitachi S-4700 field-emission scanning electron microscope operated at 12

kV. The following standards were used for EDX analyses: $CaCO_3$ (C), SiO_2 (O), MgF (F), GaP (P), Cl (KCl), Fe (Fe), and Co (Co).

5.4.4. Atomic absorption spectroscopy

For atomic absorption spectroscopy, 100 mg of ceramics sample was digested in 20 mL of aqua regia for 72 hours at room temperature. Then, 10 mL of deionized water was added to the digest and the resulting solution was filtered into a 50-mL volumetric flask. The solution was made up to the mark with deionized water. An aliquot was pipetted into 25-mL volumetric flask, diluted to the mark with deionized water. The solution was analyzed for iron at 248.3 nm using Varian SpectrAA 10 Plus Flame Spectrometer fitted with Hamamatsu hollow cathode Fe lamp model L233.

5.4.5. Magnetic measurements

The magnetization (hysteresis) curves and the temperature-dependence magnetization of the ceramics were obtained using the Quantum Design 9T-Physical Properties Measurement System (PPMS) DC magnetometer/AC susceptometer. The powdered ceramics were filled into a polycarbonate capsule, purged, pressurized, and sealed with non-magnetic Kapton® tape. The hysteresis curves were obtained at 300 K from 9 T to –9 T while the temperature-dependence magnetization curves were obtained in the temperature range of 300–2 K at a field of 1000 Oe.

5.4.6. Synthesis of G_0 alkyne-dendrimer

This dendrimer was synthesized as follows: in a 25-mL round-bottom flask was added 490 mg (0.09) of **G_0 COOH-dendrimer**, 270 mg (2.16 mmol) of 2-butyne-1,4-diol, 67 mg (0.55 mmol) of 4-(dimethylamino)pyridine (DMAP), and 10 mL of 5:1 DCM/DMSO solvent mixture. While

stirring, the mixture was cooled to 0 °C and 163 mg (0.79 mmol) of *N*,*N′*-dicyclohexylcarboiimide (DCC) was added over 30 minutes. Next, the mixture was warmed to room temperature and stirred under nitrogen overnight. Thereafter, the reaction was stopped, filtered to remove precipitated dicyclohexylurea (DCU), and the filtrate added to 50 mL of ice water. The mixture was extracted twice with 20 mL portion of DCM/$(CH_3)_2CO$ solvent mixture, and the organic extract washed twice with 50 mL of H_2O, then sequentially with 50 mL of 5% (v/v) aqueous HCl and 10 mL of 74 mM aqueous solution of NH_4PF_6. The organic extract was dried using Na_2SO_4, filtered, and the solvent removed under vacuum. The residue was dissolved in $(CH_3)_2CO$, cooled in a freezer for one hour to precipitate residual DCU, which was separated by filtration. The filtrate was added dropwise to $(C_2H_5)_2O$ to precipitate the product, which was filtered and dried at room temperature to give the final product. Yield: 78%. ^{1}H NMR (300 MHz, DMSO-d_6): δ (ppm) 7.35–6.87 (64 H, br s, Ar*H*), 6.21 (32 H, br s, complexed Ar*H*), 5.18 (40 H, s, Cp*H*), 5.02 (8 H, br s, OH), 4.70 (16 H, s, CH_2), 4.10 (16 H, s, CH_2), 4.00 (8 H, br s, CH_2), 2.64–2.10 (80 H, br s, CH_2), 1.59 (12 H, br s, CH_3). ^{13}C{^{1}H} NMR (75 MHz, DMSO-d_6): δ (ppm) 172.5, 172.1, 151.6, 151.1, 145.7, 140.1, 130.4, 129.0, 120.5, 120.3, 129.8, 129.7, 86.4, 78.4, 77.7, 75.0, 74.4, 61.9, 51.6, 51.4, 48.8, 44.8, 44.3, 35.8, 33.9, 33.2, 30.2, 26.8, 23.8. Elemental analyses: calculated for C, 55.99; H, 4.62; found for C, 55.63; H, 4.89.

5.4.7. Synthesis of G_0 Co/Fe-dendrimer

The dendrimer was synthesized using a previously reported method,[32,34,46] which was slightly modified. In a nitrogen-filled glovebox, 200 mg (0.032 mmol) of **G_0 alkyne-dendrimer** was charged into 25-mL round-bottom flask. Then, 10 mL of dried THF and 1 mL of dried DMF were added to the flask to dissolve the dendrimer. On complete dissolution, dicobalt octacarbonyl was

added and the mixture stirred at room temperature inside the glovebox for 72 hours. The mixture was filtered through Celite and precipitated into 10-fold excess of C_6H_{14}. The precipitate was re-dissolved in dried THF/DMF solvent mixture, filtered and re-precipitated into 10-fold excess of C_6H_{14} to obtain the final product as a brown solid. Yield: 66%. ^{1}H NMR (300 MHz, DMSO-d_6): δ (ppm) 7.33–6.94, (64 H, br s, Ar*H*), 6.23 (32 H, br s, complexed Ar*H*), 5.63 (16 H, s, CH_2) 5.22 (40 H, s, Cp*H*), 4.62 (16 H, s, CH_2), 4.02 (8 H, br s, CH_2), 2.61–2.27 (80 H, br s, CH_2), 1.59 (12 H, br s, CH_3). ^{13}C{^{1}H} NMR (75 MHz, DMSO-d_6): δ (ppm) 196.8, 169.7, 160.3, 152.4, 148.9, 137.3, 127.7, 126.9, 126.2, 125.8, 118.8, 117.8, 117.2, 115.4, 114.6, 75.4, 72.6, 70.4, 61.4, 58.7, 45.3, 44.1, 33.3, 31.3, 30.4, 28.2, 27.5, 24.5, 21.1. ATR-FTIR: ν_{max} (cm^{-1}) 2095 (m), 2057 (s), 2024 (s, br) (CO) cm^{-1}. Elemental analyses: calculated for C, 47.52; H, 3.35; found for C, 47.03; H, 3.74.

5.4.8. Synthesis of G_1 alkyne-dendrimer

The dendrimer was synthesized using similar procedure used in the synthesis of **G_0 alkyne-dendrimer**. In brief, 581 mg (0.037 mmol) of **G_1 COOH-dendrimer**, 153 mg (1.78 mmol) of 2-butyne-1,4-diol, 56 mg (0.46 mmol) of DMAP, 134 mg (0.65 mmol) of DCC and 10 mL of 5:1 DCM/DMSO solvent mixture were used. Yield: 80%. ^{1}H NMR (300 MHz, DMSO-d_6): δ (ppm) 7.52–6.92 (192 H, br s, Ar*H*), 6.24 (96 H, br s, complexed Ar*H*), 5.22 (120 H, s, Cp*H*), 5.12 (16 H, br s, BnCH_2), 5.08 (16 H, br s, OH), 4.73 (32 H, s, CH_2), 4.10 (32 H, s, CH_2), 4.00 (8 H, br s, CH_2), 2.64–2.20 (176 H, br s, CH_2), 1.67 (12 H, br s, CH_3), 1.67 (24 H, br s, CH_3). ^{13}C{^{1}H} NMR (75 MHz, DMSO-d_6): δ (ppm) 174.1, 172.6, 172.1, 155.4, 155.2, 155.0, 151.7, 151.5, 146.5, 146.0, 140.1, 130.5, 130.3, 130.1, 129.8, 129.6, 129.1, 129.0, 128.5, 120.5, 120.3, 120.0, 119.8, 86.5, 78.4, 77.8, 77.7, 75.4, 75.1, 75.0, 74.9, 64.9, 51.7, 48.8, 44.9, 44.7, 44.6, 35.9, 36.0, 35.7, 33.9,

33.8, 30.7, 30.3, 29.8, 29.6, 26.9, 23.9. Elemental analyses: calculated for C, 55.29; H, 4.37; found for C, 55.40; H, 4.64.

5.4.9. Synthesis of G_1 Co/Fe-dendrimer

The dendrimer was synthesized using a procedure similar to that of **G_0 Co/Fe-dendrimer**. Briefly, 200 mg (0.012 mmol) of **G_1 alkyne-dendrimer**, 10 mL of dried THF, 0.192 mmol of dicobalt octacarbonyl and 1 mL of dried DMF were used and the product was obtained as a brown solid. Yield: 63%. The product was partially soluble in common laboratory solvents, limiting characterization to ^{1}H NMR, ATR-FTIR and elemental analyses. ^{1}H NMR (300 MHz, DMSO-d_6): δ (ppm) 7.37–6.98, (192 H, br s, Ar*H*), 6.25 (92 H, br s, complexed Ar*H*), 5.76 (32 H, s, C*H*$_2$) 5.20 (120 H, s, Cp*H*), 4.69 (32 H, s, C*H*$_2$), 2.87–2.20 (176 H, br s, C*H*$_2$), 1.67, 1.59 (36 H, br s, C*H*$_3$) (O*H* and Bn*H*, and a C*H*$_2$ were not observed). ATR-FTIR: ν_{max} (cm^{-1}) 2095 (m), 2057 (s), 2024 (s, br) (CO) cm^{-1}. Elemental analyses calcd for C: 48.82; H: 3.43; found: C: 47.05; H: 3.81.

5.4.10 Synthesis of G_2 COOH-dendrimer

The dendrimer was synthesized using a procedure similar to that used in the synthesis of **G_0 COOH-dendrimer** (*Chapter Four*). In brief, 1.24 g (0.040 mmol) of **G_2 Cl-dendrimer**, 249 mg (1.28 mmol) of 5-(4-hydroxyphenyl)pentanoic acid, 442 mg (3.20 mmol) of K_2CO_3, and 3 mL of DMF were weighed into a 25-mL round-bottomed flask, and heated at 65 °C for 24 hours under nitrogen atmosphere. Yield: 90%. ^{1}H NMR (300 MHz, DMSO-d_6): δ (ppm) 12.05 (32 H, br s, COO*H*), 7.51–6.99 (448 H, br s, Ar*H*), 6.24 (224 H, br s, complexed Ar*H*), 5.24 (280 H, s, Cp*H*), 5.12, 5.04 (48 H, br s, C*H*$_2$), 4.04 (8 H, br s, C*H*$_2$), 2.64–2.06 (284 H, br s, C*H*$_2$), 1.66, 1.61, 1.57 (84 H, br s, C*H*$_3$). ^{13}C{^{1}H} NMR (75 MHz, DMSO-d_6): δ (ppm) 174.8, 173.2, 173.1, 152.0, 151.6, 140.7, 134.5, 130.9, 130.8, 130.3, 129.6, 129.0, 128.8, 121.0, 120.8, 120.3, 78.3, 78.2, 77.4, 75.5,

75.0, 73.2, 47.9, 45.4, 45.2, 34.5, 33.9, 33.7, 30.7, 27.4, 25.7, 24.8, 24.5 Elemental analyses: calculated for C, 54.16; H, 4.19; found for C, 54.35; H, 4.40.

5.4.11. Synthesis of G_2 alkyne-dendrimer

The dendrimer was synthesized using a procedure similar to that used in the synthesis of **G_1 alkyne-dendrimer**. In brief, 1.20 g (0.033) of **G_2 COOH-dendrimer**, 273 mg (3.17 mmol) of 2-butyne-1,4-diol, 99.2 mg (0.812 mmol) of DMAP, 239 mg (1.16 mmol) of DCC, and 10 mL of 5:1 DCM/DMSO solvent mixture. Yield: 60%. ^{1}H NMR (300 MHz, DMSO-d_6): δ (ppm) 7.50–6.93 (448 H, br s, Ar*H*), 6.25 (224 H, br s, complexed Ar*H*), 5.23, 5.19 (280 H, s, Cp*H*), 5.12, 5.05 (48 H, br s, CH_2), 5.08 (32 H, br s, O*H*), 4.74 (64 H, br s, CH_2), 4.09 (64 H, br s, CH_2), 4.04 (8 H, br s, CH_2), 2.65–2.15 (284 H, br s, CH_2), 1.73, 1.68, 1.61 (84 H, br s, CH_3).^{13}C{^{1}H} NMR (75 MHz, DMSO-d_6): δ (ppm) 172.6, 171.8, 157.0, 153.1, 152.1, 151.6, 140.6, 137.3, 130.8, 130.2, 130.0, 129.5, 128.9, 121.0, 120.8, 120.5, 120.3, 118.7, 118.6, 117.9, 86.9, 78.9, 78.2, 77.4, 75.6, 75.5, 75.0, 52.2, 49.3, 47.9, 36.3, 34.4, 34.3, 33.7, 33.4, 33.3, 30.7, 30.5, 27.3, 25.7, 24.8, 24.3. Elemental analyses: calculated for C, 55.10; H, 4.29; found for C, 55.44; H, 4.54.

5.4.12. Synthesis of G_2 Co/Fe-dendrimer

The dendrimer was synthesized using a procedure similar to the synthesis of dendrimer **G_1 Co/Fe-dendrimer**. In brief, 200 mg (0.005 mmol) of **G_2 alkyne-dendrimer**, 0.160 mmol of dicobalt octacarbonyl, 9 mL of dried THF and 2 mL of dried DMF were used. The product was partially soluble in common laboratory solvents limiting characterization to ATR-FTIR and elemental analyses. Yield: 84%. ATR-FTIR: ν_{max} (cm^{-1}) 2095 (m), 2057 (s), 2024 (s, br) (CO) cm^{-1}. Elemental analyses: calculated for C, 49.30; H, 3.46; found for C, 49.01; H, 3.97.

5.4.13. Formation of ceramics

The ceramics were prepared using a previously described method.[7] In brief, powdered dendrimer sample was weighed into a quartz boat, transferred inside a quartz tube connected to ultrapure nitrogen gas and placed in a pyrolysis furnace. Under the flow of nitrogen, the furnace temperature was gradually raised to 900 °C over 3 hours and held constant for 12 hours. Next, the furnace was cooled to room temperature under a flow of nitrogen and the black ceramic was collected and weighed.

References

1. AL-Badri, Z. M.; Maddikeri, R. R.; Zha, Y.; Thaker, H. D.; Dobriyal, P.; Shunmugam, R.; Russell, T. P.; Tew, G. N. *Nat. Commun*., **2011**, *2*, 482.
2. Gutfleisch, O.; Willard, M. A.; Brück, E.; Chen, C. H.; Sankar, S. G.; Liu, J. P. *Adv. Mater*., **2011**, *23*, 821.
3. Kahn, O. *Acc. Chem. Res*., **2000**, *33*, 647.
4. Wu, W.; Tang, R.; Li, Q.; Li, Z. *Chem. Soc. Rev*. **2015**, *44*, 3997.
5. Jiles, D. C. *Acta Mater*., **2003**, *51*, 5907.
6. MacLachlan, M. J.; Ginzburg, M.; Coombs, N.; Coyle, T. W.; Raju, N. P.; Greedan, J. E.; Ozin, G. A.; Manners, I. *Science*, **2000**, *287*, 1460.
7. Berenbaum, A.; Ginzburg-Margau, M.; Coombs, N.; Lough, A. J.; Safa-Sefat, A.; Greedan, J. E.; Ozin, G. A.; Manners, I. *Adv. Mater*., **2003**, *15*, 51.
8. Kulbaba, K.; Cheng, A.; Bartole, A.; Greenberg, S.; Resendes, R.; Coombes, N.; Safa-Sefat, A.; Greedan, J. E.; Stöver, H. D. H.; Ozin, G. A.; Manners, I. *J. Am. Chem. Soc*., **2002**, *124*, 12522.
9. Häussler, M.; Zheng, R.; Lam, J. W. Y.; Tong, H.; Dong, H.; Tang, B. Z. *J. Phys. Chem. B*, **2004**, *108*, 10645.
10. Shi, J.; Tong, B.; Li, Z.; Shen, J.; Zhao, W.; Fu, H.; Zhi, J.; Dong, Y.; Häussler, M.; Lam, J. W. Y.; Tang, B. Z. *Macromolecules*, **2007**, *40*, 8195.
11. Shi, J.; Jim, C. J. W.; Mahtab, F.; Liu, J.; Lam, J. W. Y.; Sung, H. H. Y.; Williams, I. D.; Dong, Y.; Tang, B. Z. *Macromolecules*, **2010**, *43*, 680.
12. Cuadrado, I.; Morán, M.; Casado, C. M.; Alonso, B.; Losada, J. *Coord. Chem. Rev*., **1999**, *193-195*, 395.
13. Caminade, A-M.; Yan, D.; Smith, D. K. *Chem. Soc. Rev*., **2015**, *44*, 3870.
14. Astruc, D.; Ornelas, C.; Ruiz, J. *Acc. Chem. Res*., **2008**, *41*, 841.
15. Hourani, R.; Kakkar, A. *Macromol. Rapid Commun*., **2010**, *31*, 947.
16. Astruc, D.; Boisselier, E.; Ornelas, C. *Chem. Rev*., **2010**, *110*, 1857.
17. Lee, C. C.; MacKay, J. A.; Fréchet, J. M. J.; Szoka, F. C. *Nat. Biotechnol*., **2005**, *23*, 1517.
18. Kong, J.; Schmalz, T.; Motz, G.; Müller, A. H. E. *J. Mater. Chem. C*, **2013**, *1*, 1507.

19. Ginzburg-Margau, M.; Fournier-Bidoz, S.; Coombs, N.; Ozin, G. A.; Manners, I. *Chem. Commun*., **2002**, 3022.
20. Li, H.; Li, L.; Wu, H.; Lam, J. W. Y.; Sun, J. Z.; Qin, A.; Tang, B. Z. *Polym. Chem*., **2013**, *4*, 5537.
21. Shi, J.; Tong, B.; Zhao, W.; Shen, J.; Zhi, J.; Dong, Y.; Häussler, M.; Lam, J. W. Y.; Tang, B. Z. *Macromolecules*, **2007**, *40*, 5612.
22. Rider, D. A.; Liu, K.; Eloi, J-C.; Vanderark, L.; Yang, L.; Wang, J-Y.; Grozea, D.; Lu, Z-H.; Russell, T. P.; Manners, I. *ACS Nano*, **2008**, *2*, 263.
23. Sun, Q.; Xu, K.; Peng, H.; Zheng, R.; Häussler, M.; Tang, B. Z. *Macromolecules*, **2003**, *36*, 2309.
24. Sun, Q.; Lam, J. W. Y.; Xu, K.; Xu, H.; Cha, J. A. K.; Wong, P. C. L.; Wen, G.; Zhang, X.; Jing, X.; Wang, F.; Tang, B. Z. *Chem. Mater*., **2000**, *12*, 2617.
25. Li, Z.; Lam, J. W. Y.; Dong, Y.; Dong, Y.; Sung, H. H. Y.; Williams, I. D.; Tang, B. Z. *Macromolecules*, **2006**, *39*, 6458.
26. Ginzburg, M.; MacLachlan, M. J.; Yang, S. M.; Coombs, N.; Coyle, T. W.; Raju, N. P.; Greedan, J. E.; Herber, R. H.; Ozin, G. A.; Manners, I. *J. Am. Chem. Soc*. **2002**, *124*, 2625.
27. Tamboli, M. S.; Palei, P. K.; Patil, S. S.; Kulkarni, M. V.; Maldar, N. N.; Kale, B. B. *Dalton Trans*., **2014**, *43*, 13232.
28. Liu, K.; Clendenning, S. B.; Friebe, L.; Chan, W. Y.; Zhu, X.; Freeman, M. R.; Yang, C. G.; Yip, C. M.; Grozea, D.; Lu, Z-H.; Manners, I. *Chem. Mater*., **2006**, *18*, 2591.
29. Luo, C.; Duan, W.; Yin, X.; Kong, J.; *J. Phys. Chem. C*, **2016**, *120*, 18721.
30. Jiang, B.; Nykypanchuk, D.; Endoh, M. K.; Chen, X.; Qian, B.; Kisslinger, K.; Koga, T.; Parise, J. B.; Grubbs, R. B. *Macromolecules*, **2016**, *49*, 853.
31. Rüttiger, C.; Pfeifer, V.; Rittscher, V.; Stock, D.; Scheid, D.; Vowinkel, S.; Roth, F.; Didzoleit, H.; Stühn, B.; Elbert, J.; Ionescu, E.; Gallei, M. *Polym. Chem*., **2016**, *7*, 1129.
32. Jiang, B.; Hom, W. L.; Chen, X.; Yu, P.; Pavelka, L. C.; Kisslinger, K.; Parise, J. B.; Bhatia, S. R.; Grubbs, R. B. *J. Am. Chem. Soc*., **2016**, *138*, 4616.
33. Friebe, L.; Liu, K.; Obermeier, B.; Petrov, S.; Dube, P.; Manners, I. *Chem. Mater*., **2007**, *19*, 2630.
34. Abd-El-Aziz, A. S.; Winram, D. J.; Shipman, P. O.; Rock, C. L.; Vandel, M. S.; Patrick, B. O. *Macromol. Chem. Phys*., **2012**, *213*, 2136.
35. Mathiowitz, E.; Ron, E.; Mathiowitz, G.; Amato, C.; Langer, R. *Macromolecules*, **1990**, *23*, 3212.
36. Zhou, Y.; Switzer, J. A. *J. Alloy. Comp*., **1996**, *237*, 1.
37. West, A. R. *Basic Solid State Chemistry*, John Wiley & Sons, Ltd, 2nd Edition, West Sussex, UK (**1999**).
38. Valenzuela, R. *Magnetic Ceramics*, Cambridge University Press, 1st Edition, Cambridge UK (**1994**).
39. Caruntu, D.; Caruntu, G.; O'Connor, C. J. *J. Phys. D: Appl. Phys.*, **2007**, *40*, 5801.
40. Sundaresan, A.; Rao, C. N. R. *Nano Today*, **2009**, *4*, 96.
41. Lu, A-H.; Salabas, E. L.; Schüth, F. *Angew. Chem. Int. Ed*., **2007**, *46*, 1222.
42. Salabas, E. L.; Rumplecker, A.; Kleitz, F.; Radu, F.; Schüth, F. *Nano Lett*., **2006**, *6*, 2977.
43. Ghosh, M.; Sampathkumaran, E. V.; Rao, C. N. R. *Chem. Mater*., **2005**, *17*, 2348.
44. Gross, A. F.; Diehl, M. R.; Beverly, K. C.; Richman, E. K.; Tolbert, S. H. *J. Phys. Chem. B*, **2003**, *107*, 5475.

45. Zha, Y.; Thaker, H. D.; Maddikeri, R. R.; Gido, S. P.; Tuominen, M. T.; Tew, G. N. *J. Am. Chem. Soc*., **2012**, *134*, 1453.
46. Abd-El-Aziz, A. S.; Winram, D. J.; Shipman, P. O.; Bichler, L. *Macromol. Rapid Commun*., **2010**, *31*, 1992.

Chapter Six: Conclusion and Future Direction

6.1. Conclusion

Demand for new antimicrobial agents to combat antimicrobial resistance provided the main impetus for this study. Indeed, antimicrobial resistance is an acknowledged global public health issue that threatens the effective treatment and prevention of common infectious diseases, increasing the cost of healthcare and in some cases, resulting in disability or death. Unfortunately, a dearth of effective antimicrobial agents and a lack of interest in the research and development of new antimicrobial agents by pharmaceutical companies accompanied the increasing virulence of resistant microorganisms. Further, the ability of microorganisms to rapidly develop new resistance mechanisms as part of their natural evolutionary process worsened the crisis. A crucial component of a coordinated strategy to address the crisis includes the research and development of new antimicrobial agents.

The work reported in this thesis introduced a new effective antimicrobial agent, η^6-arene-η^5-cyclopentadienyliron(II) ($[\eta^6$-arene-η^5-CpFe$]^+$) complexes to replenish the already exhausted antimicrobial pipeline. The chemistry of these complexes is versatile and was exploited to synthesize a new family organometallic dendrimers. Also, the presence of iron in these dendrimers implies ferromagnetism since this metal is ferromagnetic. This study, therefore, focused on the synthesis of $[\eta^6$-arene-η^5-CpFe$]^+$ -containing dendrimers and explored their antimicrobial and magnetic properties.

Chapter Two reports the synthesis route to this new family of $[\eta^6$-arene-η^5-CpFe$]^+$-containing dendrimers. These dendrimers were intrinsically redox-active due to the presence of

the $[\eta^6$-arene-η^5-CpFe$]^+$ complex. Further, the susceptibility of the complex towards nucleophilic aromatic substitution allows the facile functionalization of the dendrimer periphery, providing a strategy to impart additional function or tune the intrinsic one. This was demonstrated by incorporating photoactive β-naphthol to obtain bifunctional, photoactive and redox-active dendrimers. UV-vis and fluorescence studies confirmed the photoactivity while CV experiments revealed that the dendrimers were redox active. UV-vis and fluorescence spectroscopy also provided information on the topology of the dendrimers, specifically indicating backfolding of peripheral groups into the dendrimer inner cavity at higher generation. Photolysis of these organometallic dendrimers yielded their organic photoactive analogs with enhanced emissive property.

In *Chapter Three*, the versatility of the synthesis route was further demonstrated by successfully incorporating bulkier tetraphenylethylene into the dendrimer periphery. The photochemistry of tetraphenylethylene-containing organometallic dendrimers was exploited to synthesize the first dual emissive tetraphenylethylene-based macromolecular system. These dendrimers emitted in solution and as aggregates. Also, the dependence of the photochemistry of the tetraphenylethylene moieties on oxygen was demonstrated to be useful in the qualitative screening of degassed and aerated solvents.

In *Chapter Four*, the antimicrobial activity of the $[\eta^6$-arene-η^5-CpFe$]^+$ complexes was demonstrated in vitro, providing the motivation to design the first organometallic dendrimer with antimicrobial activity against drug resistant strains of microorganisms, such as methicillin-resistant *Staphylococcus aureus* and vancomycin-resistant *Enterococcus faecium*. The cationic charge on the dendrimers contributed to the activity because changing the PF_6^- counteranion to a BF_4^- altered the activity. Further, the dendrimers induced oxidative stress on methicillin-resistant

Staphylococcus aureus, suggesting another mechanism of action. These dendrimers were functionalized with quaternary ammonium groups or 2-mercaptobenzthiazole to obtain hybrid antimicrobial organometallic dendrimers with enhanced activity at the higher generation compared with the parent dendrimers. Also, in vitro, the dendrimers were non-toxic to human epidermal cell lines.

In *Chapter Five*, it was conclusively demonstrated that ceramics generated from these [η^6-arene-η^5-CpFe]$^+$-containing dendrimers exhibited room temperature, soft ferromagnetism. The ferromagnetism was tunable *via* changing the generation of the dendrimer or functionalizing the periphery with cobalt. Indeed, softness increased as the generation increased. The effect of the peripheral cobalt was more complicated because it increases the saturation magnetization and coercivity at the second-generation but decreased these properties at the zeroth- and first-generation. Again, in the ceramics derived from the iron/cobalt-containing dendrimers, the Co and Fe nano-crystallites existed in separate crystalline domains. Indeed, in these heterometallic dendrimers, Co and Fe are in distinct regions with the former metal being at the periphery and the latter in the inner cavity. Such spatial separation could favor separate crystallization of the Co and Fe nanoparticles.

Taken together, the work reported in this thesis demonstrated, for the first time, the antimicrobial and magnetic properties of [η^6-arene-η^5-CpFe]$^+$-derived materials. The original contribution, therefore, includes:

1. the synthesis of a new family of organometallic dendrimers.
2. the synthesis of the first TPE-based dual-emissive macromolecule
3. the demonstrated antimicrobial activity of [η^6-arene-η^5-CpFe]$^+$ complexes
4. the synthesis of the first organometallic dendrimers with antimicrobial activity

5. the identification of parameters that tune antimicrobial activity of these dendrimers.
6. the demonstrated magnetic properties of [η^6-arene-η^5-CpFe]$^+$-derived materials.
7. the synthesis of the first dendrimer-derived magnetoceramics.
8. the identification of parameters that tune magnetism in dendrimer-derived ceramics.

6.2. Future Work

Despite these contributions, gaps exist that need to be addressed in the future. First, characterization of these organometallic dendrimers was limited to NMR spectroscopy and elemental analyses. Information on the molecular weight, obtainable from gel permeation chromatography (GPC) or mass spectrometry (MS), will be helpful. The unique topology of dendrimers requires the use of a GPC coupled to a molecular weight-sensitive detector, such as light scattering detector, which were not available for this study. Attempts to use electrospray ionization mass spectrometry failed due to the insolubility of these dendrimers in solvents that are compatible with the instrument. Matrix-assisted laser desorption/ionization mass spectrometry (MALDI-MS) is a very promising technique to ascertain the molecular weight of these cationic dendrimers but attempts also failed due to lack of an appropriate matrix. Therefore, future work, which may involve a collaboration with an analytical chemist, should include the development of analytical method for the characterization of the molecular weights of these cationic dendrimers. Towards this, MALDI-MS is preferred and focus can be directed at identifying a suitable matrix for MALDI-MS characterization of these dendrimers. Such a suitable matrix will also be helpful in using MALDI-MS to characterize other [η^6-arene-η^5-CpFe]$^+$-derived macromolecules. Also, DOSY NMR is emerging as an analytical tool to determine the molecular weight of polymers and could be explored but will require a calibration curve to ascertain the molecular weight.

Also, it is fundamentally essential to understand the killing kinetics of these antimicrobial dendrimers. Such information will provide insight into whether the dendrimers are bacteriostatic or bactericidal in activity. Also of fundamental interest is the mechanism through which these dendrimers initiate the generation of free radicals. This understanding will afford a means to controlling the antimicrobial activity better.

While the narrow spectrum of activity of the dendrimers against Gram-positive drug-resistant bacteria is exciting and preferred in some cases, it is still a worthy challenge to broaden their scope of activity to Gram-negative bacteria as well as fungi. In this regards, other polymeric architecture, such as linear polymers with a pendant $[\eta^6\text{-arene-}\eta^5\text{-CpFe}]^+$ complex, need to be examined. Considering that dendrimers are explored in drug delivery, it is reasonable to position these antimicrobial dendrimers as dual functional materials, acting as drug delivery vectors and as antimicrobial agents. Such dual functional materials will be useful in wound care, where the antimicrobial dendrimer prevents and treat infections while an encapsulated analgesic can be delivered to relief pain. Also of interest is the in vivo antimicrobial activity of these dendrimers, which need to be established

The threat of resistance is not limited to bacteria. Indeed, it is also important to tackle drug resistance in malaria, tuberculosis, and HIV, which are acknowledged as serious threats. Thus, investigating the antivirals, antimalarial, antituberculosis, and anthelmintic property of $[\eta^6\text{-arene-}\eta^5\text{-CpFe}]^+$ complexes is an attractive research interest. A strategy may involve developing $[\eta^6\text{-arene-}\eta^5\text{-CpFe}]^+$ complex-drug conjugates, aiming to improve the effectiveness of the drug to combat resistance.

It is obvious that ceramics derived from $[\eta^6\text{-arene-}\eta^5\text{-CpFe}]^+$ containing dendrimers were magnetic, and this property was influenced by structure. Thus, it will be necessary to examine

other polymer types, such as star and linear poly(aromatic ether)s containing the complex in the backbone or as a pendant. Given the temperature resistance of the poly(aromatic ethers), it will be possible to increase the ceramic yield *via* the approach. Further, effort should be directed at replacing oxygen in the structure of these polymer preceramics since the formation of oxides reduces the magnetic response. Towards this, it will be attractive to examine poly(amine)s or poly(thiol)s as alternatives to poly(aromatic ether)s.